Condition Monitoring of Capacitors for DC-link Application in Power Electronic Converters

Soliman, Hammam Abdelaal Hammam

Publication date:
2017

Document Version
Publisher's PDF, also known as Version of record

CONDITION MONITORING OF CAPACITORS FOR DC-LINK APPLICATION IN POWER ELECTRONIC CONVERTERS

BY
HAMMAM SOLIMAN

DISSERTATION SUBMITTED 2017

AALBORG UNIVERSITY
DENMARK

Condition Monitoring of Capacitors for DC-link Application in Power Electronic Converters

by

Hammam Soliman

AALBORG UNIVERSITY
DENMARK

Dissertation submitted

Dissertation submitted: June, 2017

PhD supervisor: Prof. Frede Blaabjerg
Aalborg University

Assistant PhD supervisor: Assoc. Prof. Huai Wang
Aalborg University

PhD committee: Dr. Dezso Sera (Chairman)
Aalborg University

Dr. J.J Liu
Xian Jiaotong University

Dr. Suresh Perinpanayagam
University of Cranfield

PhD Series: Faculty of Engineering and Science, Aalborg University

ISSN (online): 2446-1636
ISBN (online): 978-87-7112-957-1

Published by:
Aalborg University Press
Skjernvej 4A, 2nd floor
DK – 9220 Aalborg Ø
Phone: +45 99407140
aauf@forlag.aau.dk
forlag.aau.dk

Printed in Denmark by Rosendahls, 2017

Acknowledgements

This PhD thesis is part of the Center of Reliable Power Electronics (*CORPE*) project. The center is supported by the *Danish Strategic Research Council* and the *Obel Foundation* under the supervision and guidance of Prof. Frede Blaabjerg. The main focus of CORPE is to design more reliable and more efficient power electronic systems for use in equipment for power generation, distribution and consumption. A small part of the center is related to the dc-link capacitors in power electronic converters "Condition Monitoring of Capacitors for DC-link Application in Power Electronic Converters", which I have been responsible for. This PhD project is partially funded by Arab Academy for Science, Technology and Maritime Transport (*AASTMT*) and Aalborg University (*AAU*).

With this important milestone in my life, I'm grateful and thankful to everyone who contributes to the outcome of this PhD thesis in one way or another. Especially, I would like to express my deepest gratitude and appreciation to my very supportive supervisor Prof. Frede Blaabjerg who always find the patience and gave me all the support, continuously guidance and motivation that I needed during my study.

My co-supervisor Prof. Huai Wang, who interviewed me in the process of my enrolment and followed me with guidance and constructive feedback from day one, and taught me many different skills on different aspects beside the research.

Prof. Claus Leth Bak, the head of doctoral program in Energy Technology Department for his support to all of the PhD fellows and students in the department and for his continuously concern and care for our PhD progress.

Prof. Yaser Gaber, who proposed me to Prof. Frede Blaabjerg and introduce me to the PhD program in Aalborg university. Who played an important role that my wife and I can be PhD students at the same time in the same university and department. Prof. Mostafa Marei for giving me all the support I needed in Egypt and abroad. Dr. Ibrahim Abdallah for his partial cooperation during my PhD. Prof. Yasser Galal, Prof. Rania El-Sharkawy, my mentors from home university Arab Academy for Science and Technology (*AAST*) who gave me the support to earn this scholarship. I want to thank them for teaching me many things in life in general.

My best regards to all CORPE members for many useful brain storming and discussions, especially to Brwene Gadalla (I have wrote a separate section just for her), my friend, colleague and student Mohamed Al-Hasheem, Pooya Davari (for his support in part of my experimental work), Hamid Soltani, Zian Qin (for his programming skills and friendship), and Paula Diaz Reigosa.

I would like to thank Lorand Bede who gave me the opportunity to attend his Digital Signal Processor (*DSP*) lectures and guided me in this part of my project by following me and finding the time to give me his constructive feedback on my results.

I am thankful and grateful to all staff at the Department of Energy Technology for their administrative support on all aspects that are related to my study and for making my study period more enjoyable. Especially, Tina Larsen, Corina Busk Gregersen, Hanne Munk, Ann Miltersen and Casper Jørgensen (for his great social events planning).

At last but not least, I would like to thank my closest friends who I met in Aalborg City during my PhD study and for making my life much easier, enjoyable and happier, Simon Mcllroy and his lovely wife Binca Mcllroy (met them after arriving Aalborg by 30 minutes), my smartest friend Mostafa Kamel and his talented wife Jeanette Thomsen, Ahmed Shawky, Mohamed Mazen, Hanan Bershany, Sarah Hassan and her lovely family, Kenan and Emina, Ali Zaib and his wife Isabella Kozon. Also I want to thank Helle Andersen and her parents for all the love and care they gave to me, my wife, and my son Yassin.

I would like to thank my family, especially my parents for their prayers, support and unconditional love. My parents in law for their prayers, moral and financial support and love. My deepest gratitude to my life time friend Omar El-Deeb for his great friendship and all the memories and good times we shared together and for more to come.

To my very dear and lovable wife, friend, and colleague *Brwene Gadalla*, who always gave me the support, and for her understanding to my unstable mood during my PhD period. For making my life easier by withstanding with all the changes and by holding a huge responsibility of me and our beloved son Yassin beside focusing on her PhD study as well. For playing the most important role in my life by providing me with love and care. To our son *Yassin* for bringing joy and happiness to our life after struggling in his birth, and for giving us the opportunity to taste the real happy life.

"*The beauty is in the knowledge that we might never arrive at truth itself but will continue the pursuit anyway. I am not concerned about what I reached if any, what concerns me the most is to not lose the urge of pursuit*"

by *Sarah H. Awad*

Hammam Soliman
Aalborg University, June 13, 2017

English Abstract

Power electronic circuits are used in variety of applications ranging from small power supplies in computers to more specialized applications such as; satellite, airplane, medical equipments and different war-machines. In all of these applications, static power converters are an essential subsystem whose failure leads to the imminent and total stoppage of the equipment. Dc-link capacitor is commonly used in all of these equipments as smoothening energy element of the converters. As a fact, in energy conversion converters, a group of series/parallel connected capacitors (capacitor bank) or a single capacitor is normally used as dc-link filter. The system may be malfunction if one or more capacitor reaches end-of-life. Since failure of a single element may lead to collapse of the entire system, it is needed to develop some kind of mechanism, which will alert the operator in advance for predictive maintenance before failure, such mechanism is known as "Condition Monitoring".

Recently, the academic research have been focusing on monitoring the conditions and the health status of dc-link capacitors. Industry applications require more reliable power electronics products with preventive maintenances. Therefore, an in-depth analysis of prior-art condition monitoring methods (advantages, shortcomings) have been done from the following aspects: a) end-of-life indicator (e.g. C, ESR); b) how to estimate the indicator (e.g. sense current, voltage); c) algorithm to obtain the value of the indicator (online or offline); d) accuracy study and sensitivity analysis; e) hardware and software realization (reliability, cost, and complexity of the additional software algorithm and hardware circuits).

From analysing the prior-art methods it was found that, the existing capacitor condition monitoring methodologies are suffering from low estimation accuracy and/or extra hardware cost, where such shortcomings are preventing these methodologies to be considered in practical applications. Therefore, development of new condition monitoring technology that

is based on software solutions with reducing the needs of extra hardware is beneficial with respect to the cost and complexity, and therefore could be more convenient for practical applications in the industry field.

This project develops new method using an Artificial Neural Network (*ANN*) algorithm in order to monitor the change of the capacitance of an electrolytic capacitor for dc-link application in order to apply predictive maintenance. The software based method is proposed in order to solve the existing issues of the prior-art research.

The ANN method estimates the end-of-life indicator (e.g. capacitance) using only the input/output terminal information of the power converter, which are readily available from the feedback signals of existing digital controller. The trained ANN is implemented with the Digital Signal Processor (*DSP*) which is normally existing for control purposes. In order to investigate the proposed method under different conditions, the ANN condition monitoring method is applied on dc-link capacitor in a Front-End diode bridge converter. Moreover, the impact of training data quality and amount on the ANN accuracy are studied. Analysing the estimation error under different capacitance conditions, different reduction level of the capacitance initial value and different loading conditions are also given.

Dansk Abstrakt

Effektelektroniske kredsløb anvendes i mange forskellige applikationer lige fra små strømforsyninger i computere til mere specialiserede applikationer såsom; satellitter, fly, medicinsk udstyr og i militære systemer. I alle disse applikationer er effektelektroniske omformere et væsentligt delsystem, hvor fejl fører til uheld og evt. total standsning af systemet. Kondensatorer er almindeligt anvendte i effektelektroniske systemer som energilagrende elementer. I effektelektroniske systemer bliver en enkelt kondensator eller flere kondensatorer anvendt i en kondensatorbank, som normalt bruges i jævnspændingsdelen. Systemet kan få en funktionsfejl, hvis en eller flere kondensatorer når deres end-of-life. Da svigt i et enkelt element kan føre til sammenbrud af hele systemet, er det nødvendigt at udvikle et system, som kan gøre operatøren opmærksom på dette på forhånd og foretage forebyggende vedligeholdelse før svigt. Sådan en mekanisme er kendt som ”tilstandsovervågning” ("Condition Monitoring") af et system.

I den sidste tid har tilstandsovervågning af DC-link kondensatorer for at estimere deres levetid tiltrukket en del opmærksomhed, da industrielle anvendelser kræver mere pålidelige produkter med forebyggende vedligehold. Derfor er en grundig analyse i denne afhandling af kendte tilstandsovervågningsmetoder (fordele, ulemper) foretaget ud fra følgende aspekter: a) end-of-life indikatorer; b) hvordan man kan finde indikatoren (fx måle strøm, spænding); c) algoritme til at opnå værdien af indikatoren (online eller offline); d) metodernes nøjagtighed og følsomhed; e) realisering af hardware og software (pålidelighed, omkostninger og kompleksiteten af de ekstra software-algoritmer og hardware-kredsløb).

Fra analysen af de kendte metoder er det konstateret, at de eksisterende tilstandsovervågningsmetoder af kondensatorer giver enten forøgede hardware-omkostninger eller en dårlig estimeringsnøjagtighed, hvilket er udfordringer, der skal løses i industrielle anvendelser. Derfor vil udvikling af en ny til-

standsovervågningsteknologi med softwareløsninger uden ekstra hardwareomkostninger være mere lovende for industrielle anvendelser. Dette projekt udvikler en ny software-baseret metode ved hjælp af en neuralt netværk (ANN) algoritme til at overvåge ændringen af de elektriske parametre i elektrolytkondensatorer til DC-link'en i en effektkonverter, som arbejder under stressede forhold, og det påtænkes at anvende den til forebyggende vedligeholdelse. Den software-baserede metode er foreslået for at kunne løse de eksisterende problemer.

ANN-metoden estimerer end-of-life-indikatorer (fx kondensatorens kapacitans) ved hjælp af måling på indgangsterminalen og udgangsterminalen af omformeren, som er let tilgængelige fra allerede eksisterende digitale styringer. Den udviklede ANN algoritme udføres med en Digital Signal Processor, der normalt bruges med henblik på kontrol af motoren. For at undersøge den foreslåede metode under forskellige betingelser er ANN tilstandsovervågningsmetoden anvendt på en DC-link-kondensator i en diodeensretterbro, som typisk anvendes i en motorstyring. Desuden er kvaliteten af træningsdata for ANN'en og dens nøjagtighed undersøgt. En fejlanalyse under forskellige DC-link kapacitansværdier er beskrevet, såvel som at forskellige niveauer af kapacitansreduktionen i forhold til den oprindelige værdi under forskellige belastningstilstande også er undersøgt. Det er konkluderet, at den foreslåede metode kan implementeres i en fremtidig motorstyring.

Table of Contents

List of Figures

List of Tables

Chapter. 1

Introduction

This chapter is the introduction of the documented Ph.D. project, which includes project motivation, background in capacitors, problem formulation, project objectives, limitations and thesis structure.

1.1 Introduction

This chapter presents a background of the dc-link capacitors in power electronic converters. It includes a description of their common types, construction, and mode of failures. Moreover, a general reliability assessment of capacitors from different aspects (e.g. physics-of-failure, design, health management, and condition monitoring) is also addressed. Then, in order to show a clear understanding of the flow of this research work, a structure of this thesis is also given. Finally, a list of the published work by the author of this PhD thesis is given by the end of this chapter.

1.1.1 DC-link capacitors in power electronic converters

Capacitors are one of the reliability critical components in power electronic systems. They are widely used for the purpose of reduce the voltage ripples in the dc-link and to equalize the power difference between the input side and the load side. They are also a storage element that can be used in the AC-side [4]. Fig. 1.1 shows the generic block diagram of a capacitive dc-link based power electronic converter [80]. Stage I and stage II could be different circuit topologies. Table 1.1 lists some scenarios for each power electronic stage [80].

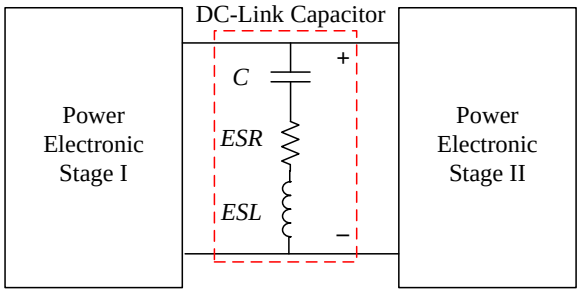

Fig. 1.1: Block diagram of a capacitive dc-link based power electronic converter with parasitic elements [80].

Table 1.1: Different Scenarios for Different Power Electronic Converters [80].

Power Electronic Stage I	**Power Electronic Stage II**
AC/DC	DC/AC or DC/DC or Load
DC/DC	Load
DC	DC/AC

However, selection of the capacitor type depends on different factors such as; dc-link voltage rating, capacitance value, operating frequency, physical size, operating temperature, cost and so on. Moreover, the design of the dc-link is required to have the matching between the capacitor characteristics and the application specifications [88]. In dc-link applications, three types of capacitors are widely used, the Electrolytic Capacitors (E-Caps), the Metallized Polypropylene Film Capacitors (MPPF-Caps) and the high capacitance Multi-Layer Ceramic Capacitors (MLC-Caps). In the following subsections, E-Caps and MPPF-Caps are discussed on details. Their constructions and mode of failures are also listed.

Electrolytic capacitors (E-Caps)

Electrolytic Capacitors (Fig. 1.2) are widely used in power converters due to the fact that they help to filter out/reduce the AC ripple voltage and also serve for coupling and decoupling applications [4]. They are also widely used due to their large capacitance and relatively small size [4]. The advantage of their small size property is due to the very thin dielectric layer where the distance between the plates is very small [4] [3]. Most of the electrolytic capacitors are polarized, which means that the polarity of the applied DC voltage must be the correct corresponding polarity; i.e. positive terminal to the positive end of the capacitor and negative terminal to the negative end of

Fig. 1.2: JIANGHAI 22 μF, 400 V electrolytic capacitor.

the capacitor [73]. Otherwise, the insulation will break down due to incorrect polarization, and hence, the capacitor may be permanently damaged [73]. In addition to the polarization disadvantage where applying an AC voltage is not applicable, the considerable voltage rating for electrolytic capacitor is relatively low [76].

Construction and mode of failures A major part in the construction of electrolytic capacitors is the oxide layer. A group of metals that are called "*Valve Metals*" are considered as electrically insulating oxides, and thereby, they can serve as an oxide layer [5]. The valve metals are; tantalum, aluminium, zirconium, hafnium, titanium, and niobium. Since the thickness of the dielectric layer in the capacitor is effected by the electrochemical changes, it is very important that the selected metal type of the dielectric layer can permit an accurate control of this thickness. Only two of the aforementioned metals (i.e. aluminium and tantalum) are having the advantage of accurate control for their thickness with respect to the electrochemical changes [8].

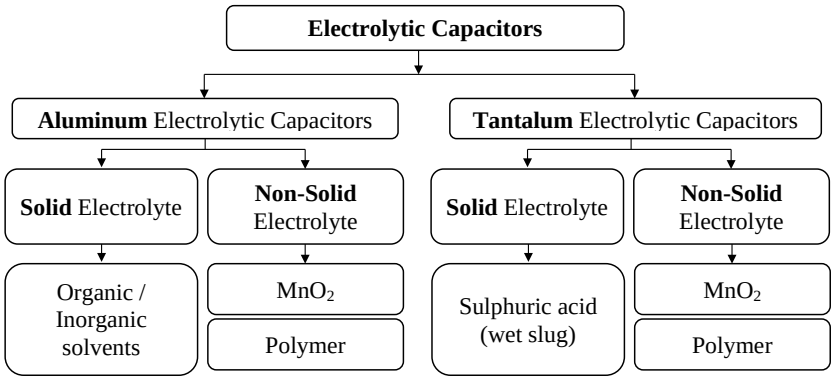

Fig. 1.3: The different types of metals and electrolytes in electrolytic capacitors [5].

As the basic construction principles of electrolytic capacitors for both aforementioned types (Al-Caps and tantalum capacitors), each of these two capacitor families are using non-solid and solid manganese dioxide or solid polymer electrolytes, so a great spread of different combinations of anode material and solid or non-solid electrolytes are available. These combinations are illustrated in Fig. 1.3 [5].

Al-Caps are consisting of three main parts; an aluminium foil, a capacitor paper, and an aluminium oxide layer. The aluminium foil that in contact with the oxide layer acts as the "*Anode*". The capacitor paper (electrolytic spacer) acts as the "*Cathode*". While the aluminium oxide layers acts as a dielectric material. Once the capacitor paper (electrolyte) gets in contact with the oxide layer, the oxide layer serves as an excellent insulation surface. Eventually, a higher capacitance becomes available according to the effective surface produced by the etched aluminium foil [5]. As mentioned earlier, Al-Caps are consisting of two aluminium foils with a capacitor paper inserted in between. After wounding the two foils and paper an impregnation process with electrolyte is applied. A simple illustrative structure of an Al-Caps is shown in Fig. 1.4.

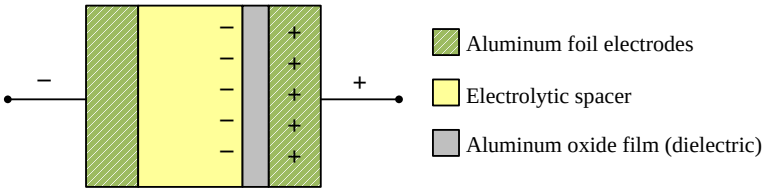

Fig. 1.4: The construction of an aluminium electrolytic capacitor [5].

Since the oxide layer has rectifying properties, an electrolytic capacitor has polarity. But if an oxide layer is attached to both cathode and anode, a bipolar capacitor type would be produced. This type refers to a "non-solid" Al-Caps, in which the electrolytic paper is soaked with a liquid electrolyte. Another type of Al-Caps is the "solid" type, in which uses a solid electrolyte 1.4. Although E-Caps are commonly used because of their low cost and small size, they still remain one of the most unreliable electrical components. Based on a collected examples of failures in power electronics systems [93], E-Caps are sharing 30% of the failure root cause distribution for power electronic systems as shown in Fig. 1.5. Here are three systematic mode of failures caused due to three failure mechanisms [4]:

1) **Over-voltage** – a leakage current in the dielectric layer due to an excessive voltage, results a **short circuit** mode of failure.

2) **Disconnection of terminals** – the soldering joints are affected by the

vibration stressor, and hence an **open circuit** mode of failure is the result.

3) **Over Temperature** – an excessive heat dries out and vaporize the electrolyte, and thereby, the life of the E-Caps is shortened causing a **wear-out** mode of failure.

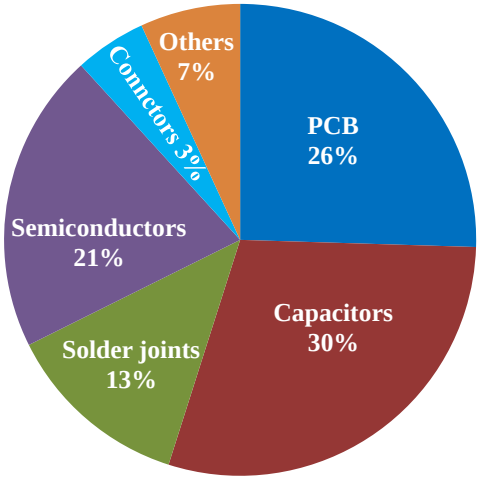

Fig. 1.5: Failure root cause distrbution for power electronic systems [93].

Metallized Polypropylene Film capacitors (MPPF-Caps)

Due to their unique self healing properties, low Equivalent Series Resistance (ESR), and wide filtering bandwidth; MPPF-Caps (Fig. 1.6) have become an acceptable substitute to E-Caps.

Fig. 1.6: EPCOS 110 μF, 450 V MPPF capacitor.

Since MPPF-Caps provide a well-balanced performance for high voltage applications, they are preferable in the aerospace and other fault-tolerant

applications. Moreover, from the manufacturing point of view, MPPF-Caps are metal based and they can withstand against the environmental changes such as temperature and humidity fluctuations. Comparing MPPF-Caps with E-Caps, MPPF-Caps are featuring the following advantages:

1) High voltage capabilities.
2) High peak and Root Mean Square (RMS) current capabilities.
3) Non-polarized.
4) Robustness (withstand up to twice rated voltage for short time).
5) Higher capacitance with lower volume.
6) Solid metal based technology.

Construction and mode of failures Film capacitors are consisting of two dielectric layers (plastic film) covered with metal foils (electrodes). These layers are attached to a terminal ends and wounded into a cylindrical shape before getting encapsulated [43]. A cross-section view of a film capacitor is shown in Fig. 1.7.

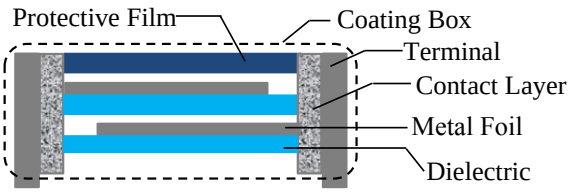

Fig. 1.7: Cross-section of a film capacitor [43].

Film capacitors are classified into two types with respect to the metal foil type as listed below [43]. Two different configuration of the electrode can be applied as seen in Fig. 1.8.

1) **Film capacitors**; where two layers of plastic film are used as dielectric layers. Each is covered with a thin metal foil which acts as the electrodes and usually they are made out of aluminium. The direct contact between the dielectric layer and the electrode is the main advantage, where surges of high current can be handled [43].
2) **Metallized film capacitors**; where two metallized metal foils are covering the dielectric layers. The difference in this type is tat, a thin layer of vacuum-deposited is attached to the aluminium metallization side to serve as electrodes [43].

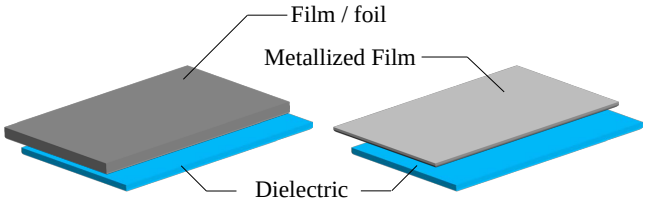

Fig. 1.8: Electrode configurations in film capacitors [43].

The configuration with metallizing the film is the reason that MPPF-Caps are having the "self-healing" property. It is applied when "the electrical properties of the capacitor are restored rapidly after a local breakdown to the values before the breakdown" [43] [7]. The self-healing property is beneficial where damaging the capacitor can be avoided in case of short circuits and/or breakdowns of the dielectric material. A "zero defect" capacitors can be made with considering this kind of property in the design stage, where a capacitor with large capacitance and relatively small case can be produced. However, since a direct contact between the dielectric and electrode is not applied in the metallized film capacitors, a main disadvantage of that is the limited current surge rating. Moreover, It is important to mention that there are many type of failures that might occur, and not all of them will necessarily lead to the self-healing property [43] [7].

As the failure modes of E-Caps and their failure mechanism were discussed, similarly, MPPF-Caps mode of failures and their failure mechanism are listed as following:

1) **Over-current** – a flow of an over-current will cause the dielectric film to breakdown, and thereby, a moisture absorption by film will occurred, resulting in a **short circuit** mode of failure.

2) **Connection instability** – the area of the electrode is reduced due to moisture absorption, in addition to a heat contraction of dielectric film will affect the connection stability, and hence an **open circuit** mode of failure is the result.

3) **Dielectric loss** – an exposure to an excessive amount of humidity dries out and vaporize the dielectric and shortens the life of the capacitor causing a **wear-out** mode of failure.

Regarding the discussion of the two types of capacitors, summary of some specific advantages and shortcomings with respect to their performance are collected by [40] in Table 1.2. E-Caps could achieve the highest energy density and lowest cost per joule, but with relatively low ripple current ratings and

high ESR, and hence some wear-out issues due to the evaporation of electrolyte material. MPPF-Caps could provide a well-balanced performance for high voltage applications (e.g. above 500 V) in terms of cost per joule, capacitance, ESR, ripple current ratings, and reliability. Nevertheless, they have the shortcomings of large volume and moderate upper operating temperature.

Table 1.2: Performance Comparison of Two Types of Capacitors for dc-links (+++ superior, ++ intermediate, + inferior) [40].

Aspects	**E-Caps**	**MPPF-Caps**
Capacitance	+++	++
Voltage	++	+++
Ripple current	+	+++
ESR	+	+++
Dissipation Factor (*DF*)	+	+++
Frequency range	+	++
Capacitance stability	++	+++
Over-voltage capability	++	+++
Temperature range	++	+
Energy density	+++	+
Reliability under electro-thermal stress	+	+++
Cost per joule	+++	++

1.1.2 General reliability assessment of capacitors

As referred earlier, in the field of power electronic converters, dc-link capacitors are considered as high significant component. They have a direct impact to the size, cost, efficiency, and failure rate of the power converter, and hence contribute to the converter's overall reliability. Therefore, reliability studies on the dc-link capacitors are very important in order to achieve reliable and robust converters. In Fig. 1.9, it can be seen that, today's perspective toward the reliability assessment of power electronic devices should be considered by three main aspects [40].

Analytical Physics

According to Fig. 1.9, it can be seen that understanding the reliability physics of a power electronic component is a major aspect. Moreover, understanding

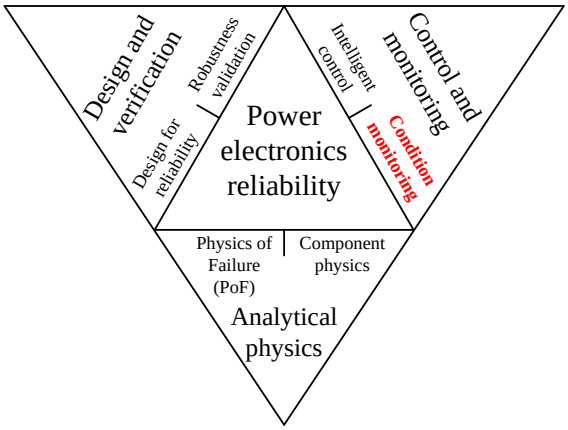

Fig. 1.9: Aspects of power electronics reliabilty assessment [40].

the failure mechanisms and the mode of failures of power electronic components are essential to the reliability lifetime prediction, and hence also the reliability improvements. In regards to the reliability of dc-link capacitor from Physics-of-Failure (*PoF*) point of view, in Chapter 1, the mode of failures, the failure mechanisms, and the basic construction are discussed in section 1.1.1 for both E-Caps and MPPF-Caps. From the capacitor user's view point, understanding the nature of the capacitor helps to design more reliable and robust power converters through an optimum selection of the capacitor's specifications. Therefore, design and verification comes as the second major aspect in capacitors reliability.

Design and verification

The Design For Reliability (*DFR*) process varies from designer to designer, due to the different reliability tools and different product requirements. In spite of these differences, there are always a common pattern, which covers the process of identification, validation, verification, and control. By following this common pattern it is guaranteed that the reliability is well considered during the design phase. The DFR applied to the dc-link capacitors is discussed in this section. Different scenarios of reliability-oriented design are reviewed in [88], and they are presented in Fig. 1.10. Fig. 1.10 shows the main existing solutions of dc-link capacitor design. The widely used design is shown in Fig. 1.10(a) either by using an Al-Caps or MPPF-Caps. Many research efforts have been carried out in two directions;

1) Reduce the dc-link requirements [87].

2) Achieve an optimal design of dc-link capacitor bank [70].

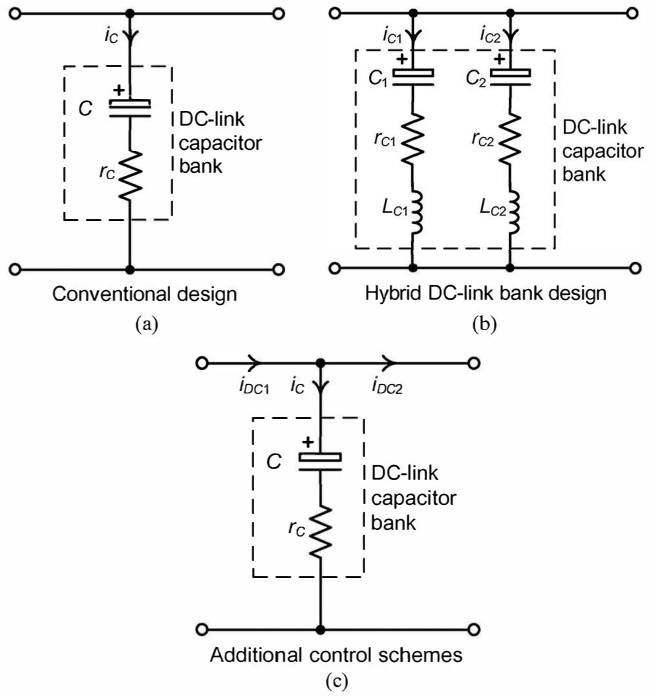

Fig. 1.10: Some types for solutions for dc-link capacitors design [88].

In the first direction, if replacing the Al-Caps with MPPF-Caps is feasible, then, the energy storage requirements can be reduced, and thereby, high level of reliability is achieved with no additional increase in both volume and cost [87]. Fig. 1.10(b) shows a recent design proposed by [34] that combines between 40 mF Al-Caps, and 2 mF MPPF-Caps for a 250 kW inverter application. If this solution is considered, the current stresses are reduced, and hence, the reliability of the Al-Caps bank is enhanced.

According to the first research direction, the design concept shown in Fig. 1.10(c) is to synchronize the current i_{DC1} and i_{DC2} through a designed control scheme that helps reducing the ripple current [42]. This design solution is feasible for the application where the two power stages connected through the dc-link are having a common control in their operating frequencies [42].

Although the design for reliability stage will improve the reliability of the capacitor part, the additional circuit components and/or control scheme will produce new failure potentials in the dc-link part. Therefore, a control configuration that monitor the the behaviour of the designed dc-link capacitor is important in sake of reliability evaluation of the whole dc-link part. Therefore, this monitoring is needed to quantify the impact of these new solutions.

Control and monitoring

Improving the reliability of a power electronic converter is not restricted to the design phase only, it should also continue to the operation phase for further improvements. Therefore, power components maintenance in power electronic converters is essential for reliability improvements. Taking dc-link capacitor as an example; the maintenance decision flow chart shown in Fig. 1.11 is a general guideline that explains how to decide a suitable kind of maintenance.

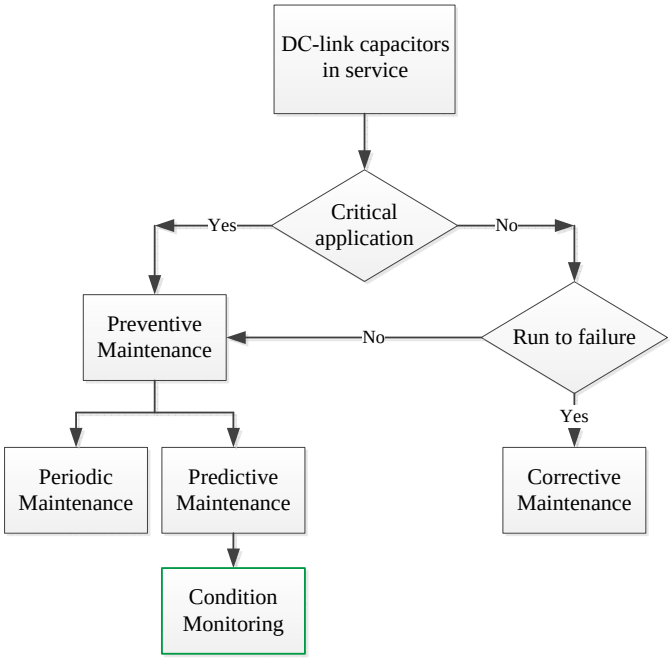

Fig. 1.11: Maintenance decision guidelines.

Controlling and monitoring the conditions of a power electronic converter during the operation is the third important aspect according to Fig. 1.9. According to [40], there are three main strategies that can improve the reliability of a power electronic converter: a) Prognostics, Health Management and Control (PHMC); b) active thermal control; and also c) fault tolerant control.

a) Prognostics Health Management and Control (PHMC) The term (prognostics) is defined as "*An engineering discipline focused on predicting the time at which a system or a component will no longer perform its intended function.*" [82]. This unintended/unplanned functionality is mostly due to a failure that makes the system unable to operate in its normal conditions any more. In

order to make a decision, the Remaining Useful Life (RUL) is a very important factor that needs to be considered. Prognostics is able to predict the component performance in the future based on an assessment of the system degradation with respect to its normal operating conditions. Linking between the failure mechanism studies of a given system and its life-cycle management is so called "Prognostics and Health Management (*PHM*)". The Prognostics, Health Management, and Control (*PHMC*) strategy will deliver methods; protocols; and tools for robust sensing; diagnostics; prognostics; and control that enable users and/or manufacturers to respond to planned and un-planned performance changes, and hence enhance the overall reliability system. The principle of condition monitoring spouts from the PHMC strategy. The condition monitoring principle is a major sub-aspect in the power electronics reliability, as shown in Fig. 1.9 and further detailed discussion is presented in this thesis.

b) Active thermal control Analysis of the thermal performance of power converters shows that some of the semiconductor components are exposed to more stress than the others, and this an uneven thermal distribution can be seen more in power converter with complex design (i.e multi-level power converter). Therefore, it is important to apply a technique that helps in regulating the thermal stress in a given application. An example of that is the regulation of the losses in an IGBT modules in order to prevent the failures; such as power cycling and over temperature [67].

c) Fault-tolerant control Requirements and conditions of a safe operation of a power electronic converter are very important and should always be followed by the users. Operating beyond these conditions may affect the nature of the components and eventually lead to damage of the power converter. Fault tolerance is defined as, "*A property that enables a system to continue operating properly in the event of the failure of (or one or more faults within) some of its components*" [59]. Designing a fault-tolerant control scheme allows the system to maintain operating in its normal conditions but with lower performance instead of shutting it down [55]. This kind of operating condition is referred as "Graceful Degradation".

1.1.3 Capacitor condition monitoring

As discussed in section 1.1.2, condition monitoring principle comes from the PHMC strategy, and it is a major sub-aspect in power electronics reliability. The research in this project is focusing on improving the reliability of the dc-link capacitors in power electronic converters. In the following subsection, the definition of condition monitoring principle in general is presented.

Moreover, the motivation behind it and why it is important for dc-link capacitor are also discussed.

Definition and motivation

In general, condition monitoring principle is defined as, *"a real-time measurement of a component parameter, such that if it drifts away from a healthy condition an appropriate action can be taken"* [94]. In some applications this real-time measurement is not directly reachable with a measurement device. Therefore, an alternative way is to estimate this parameter instead of measuring it. Condition monitoring is a principle that estimates and predicts the health status and operating conditions of a given system or component. It is very recommended to be applied in safety-critical systems and reliable applications, such as; air-crafts, wind turbines, and electric vehicles. Applying condition monitoring helps in applying preventive maintenance instead of corrective maintenance through predicting future failures.

According to a review based on condition monitoring for Device reliability in power electronics presented in [94], semiconductor and soldering failures in device modules are sharing totals 34% of converter system failures as shown earlier in Fig. 1.5, while for E-Caps, they are sharing 30% of the failure distribution in power electronic components.

As a fact, in energy conversion systems, a group of series/parallel connected capacitors (capacitor bank) or a single capacitor is normally used as dc-link filter. In systems using capacitor banks, although the system will keep operating under a failure of a single capacitor, it is very recommended to replace all the capacitors in order to ensure reliable operation. The recommendation to replace all capacitors is due to the fact that, other capacitors may exposed to an increased stress, and thereby, the capacitors life-time degradation is accelerated [80].

Due to the aforementioned preamble on condition monitoring and dc-link capacitors, monitoring the health status and operating condition of dc-link capacitors is one of the most critical aspects that must be considered in modern design of power electronic converters [78].

1.2 Problem formulation

In most applications that require power conversion, a dc-link capacitor is located between the two power stages. Dc-link capacitors are essential for filtering purposes by reducing the voltage ripples and equalizing the power difference between the input side and the output side. As a smoothing energy element, dc-link capacitors are exposed to a high stressful environment. Exposure to stressors (e.g. over voltage, over temperature, humidity ...etc) by

time will affect the initial conditions of the capacitor construction (e.g. vaporization of electrolyte material) causing a capacitance degradation which shortens the life time of the capacitor. Since failure of a single element may lead to collapse of the entire system, development of a monitoring system that monitors the health condition of the capacitor before reaching End-of-Life (EOL) is required. An EOL criterion for a capacitor is decided based on the Capacitance (C) and/or the Equivalent Series Resistance (ESR) compared with their initial values. The absence of cost-effective and practical solutions are the main reasons why capacitor condition monitoring is not adopted by industry. A main challenge is the way to obtain the dc-link current without the usage of extra hardware and/or extra signal injection. Therefore, new methodologies that overcome the aforementioned challenge are needed.

1.3 Project objectives

The hypotheses of this project is that, the health status of the dc-link capacitor should be known by estimating its capacitance value, also the objective of this project can be achieved by answering the following questions:

- How does capacitor condition monitoring improve the reliability of a given power electronic dc-link based system?

In energy conversion power electronic systems, a capacitor bank or a single capacitor is normally used. The systems could be stop operating properly if a single capacitor degrades. In systems using capacitor banks, although the system will keep operating under a failure of single capacitor, it is very recommended to replace all the capacitors in order to ensure reliable operation. The recommendation to replace all capacitors is due to the fact that, other capacitors may exposed to an increased stress, and thereby, the capacitors life-time degradation is accelerated. The estimation of capacitance value can be correlated to the capacitor reliability in one of the following three options:

1) An indicative sign that decide if the capacitor have failed or not by comparing the estimated status to a specific EOL criteria.

2) A capacitor degradation level, where the difference between the estimated value and the specific EOL threshold criteria is observed. For this option, a detailed degradation curve for the capacitance or the equivalent series resistance is not necessary.

3) An estimation of the Remaining Useful Lifetime (RUL). Where degradation curves of the capacitance or the equivalent series resistance under certain conditions are required to be known. In such cases, an accelerated degradation testing data must be conducted.

- What are the main shortcomings in the previous methodologies?

The existing methodologies of capacitor condition monitoring require additional hardware circuitry in order to obtain the dc-link capacitor current. Those extra circuits are used whether for measuring the dc-link capacitor current (e.g. PCB based Rogowski coils) and/or external signal injection. Extra hardware leads to high cost and high complexity as well. Moreover, comparing the resulted accuracy with respect to the required effort makes it less attractive for practical industry applications.

- How can the main disadvantages of the previous methods be avoided?

Methodologies based on software solutions with limited or no hardware are expected to be preferable for practical applications, which normally requires high reliability performance and low cost solutions. Such software-based methodologies could be beneficial in two ways: a) it could be applied for already existing power converters by upgrading and integrating the algorithm in their digital controllers; b) as nowadays the cost of digital controllers are getting reduced, hence, it could be also applied for new power converters.

1.4 Limitations of the project

The proposed capacitor condition monitoring method in this project is limited to Electrolytic Capacitors (*E-Caps*). Both simulation and experimental case studies are limited to 4 kW power converters with an operating switching frequency of 10 kHz. Two different topologies are considered in this project for capacitor condition monitoring based on ANN algorithm. Differences are with respect to the load type, line inductance location and nominal dc-link capacitance value. The first topology is a resistive load front-end diode bridge converter with line inductance located between three-phase voltage source and the diode bridge. The nominal dc-link capacitance value is limited to 1.1 mF.

The second topology is a three-phase front-end diode bridge motor drive provided by *Danfoss* where dc-link inductances are considered. Additionally, the nominal power level of the system is up to 7.5 kW, but as stated earlier, for the cases studied in this project, up to 4 kW power level is considered. Two series capacitors are connected as a dc-link capacitor bank equals to 0.5 mF with 800 V operating dc-link voltages.

1.5 Thesis outline and structures

This thesis deals with development of new methods that monitors the health status of the E-Caps for dc-link application under stressed conditions by esti-

mating the changes in the electrical parameters of the capacitor. An in-depth analysis of prior-art condition monitoring methods (advantages, shortcomings) have been done and it was found that the existing methodologies of condition monitoring applied for capacitors are having deficiencies regarding the accuracy level and hardware cost. Therefore, development of new condition monitoring technology based on software solutions and minimum usage of hardware components will significantly be more cost-effective.

This project develops new methods using an Artificial Neural Network (*ANN*) algorithm in order to estimate the capacitance value which represent the health status of the electrolytic capacitors in dc-link application. The application of the method is condition monitoring of capacitors under field operation in power electronic systems in order to apply predictive maintenance. The software based method is proposed in order to solve the existing issues of the prior-art research.

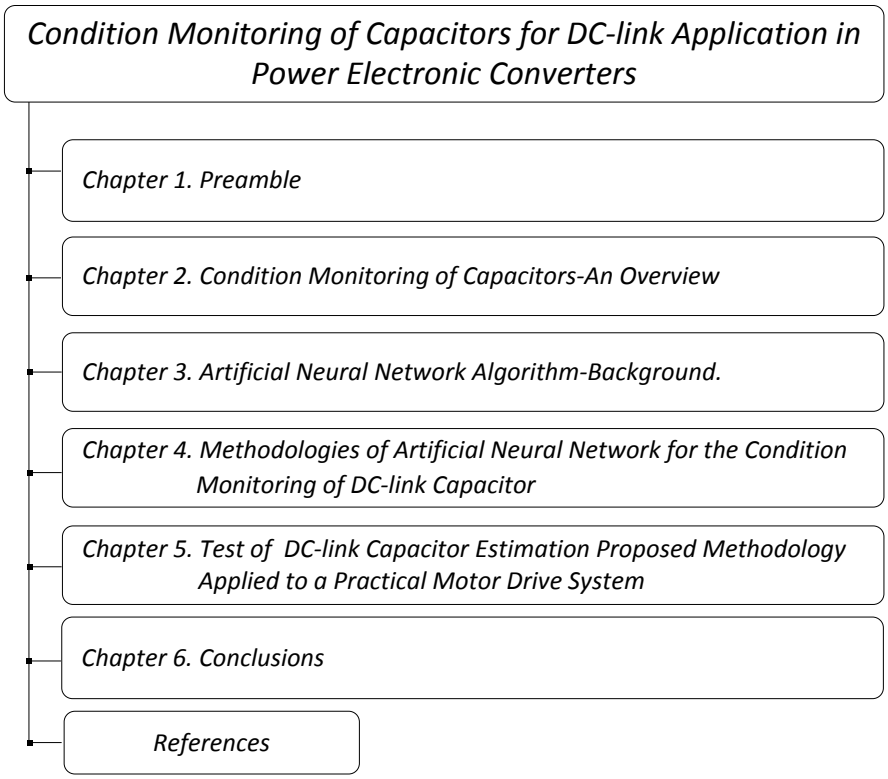

Fig. 1.12: Detailed paper-based thesis structure.

The structures and details of this paper-based thesis can be seen in the diagram shown in Fig. 1.12. The introduction of this thesis is presented in *Chapter 1* and includes a background of the dc-link capacitor types, their construction and mode of failure, general reliability assessment methods. Moreover, problem formulation, project motivation, objectives and limitations of this project are also included.

In *Chapter 2*, an overview of the existing technologies of capacitor condition monitoring and a classification according to their methodologies is given. The given overview is beneficial to both the academic research and the industry. The following two purposes are served by this overview: a) identify the limitations of the existing technologies and the promising aspects of them; b) explore the points of strength to develop future research that contribute to more practical applications.

In *Chapter 3*, the background of the ANN algorithm technology to be used in this project is given. It also discusses the basic concept of the ANN and its structure, and then describes the training process. In addition, description of the ANN type and its mathematical details used in this project is discussed.

Applying of the proposed method in simulation is analysed in *Chapter 4*. The proposed condition monitoring method based on ANN is applied on a three-phase front-end diode bridge converter where the dc-link voltage is not controlled and thereby only unidirectional power flow. In order to validate the proposed condition monitoring method, a proof of the concept using a Digital Signal Processor (DSP) is also presented. The proposed ANN is implemented in a DSP to verify the capacitor condition monitoring in practice. However, *Chapter 4* is a mid-way step between simulation and practice. This is due to the fact that, the inputs to the ANN integrated with the DSP are still sourced from simulation. In addition, part of *Chapter 4* concerns also the integration steps of the trained ANN with the DSP and issues of Analog-to-Digital Conversion (ADC) and Digital-to-Analog Conversion (DAC).

In *Chapter 5*, verification of condition monitoring based on ANN algorithm is applied on a 4 kW three-phase front-end diode bridge motor drive. The motor drive is provided by Danfoss. The approach to apply the proposed methodology is to estimate the total capacitance value of the dc-link capacitor bank using a trained ANN. The ANN is trained and tested using input and output terminal information from the practical. In addition, capacitance estimation based on measured dc-link voltage harmonics are also included. Finally, a conclusion is provided in *Chapter 6* including main contributions and future work.

1.6 List of publications

A list of the papers derived from this project, which are published till now or have been submitted, is given as follows:

Journal Papers

J1. H. Soliman, H. Wang and F. Blaabjerg, "A Review of the Condition Monitoring of Capacitors in Power Electronics Converters," *IEEE Transactions on Industry Applications*, vol. 52, No. 6 PP. 4976-4989 pages, 2016. [Open Access]. DOI:10.1109/TIA.2016.2591906.

J2. H. Soliman, B. Gadalla, H. Wang and F. Blaabjerg, "Artificial Neural Network Algorithm for Condition Monitoring of DC-link Capacitors Based on Capacitance Estimation," *Journal of Renewable Energy and Sustainable Development (RESD)*, vol. 1, PP. 294-299, 2016. [Open Access]. ISSN:2356-8569.

J3. H. Soliman, P. Davari, H. Wang and F. Blaabjerg, "Capacitance Estimation Algorithm based on DC-Link Voltage Harmonics Using ANN in Three-Phase Motor Drive Systems," *IEEE Transactions on Power Electronics*, 2017. [Under Preparation].

Conference Contributions

C1. H. Soliman, B. Gadalla, H. Wang and F. Blaabjerg, "Condition monitoring of dc-link capacitors based on artificial neural network algorithm," in *Proc. of IEEE Fifth International Conference on Power Engineering, Energy and Electrical Drives (POWERENG),* pp. 1-5, May. 2015.

C2. H. Soliman, H. Wang and F. Blaabjerg, "A Review of the Condition Monitoring of Capacitors in Power Electronic Converters," in *Proc. of IEEE INTERNATIONAL ACEMP - OPTIM - ELECTROMOTION JOINT CONFERENCE: ACEMP – OPTIM*, pp. 243-249, May. 2015.

C3. H. Soliman, H. Wang and F. Blaabjerg, "Capacitance estimation for dc-link capacitors in a back-to-back converter based on Artificial Neural Network algorithm," in *IEEE 8th International Power Electronics and Motion Control Conference (IPEMC-ECCE Asia),* pp. 3682-3688, May. 2016.

C4. H. Soliman, I. Abdelsalam, H. Wang and F. Blaabjerg, "Artificial Neural Network based DC-link Capacitance Estimation in a Diode-bridge Front-end Inverter System," in *IEEE 8th International Future Energy Electronics Conference (IFEEC-ECCE Asia),* pp. 1-6, June. 2017.

C5. H. Soliman, P. Davari, H. Wang and F. Blaabjerg, "Capacitance Estimation Algorithm based on DC-Link Voltage Harmonics Using ANN in Three-Phase Motor Drive Systems," in *IEEE Energy Conversion Congress and Exposition (ECCE 2017),* **Accepted Digest**, Oct. 2017.

Chapter. 2

Condition Monitoring of Capacitors - an overview

In this chapter, an overview of the existing technologies to do capacitor condition monitoring and a classification according to their methodologies is given. This given overview is one of the main contribution in this PhD project and it is a direct copy from my paper [80] which is published during my PhD study with the following details:
***H. Soliman, H. Wang and F. Blaabjerg, "A Review of the Condition Monitoring of Capacitors in Power Electronics Converters," IEEE Transactions on Industry Applications, 2016**. The following two purposes are served by this overview: a) identify the limitations of the existing technologies and the promising aspects of them; b) explore the points of strength to develop future research that contribute to more practical applications.*

2.1 Introduction

The condition monitoring of semiconductor devices used in power electronics is well reviewed in [94]. In addition to active semiconductor devices, capacitors are another type of components which fail more frequently than other components in power electronic systems [94]. During the last two decades, there are a large number of scientific publications on the condition monitoring of capacitors, of which the relevant ones are collected and reviewed in this chapter [11–32, 35–39, 41, 44–47, 49–54, 56–58, 60–66, 68, 69, 71, 72, 75, 77, 81, 83–86, 91, 92, 95]. Nevertheless, the developed technologies are rarely adopted in industrial applications, due to the complexity, increased cost, and

other relevant issues. Therefore, an overview of the existing methods is beneficial to both the industry application and academic research. It serves the following two purposes: a) a benchmark of different condition monitoring solutions and identify the most promising aspects and limitations of them; b) trace the process history of the technology evolution and explore the future research opportunities that have the potential to contribute to more practical applications.

A single capacitor or a capacitor bank is usually used in power electronics conversion systems. If the single capacitor reaches its End-Of-Life (*EOL*), the systems may be malfunction. For the systems with capacitor banks, once one of the capacitor fails, the other capacitors may withstand increased stresses, which then accelerate the degradation of them. Therefore, the time-to-failure of the multiple capacitors could vary. In order to ensure a reliable operation, it is recommended to replace the entire bank once one of the capacitors reaches the end-of-life [10].

A simplified equivalent model of capacitors is shown in Fig. 2.1(a), and the corresponding frequency characteristics is plotted in Fig. 2.1(b). It can be seen that the capacitor impedance is distinguished by three frequency regions dominated by capacitance (*C*), the Equivalent Series Resistance (*ESR*) and the Equivalent Series Inductance (*ESL*), respectively.

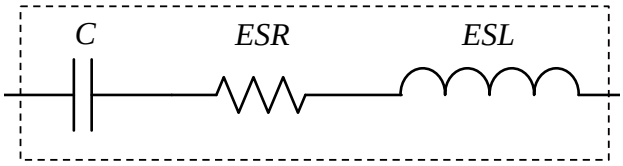

(a) A simplified equivalent model of capacitors.

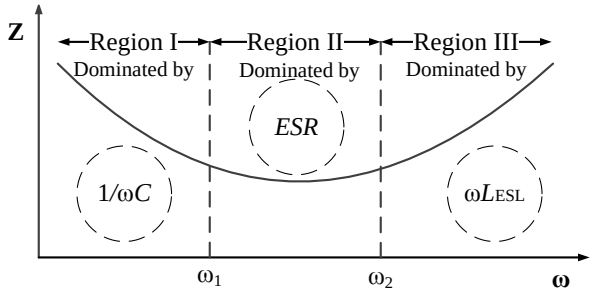

(b) The impedance characteristics of capacitors.

Fig. 2.1: The equivalent model and impedance characteristics of capacitors [80].

The majority of the condition monitoring methods for both individual capacitors and capacitor banks are based on the estimation of the capacitance

C and Equivalent Series Resistance (*ESR*), which are typical indicators of the degradation of capacitors [88].

According to the degradation curves in Fig.2.2(a), and based on the block diagram shown in Fig. 2.2(b), an end-of-life or a threshold criteria is needed before going further and decide the health condition of the capacitor. For electrolytic capacitors, the widely accepted end-of-life criteria is 20% capacitance reduction or double of the *ESR*. For film capacitors, a reduction of 2% to 5% capacitance may indicate the reach of end-of-life. The range in between the initial value of capacitance/*ESR* and the aged value, is the condition monitoring range, as shown in Fig. 2.2(a).

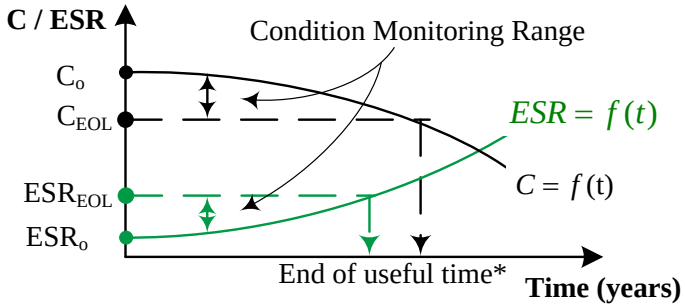

C_o = Initial capacitance. C_{EOL} = Capacitance at End-Of-Life.
ESR_o = Initial equivalent series resistance. ESR_{EOL} = equivalent series resistance at End-Of-Life.
*C_{EOL} could be larger or smaller than ESR_{EOL}, it depends on the application and the capacitor type.

(a) Capacitance and *ESR* curves as an indication of capacitor degradation level.

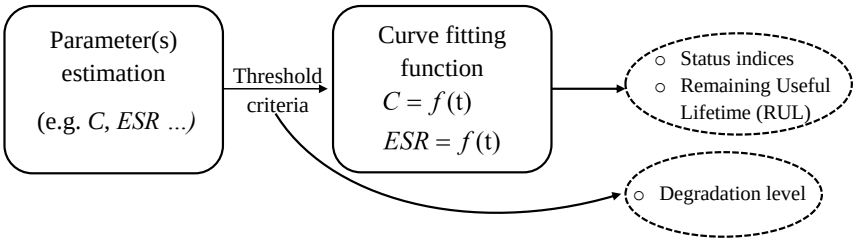

(b) Major steps in condition monitoring of capacitors.

Fig. 2.2: Key indicators of condition monitoring and their steps [80].

The selection of those end-of-life criteria are based on two aspects to consider: 1) The capacitor degradation rate becomes considerably faster (e.g. *dC/dt* , *dESR/dt*) after the capacitance or *ESR* reaches the specified end-of-life criteria, 2) The power electronic conversion systems may not function appropriately when the capacitance drops or the *ESR* increases to a specified level [89]. The estimated capacitance *C* or *ESR* value can be correlated to the

health conditions of the capacitor in one of the following:

1) An EOL indication by comparing the estimated value to the specific end-of-life criteria.

2) A degradation level, by observing the difference between the estimated value of C and/or ESR and the specific EOL criteria. For this purpose, a detailed C or ESR degradation curve is not necessary.

3) An estimation of the Remaining Useful Lifetime (RUL). It requires the knowledge of the C and/or ESR degradation curves under specific operation conditions, which are usually obtained from the accelerated degradation testing data.

An overview of the reliability of capacitors in dc-link applications is presented in [88]. Failure mechanisms, lifetime models and dc-link design solutions are discussed. A brief discussion on the condition monitoring of capacitors is also given. Since the scope of [88] does not focus on the condition monitoring, no detailed discussion and critical comparison of the prior-art methods are provided. The review in this chapter intends to fill the gap in the literature and conducts a comprehensive overview on the research topic. Section 2.2 gives the classification of the existing condition monitoring methods. Section 2.3 outlines the technology development history of capacitor condition monitoring for the last two decades and the benchmark of these technologies. A summary of the future research opportunities is given in Section 2.4.

2.2 Classification of condition monitoring literature according to their methodologies

As shown in Fig. 2.3, the capacitors condition monitoring methods can be classified from three perspectives. Availability is the first perspective, where the health indicator can be obtained during the operation of the system, and thereby it is called an online condition monitoring. If an interruption of the system is required to obtain the health indicator it is called an offline condition monitoring. The second perspective shows the type of the health indicator that is used for the condition monitoring. The third perspective is the methods to obtain the values of the specific indicator.

Accordingly, Fig. 2.3 shows the classification of the methods to obtain different health indicators. They are divided into three categories to be discussed and they are mainly applied for single-stage DC-DC converters, DC-AC inverters, and two stage AC/DC/AC converters. The topologies that are

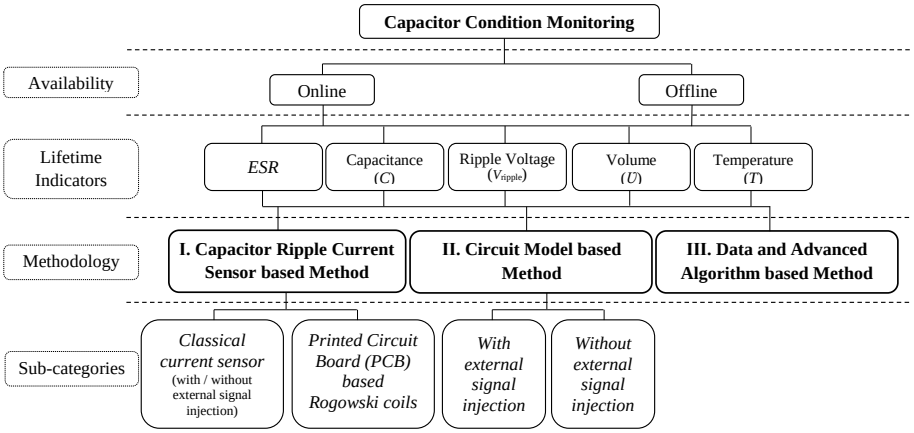

Fig. 2.3: A classification of capacitor condition monitoring technology and their indicators [80].

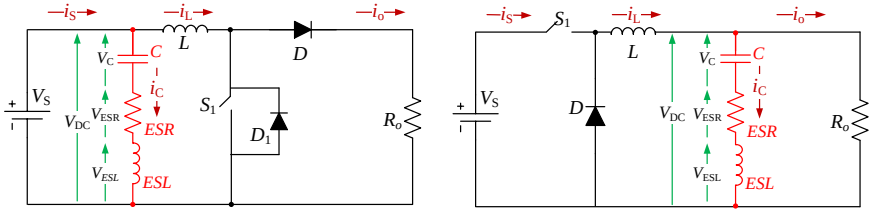

(a) The boost converter circuit. (b) The buck converter circuit.

Fig. 2.4: Condition monitoring applications for single-stage DC-DC converters discussed in this thesis [80].

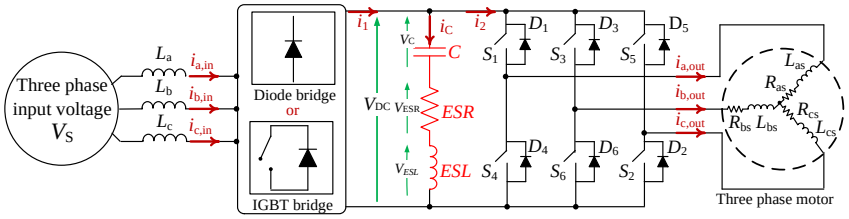

Fig. 2.5: Condition monitoring applications for two-stage AC/DC/AC power converters being discussed in this chapter [80].

discussed in this section are shown in Fig. 2.4 and Fig. 2.5, where Fig. 2.4(a) is a boost converter and Fig. 2.4(b) is a buck converter.

Fig. 2.5 shows a generic structure of AC/DC/AC converters with either a diode-bridge rectifier or PWM rectifier as the first AC-DC stage. The definitions of the voltages, currents, and components are shown in the figure.

Table 2.1: Condition Monitoring Methods of Capacitors in Power Electronic Converters from Different Literature [70].

Methodology	*C* / *ESR*	Used Approach	Topologies	Advantages/Disadvantages	Capacitance/power rating	Used in Ref.
I	*C* (E-Caps)	$C = \frac{1}{\Delta v_C}\int i_C dt$	Fig. 2.5 Diode bridge	Avoids the use of extensive filters.	4700 µF - 15 kW 2200 µF - 15 kW	[6] [7]
	ESR (E-Caps)	$ESR = \frac{V_{DC} - V_C}{i_C}$	Fig. 2.5 PWM IGBT bridge	Extra effort and many filters to be used because of the current injection.	2500 µF - 3 kW 63.5 mΩ	[21]
	ESR (E-Caps)	$ESR = \frac{\Delta v_{Cf}}{\Delta i_{Cf}}$	Fig. 2.4 (b) Buck converter	Requires additional hardware for implementation.	2200 µF - 40 W	[5] [55]
	ESR (E-Caps)	$\frac{ESR}{ESR_O} = \left(\frac{\vartheta_{ol,O}}{\vartheta_{ol}}\right)^2$ $ESR_{HOT} = \frac{\Delta T \times H \times S}{I^2}$	Fig. 2.5 Diode bridge	High accuracy level of ESR estimation.	470 µF - 0.4 Ω	[41] [42]
	C (E-Caps)	$C = \frac{1}{\Delta v_C}\int i_C dt$	Fig. 2.5 PWM IGBT bridge	Extra effort and many filters to be used because of the current injection.	6150 µF - 3 kW	[22]
	ESR (E-Caps)	$ESR = \frac{P_C}{i_C^2}$	Fig. 2.5 Diode bridge	Simple analog circuit is required for the capacitor voltage measurement.	1800 / 5600 µF - 6 kW	[4]
II	ESR (E-Caps)	$ESR \propto V_C$	Fig. 2.4 (b) Buck converter	Forming an LC filter is important for achieving the proposed approach.	68 µF - 72 W	[29]
	C (MPPF-Caps)	$C\frac{dv_C}{dt} + \frac{1}{R_{th}}V_C = -i_{2f}$	Fig. 2.13 Fig. 2.14	Applied for specific kind of application systems (traction systems).	9 mF - 1.2 MW	[33]
	ESR (E-Caps)	$ESR \propto V_C$	Fig. 2.4 (b) Buck converter	Difficult due to requirement for additional measurements and prior data for the reference model.	2200 µF - 40 W	[34]
	ESR (E-Caps)	$ESR = \frac{\Delta v_C \times R}{R \times \Delta I_L - \Delta v_C}$	Fig. 2.4 (a) Boost converter	The temperature effect is considered.	N/A	[39]
	ESR (E-Caps)	$ESR = \frac{\Delta v_C \times R}{R \times \Delta I_L - \Delta v_C}$	Fig. 2.4 (b) Buck converter	The temperature effect is considered.	N/A	[59]
	C (E-Caps)	$C = \frac{1}{\Delta v_C}\int i_C dt$	Fig. 2.5 Diode bridge	Low accuracy under dynamic operation.	80 µF - 1.1 kW	[28]
	C (E-Caps and MPPF-Caps)	$C = \frac{1}{\Delta v_C}\int i_C dt$	Fig. 2.5 Diode bridge	Applied on both E-Caps and MPPF-Caps.	470 µF - 250 mΩ	[43]
	C (E-Caps)	$C = \frac{1}{\Delta v_C}\int i_C dt$	Fig. 5 Diode bridge	Low accuracy under dynamic operation.	3280 µF - 100 W	[44]
	C and *ESR* (E-Caps)	$C = \frac{V_S D T_S}{8L\left(V_{S_{i=\frac{DT_S}{2}}} - V_{S_{i=\frac{(1+D)T_S}{2}}}\right)}$	Fig. 4 (a) Boost converter	The condition monitoring method can be implemented in the same microcontroller used for MPPT purpose.	47 µF - 750 W	[45]
III	*C* (E-Caps)	$C = \frac{BPF[P_C]}{BPF\left[\frac{1}{2}\frac{\Delta v_C^2}{dt}\right]}$	Fig. 2.5 PWM IGBT bridge	Current measurement is not required.	3950 µF - 3 kW	[20]
	C (E-Caps)	Trained information on ANFIS	Fig. 2.17	Based on software – no extra hardware is required.	1500/2500 µF - 12 kW	[32]

i_{2f} - current through the capacitance in the frequency filter, R_{th} - braking rheostat, V_{DC} - dc-link voltage, V_C - capacitor voltage, i_C - capacitor current, V_{Cf} - capacitor voltage at certain switching frequency, $i_{Cf\_}$ - capacitor current at certain switching frequency, Δv_C - capacitor ripple voltage, Δi_{Cf} - fundamental capacitor ripple current, Δv_{Cf} - fundamental capacitor ripple voltage, $\vartheta_{ol,0}$ - initial volume of E-Caps, ϑ_{ol} - volume of E-Caps, ESR_o - initial value of equivalent series resistance, ESR_{HOT} - ESR at operating temperature, H - heat transfer per surface area, S - surface area, ΔT - element temperature rise, ΔI_L - inductor ripple current, R - load resistance, V_S - solar PV voltage, T_S - switching time, D - duty cycle, L - inductor, $BPF[P_C]$ - output capacitor power from band pass filter, ANFIS - Adaptive Neuro Fuzzy Inference System, ANN - Artificial Neural Network.

Part of the representative condition monitoring methods discussed in [15] - [41] are listed in Table 2.1. Table 2.1 categorise the respective methods, the applied health indicator, and also the principle for the indicator estimation. The information of the application case in terms of topology, power rating,

and capacitance value are listed. A brief discussion of the advantages and disadvantages is also included. More specific details of these methods and applications will be discussed in this section.

2.2.1 Capacitor ripple current sensor based methods

The basic concept in this category is to obtain the capacitance and/or *ESR* by using the capacitor voltage and ripple current information at region I and region II, respectively (as illustrated in Fig. 2.1(b)). Some of the presented methods in the literature have applied this concept [17, 19–24, 26, 28, 31]. To obtain the voltage and current information at a certain frequency, external signals are injected. The signal is injected into the power electronic circuits with the frequency of interest. A large number of papers discuss the methods in this category. The capacitor voltage information is readily available since it is usually required for the control of power electronic converters, (e.g., the dc-link voltage). The ripple current is measured by an additional current sensor. The current sensors used for capacitor current measurements can be divided into classical current sensors (e.g., resistors, hall sensors) and Printed Circuit Board (PCB) based Rogowski coils. PCB based Rogowski coils are a designed PCBs which are fixed to the capacitor terminal to sense both the capacitor currents and voltages.

Classical current sensors

Without signal injection Methods that are using direct classical current sensors are not very common. Three examples illustrate the concept of using a direct sensor [15], [49] and [83]. All are using a direct current sensor to obtain the capacitor ripple current which is in addition to the ripple voltage obtained through an existing voltage sensor. In [15], the Root-Mean-Square (*RMS*) value of the capacitor current measured by a current sensor is obtained. The average capacitor power (P_C) can be calculated by multiplying the capacitor's current and capacitor's ripple voltage. The calculation of the ESR is achieved by (2.1)

$$ESR = \frac{P_C}{i_C^2} \tag{2.1}$$

where i_C is the current flowing through the dc-link capacitor.

In [49], the measured capacitor current is filtered by a Band Pass Filter (BPF) before calculating the *RMS* value. The usage of the filter is due to the calculation of *ESR* in a certain range of frequencies -as discussed previously- and it is given in (2.2) as

$$ESR = \frac{V_{Cf}}{i_{Cf}} \tag{2.2}$$

where, V_{Cf} and i_{Cf} are the dc-link capacitor voltage and current at a certain switching frequency, respectively.

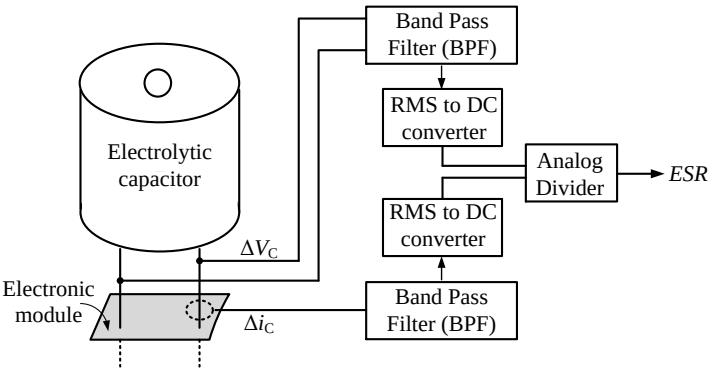

Fig. 2.6: ESR computational circuit in capacitors [83].

In [83], an electronic module is designed and integrated with an electrolytic capacitor. The electronic circuit is able to calculate the *ESR* by sensing the capacitor ripple current and voltage. The calculated *ESR* value are then compared with the initial value of the ESR_o in order to decide the capacitor status. The computational circuit is shown in Fig. 2.6.

Although this method requires additional hardware and the maximum error of the *ESR* estimation is 10%, the main advantage is the usage of a toroidal core to sense the ripple current. The authors claimed that the additional parasitic inductance due to the usage of the toroidal core is negligible in this application case.

It is important to notice that the estimation of the *ESR* based on the average capacitor power is achieved with 10% estimation error, which is acceptable in some applications. Moreover, it is achieved without the usage of filters, which also reduces effort and cost. But in some applications, the usage of the filter is required in order to achieve higher accuracy with an estimation error lower than 10%.

With signal injection An alternative way is to externally inject a desirable signal of current or voltage at a certain frequency into the circuit where the capacitor of interest is located. This basic methodology is the most widely used. Various applications and different methods can be used, and most are applied on an experimental setup as illustrated in Fig. 2.7.

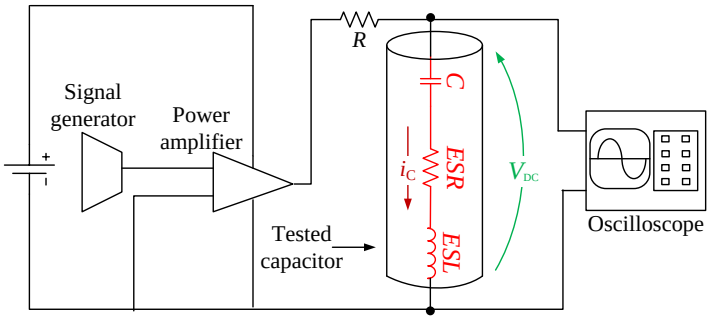

Fig. 2.7: Experimental setup with signal injection used in [20]- [28].

In [20] and [19], an experimental technique that allows the determination of the *ESR* value of aluminium electrolytic capacitors based on sinusoidal analysis technique is reported. The technique has been applied on a capacitor existing in an LC filter with 25 V input voltage, and 4700 μF filter capacitor. However, the technique presented some drawbacks due to the fact that both capacitance and inductance values are frequency dependent. In these two references, the estimated *ESR*s from the experimental test are not compared with the simulations. This is due to the fact that both tests are done at different frequencies. Moreover, the obtained results are not compared to the initial values due to the lack of information from the manufacturer of the tested capacitors. The manufacturer is typically providing the data sheets with a dissipation factor (*DF*) at 120 Hz.

In order to overcome the aforementioned shortcomings, different algorithms were used in [17, 21–24, 26, 28, 31]. Laplace transform algorithm in [21], Newton Raphson (*NR*) in [22] and [24], Discrete Fourier Transform (*DFT*) in [17, 26, 28], and Least Mean Square (*LMS*) in [23, 31]. All the algorithms are used to calculate the relationship between the input voltage and the output voltage of the experimental circuit shown in Fig. 2.7. The differences between these algorithms are summarized at the end of this section.

In [22] and [17], the same setup as shown in Fig. 2.7 is used to estimate the equivalent circuit of the capacitor by using the *NR* method and *DFT*, respectively, instead of Laplace analysis. The measured values of the capacitance and *ESR* are compared with those obtained in [21]. The *NR* based method gave values, which were very close to the measured values using an LCR meter with a maximum error of 1.5%. Comparing the obtained values based on the *DFT* method in [17] with the values obtained by the Laplace transform method in [21], the *DFT* method estimated the *ESR* with a maximum error of 8%, and the method using the Laplace method estimated the *ESR* with a maximum error of 18%.

Another method based on *DFT* analysis is considered in [26] and it is

applied on the same setup as shown in Fig. 2.7. The method estimated the *ESR* and capacitance with a maximum error of 11% and 2.8% respectively. In [23], a simple modification to the same setup shown in Fig. 2.7 is carried out to estimate the *ESR* and capacitance. The modified circuit uses a control circuit to charge and discharge the capacitor. Therefore, from the relationship between the capacitor current and the capacitor voltage, the capacitance value is estimated by applying an *LMS* Algorithm using a sinusoidal curve fitting technique instead of using the Laplace transform.

Based on the same method proposed in [23] and the setup shown in Fig. 2.7, a wider range of frequencies and temperatures are considered in [31] for the estimation of *ESR* and capacitance. In addition, [31] uses two methods; a) based on sinusoidal generator, b) based on charge/discharge circuit, and compares each method. It is concluded that for the *ESR* estimation the first method is better, while the opposite is correct for the capacitance estimation.

Table 2.2: A Summary of Condition Monitoring Analysis Algorithms [70].

Analysis Algorithm	**Operating frequency [Hz]**		***(C)* Estimation error [%]**	***(ESR)* Estimation error [%]**
Laplace Transform	120		17.6% [10]	N/A
	750		N/A	18% [11]
	10 k		N/A	5% [10]
Discrete Fourier Transform (*DFT*)	750		N/A	8% [11]
	1 k		2.8% [12]	11% [12]
	10 k		N/A	10% [10] 12% [16]
Newton-Raphson (*NR*)	120		1.5% [10]	8.4% [15]
Least Mean Square (*LMS*)	1 kHz	Method (1)*	2.6% [13] 1.0% [14]	0.4% [14]
		Method (2)*	0.3% [14]	9.7% [14]

*Method (1): based on sinusoidal generator. Method (2): based on charge/discharge circuit.

Table 2.2 summarizes the comparison between all algorithms with respect to the operating frequency. Based on the review of these algorithms, the following can be concluded:

1) In order to use the Laplace transform algorithm, a certain requirement must be fulfilled. The requirement is that the input resistance *R* must be two to three times higher than both the *ESR* and the *ESL*. Otherwise, the Laplace transform algorithm shows high error percentages.

2) The *NR* Algorithm is an iteration based algorithm, and from the results listed in Table 2.2, *NR* is recommended for the frequency region I, and

hence, for capacitance estimation.

3) The *DFT* algorithm is considering only the first harmonic component in the computation of the gain and phase displacement between the input and output voltage, and hence, it needs low effort.

4) All of the four algorithms are applied for offline condition monitoring of capacitors.

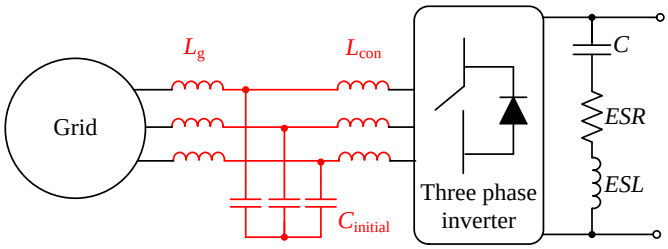

Fig. 2.8: LCL filter interfaced PWM inverter connected to the grid [47].

For the LCL filter of a grid connected PWM converter shown in Fig. 2.8, a condition monitoring method is proposed in [60] and [47]. This methodology is based on using the corresponding variation in the filter capacitor operating frequency region as the capacitance drop is an indication to the health status. Assuming the capacitance is reduced up to 80% of the initial value, the frequency caused due the drop is calculated by

$$f = \frac{1}{2\pi} \times \sqrt{\frac{L_{con} + L_g}{L_{con} \times L_g \times 0.8 C_{initial}}} \tag{2.3}$$

where L_{con} is the line inductance on the converter side, L_g is the line inductance on the grid side, and $C_{initial}$ is the initial value of the capacitance. The initial frequency corresponding to the initial capacitance is 2185 Hz. Due to a 20% capacitance drop, the corresponding frequency to is 2440 Hz. To obtain the frequency of the aged capacitor, a voltage is injected into the reference voltage of the capacitor in the LCL filter with the frequency ω_{inj}. Although this method is similar to the one proposed in [14] since both are using voltage injection, the difference is the usage of the measured capacitance frequency and comparing it to the initial frequency to identify the deterioration of the capacitor. Moreover, as shown in Fig. 2.9.

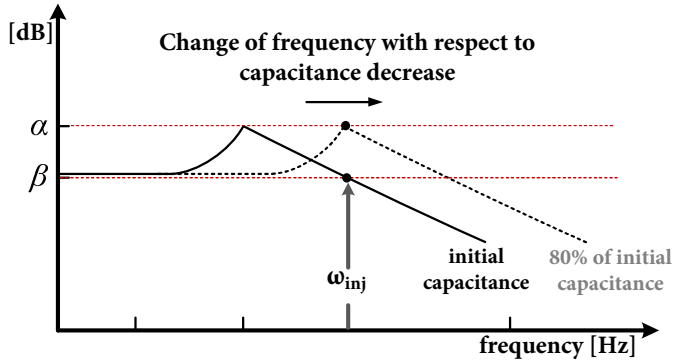

Fig. 2.9: Difference of dB gain between initial capacitance and faulty capacitance. [47].

The resonant frequency is moved by the decrease in capacitance, the response gain to the injection component is increased from point β to point α due to the changed transfer function of the LCL filter. Thereby, the replacement time of the capacitors is determined according to the following condition:

$$(\alpha - \beta) \geq 80\% \tag{2.4}$$

where (α) and (β) are the dB frequency magnitude of the initial and degraded capacitance, respectively.

PCB based Rogowski coils

Capacitor condition monitoring based on PCB based *Rogowski* coils is summarized in this sub-section. Sample of a PCB based Rogowski current sensors is shown in Fig. 2.10.

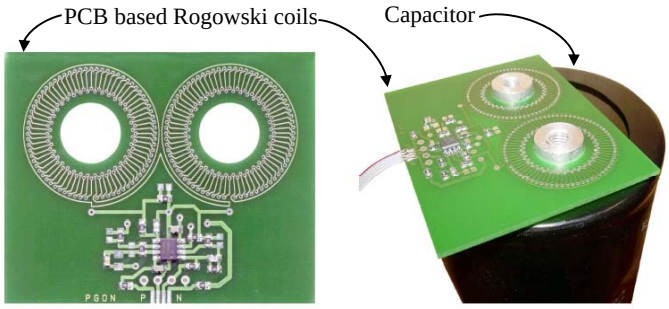

Fig. 2.10: Sample of a PCB based Rogowski current sensor connected to a capacitor [84, 92].

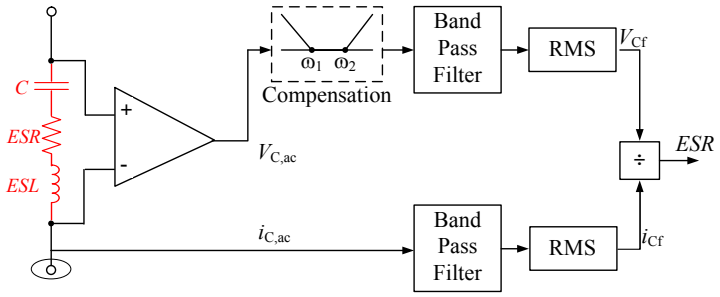

(a) ESR estimation done within the capacitor's ohmic frequency range as illustrated in Fig.2.1(b) [83].

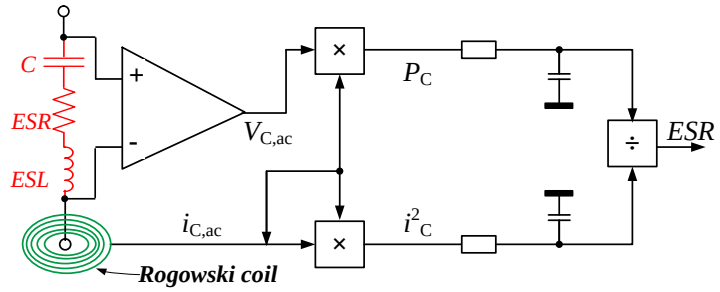

(b) ESR estimation based on Rogowski coil current sensor [84, 92].

Fig. 2.11: Condition monitoring by *ESR* estimation based on designed PCBs.

The methods described in [84] and [92] are based on the *Rogowski* current sensor concept, where a designed PCB is fixed to the capacitor terminal to sense both capacitor's current $i_{C,ac}$ and voltages $V_{C,ac}$ as shown in Fig. 2.11(b). The difference between *Rogowski* based methods and the method in [83] is illustrated in Fig. 2.11. The advantage with the *Rogowski* based methods is the avoidance of using extensive filters since the total active power P_C drawn by the capacitor is represented by the *ESR*. In Fig. 2.11(a), V_{Cf} and i_{Cf} are the capacitor voltage and current at a certain frequency, respectively.

2.2.2 Circuit model based methods

Without signal injection

Instead of the current sensors connected in series with the capacitors, the capacitor ripple currents can also be obtained indirectly based on the operation principle of PWM switching converters [91], and the switching status of DC-DC power converters with LC filters [39].

An on-line condition monitoring method based on capacitance estimation

is presented in [91], and the capacitance is estimated by

$$C = \frac{1}{\Delta V_{DC}} \int i_C dt \tag{2.5}$$

Referring to Fig. 2.5, the electrical information i_1, $i_{a,out}$, $i_{b,out}$ and V_{DC} are obtained by using the three existing current sensors and one voltage sensor, respectively. These sensors are already existing for the control purpose of the converter. The electrical information i_C, i_2, $i_{c,out}$ are estimated indirectly.

The capacitor ripple current i_C is calculated using the difference between the input current sensor i_1 and the current flows to the inverter i_2 which is based on the transistor switching sequences. The assumption of this calculation is that the three phase output currents are balanced.

Due to the high switching frequency in the DC-DC converters, the impedance of the electrolytic capacitor is dominated by the *ESR*. Since the *ESR* is very small compared to the load resistance, the output ripple voltage is determined by the capacitor *ESR* and the inductor ripple current. For a DC-DC power converter operated in steady state, three factors in which the inductor current depends on remains unchanged. The factors are duty cycle, the inductance, and the difference between input and output voltage. Therefore, the amplitude of the output AC ripple voltage is determined directly by the *ESR*. The experimental test is based on a comparison between the output ripple voltage in the case of using predetermined un-aged capacitor, with the output ripple voltage in case of using an aged capacitor.

In [16], an online methodology that belongs to this category and requires no signal injection is proposed. The methodology is applied on a dc-link capacitor in a boost converter as shown in Fig. 2.4(a). The boost converter is supplied from a PV panel. The main advantage of this methodology is that, the sensing voltage for the Maximum Power Point Tracking (*MPPT*) purpose is utilized for the *ESR* and capacitance estimation according to (2.6) and (2.7), respectively.

$$ESR = \frac{\left[V_{S|_{t=0}} - V_{S|_{t=DTs}}\right] \times L}{V_S \times DTs} \tag{2.6}$$

$$C = \frac{V_S \times DTs}{8 \times L \times \left[V_{S|_{t=\frac{DTs}{2}}} - V_{S|_{t=\frac{(1+D)Ts}{2}}}\right]} \tag{2.7}$$

where, V_S, T_s, D, and L are the solar PV voltage, switching time, duty cycle, and the inductor, respectively as illustrated in Fig. 2.12.

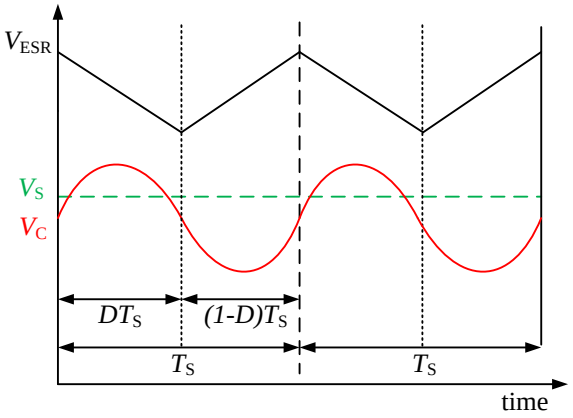

Fig. 2.12: Voltages waveform with respect to sampling time and duty cycle. [16].

However, the *ESR* and the capacitance can be estimated only during steady state, when the MPPT system settles to a point. Since the same sensing voltage is used for the MPPT, *ESR* and capacitance estimation, the condition monitoring method is implemented in the same microcontroller, which is also used for the MPPT. This helps to avoid additional hardware, and hence reduces the cost.

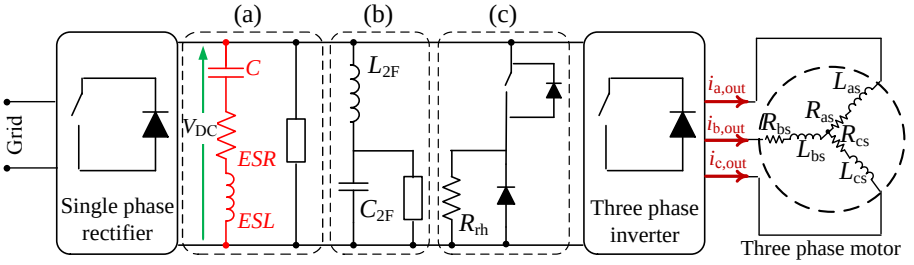

Fig. 2.13: General traction power converter scheme. (a) dc-link capacitor. (b) Frequency filter. (c) Braking chopper. [37].

Another methodology that is applied to the capacitor condition monitoring is based on the circuit model presented in [37]. The condition monitoring is based on the capacitance estimation of a dc-link Metallized Polypropylene Film (MPPF) capacitor in a traction system. The general traction power converter topology for the railway trains is shown in Fig. 2.13. In respect to the operation nature of the traction systems, during the capacitor discharge period, the obtained equivalent circuit of the dc-link is shown in Fig. 2.14. Normally in the traction system applications both current and voltage sensors

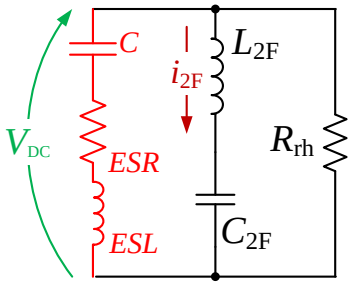

Fig. 2.14: Equivalent dc-link circuit during dc-link capacitor discharge [37].

are already installed and available in some auxiliary measurement blocks. Thereby, an insertion of an additional current sensor in series with the dc-link capacitor or a voltage sensor is avoided, and the dc-link capacitor will be obtained by applying the Least Mean Square (*LMS*) optimization algorithm to

$$C\frac{dv_{DC}}{dt} + \frac{1}{R_{rh}} \times V_{DC} = -i_{2F} \tag{2.8}$$

where C, i_{2F}, L_{2F}, C_{2F}, R_{rh}, V_{DC} are the dc-link capacitor, current passes through the frequency filter, frequency filter inductance, frequency filter capacitance, braking rheostat, and dc-link voltage, respectively in the motor.

A similar concept that estimates the *ESR* and the capacitance at a certain time is also presented in [95]. The estimation is applied to a dc-link capacitor in a three phase diode bridge AC/DC/AC converter that drives an induction motor as shown in Fig. 2.5. The main idea is to apply the condition monitoring method whenever the motor is stopped. During this instant, the equivalent circuit is given as shown in Fig. 2.15.

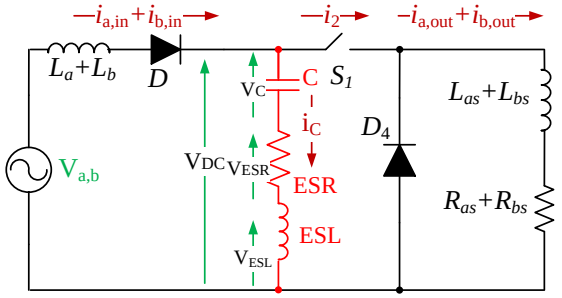

Fig. 2.15: Equivalent circuit of the 3-phase AC/DC/AC converter shown in Fig. 2.5 when the motor is stopped [95].

In Fig. 2.15, L_a, L_b, L_{as}, L_{bs}, R_{as}, R_{bs}, are the line inductances of phase A

and phase B, the stator inductances and resistances of phase A and phase B, respectively.

With signal injection

A few examples that are based is on the circuit model methodology in addition to external signal injection are proposed in [54, 58, 62, 68, 71, 72]. The current injection methods in [71], [62], [68], and [72] are applied on the PWM AC/DC/AC converter, while in [54] and [58] they are applied to a sub-module capacitor in a modular multilevel converter, and a drive system for electric vehicles, respectively.

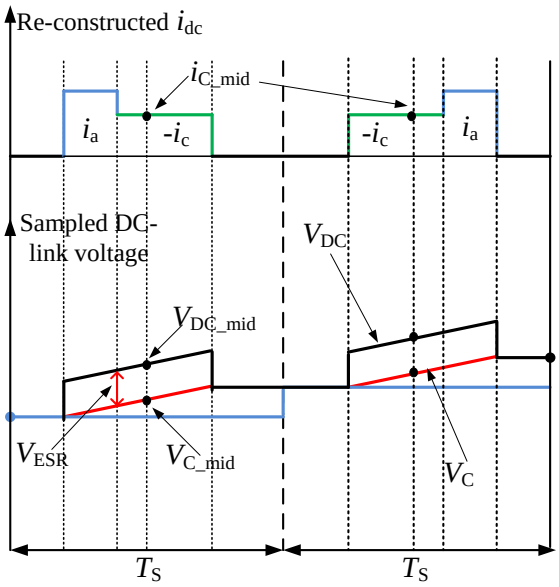

Fig. 2.16: Behavior of the dc-link current and voltage according to the gating pulses in an AC/DC/AC converter shown in Fig. 2.5 [71].

The injected current is of a frequency lower than the line frequency, inducing two voltages, which follows the relationship of

$$V_{DC} = V_C + V_{ESR} \tag{2.9}$$

By considering the generation of the zero voltage vectors in the switching periods, the values at the mid-point of the switching periods are used in order to obtain the ESR value as

$$ESR = \frac{V_{ESR}}{i_C} = \frac{V_{DC\_mid} - V_{C\_mid}}{i_{C\_mid}} \tag{2.10}$$

where the term (mid) in the subscripts indicates the quantities measured at the midpoint of the normal sampling period as in the signals shown in Fig. 2.16.

In [62] the estimated capacitance is obtained by 2.5. Although it can be noticed that the current injection method is applied on various applications, the need of external signals, extra hardware and filters are the main shortcomings in such a method.

2.2.3 Data and advanced algorithm based methods

In this category, the power electronic converters are treated as a black-box or semi-black-box. Black-box approaches are based on the information of voltages and currents at the input side and output side only. The internal properties of the converters are assumed unknown. Semi-black-box approaches use also some of the available information inside the power converter structure. The relationship between the parameters to be estimated and the available parameters (e.g., input and output side terminal voltage and current information, dc-link voltage) are obtained through the data training.

In [14], a low frequency AC voltage is injected to the dc-link reference, which is used as training data in order to find the identification model based on a Support Vector Regression (*SVR*) method. After using a set of training data, a function that finds the relationship between the capacitor's power P_C and its corresponding capacitance is designed, and the capacitance C is determined according to

$$C = \frac{BPF[P_C]}{BPF[1/2][\frac{\Delta V_C^2}{dt}]} \tag{2.11}$$

where, the term $BPF[P_C]$ refers to the capacitor's power filtered by using a *Band Pass Filter*. The cut-off frequency of the used BPF equals to 30 Hz. As claimed in [14], this method is simpler than the current injection, since the estimation is based on the capacitor power and no dc-link ripple current information is required. Since the SVR is an algorithm, which is based on off-line trained data, the Recursive Least Square (RLS) algorithm can be applied to allow the estimated capacitance to be updated, when new data become available [61].

A method for condition monitoring of capacitors based on data training using software algorithms is presented in [57]. Its structure is shown in Fig.

2.17. The method is applied to a power electronic converter shown in Fig. 2.17(b) and based on Adaptive Neuro-Fuzzy Inference System (ANFIS) algorithm. The methodology is based on collecting data and training the ANFIS on them in sake of predicting future non-trained outputs according to the basic structure shown in Fig. 2.17(a). The supply voltage V_s and ripple voltages V_1 and V_2 of both filter capacitors C_1 and C_2 are inputs to the ANFIS.

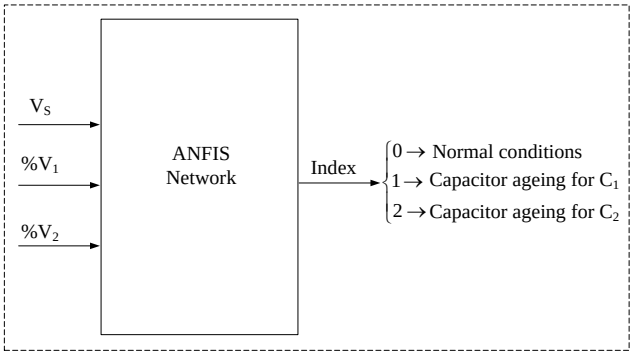

(a) Structure of Adaptive Neuro-Fuzzy Inference System (ANFIS) network [57].

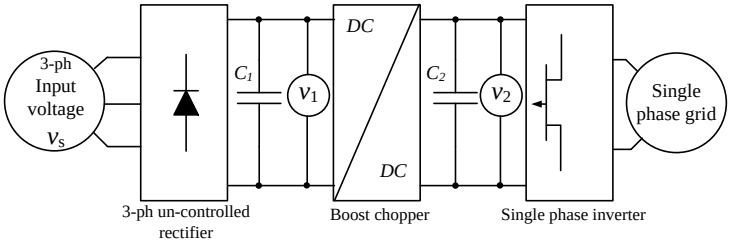

(b) Power electronic converter circuit [57].

Fig. 2.17: Condition monitoring of capacitors based on data training proposed by [57].

Both V_1 and V_2 are going through an interpolation process before implementing them in order to assure that a strong mapping between the input and output is obtained.

In order to investigate the ageing process, V_1 and V_2 are calculated at the end-of-life states and denoted by $V_{1\text{th}}$ and $V_{2\text{th}}$, respectively. A relationship between the supply voltage and the end-of-life voltages is linearly interpolated using curve fitting techniques. The two factors $\hat{V}_{1th}$ and $\hat{V}_{2th}$ are obtained, where $\hat{V}_{1th}$ and $\hat{V}_{2th}$ are the estimated values of $V_{1\text{th}}$ and $V_{2\text{th}}$ according to V_s respectively. Finally, in order to obtain the data implemented as input to the ANFIS, a percentage value is calculated as the following

$$\%V_1 = \frac{V_{1m}}{V_{1th}} \times 100 \tag{2.12}$$

$$\%V_2 = \frac{V_{2m}}{V_{2th}} \times 100 \tag{2.13}$$

where V_{1m} and V_{2m} are the measured values of V_1 and V_2 respectively at any current level.

The ANFIS network is trained on 366 pair of input and output. The network estimates one index out of two indices for capacitance and *ESR* of both capacitors in the converter. Moreover, the ANFIS can show decreasing/increasing percentages in the capacitance and the *ESR*, respectively. The method based on the ANFIS gives a high accuracy (0.5% maximum error) according to the results and it is useful for fault detection.

2.3 Historical summary of the existing methodologies of condition monitoring

The technology evolution of the capacitor condition monitoring technologies is illustrated in Fig. 2.18 with respect to the history. Different methods are represented according to the selected indicators, online or offline, and the methodologies discussed in Section 2.2. The maximum estimation error corresponding to each methodology is also given in Fig. 2.18.

Since the estimation accuracy is an important performance factor, Fig.2.19 compares the estimation errors with respect to the range of capacitance *C* and *ESR*. The comparison is according to the available data in different literatures and with respect to the methodologies classified earlier in Section 2.2. It can be seen that the lowest error percentages are captured by the methods that belongs to methodology III. This conclude that software solutions (e.g. requires less/no extra hardware and/or signal injection) have a strong potential to be considered in the future condition monitoring methods.

Fig. 2.20 summarizes the share of the considered lifetime indicators, and the share of each methodology listed in this chapter. Almost 60% of the used health indicator is captured by the *ESR*. This percentage conclude that (E-Caps) are the widely used capacitor type in power electronic applications.

2.4 Summary

Based on the above analysis, the following conclusion can be given in the overview:

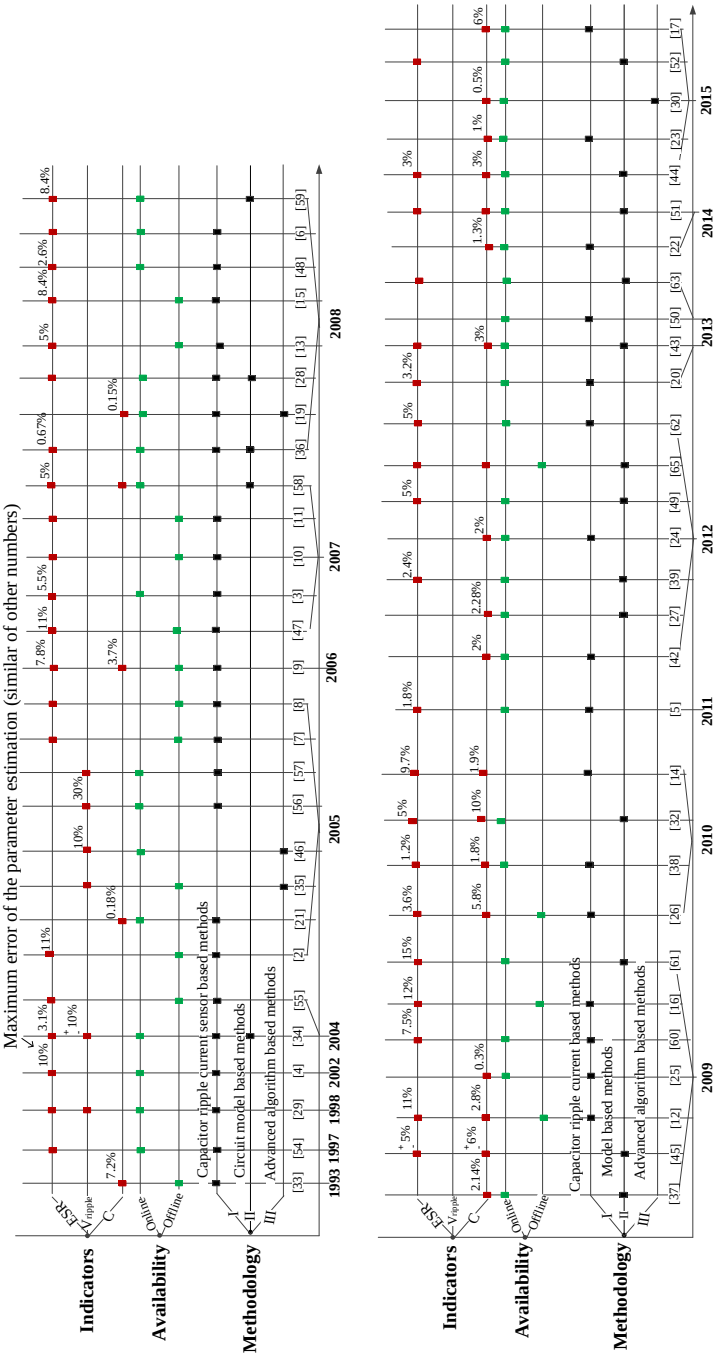

Fig. 2.18: History of the condition monitoring technology development for capacitors from 1993-2015 [80].

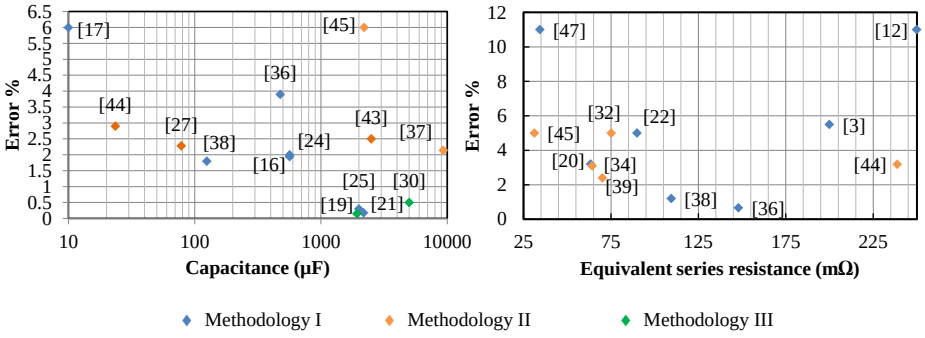

Fig. 2.19: Comparison of the parameter estimation in prior-art literatures [80].

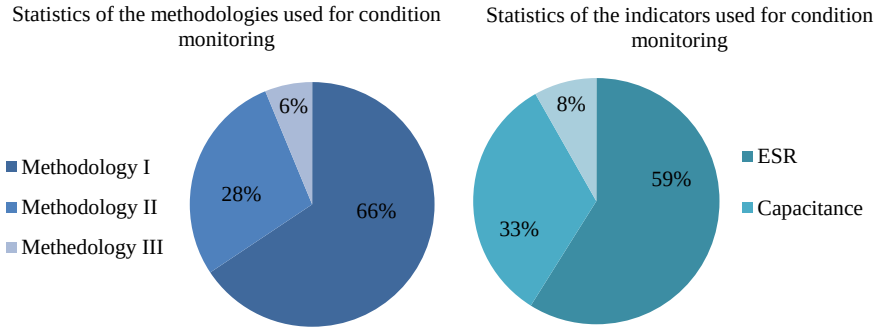

Fig. 2.20: Sharing percentages of the used methods and the considered indicators summarized in Fig. 2.18 [80].

1) Fig. 2.19 shows that the condition monitoring methods based on Methodology III have achieved a relatively higher accuracy than those based on Methodology I and Methodology II.

2) The majority of the condition monitoring methods are based on themethodology I as shown in Fig. 2.20, which is based on capacitor ripple current measurements.

3) Fig. 2.20 shows that the ripple voltage estimation is the least considered indicator. However, the capacitor ripple voltage is the main factor in *ESR* and capacitance estimation.

4) According to the development history shown in Fig. 2.18, the *ESR* is a common indicator for capacitor condition monitoring due to the widely

usage of electrolytic capacitors where both capacitance and *ESR* can indicate the health status. For film capacitors, the capacitance is a preferred indicator, since the ESR of the film capacitors are significantly smaller than that for the electrolytic capacitors.

5) It can be noted from Fig. 2.18 that the majority of the condition monitoring methods are online. By considering that the degradation of capacitors are usually very slow, offline condition monitoring is sufficient in most applications (e.g., in motor drives) to detect the wear out of capacitors. It implies that simpler estimation methods can be applied (e.g., during the start-up of motor drives).

6) The capacitor ripple current sensor based methods are not attractive for practical industry applications due to they need additional hardware circuitry, meaning cost and extra reliability issues are introduced into the circuit. Table 2.4 shows the hardware/software complexity with respect to each methodology. It can be seen that the hardware complexity is reduced compared to an increase in software complexity.

7) Software based methods with reduced or no additional hardware efforts are expected to be attractive for industry applications, which requires high reliability performance and low cost. The advantages of this kind of methods are twofold: a) it could be applied for both new power converters or existing power converters by upgrading the algorithms in the digital controllers; b) it is a trend that the cost of digital controllers and computation resources is reducing. Moreover, methods that are based on software algorithms are less exposed to be copied from other users or competitors.

8) Cost-effective and low-inductive current sensing methods could overcome many of the shortcomings of existing current sensor based methods. PCB-based Rogowski coils are promising for the capacitor current measurement, while more research efforts are needed to achieve better integration with the capacitors and more robust and cost-effective design.

9) Integrated implementation of condition monitoring, protection, and other ancillary functions for capacitors in applications requiring high reliability performance.

Table 2.4: The Associated Levels of Complexity With Respect to Each Methodology [70].

Methodology	Hardware Complexity	Software Complexity
I	+ + +	+
II	+ +	+ +
III	+	+ + +

10) Condition monitoring of capacitors discussed here is limited to the wear out detection. To extend the scope, in reliability critical applications, the online monitoring of the operation status (e.g., hot spot temperature, abnormal voltage and current stresses) is also of much interest. For this perspective, the online monitoring of capacitance and *ESR* value might be necessary to indirectly monitor the temperature and other abnormal stressors.

11) Based on the investigation carried out in this chapter, Fig. 2.21 shows that new methods based on software solutions and existing feedback signals, without adding any hardware cost, could avoid the critical shortcomings in the existing methodologies, and hence could be attractive for industry applications.

In the next chapter, a proposed methodology based on data and advanced algorithm is presented. The Artificial Neural Network (*ANN*) algorithm is selected for condition monitoring based on capacitance estimation. The following bullets explains why ANN is selected for solving this problem:

- ANN algorithm belongs to *Methodology III* (e.g. data and advanced algorithm), therefore, ANN have the properties mentioned earlier.

- Condition monitoring based on capacitance estimation is classified as a prediction, regression and curve fitting problem and ANN is specifically designed for such kind of problems.

- Condition monitoring is defined as; "*By accumulating component life data, preventive maintenance activities can be refined. This activity should consist of taking measurements to determine equipment condition. Data should be collected over time*". Therefore, accumulated measurements is essential for condition monitoring. ANN is based on using part of the accumulated data for the training stage, then, accumulated measurements are not

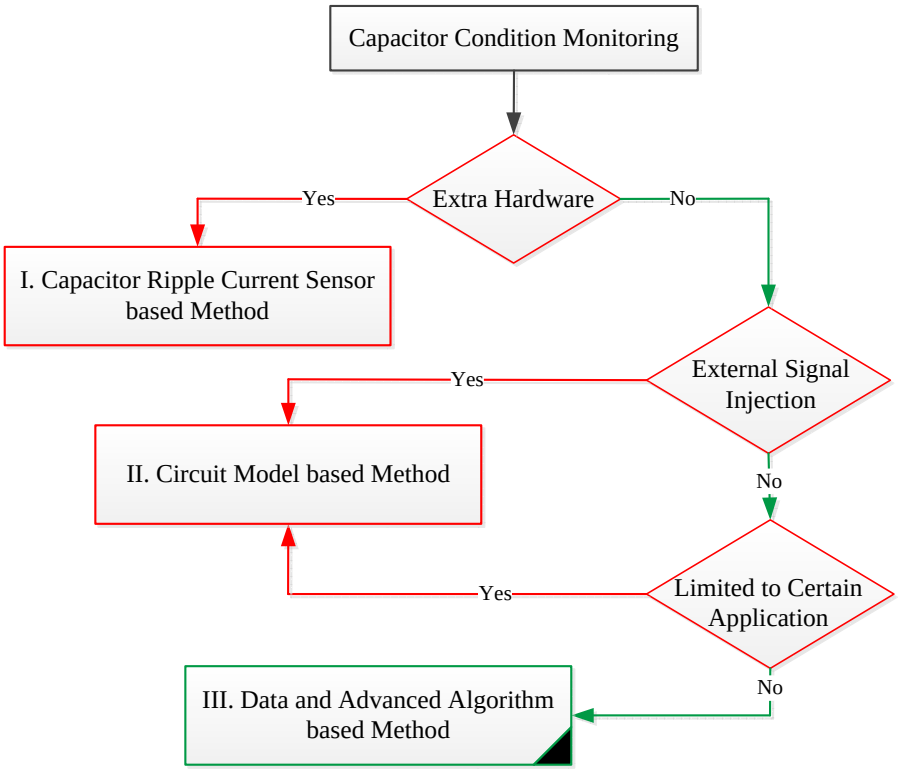

Fig. 2.21: Capacitor condition monitoring decision guideline.

needed any more, due to the ANN prediction ability using untrained data.

- ANN toolbox in *MATLAB* is a friendly use toolbox. The frequent updates applied to the ANN toolbox by MATLAB are improving the ANN algorithm and promoting it to be adopted in critical and practical applications.

- The ANN toolbox is very flexible to generate different versions of trained ANN. Trained ANN can be generated as a *SIMULINK* model, C/C++ code file, or M-code file.

- Integration of ANN within an existing and/or under-constructing system can be achieved simply.

- The ANN has a common platform with other software program (e.g. Code Composer Studio (*CCS*), *LABVIEW*, *dSPACE*).

Chapter. 3

Artificial Neural Network Algorithm - Background

In this chapter, the background of the ANN algorithm technology to be used in this project is given. It also discusses the basic concept of the ANN and its structure, and then describes the training process and the training types. In addition, a description of the ANN type used in this project is discussed.

3.1 Introduction

The Artificial Neural Network (ANN) is the proposed algorithm to be used in this thesis to overcome the existing challenges in capacitor condition monitoring applications. In addition, part of this thesis concerns also the integration of the trained ANN inside a Digital Signal Processor (*DSP*) in order to be suitable for practical applications.

3.2 Basic concept and structure

Artificial neural networks were originally designed to model the functionality of the biological neural networks, which are a part of the human brain. The human brain is the decision system for the human which has millions of neuron interacted and connected in a complicated way. The brain is more powerful and faster than any computer processor in handling complicated problems related to human performance problems. The human brain has multiple layers of neurons that interact with each other in parallel. The par-

allel interaction means that each neuron receives input lines from all neurons in the previous layer (input layer) and sends different output lines to all neurons in the next layer (output layer) [90].

The brain has powerful decision abilities to solve various complex problems like motion, posture, mathematical calculations, etc. The decision abilities in the human brain are gained by memorizing and learning previous cases that are similar to these problems. Likewise, ANN is an intelligent mathematical algorithm that consists of three main layers; input layer, hidden layer, and output layer. Fig. 3.1 shows a general structure of an ANN, where $(x_{0,n})$ represents the input vector/matrix, $(h_{0,m})$ is the number of hidden neurons, and $(u_{0,y})$ is the output vector/matrix. The input layer could be a vector or a matrix that contains a given system's inputs. The hidden layer represents the core of the ANN and contains amount of units called "hidden neurons".

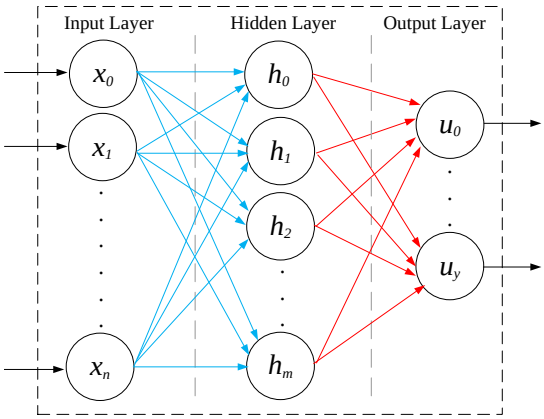

Fig. 3.1: Generic structure of an Artificial Neural Network [90].

The main mathematical calculations to process the available inputs and provide the required output takes place inside the hidden layer. Similar to the human neurons in the brain where the hidden neurons receives and sends sets of data from the input layer to the output layer. The received and sent data to and from the neuron differs depending on the weight value of the channel that are used for data transfer. The weight of the channel means, the value/gain that is multiplied by the carried data (i.e., multiplying the weights value by the coming data from the previous neuron) before passing the result to the next neuron. The weight value changes by changing the intended task and it is decided by learning and memorizing performing that task. The optimization of the weight value decided by learning is explained sufficiently in the following section.

The complexity of the ANN depends on the problem to be solved. More-

over, it depends on the amount of inputs that the ANN need to handle in order to create a correlation between inputs and the required outputs to be predicted. Complex problems requires more hidden neurons. Usually, single hidden layer is able to predict any non-linear system [33]. Beside, researchers have acknowledged that a better performance for the ANN is achieved when using one hidden layer considering the change of the hidden neurons amount according to the needs. The reasons for not using more than one hidden layer are as follows:

1) Multiple hidden layers expose the ANN to more noise because more neurons and connected channels between the layers will exist, and hence, an unstable network performance will be the case.

2) The curve fitting becomes very specialized towards certain training cases. This reduces the prediction ability of the ANN towards new inputs other than the trained ones.

3) Multiple hidden layers increase the risk to reach a local optimized solution. Eventually, locally optimized ANN will produce wrong predicted outputs.

As stated previously, the ANN could need more hidden neurons according to the complexity of the problem and the amount of data the ANN needs to handle. Therefore, calculation and selection of the optimal or nearly-optimal amount of hidden neurons is an important task. In [48], it is suggested that the sufficient amount of hidden neurons is calculated by:

$$\sqrt{(y+2)n} + 2\sqrt{\frac{n}{y+2}} \tag{3.1}$$

where, y, n are the number of outputs and the number of the training sets, respectively. However, in the absence of an exact method to calculate the optimal amount of hidden neurons, the trial and error method is the most primitive one. It is usually common to achieve nearly-optimal output when adopting the trial and error method. The user would change the amount of hidden neurons during the training process in most applications till the best trained ANN is generated.

3.3 Training process

In the phase of creating a new ANN, the training phase is the most important part for a proper performance. Basically, there are two different types of training; supervised and unsupervised training. The supervised training is used in regression problems, where a set of training data that includes inputs

and their corresponding outputs is used. The unsupervised training is used in clustering problems, where only the inputs are known. In this thesis, the supervised training is considered. Fig. 3.2 explains the theory of the supervised training. The *ADALINE* is an abbreviation for Adaptive Linear Neuron which is the simplest artificial neural network model [74].

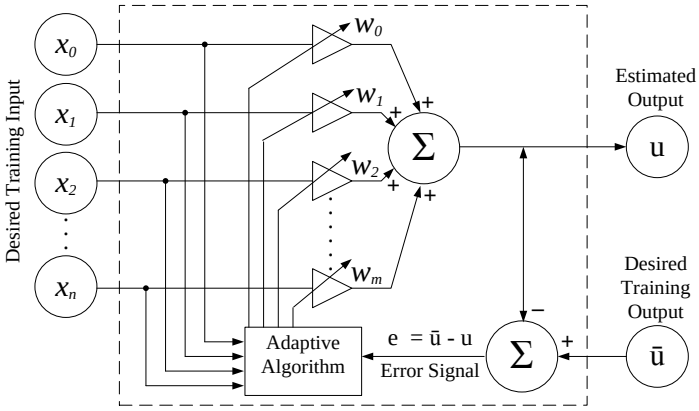

Fig. 3.2: Simplest Artificial Neural Model - (ADALINE) [74].

As shown in Fig. 3.2, the model consists of n inputs, a linear accumulation functions, and an adaptive algorithm. The adaptive algorithm is for error minimization purposes. The minimization function is the Least Mean Square (*LMS*). The output estimated by the model is described by the following mathematical formula:

$$u = \sum_{i=0}^{n} w_i x_i \tag{3.2}$$

where, w_i is the ith weight value of the channel, and x_i is the ith input to the model.

Since condition monitoring applications are regression and prediction problems, this thesis is considering a supervised training based on a curve fitting regression solution. Regression means creating a curve (i.e as shown in Fig. 3.3) that passes and fits between the training data set. A factor called regression response (R) is always observed during the training process. The regression factor is a value between 0 and 1. As long as the regression factor is close to 1, a strong correlation between inputs and outputs can be achieved.

The training process starts by data collection for capacitor condition monitoring. The collected data will be prepared as training sets. In addition, the source of input/output training sets should be a reliable source in order to predict the exact output for the provided training sets. The collected training sets and their sources are well described in the following chapters.

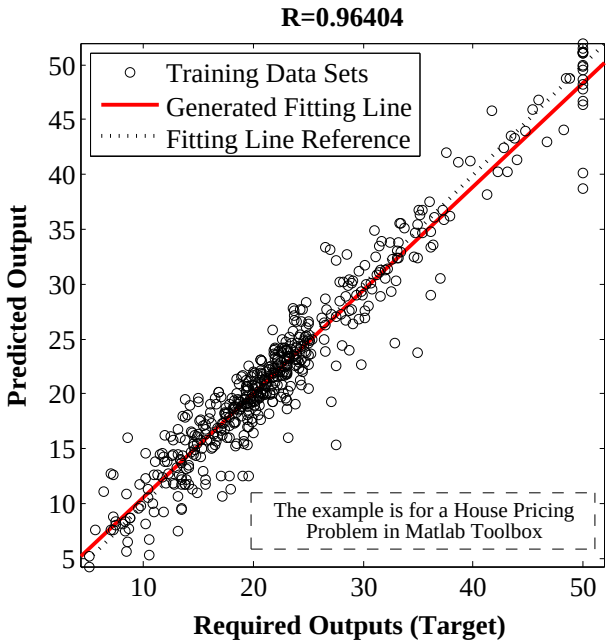

Fig. 3.3: Curve Fitting Regression Diagram [6].

After preparing and feeding the training sets to the appropriate layers in the network, the next step is to optimize the network parameters. The amount of hidden neurons is optimized and changed during the training process allowing the network to achieve the highest performance, (i.e the highest regression factor). The training process is finished, when the generated output stopped improving. When the training process is finished, and the generated regression factor is satisfied, then the network can be generated and ready to be used. Otherwise, re-training the network is necessary in order to avoid poor results. Low regression response mean that the network is not able to handle the correlation between inputs and outputs. Therefore, two paths can be considered to overcome this problem. First, increasing the amount of hidden neurons in the hidden layer and re-train the network. Increasing the amount of hidden neurons will expand the dimension of the fitting curve to fit more training data. In the case that an increase of the hidden neurons do not improve the network, it means that the amount of training sets are not sufficient, and more training sets are required as a second path.

In the following chapters, the amount of training sets and the amount of hidden neurons and their impact on the ANN accuracy will be discussed.

3.4 Feed-Forward artificial neural network

Feed-Forward Artificial Neural Network (*FFANN*), which can be seen in Fig. 3.1, is one of the most common types of ANN. The inputs which are represented as a set of circles are included in the input layer. The input enter the hidden layer by the neurons weight. The hidden neurons are represented as circles inside with a sigmoidal transfer function. The output layer receives the output of the hidden layer by another neurons weight. Inside each neuron there is linear transfer function as shown in the same figure, to provide the final results (estimated outputs). Generally, the sigmoidal and linear transfer functions are used on the hidden and output layers, respectively [33].

FFANN is normally used in applications including classification and regression problems. The advantages of using FFANN are as following:

1) Working well for many applications and especially curve fitting of the time series data (i.e., data that come in different times and values).

2) Generalizing the system prediction at any input or extrapolating off-grid training phase. After the network is trained, it will be able to predict any new input, even those are out of the training limits.

3.5 Summary

In this chapter, the neural fitting application (*nftool*) in Matlab software is used for capacitor condition monitoring. The tool helps selecting the training data sets, creating and training a network, and evaluating its performance using Least Mean Square (*LMS*) error and regression analysis. A feed-forward artificial neural network will be used to estimate the dc-link capacitance value. In the following chapter, the proposed capacitor condition monitoring based on ANN is applied and presented.

Chapter. 4

Methodologies of Artificial Neural Network for the Condition Monitoring of DC-link Capacitor and Proof - of - Concept

This chapter includes the simulation analysis of the proposed methodology applied on three-phase power converter. Moreover, a proof of concept in a hardware platform is also presented. The given work in this chapter is copied and derived from my papers [78], [81] which are published during my PhD study with the following details:

[78] H. Soliman, H. Wang and F. Blaabjerg, "Capacitance estimation for dc-link capacitors in a back-to-back converter based on Artificial Neural Network algorithm".
[81] H. Soliman, B. Gadalla, H. Wang and F. Blaabjerg, "Condition monitoring of dc-link capacitors based on artificial neural network algorithm"..

4.1 Introduction

As shown in Fig. 4.1, the main objective of this chapter is to simplify the proposed ANN methodology with respect to the amount and/or type of ANN inputs. In this chapter, three different ANNs (ANN1, ANN2 and ANN3) are studied. Methodology simplification is studied in order to minimize the amount of ANN inputs. Moreover, the impact of input/output current on the ANN estimation accuracy is also studied.

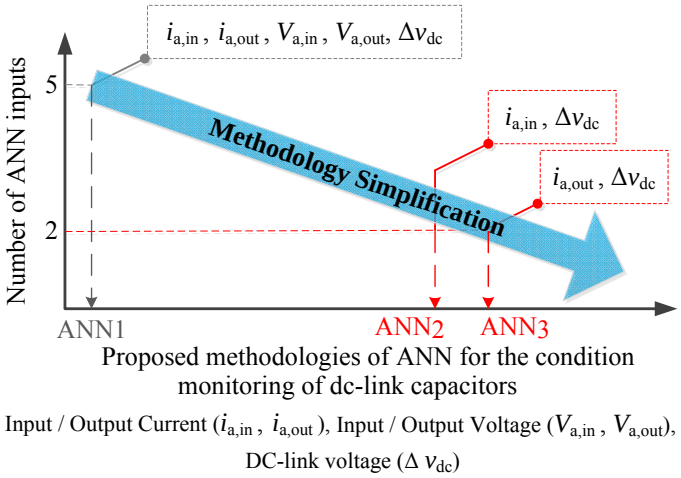

Fig. 4.1: ANN methodology simplification in terms of ANN inputs.

4.2 System configuration

The proposed condition monitoring method is applied to estimate the capacitance value of the dc-link capacitor in a three phase AC/AC power converter as shown in Fig. 4.2. Specifications of the converter are listed in Table 4.1.

Table 4.1: Specifications of The Case Study of Three-Phase Inverter with Diode Bridge Rectifier Front-End. .

Load Type	Resistive
Input AC Voltage (V_{L-L})	400 V
Output AC Voltage (V_{L-L})	400 V
Rated DC-link Voltage (V_{dc})	500 V $\sim$ 565 V
Full Power Level (P_o)	4 kW
Nominal Capacitance (C_0)	1100 μF
Line Inductance $(L_a), (L_b), (L_c)$	3.67 mH

The AC/AC power converter consists of two power stages; 1) front-end diode bridge rectifier connected to three phase input voltage power supply; 2) IGBT bridge connected to a three phase resistive load. The two power stages are connected to each other through a dc-link capacitor.

In this simulation model, the dc-link voltage is uncontrolled and the three phase output voltages fed to the resistive load are controlled using feedback control as shown in Fig. 4.3. The measured output voltage $(V_{abc,out-mes})$ is

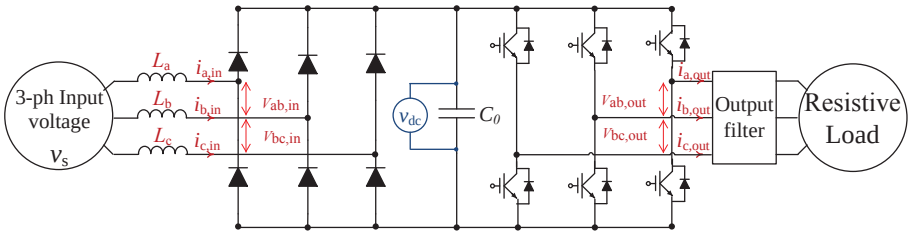

Fig. 4.2: An AC-AC power converter with a capacitor dc-link [81].

compared to the reference output voltage ($V_{abc,out-ref}$) in the Direct–Quadrature (dq) axis. A comparison takes place in the voltage regulator where the obtained difference between reference and measured signal is adjusted. Based on this adjustment, a transformation from dq to three phase system (abc) is required before generating the Pulse Width Modulation (PWM) signals. The generated signal controls the IGBT bridge to maintain the output voltage constant at the nominal value. However, the signal controls only the voltage, and therefore, the variation of the load power is considered during the capacitance estimation.

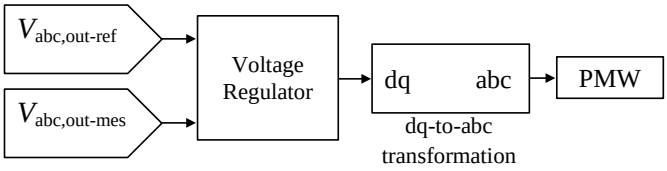

Fig. 4.3: Generation of the PWM control signals to the IGBT bridge of the convetrer simulation model shown in Fig. 4.2.

4.2.1 Structure and optimizing of artificial neural network

Considering the ANN algorithm as a concept for capacitance estimation has first been discussed in [79]. The main motivation is that the estimated value of C is possible to be obtained using the available input and output terminal information of the converter, without sensing the capacitor current i_C. The available information are phase A input/output; voltages $V_{a,in}$, $V_{a,out}$, currents $i_{a,in}$, $i_{a,out}$, and the ripple dc-link voltage Δv_{dc}, respectively. The aforementioned information will be used as *input* to the ANN that is referred as *ANN1*, while the corresponding value of C is used as a *target*. The basic structure is shown in Fig.4.4. Afterwards, ANN1 is responsible to estimate the value of C when using different inputs than the trained ones.

To collect a training set, the capacitance values in the range between 900 μF and 1300 μF with 10 μF step are used as targets to the network in this

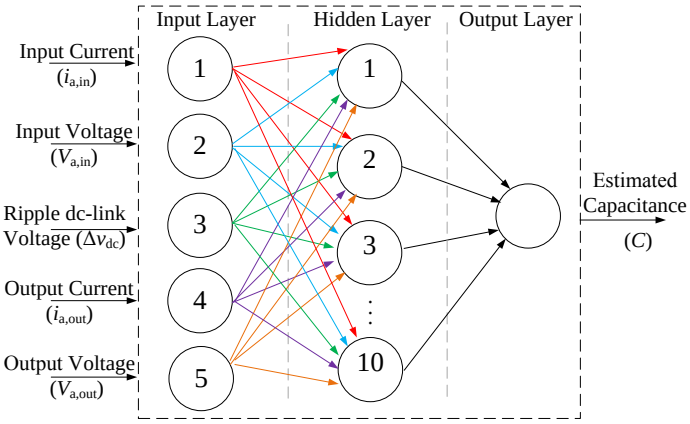

Fig. 4.4: Structure of the proposed *ANN1* for capacitance estimation.

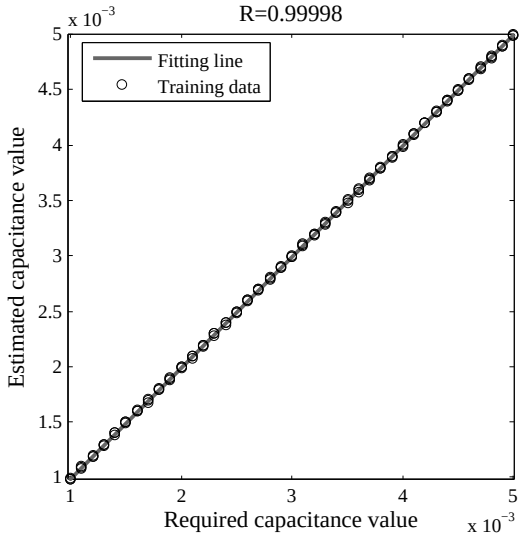

Fig. 4.5: Regression response of the trained *ANN1*.

case. Those 41 datasets have single phase A RMS input/output voltages, currents, and the ripple dc-link voltage. Since different loading conditions of the converter are also considered, three training sets of 41 data under the respective loading level of 4 kW, 3 kW and 3 kW are used. The total amount of training datasets are 123 data. All the 123 datasets are fed to a single hidden layer ANN1 consisting of 10 neurons using the Neural Fitting Tool nftool in MATLAB software. Where a single hidden layer consisting of 10 neurons are the simplest design specifications for a given ANN. The iteration

algorithm used in this training is *Levenberg-Marquardt*, which typically takes more memory but less calculation time.

As stated in chapter 3, the training automatically stops when the generated correlation stops improving. The trained ANN1 has achieved a regression of R= 0.99998 as shown in Fig. 4.5 using this method. Therefore, the trained ANN1 is acceptable and generated for testing purposes.

4.2.2 Testing of the trained ANN1

In this subsection, the trained ANN1 is tested for verification. The input to the ANN1 are stored in the Matlab workspace, which are sent to the ANN's input layer as a group set. Each group set results in one corresponding output (estimated C value). The same group set of inputs are saved in the input layer until a new set is available in the workspace.

In order to simulate a capacitance drop, two capacitors C_1 and C_2 are connected in parallel through switches in order to have the option to switch between them. At the instant of 5 sec, C_2 will be switched on instead of C_1, and a capacitance drop from 1100 μF to 880 μF is simulated. Fig. 4.6 shows the capacitance value estimated by the trained ANN1 and their corresponding error percentages.

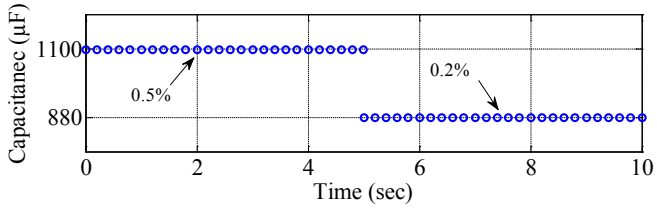

Fig. 4.6: Capacitance estimation of a simulated capacitance drop of 220 μF from 1100 μF to 880 μF at 4 kW power level.

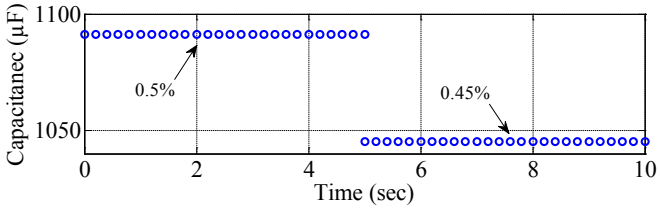

Fig. 4.7: Capacitance estimation of a simulated capacitance drop of 50 μF from 1100 μF to 1050 μF at 4 kW power level.

The estimated results verify that the trained ANN1 can respond to the changes in the capacitance value, and the value of the capacitor can be easily

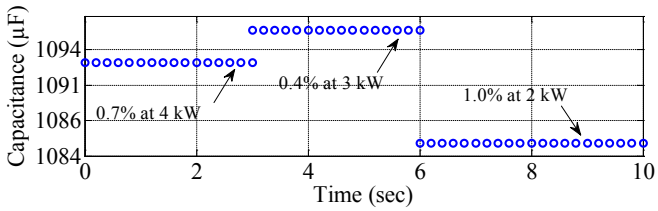

Fig. 4.8: Trained ANN1 accuracy against changes in load power.

identified. Moreover, the trained ANN1 is tested to identify the reduction of 50 μF out of 1100 μF and the resulting estimation is shown in Fig. 4.7. For the initial stage, the estimated value is 1098 μF and for the degraded case, the estimated value is 1048 μF, which gives a maximum error of 0.5%.

To test the robustness of the trained ANN1 against loading power variations, the ANN1 is tested to estimate the nominal capacitance value of 1100 μF during a load power change. The estimated results with their corresponding errors are shown in Fig. 4.8.

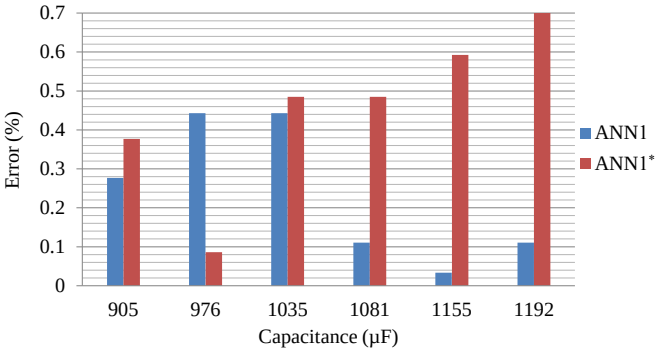

Fig. 4.9: Estimation error analysis by different trained ANNs under 4 kW powel level.

As stated in chapter 3, the amount of training datasets affect the ANN accuracy. In order to show the impact of the training datasets on the ANN estimation accuracy, another network ($ANN1^{\star}$) is trained by using 63 dataset instead of 123 dataset and considers the same conditions of ($ANN1^{\star}$) which is trained earlier. 20 μF step instead of 10 μF step is considered during collection of training datasets for $ANN1^{\star}$. Fig. 4.9 shows that the errors estimated by $ANN1^{\star}$ are higher than the ones estimated previously by the ANN1, implying a trade-off between the estimation accuracy and the required computation resource.

The last accuracy analysis is performed in order to analyse the error of the estimated capacitance with respect to different degree of changes of the original capacitance value of 1100 μF and the results are shown in Fig. 4.10. It can

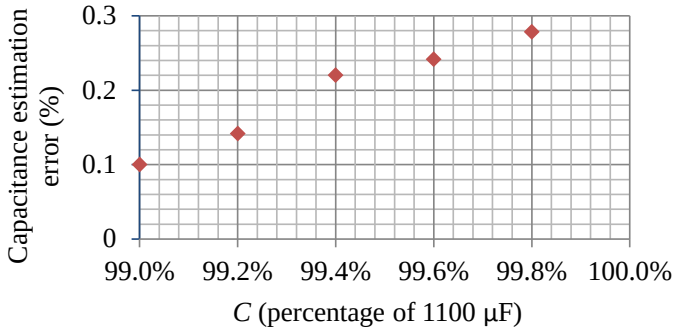

Fig. 4.10: Error analysis under different levels of capacitor reduction at rated power level.

be noted that the estimation errors of the proposed ANN1 are below 0.3%. That means it can respond and estimate correctly the capacitance values even under a very low level of capacitance reduction as of 0.1% changes.

In the light of the presented results, the following remarks are given:

1) The simulation results of the proposed method based on ANN1 verify that the condition monitoring methods based on only a software solution can be an attractive alternative for practical industry applications.

2) It can be noted from the results that the trained ANN1 is capable to respond for a very small change of the capacitance, and estimate the capacitance value within the range which the network is trained.

3) It should be noted that the accuracy of a trained ANN strongly depends on the amount, quality, and accuracy of the data used in the training.

Although of the positive remarks above, it have been realized that the proposed method can be improved. The dc-link capacitance value could be estimated using less information. Estimation of the capacitance using the ripple dc-link voltage Δv_{dc} and phase A input current $i_{a,in}$, or phase A output current $i_{a,out}$ can be sufficient. Moreover, it is also addressed that using instantaneous training information is not a realistic method in practice. Therefore, an improved method in collecting the training information is considered in further investigations in this thesis.

4.3 Training data preparation for ANN improvement

In this section the same basic structure in the previous subsection is used, but with two inputs to the ANN instead of five. Moreover, in order to investigate

the impact of input current and output current on the estimation accuracy, two ANNs are trained. In addition to Δv_{dc}, the first ANN (*ANN2*) is trained using phase A input current $i_{a,in}$, and the second ANN (*ANN3*) is trained using phase A output current $i_{a,out}$ as shown in Fig. 4.11.

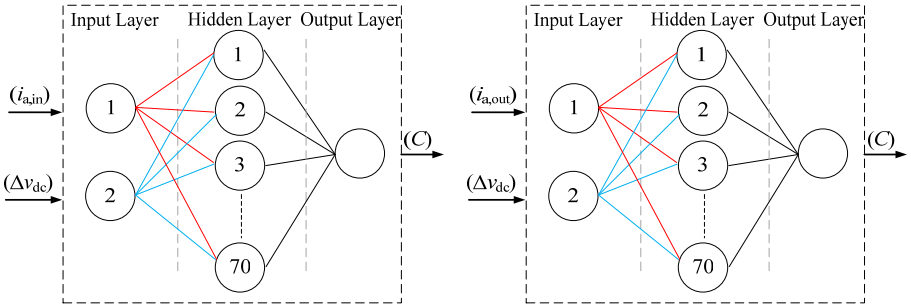

Fig. 4.11: Simplified structure of the two ANNs (*ANN2* and *ANN3*) applied for front-end diode bridge and back-to-back converters.

Also the same front-end diode converter as shown in Fig. 4.2 is considered with rating conditions referred in Table 4.1.

Since the amount of inputs are reduced, the strength of the correlation between inputs and targets has become more challenging. Therefore, another training algorithm called *Bayesian Regularization* is considered, which is suitable for the challenging problems. In addition, different amount of hidden neurons (70 hidden neurons) are selected.

Since the ripple dc-link voltage depends on both the capacitance and the loading conditions, the prepared training datasets are collected from the operation of five different power loading conditions. The same previously operational power of 4 kW is also considered. The boundaries of the power levels are between 4 kW power and 400 W as 10% of the selected operating power. For each power level, there are 41 data of the capacitance values used to train the ANNs, covering the range between 900 μF and 1300 μF with 10 μF step. Each capacitance value corresponds to one value of the input current and one value of the ripple dc-link voltage. The process of the training datasets collection is as following:

1) Starting from the lower boundary of the capacitance range (900 μF), the front-end diode bridge converter SIMULINK model starts running with 1 μs sampling time.

2) During the simulation, the Root Mean Square (*RMS*) values of phase A input current $i_{a,in}$, phase A output current $i_{a,out}$, and ripple dc-link voltage Δv_{dc} are sent and saved into the MATLAB memory workspace.

3) After the simulation under a specific dc-link capacitance stops, $1e^6 + 1$ instantaneous values for each parameter (sampling time of $1e^{-6}$ is considered for the simulation) are available. A designed Matlab code calculates the mean and peak of the least 7,000 instantaneous values for each 0.1 sec simulation time. In order to have enough time to simulate different cases and avoid the transient time, the simulation time is selected to be 1.3 sec. By the end of each 0.1 sec, one average RMS value for the phase A input current $i_{a,in}$, A output current $i_{a,out}$, and one peak RMS value of the ripple dc-link voltage Δv_{dc} are available. An explanation diagram for the Matlab code is shown in Fig. 4.12

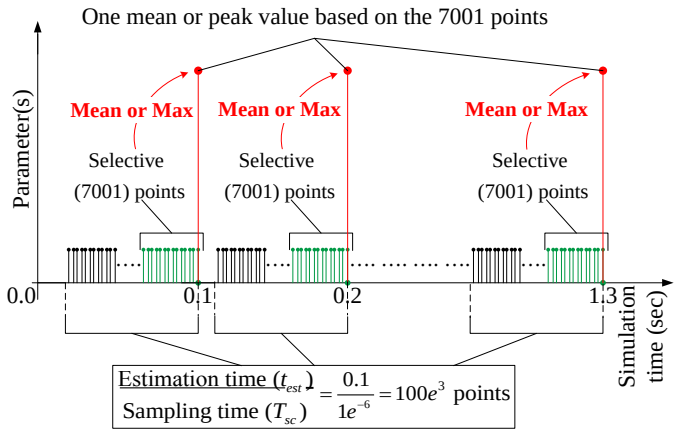

Fig. 4.12: Explanation of the designed Matlab code to prepare the training data of Phase A input and output current and ripple dc-link voltage.

4) By reaching the upper boundary of the capacitance range (1300 μF), 4 datasets are available. One dataset for phase A input current $i_{a,in}$, One dataset for phase A output current $i_{a,out}$, and one dataset for ripple dc-link voltage Δv_{dc}, and one dataset for the capacitance. Each dataset consists of 41 data.

5) The above process is done for the operating power level of 4 kW, 3 kW, 2 kW, 1 kW, and 400 W respectively. Finally, there are 205 data in each dataset.

In addition to the ripple dc-link voltage Δv_{dc}, the datasets of phase A input current $i_{a,in}$ and the datasets of phase A output current $i_{a,out}$ are loaded to the input layer of ANN2 and ANN3 respectively as a matrix with a dimension of 2×205. While the dataset of the capacitance is loaded to the output

layer of both ANNs as a matrix with a dimension of 1×205. Due to the usage of the average values, the error of the estimated capacitance is reduced. The trained ANNs can be used to estimate the dc-link capacitance under different loading conditions with any capacitor value within the trained range.

The used iteration algorithm in this training is the *Bayesian Regularization* [1], which typically takes longer time but it is definitely better for challenging problems. Moreover, the used training algorithm avoids the overfitting issues by stopping the training automatically, when the generated results stop to be improved.

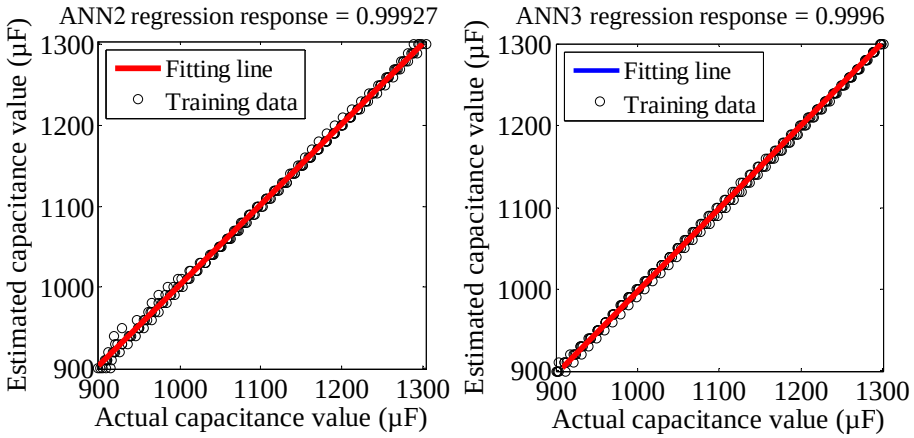

Fig. 4.13: Regression response of the trained ANNs (ANN2 and ANN3) based on the improved training data.

The regression response of the trained ANNs (ANN2 and ANN3) are shown in Fig. 4.13. It can be noted that all of the 205 input data are aligned to the fitting line and the values of R is close to 1 giving a strong regression. Based on the results, the network stopped training and the ANNs are generated and ready to be tested. In the final step in generating the trained ANNs, Matlab toolbox offers to generate the trained ANNs as a *SIMULINK* model for each ANN. In the following sections, the testing of the trained ANNs SIMULINK models are studied.

4.3.1 Capacitance estimation under different conditions

In this section, the generated ANN2 and ANN3 are tested under different case studies for verification purpose. The same converter as shown in Fig. 4.2 is used. The two ANNs are fed with updated dataset every 0.1 sec. For ANN2, each dataset consists of one averaged value of the root-mean-square of the input current $i_{a,in}$ and dc-link ripple voltage Δv_{dc}, while for ANN3, each dataset consists of one averaged value of the root-mean-square of the

output current $i_{a,out}$ and dc-link ripple voltage Δv_{dc}. Three cases are studied for the trained ANNs in the following subsections.

Case I: Constant capacitance conditions

In this case, the trained ANN2 and ANN3 are tested to check whether they are able to estimate the correct value of the capacitance or not. Two random values within the trained capacitance range C_1 = 1182 μF and C_2 = 975 μF are chosen for this test. ANN2 and ANN3 are fed with the same peak values of Δv_{dc} shown in Fig. 4.14. The behaviour of the phase A input and output current is shown in Fig. 4.15.

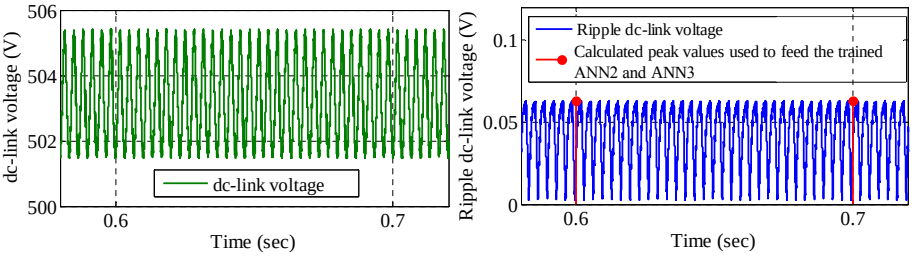

Fig. 4.14: Zoom-in on the behaviour of the original dc-link voltage, its ripple and the calculated peaks of the ripple used to feed the trained ANN2 and ANN3 for the estimation of C_1=1182 μF.

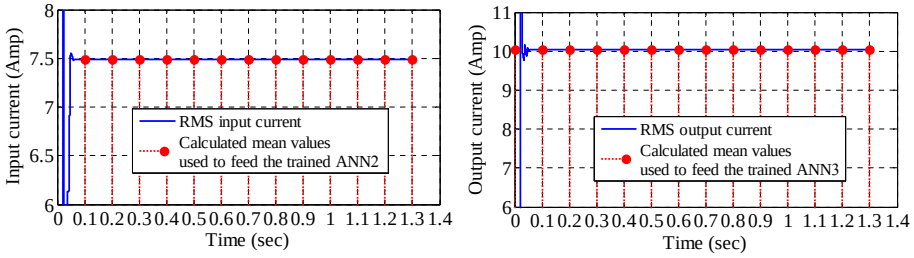

Fig. 4.15: Behaviour of the original RMS phase A input and output current and the selected mean values used to feed the trained ANN2 and ANN3 for the estimation of C_1 = 1182 μF.

The estimated capacitance values from ANN2 and ANN3 are shown in Fig. 4.16. Moreover, the corresponding percentage error of each capacitance values for both ANNs are shown in Fig. 4.17.

In Fig. 4.16 it can be seen that the estimated capacitance values are aligned with the actual values with very low estimation errors, which are less than 0.4% as shown in Fig. 4.17.

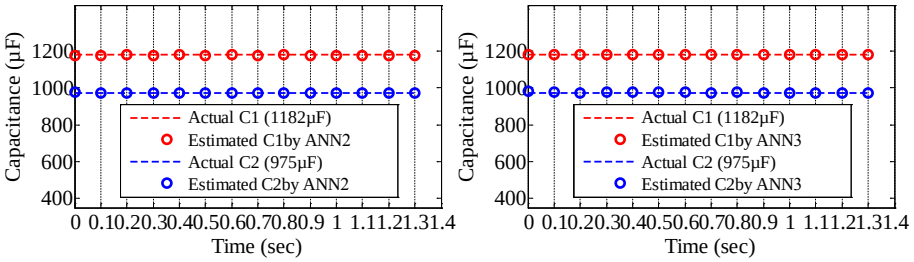

Fig. 4.16: The capacitance estimation of C_1=1182 μF and C_2=975 μF by the trained ANN2 and ANN3 at 4 kW load.

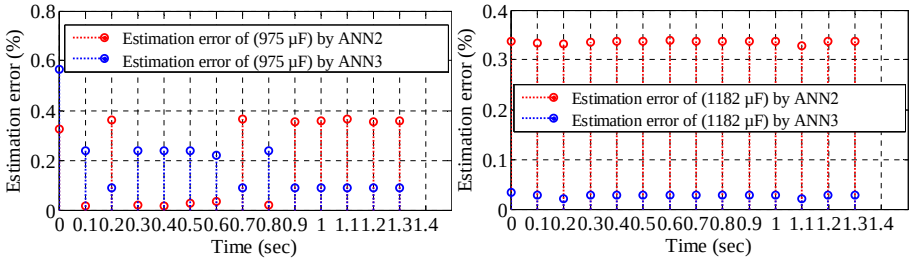

Fig. 4.17: The corresponding error of the capacitance estimation in Fig. 4.16 by the trained ANN2 and ANN3 at 4 kW load.

Case II: Varying load conditions

In this test, the impact of the load (power) variation on the estimation accuracy for both ANN2 and ANN3 is analysed. A simulated drop in the load power is subject to the model. The load power is dropped from 4 kW to 400 W at the instant of 0.7 sec.

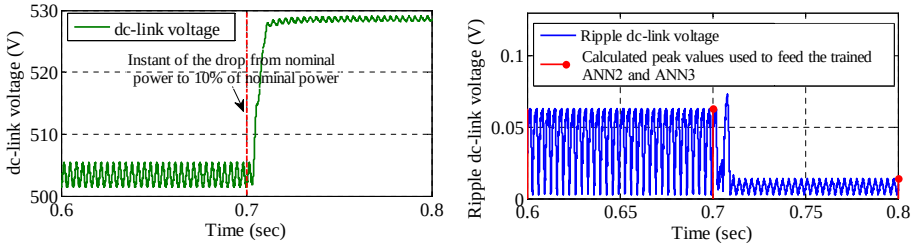

Fig. 4.18: Zoom-in on the behaviour of the original dc-link voltage, its ripple and the calculated peaks of the ripple used to feed the trained ANN2 and ANN3 for the estimation of 1182μF under load variation.

The behaviour of dc-link voltage and its ripple are shown in Fig. 4.18. It can be seen that the dc-link voltage amplitude is increased, while the ripple

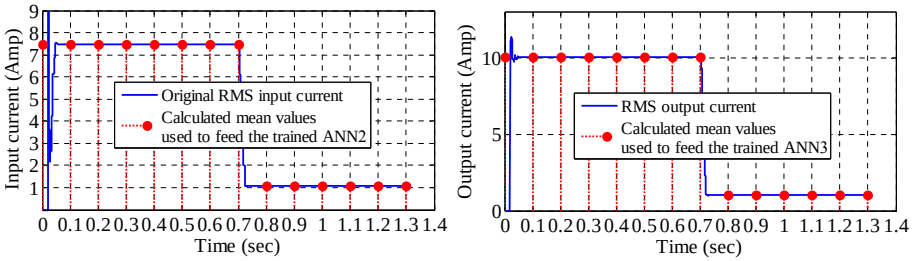

Fig. 4.19: Behaviour of the original RMS phase A input and output current and the selected mean values used to feed the trained ANN2 and ANN3 for the estimation of 1182μF under load variation.

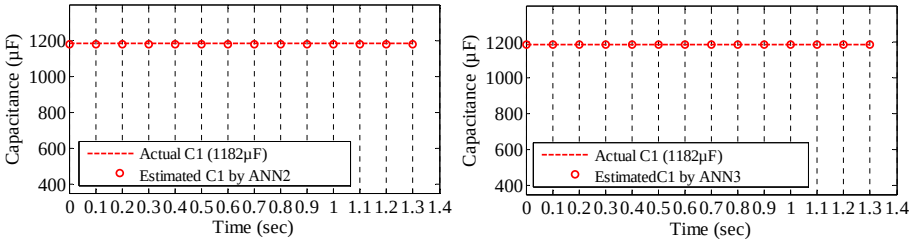

Fig. 4.20: The capacitance estimation by the trained ANN2 and ANN3 under load variation.

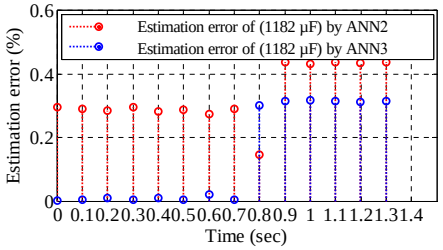

Fig. 4.21: The capacitance estimation error by the trained ANN2 and ANN3 under load variation.

voltage is decreased. In addition, the behaviour of the phase A input $i_{a,in}$ and output $i_{a,out}$ current are shown in Fig. 4.19. It can also be seen that the input current amplitude is dropping according to the updated loading condition.

The estimation of capacitance values and their corresponding errors are shown in Fig. 4.20 and Fig. 4.21, respectively. It can be seen that the variation impact took place just after 0.1 sec. In addition, both ANNs are still able to estimate the correct capacitance value even after the updated loading conditions with an estimation error less than 0.5%. Moreover, Fig. 4.21 shows that ANN2 estimated the capacitance value with less error at the case of a load variation. However, ANN3 has higher estimation accuracy during nominal

conditions.

Case III: Varying capacitance conditions

In this test a 1% drop in capacitance is simulated by using two capacitors connected in parallel.

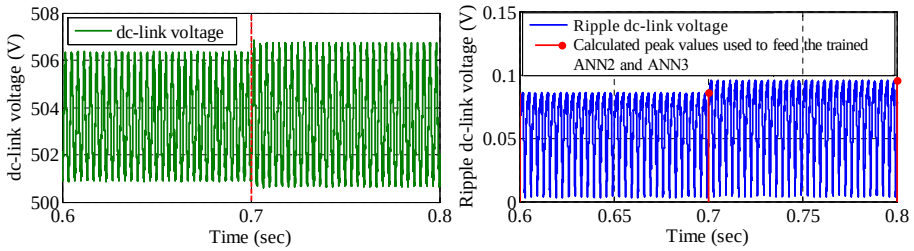

Fig. 4.22: Zoom-in on the behaviour of the original dc-link voltage, its ripple and the calculated peaks of the ripple used to feed the trained ANN2 and ANN3 for the estimation of 1100 μF with 11 μF capacitance drop.

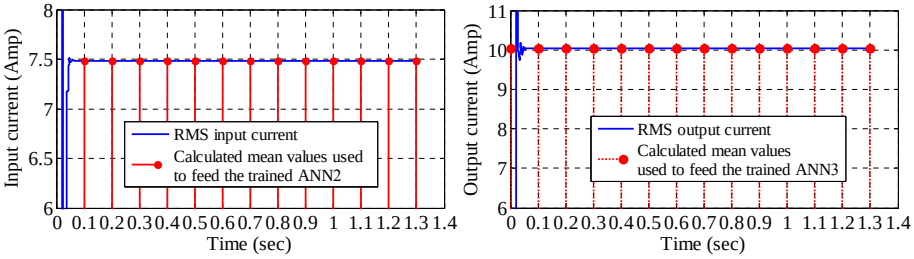

Fig. 4.23: Behaviour of the original RMS phase A input and output current and the selected mean values used to feed the trained ANN2 and ANN3 for the estimation of 1100 μF with 11 μF capacitance drop.

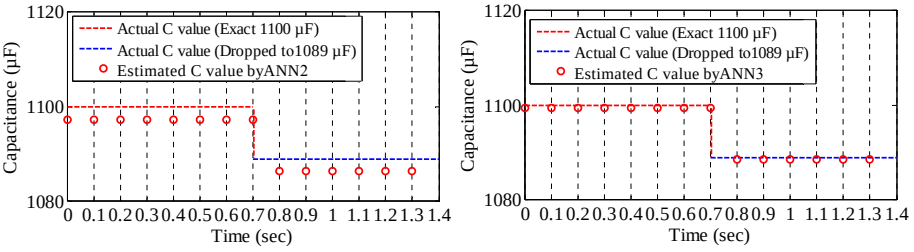

Fig. 4.24: The capacitance estimation by the trained ANN2 and ANN3 under 11 μF capacitance drop.

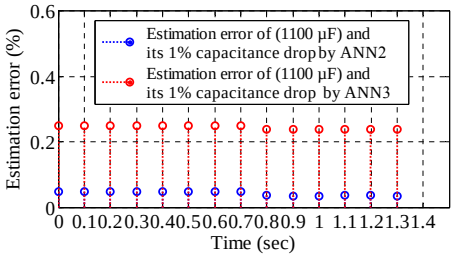

Fig. 4.25: The capacitance estimation error by the trained ANN2 and ANN3 under 11 μF capacitance drop.

Where C_1 equals to 1089 μF, and C_2 equals to 11 μF and connected through a switch to have the option to switch between 1100 μF and 1089 μF. The behaviour of the dc-link voltage, its ripple, and the behaviour of the phase A input and output currents, are shown in Fig. 4.22 and Fig. 4.23, respectively.

It can be noted that the dc-link voltage and its ripple increased against the drop in the dc-link capacitance value. In addition, the input current is also had a neglected slight drop with respect to the capacitance drop, which means that estimation of capacitance in case of loading variation is more dependant on the variation in the dc-link voltage ripple.

In Fig. 4.24 and Fig. 4.25 the estimated capacitance value with the corresponding estimation error are given. Both ANNs are able to estimate a correct value of capacitance before, after, and during the capacitance variation instant with estimation error less than 0.3%.

The following remarks and comments are based on the resulting capacitance estimation obtained by the trained ANN3.

1) In the resulting estimation error in the previous three cases, it can be seen that ANN3 have achieved more accuracy comparing to the achieved ones by ANN2.

2) It can be seen that the trained ANN3 estimates the actual value in steady state with a maximum error less than 0.4% as shown in Fig. 4.17.

3) The trained ANN3 detects 1% variation in the capacitance value with maximum error less than 0.2% as shown in Fig. 4.25.

4) A proof of the concept is beneficial in order to validate the proposed capacitor condition monitoring based on ANN. Therefore, an implementation of the trained ANN3 in a Digital Signal Processor (*DSP*) is given in Section 4.4.

4.4 Proof of Concept Using a Digital Signal Processor (DSP)

In order to proof the concept, the proposed ANN3 is implemented in a Digital Signal Processor (DSP). The main objective is to verify that a trained ANN in Matlab can be integrated in a hardware controller. In addition, the validation part in this section aims to proof the concept by feeding the DSP with digital data, but those data are obtained from the front-end diode bridge SIMULINK model shown in Fig. 4.2. The used DSP is Texas Instrument TMS320F28335 [2]. Code Composer Studio (*CCS v5.4*) is used for interacting with the C-code files. Since the *CCS v5.4* version does not have the option to connect directly to Matlab, therefore, the code composer version (*CCS v3.3*) is used as an intermediate step in addition to *CCS v5.4*.

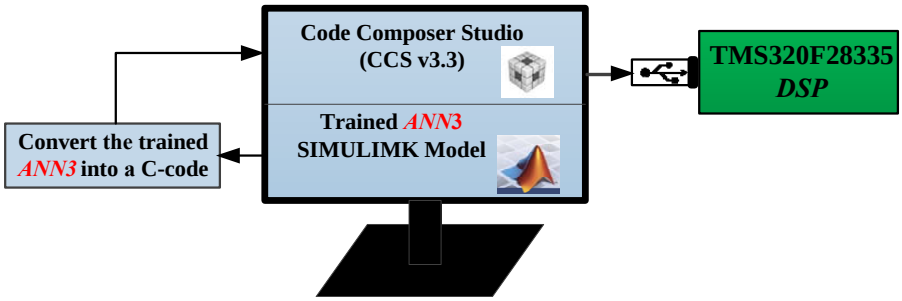

Fig. 4.26: The process of the ANN3 establishement to DSP from Matlab

The establishment process of the (*CCS v3.3*) from Matlab is shown in Fig. 4.26 and explained in the following steps:

1) Connecting the DSP board to the PC using the proper USP cable.

2) Run the (*CCS v3.3*) program on the PC and connect the DSP board, a green led on the DSP board is turned on, then the (*CCS v3.3*) program is closed.

3) Inside the Matlab editor, command 1 and command 2 are written, respectively. The lines in-between are generated automatically after entering command 1 as status of the establishment progress.

```
» cc=ticcs % command 1
TICCS Object:
Processor type : TMS320C28xx
Processor name : TMS320C2800-0
Running? : No
Board number : 0
```

Processor number : 0
Default timeout : 10.00 secs
RTDX channels : 0
» cc.visible(1) % command 2

4) Once the above commands are entered, the (*CCS v3.3*) program is re-opened again, and the DSP board is ready to be uploaded with the trained ANN3.

5) When the trained ANN3 is built inside the DSP, an equivalent project that consists of the C-code and header files is generated and saved as a project folder.

6) Afterwards, the (*CCS v5.4*) is opened. The (*CCS v5.4*) imported the built project as "Legacy *CCS v3.3* Projects". Finally, the ANN3 can be fed with inputs according to the registered ports.

However, the ANN3 should fulfil important specifications that met the requirements of the DSP as it is a new environment instead the Matlab. The process of preparing and implementing the ANN3 in the DSP is explained and illustrated in details in the following section.

4.4.1 ANN3 preparation and implementation in DSP

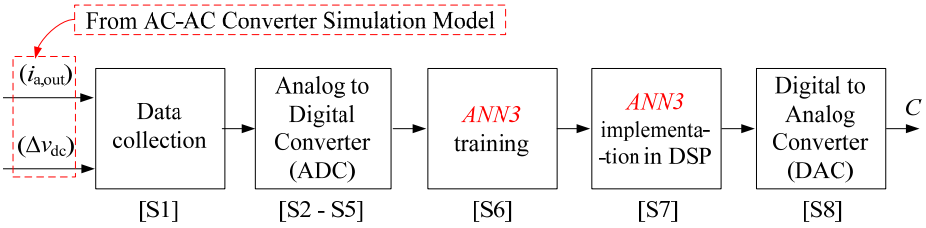

Fig. 4.27: The process of ANN3 implementation in DSP using the input signals from AC-AC convetrer shown in Fig. 4.2.

The block diagram shown in Fig. 4.27 illustrates the implementation process with the following steps:

S1) The training datasets obtained from the front-end diode bridge SIMULINK model and used earlier in Chapter 4.1, are collected and stored in an excel sheet.

S2) In a real prototype applications, readings of current and voltage are fed to the DSP into a digital form. Therefore, three gain factors (i.e shown

in the equations 4.1, 4.2, and 4.3) are calculated to obtain the equivalent digital values of phase A input current $i_{a,out}$, ripple dc-link voltage ΔV_{dc}, and capacitance values.

S3) The DSP maximum voltage rating of a digital input $DSP_{max,volt_1}$ equals to 3 V, and the maximum number of bits $DSP_{max,bits}$ are 4096 bits, therefore, the calculated gain factors are based on 2.7 V $DSP_{max,volt_2}$, and 4096 bits as usable peak limits. Moreover, 10 Amp, 0.04 V, and 1300 μF are used as the maximum limits for phase A input current $i_{max,a,in}$, ripple dc-link voltage $\Delta V_{max,dc}$, and capacitance C_{max}, respectively.

S4) Based on the previous considerations mentioned in S3, the gains are calculated as the following:

$$K_I = \frac{DSP_{max,volt_2} \times DSP_{max,bits}}{i_{max,a,out} \times DSP_{max,volt_1}} = \frac{2.7 \times 4096}{10 \times 3} = 368 \tag{4.1}$$

$$K_V = \frac{DSP_{max,volt_2} \times DSP_{max,bits}}{\Delta V_{max,dc} \times DSP_{max,volt_1}} = \frac{2.7 \times 4096}{0.04 \times 3} = 92160 \tag{4.2}$$

$$K_C = \frac{DSP_{max,volt_2} \times DSP_{max,bits}}{C_{max} \times DSP_{max,volt_1}} = \frac{2.7 \times 4096}{0.0013 \times 3} = 2835692 \tag{4.3}$$

Where, K_I, K_V, and K_C, are the gain factors, phase A input current $i_{a,out}$, ripple dc-link voltage ΔV_{dc}, and capacitance C, respectively.

S5) Afterwards, all the collected datasets stored in the excel sheet are multiplied by the corresponding gain factor, and hence, three datasets each consisting of 205 data are put into a digital form and ready to be used as training data.

S6) The same ANN3 structure shown in Fig. 4.11 is applied to train the available digital data. The regression response is the same as that in Fig. 4.13.

S7) The implementation of the trained ANN3 in the DSP is achieved by generating a C-code, that is equivalent to the generated SIMULINK trained ANN3 model. Afterwards, this C-code is compiled using the Code Composer Studio (*CCS*), and then, a new ANN3 is built by the DSP

S8) In sake of testing the trained ANN3 by the DSP, the streaming of data coming from the front-end diode bridge converter SIMULINK model are first converted into digital forms according to (4.1), (4.2) and (4.3).

The estimated capacitance value in a digital format is converted into a physical value according to (4.3).

4.4.2 Testing Results of the Implemented ANN3 in DSP

In this section, three different capacitance values are selected to be estimated by the trained ANN3 on the *DSP* system. This is done by adjusting the capacitance value in the simulation model of the converter. The estimated results by the *DSP* are listed in Table 4.2.

Table 4.2: Estimated Capacitance Values and the Corresponding Error Percentages by DSP Used in a front-end diode bridge Converter.

Actual C value	Estimated by *DSP*	Estimation error
1182 μF	1182.2 μF	0.02 %
1093 μF	1093.2 μF	0.02 %
975 μF	974.9 μF	0.01 %

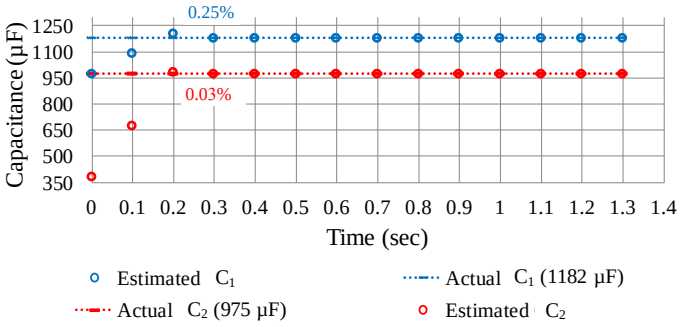

Fig. 4.28: The capacitance estimation by the trained ANN3 in DSP at 4 kW load.

The error of the estimated capacitance values from the DSP is less than 0.1%. To verify the simulation results presented in Chapter 4.1, similar three case studies are applied on the implemented ANN3 in DSP. The estimated capacitance by using the DSP are presented in Fig. 4.28 to Fig. 4.31. It can be seen in Fig. 4.28 that the maximum error is 0.25% and 0.03%, respectively, for the two estimated capacitors. In Fig. 4.29 and Fig. 4.30, it can be noted that the maximum error is 18% during the transient load variation from 4 kW to 400 W. During steady state, the errors are below 0.35%.

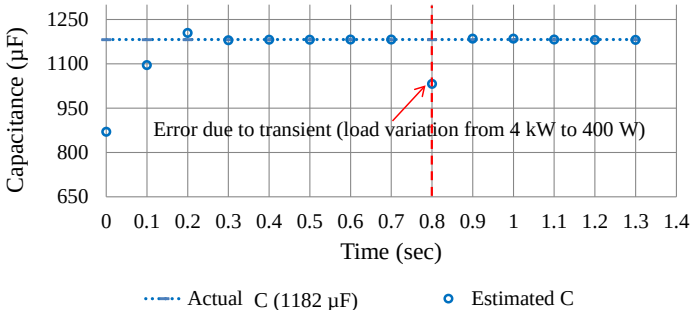

Fig. 4.29: The trained ANN3 using DSP under load variations.

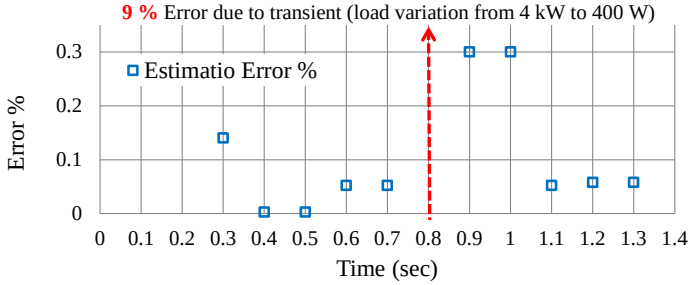

Fig. 4.30: Estimation error by ANN3 using a DSP corresponding to Fig. 4.29 under load variations.

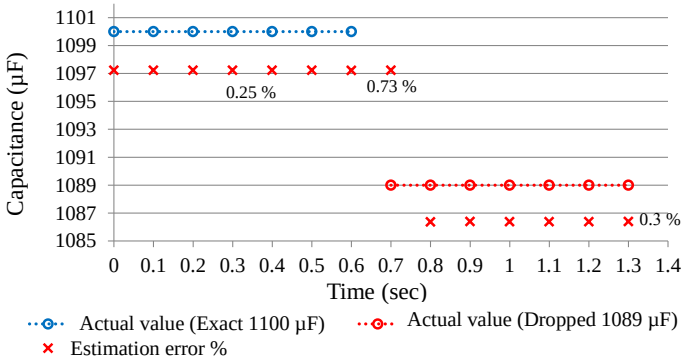

Fig. 4.31: Estimation error analysis using DSP with a capacitance variation at 4 kW load.

4.5 Summary

The following remarks and comments are based on the resulting capacitance estimation obtained from the DSP operation.

1) The proposed capacitor condition monitoring method based on ANN3 is implemented in both simulation software and DSP.

2) It can be seen that the trained ANN3 estimates the actual value in steady state with a maximum error of 0.25%.

3) An error of 9% is observed at the instant of load variation, which should then be discarded when operating.

4) The trained ANN3 estimates the correct value during the steady state operation with error less than 0.8%.

5) The trained ANN3 detects 1% variation in the capacitance value with maximum error equal to 0.73% at the instant of drop.

5) Although a proof of the concept is given, feeding a trained ANN with signals obtained from practical application still required for further verification. Therefore, a practical case study that applied on a motor drive is given in Chapter 5.

Chapter. 5

Application of the Proposed Method to a Practical Motor Drive System

This chapter presents a verification of condition monitoring based on ANN algorithm.

5.1 Introduction

In order to validate the proposed capacitor condition monitoring method based on ANN, an experimental study is conducted in this chapter. The ANN methodology is applied on a practical motor drive system. As stated earlier, simplifying the ANN methodology is one of the main objectives in this project. Therefore, more simplified ANN method is also proposed.

Since the AC component (dc-link voltage ripple) is both capacitance and load dependent, using dc-link voltage ripple and current information is important in order to differentiate between the impact of capacitance and load change as shown in Fig. 5.1. Another alternative is to use the dc-link voltage harmonics which includes both DC and AC components, where the DC component is only load dependent. Therefore, as shown in Fig. 5.2, in addition to the ANN trained on dc-link voltage ripple and current (*ANN4*), a new simplified ANN is trained on dc-link voltage harmonics (*ANN5*), and thereby, an analysis of the dc-link voltage harmonics using Fast Fourier Transform (*FFT*) is also given in this chapter. The structure of the proposed ANNs in this section are shown in Fig. 5.3.

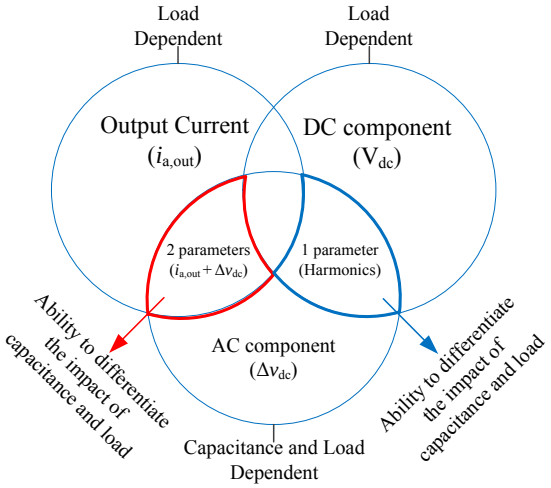

Fig. 5.1: Dependent parameters of capacitance and load variation impact in terms of dc-link capacitance estimation.

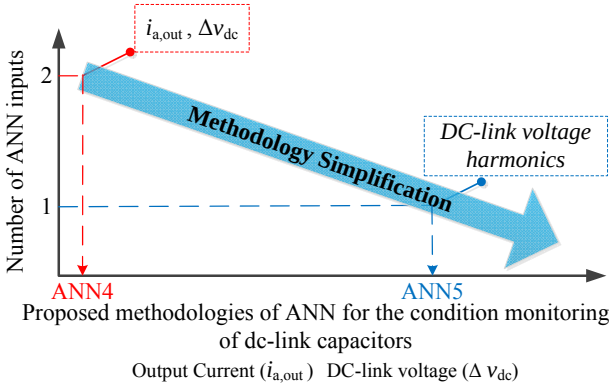

Fig. 5.2: ANN methodology simplification with respect to the ANN inputs.

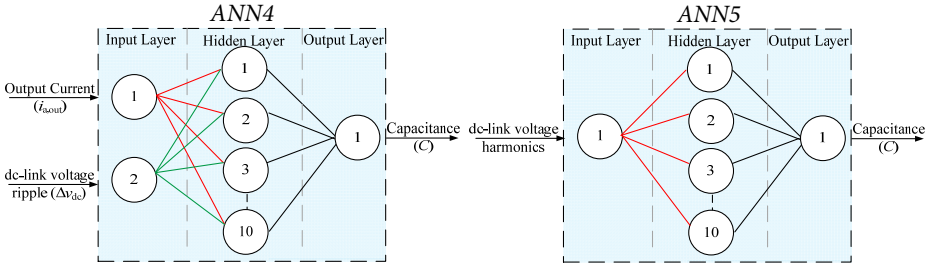

Fig. 5.3: Structure of the proposed *ANN4* and *ANN5*.

5.2 System configuration

The validation of the proposed methodology is applied on a 4 kW three-phase, front-end diode bridge motor drive provided by *Danfoss* [9]. The circuit diagram of the experimental platform is shown in Fig. 5.4, and the considered operating conditions and specifications of the motor drive are listed in Table 5.1.

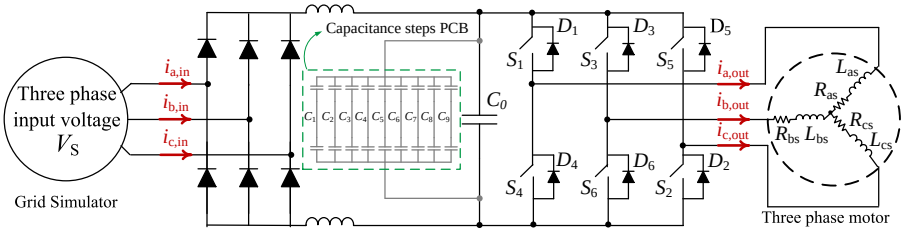

Fig. 5.4: An AC-AC power conversion system using a front-end diode bridge with a capacitor dc-link.

Table 5.1: Specifications of the Front-End Motor Drive from *Danfoss* [9].

Parameter	**Rating**
Rectifier Input AC Voltage (V_{L-L})	400 V
AC IGBT Inverter Output Voltage (V_{L-L})	400 V
Nominal DC-link Voltage (V_{dc})	550 V
Operating Power Level (P_o)	4 kW
Nominal Rotor Speed (N_r)	1500 rpm
Nominal Torque (T)	26 N.m
Nominal DC-link Capacitance (C_0)	500 μF
DC-link Inductances (L_{dc})	4 mH

A description of the experimental platform is shown in Fig. 5.5. The motor drive consists of different stages as listed in the Table in Fig. 5.5. The rectifier bridge converts the three-phase AC input fed from the main supply (grid) to DC current to supply inverter power. In order to filter the intermediate DC voltage, DC reactors are connected in the dc-bus. The DC reactors are also reducing the RMS current and harmonics on the AC side, and raising the power factor reflected back to the line. An installed capacitor bank (2 E-caps connected in series each 1000 μF) stores the DC power and provides

Equivalent circuits

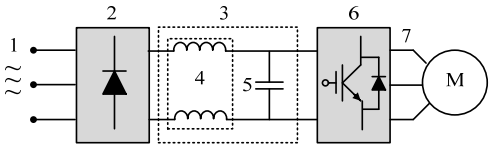

Area	Title
1	Main bus
2	Rectifier
3	DC bus
4	DC reactors
5	DC-link capacitor bank
6	Inverter
7	Motor bus

(a)

Hardware units

(b)

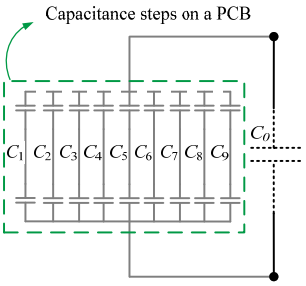

(c)

(d)

Fig. 5.5: Overview of the experimental platform used for applying the capacitor condition monitoring based on ANN. (a). Equivalent circuit of the motor drive. (b). Front-end diode bridge motor drive provided by *Danfoss*. (c) Equivalent circuit of the designed capacitance PCB. (d). Designed PCB capacitance board.

ride-through protection for short power losses. The equivalent capacitor of the complete DC bus is 500 μF with a total rated dc-link voltage of 800 V. Although the nominal dc-link voltage across the capacitor bank is 800 V, in this project, the motor drive is operated at 4 kW with 550 V dc-link voltage. Finally, a full bridge inverter that converts the DC into a controlled PWM AC waveform to control output voltage to the motor.

In order to apply varying conditions to the dc-link capacitor in the motor drive, a capacitor Printed Circuit Board (*PCB*) shown in Fig. 5.5(d) is designed and connected in parallel with the existing nominal dc-link capacitor (C_0) as shown in Fig. 5.5(c). The PCB consists of additional 9 individual (C_1 - C_9) steps of identical E-Caps, each step equals to 11 μF to analyse different capacitor values. The first time the system is operated at nominal conditions

with nominal capacitance C_0; afterwards, the system is operated by adding additional capacitances in a step. Each time the system is in operation, a corresponding waveform of the dc-link voltage and phase A output current are obtained and imported into Matlab. These imported waveforms are then processed for the relevant ANN training purposes. Considering three power levels, eventually [2x30] dataset is available for training and/or testing purposes.

5.3 Simulation Case of ANN4

Comparing to the previous simulation cases in *Chapter 4*, In this chapter, only 10 steps of capacitance are considered (C_0 - C_9). Therefore, a simulation case study is analysed first in order to show the feasibility of the proposed method with few steps of capacitance. In the simulation case, similar motor drive system is modelled in Matlab with the specifications listed in Table 5.1.

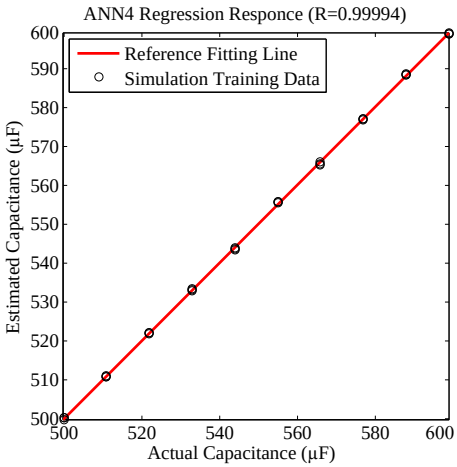

Fig. 5.6: Regression response of the proposed trained *ANN4* based on simulation training dataset.

The process of training data collection and training is the same as described in Section 5.2. The regression response of ANN4 based on simulation is satisfactory as shown in Fig. 5.6. It can be noted that ANN4 is trained using [2x30] dataset. The behaviour of the dc-link voltage at nominal power level obtained from the simulation is shown in Fig. 5.7. Moreover, the motor speed and torque waveforms are shown in Fig. 5.8. ANN4 is tested to estimate the capacitance value at constant capacitance condition under different loading conditions. The estimated capacitance by ANN4 with the corresponding estimation error are listed in Table 5.2.

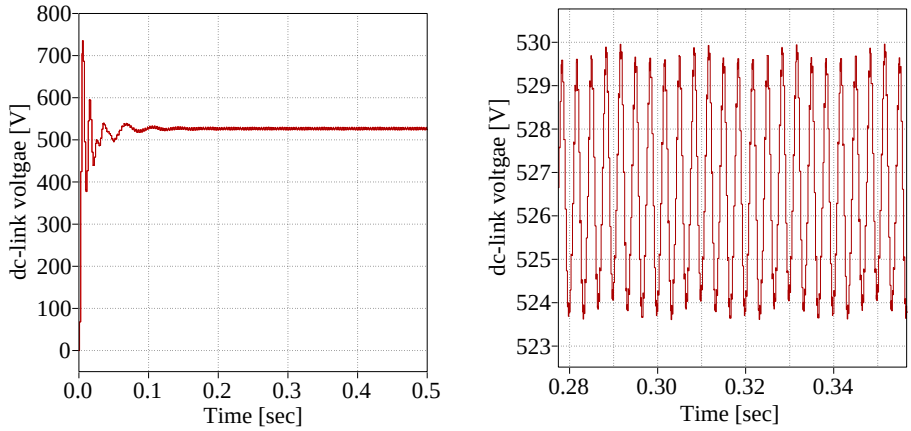

Fig. 5.7: Behaviour of the dc-link voltage at nominal power level obtained from the simulation.

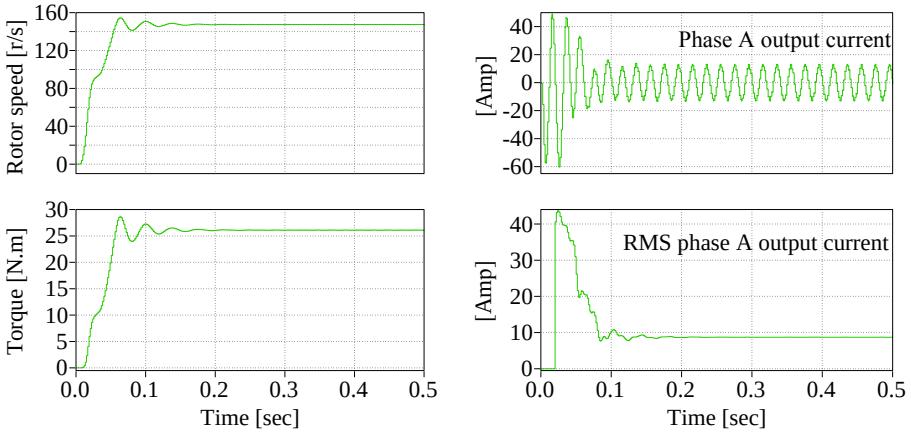

Fig. 5.8: The motor speed and torque waveforms obtained from simulation.

Table 5.2: Simulation Results for Estimated Capacitance by ***ANN4*** Under Different Loading Conditions.

Actual Value	ANN4$_{Estimation}$	ANN4$_{Error}$	Power Level
566 μF	565.1 μF	0.16%	2 kW
555 μF	555.7 μF	0.12%	3 kW
544 μF	543.2 μF	0.15%	4 kW
566 μF	566.9 μF	0.16%	4 kW

In order to simplify the training data collection process, additional ANN is trained based on minimum and maximum boundaries; (C_0, C_1, C_8 and C_9). The ANN trained based on boundaries is referred to as ANN4$_{BOUNDARY}$. The regression response of ANN4$_{BOUNDARY}$ based on simulation is satisfactory as shown in Fig. 5.9. It can be noted that ANN4$_{BOUNDARY}$ is trained using [2x12] dataset. It is Expected that ANN4$_{BOUNDARY}$ is able to estimate the in-between capacitance values which ANN4$_{BOUNDARY}$ did not consider in the training.

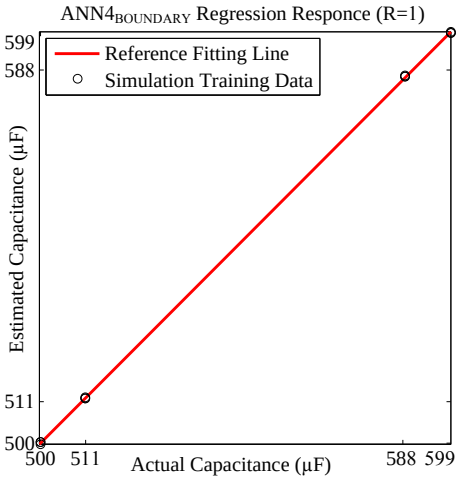

Fig. 5.9: Regression response of the proposed trained *ANN4$_{BOUNDARY}$* based on simulation training dataset.

ANN4$_{BOUNDARY}$ is tested to estimate the capacitance value at constant capacitance condition under different loading conditions. The estimated capacitance by ANN4$_{BOUNDARY}$ with the corresponding estimation error are listed in Table 5.3. More detailed discription of the training based on boundaries is given in the experimental case study.

Table 5.3: Simulation Results for Estimated Capacitance by ***ANN4$_{BOUNDARY}$*** Under Different Loading Conditions.

Actual Value	ANN4$_{Estimation}$	ANN4$_{Error}$	Power Level
566 μF	565.2 μF	0.14%	2 kW
555 μF	556 μF	0.18%	3 kW
544 μF	549.9 μF	1.0%	4 kW
566 μF	566.8 μF	0.14%	4 kW

By comparing the estimated error from Table 5.2 and Table 5.3, it is concluded that using boundaries information could be satisfying for capacitance estimation.

5.4 Experimental Case of ANN4

For ANN4, the estimation is based on the dc-link voltage harmonics. Three different power ratings including the nominal power level are also considered. The training data are obtained from the motor drive shown in Fig. 5.4. The training data collected for ANN4 with respect to capacitance steps and the three considered power levels are shown in Fig. 5.10.

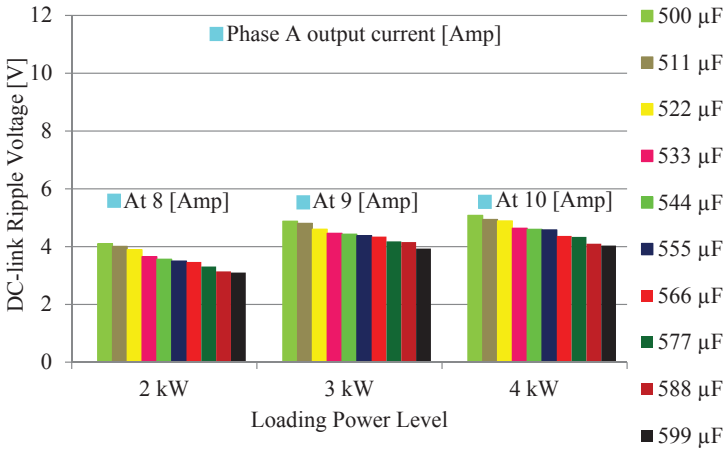

Fig. 5.10: Measured dc-link voltage ripple ΔV_{dc} and phase A output current $i_{a,out}$ dataset for training and testing of *ANN4*.

It can be seen that the dc-link voltage ripple and output current have a linear relationship with respect to the capacitance and loading power variation. For each power rating, there are 10 dataset of the capacitance values used to train ANN4. These 10 dataset are in the range between 500 μF and 599 μF with 11 μF step. Since there are 3 power levels are considered, 30 training dataset are collected. ANN4 is fed with a training dataset dimension of [2x30].

The regression response of ANN4 is shown in Fig. 5.11. For ANN4 the regression response equals to 0.99913. The regression response for ANN4 means a very strong correlation between inputs and targets. Since the regression response is satisfactory, trained ANN4 is generated as a SIMULINK models for capacitance estimation. Afterwards, the generated ANN4 is ready for testing.

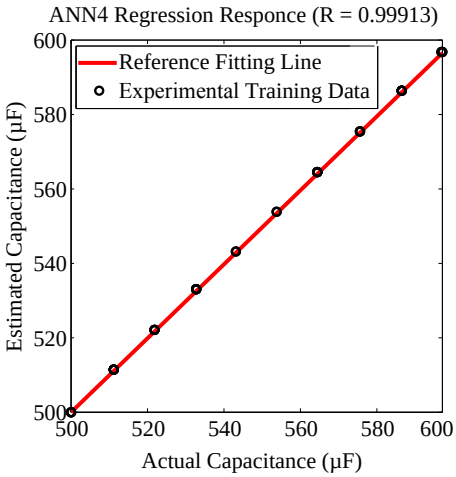

Fig. 5.11: Regression response of the proposed trained *ANN4* based on experimental training data.

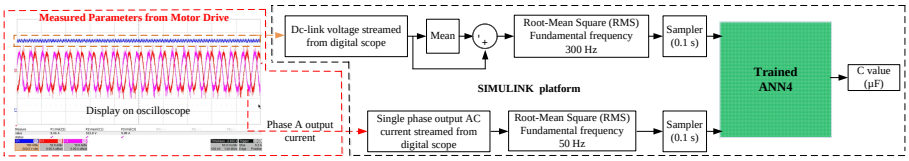

Fig. 5.12: Process of the proposed capacitor condition monitoring methodology based on the proposed *ANN4*.

The process of the capacitor condition monitoring method for ANN4 is shown in Fig. 5.12. For ANN4, the corresponding phase A output current $i_{a,out}$ and dc-link voltage ripple ΔV_{dc} from each capacitance step are obtained in MATLAB. In order to obtain the AC ripple of the dc-link voltage, the dc-link voltage measured in the motor drive is streamed to a MATLAB model that extracted the AC ripple of the dc-link voltage. Moreover, since ANN4 is considering the rms current, an rms block in MATLAB model is considered as well.

In order to test the generated ANN4, 2 case studies are applied. The purpose of studying these cases are in the sake of testing the trained ANN4 and whether it is able to estimate the capacitance value under different conditions. Analysing the estimation error for ANN4 is also included. Accuracy analysis with respect to the training data amount, source and type are also given.

5.4.1 Constant Capacitance Condition

In this case study, different capacitance values are selected to be estimated by the trained ANN4 used on the test system.

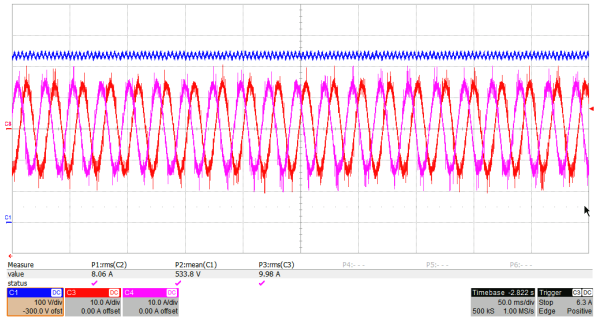

Fig. 5.13: Captured signals of the dc-link voltage and Phase A and B output current waveforms at C = 533 μF and the corresponding harmonic amplitude at 300 Hz operating at 4 kW.

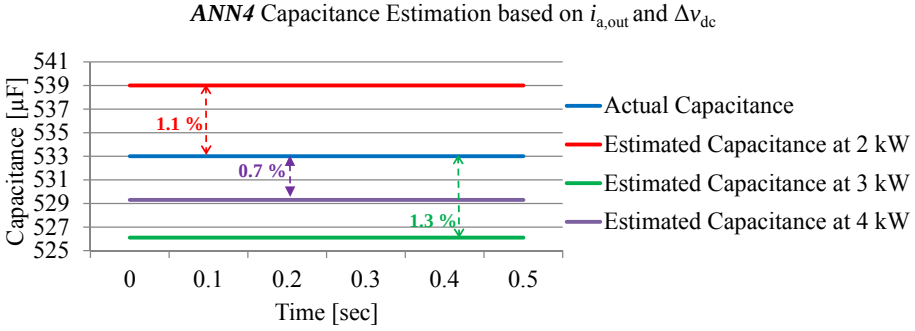

Fig. 5.14: The capacitance estimation of C = 533 μF capacitor by the trained *ANN4* under different loading conditions.

Table 5.4: Experimental Results for Estimated Capacitance by ***ANN4*** Under Different Loading Conditions.

Actual Value	ANN4$_{Estimation}$	ANN4$_{Error}$	Power Level
566 μF	561.6 μF	0.8%	2 kW
555 μF	553.8 μF	0.2%	3 kW
544 μF	543.2 μF	0.15%	4 kW
566 μF	564.9 μF	0.2%	4 kW

The dc-link capacitance value in the motor drive is adjusted to 533 μF. The corresponding waveform of dc-link voltage and output current are captured with a window width of 0.5 sec as shown in Fig. 5.13. The estimated results and the estimation error by ANN4 are shown in Fig. 5.14. More capacitance estimation results are listed in Table 5.4.

5.4.2 ANN4 Boundaries Training

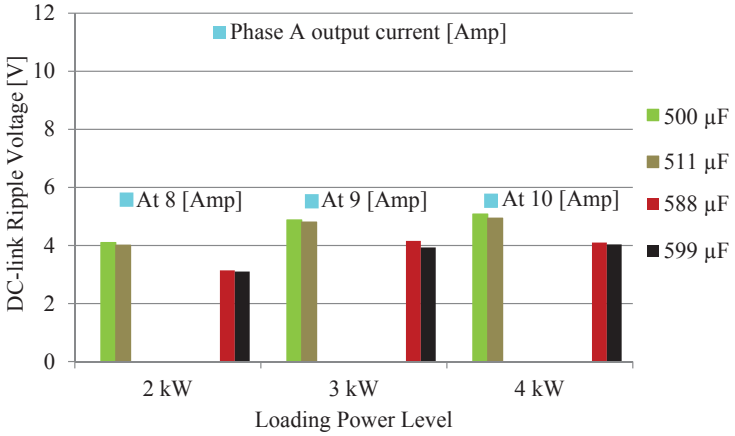

Fig. 5.15: Considered boundaries of dc-link voltage ripple ΔV_{dc} and phase A output current $i_{a,out}$ dataset for training ANN4$_{BOUNDARY}$.

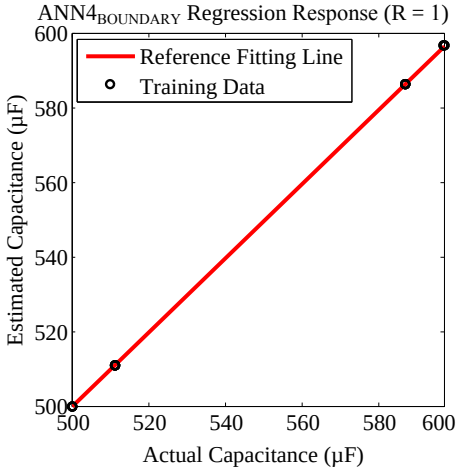

Fig. 5.16: Regression response of the proposed trained ANN4$_{BOUNDARY}$.

In this case study, the impact of training data amount, type and source is investigated. The purpose is to analyse the ANN behaviour and estimation error with respect to the considered training dataset. The same structure of ANN4 is studied in this section and referred to as ANN4$_{BOUNDARY}$. The considered training dataset for ANN4$_{BOUNDARY}$ is shown in Fig. 5.15. It can be seen that the considered training dataset are covering only the minimum and maximum boundaries. ANN4$_{BOUNDARY}$ is fed with a training dataset dimension of [2x12]. The regression response of ANN4$_{BOUNDARY}$ is shown in Fig. 5.16. The trained ANN4$_{BOUNDARY}$ is expected to estimate the values between these boundaries. Similar setting in 5.4.1 is considered. The estimated results and the estimation error by ANN4$_{BOUNDARY}$ are shown in Fig. 5.17. More capacitance estimation results are listed in Table 5.5.

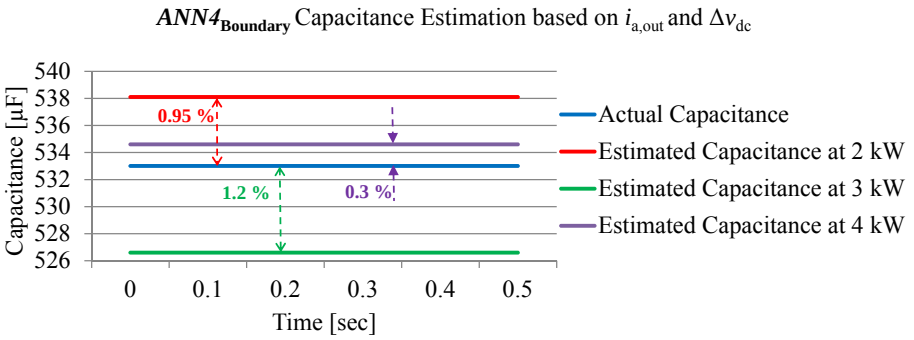

Fig. 5.17: The capacitance estimation of C = 533 μF by the trained $ANN4_{BOUNDARY}$ under different loading conditions.

Table 5.5: Experimental Results for Estimated Capacitance by ***ANN4***$_{BOUNDARY}$ Under Different Loading Conditions.

Actual Value	ANN4$_{Estimation}$	ANN4$_{Error}$	Power Level
566 μF	572.1 μF	1%	2 kW
555 μF	569.2 μF	2.5%	3 kW
544 μF	539.7 μF	0.8%	4 kW
566 μF	555.8 μF	1.8%	4 kW

5.5 DC-link voltage harmonics analysis

As stated earlier in this chapter, an alternative to estimate dc-link capacitance values based on ANN is to consider DC and AC components which can be found in dc-link voltage harmonics. Therefore, studying the impact of capacitance value on the dc-link ripple voltage has motivated this research to investigate the behaviour of the dc-link voltage harmonics.

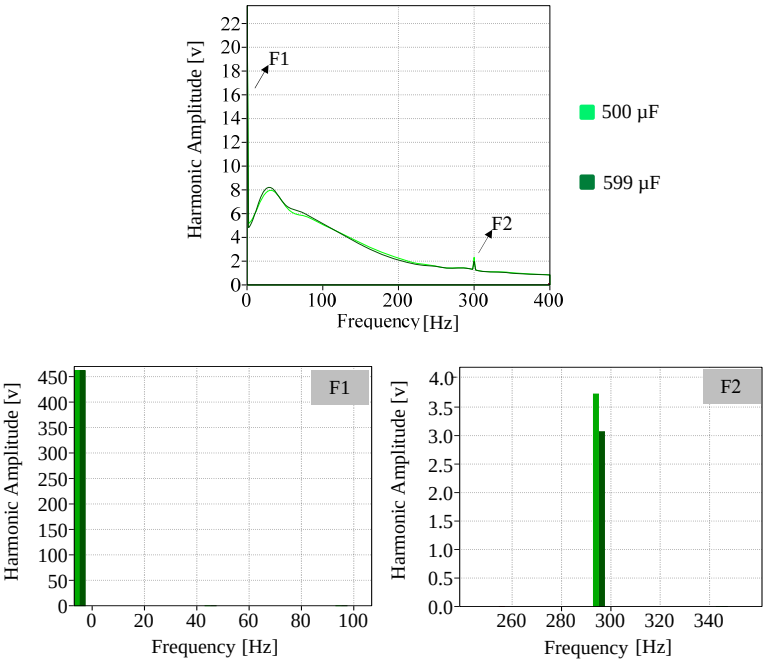

Fig. 5.18: DC-link voltage harmonic analysis under constant loading and balanced grid conditions with respect to the capacitance variation.

Analysing the dc-link voltage signals using Fast Fourier Transform (*FFT*) have proved the expectations to find a liner relationship between the capacitance value and the harmonics amplitude. The analysis is applied to a Front-End diode bridge motor drive as shown in Fig. 5.4. For a balanced grid conditions, the analysed dc-link voltage harmonics are classified into 2 features *F1 and F2* with respect to their frequencies. For a simulation analysis, the impact of capacitance variation at constant loading conditions and balanced grid conditions on the harmonic amplitudes is shown in Fig. 5.18.

It can be seen that feature F2 is the most dominant feature, where the capacitance variation impact can be reflected into the harmonic amplitude. Based on this reflection, the ANN is able to identify the capacitance value. Moreover, the harmonics amplitude are also reflecting the loading power

level. Therefore, a proposed ANN that estimates the capacitance value based on the dc-link voltage harmonic amplitude is also given in this chapter.

Since a simulation case study in Section 5.3 has proved the feasibility of training an ANN on few dataset, an experimental case is studied directly in the following section.

5.6 Simulation Case of ANN5

As stated earlier in Section 5.3, a simulation case study is analysed first in order to show the feasibility of the proposed method with few steps of capacitance.

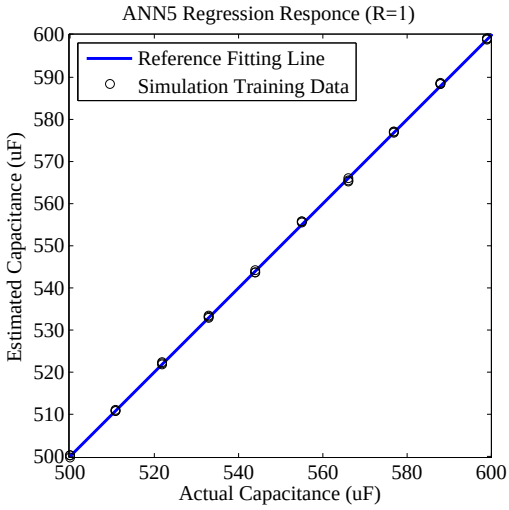

Fig. 5.19: Regression response of the proposed trained *ANN5* based on simulation training dataset.

In the simulation case, similar motor drive system is modelled in Matlab with the specifications listed in Table 5.1. The regression response of ANN5 based on simulation is satisfactory as shown in Fig. 5.19. It can be noted that ANN5 is trained using [1x30] dataset. As presented in Section 5.3, the behaviour of the dc-link voltage at nominal power level, the motor speed and torque waveforms obtained from the simulation is shown in Fig. 5.7 and Fig. 5.8. ANN5 is tested to estimate the capacitance value at constant capacitance condition under different loading conditions. The estimated capacitance by ANN5 with the corresponding estimation error are listed in Table 5.6.

In order to simplify the training data collection process, additional ANN is trained based on minimum and maximum boundaries that corresponds to the capacitance steps; (C_0, C_1, C_8 and C_9). The ANN trained based on

Table 5.6: Simulation Results for Estimated Capacitance by ***ANN5*** Under Different Loading Conditions.

Actual Value	$ANN4_{Estimation}$	$ANN4_{Error}$	Power Level
566 μF	566.5 μF	0.08%	2 kW
555 μF	554.1 μF	0.16%	3 kW
544 μF	544.9 μF	0.16%	4 kW
566 μF	561.9 μF	0.8%	4 kW

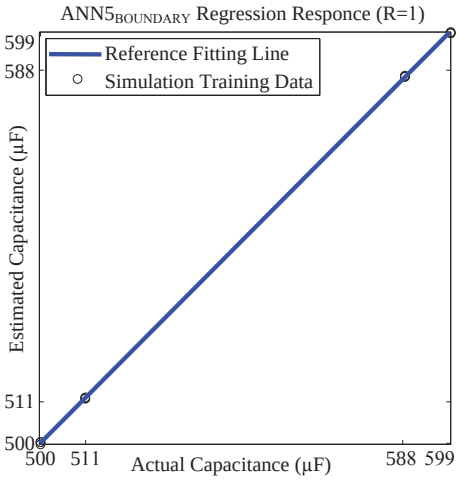

Fig. 5.20: Regression response of the proposed trained $ANN5_{BOUNDARY}$ based on simulation training dataset.

boundaries is referred to as $ANN5_{BOUNDARY}$. The regression response of $ANN5_{BOUNDARY}$ based on simulation is satisfactory as shown in Fig. 5.20. It can be noted that $ANN5_{BOUNDARY}$ is trained using [1x12] dataset. It is Expected that $ANN5_{BOUNDARY}$ is able to estimate the in-between capacitance values which $ANN5_{BOUNDARY}$ did not consider in the training. $ANN5_{BOUNDARY}$ is tested to estimate the capacitance value at constant capacitance condition under different loading conditions. The estimated capacitance by $ANN5_{BOUNDARY}$ with the corresponding estimation error are listed in Table 5.7. More detailed description of the training based on boundaries is given in the experimental case study.

By comparing the estimated error from Table 5.6 and Table 5.7, it is concluded that using boundaries information could be satisfying for capacitance estimation.

Table 5.7: Simulation Results for Estimated Capacitance by $ANN5_{BOUNDARY}$ Under Different Loading Conditions.

Actual Value	$ANN4_{Estimation}$	$ANN4_{Error}$	Power Level
566 μF	553 μF	2.3%	2 kW
555 μF	553.5 μF	0.3%	3 kW
544 μF	549.5 μF	1.0%	4 kW
566 μF	574.5 μF	1.5%	4 kW

5.7 Experimental Case of ANN5

For ANN5, the estimation is based on the dc-link voltage harmonics. Three different power ratings including the nominal power level are also considered. The training data are obtained from the motor drive shown in Fig. 5.4. The training data collected for ANN5 with respect to capacitance steps and the three considered power levels are shown in Fig. 5.21.

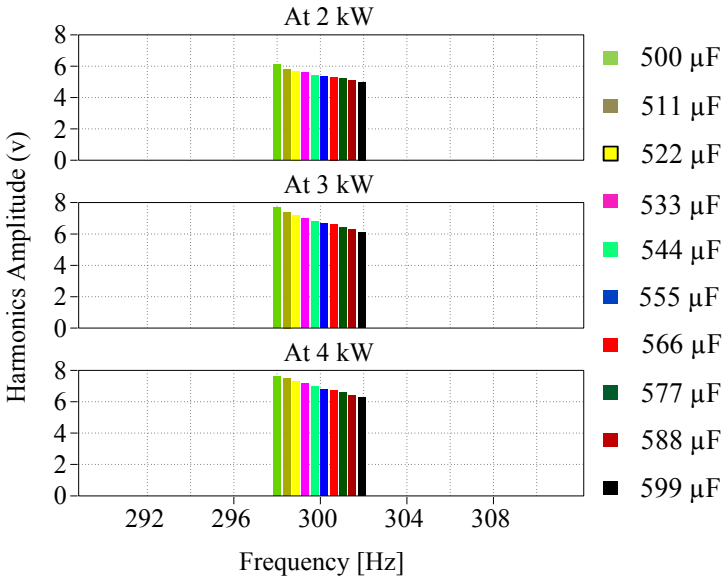

Fig. 5.21: Collected dc-link voltage harmonics dataset for training and testing of *ANN5*.

A linear relationship between dc-link voltage harmonic amplitudes and the capacitance and loading power variation can be seen. For each power rating, there are 10 dataset of the capacitance values used to train ANN5. These 10 dataset are in the range between 500 μF and 599 μF with 11 μF step.

ANN5 is using the corresponding dc-link voltage harmonics component at 300 Hz frequency to each capacitance step. Since there are 3 power levels are considered, 30 training dataset are collected. ANN5 is fed with a training dataset dimension of [1x30].

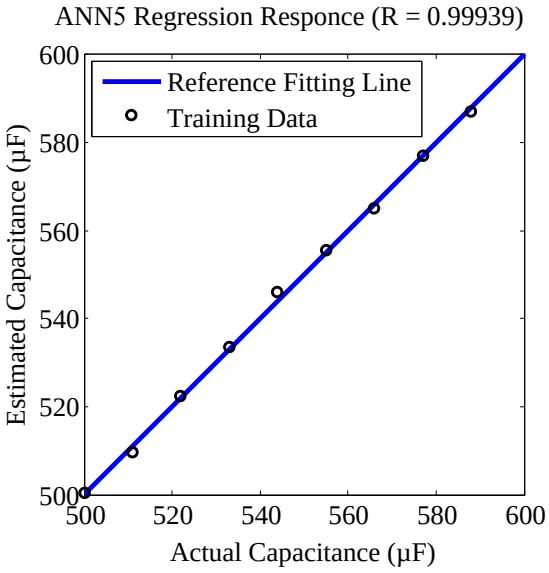

Fig. 5.22: Regression response of the proposed trained *ANN5*.

The regression response of ANN5 is shown in Fig. 5.22. For ANN5 the regression response equals to 0.99939. The regression response for ANN5 means a very strong correlation between inputs and targets. Since the regression response is satisfactory, trained ANN5 is generated as a SIMULINK models for capacitance estimation. Afterwards, the generated ANN5 is ready for testing.

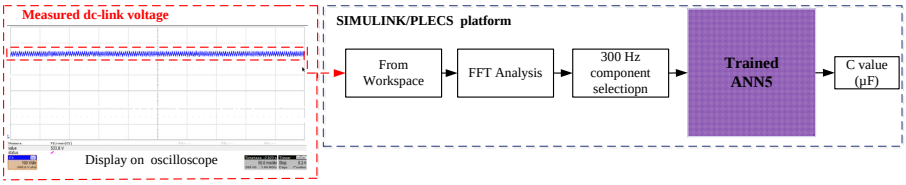

Fig. 5.23: Process of the proposed capacitor condition monitoring methodology based on the proposed *ANN5*.

The process of the capacitor condition monitoring method for ANN5 is shown in Fig. 5.23. For ANN5, the dc-link voltage waveform is imported to

Matlab workspace and applied to an FFT analysis. Only the 300 Hz component is considered in capacitance estimation. In order to test the generated ANN5, 2 case studies are applied. The purpose of studying these cases are in the sake of testing the trained ANN5 and whether it is able to estimate the capacitance value under different conditions. Analysing the estimation error for ANN5 is also included. Accuracy analysis with respect to the training data amount, source and type are also given.

5.7.1 Constant Capacitance Condition

In this case study, different capacitance values are selected to be estimated by the trained ANN5. The dc-link capacitance value in the motor drive is adjusted to 533 μF.

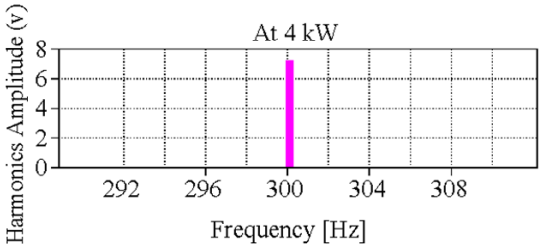

Fig. 5.24: Captured signal of the corresponding dc-link voltage harmonic amplitude at C = 533 μF, and at 300 Hz operating at 4 kW.

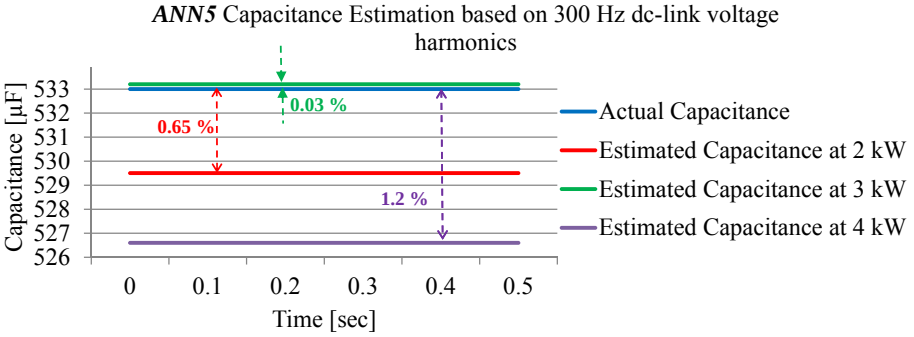

Fig. 5.25: The capacitance estimation of C = 533 μF by the trained *ANN5* under different loading conditions.

The estimated results and the estimation error by ANN5 are shown in Fig. 5.25. More capacitance estimation results are listed in Table 5.8.

Table 5.8: Experimental Results for Estimated Capacitance by ***ANN5*** Under Different Loading Conditions.

Actual Value	$ANN5_{Estimation}$	$ANN5_{Error}$	Power Level
566 μF	560.4 μF	0.1%	2 kW
555 μF	555.4 μF	0.07%	3 kW
544 μF	545.3 μF	0.2%	4 kW
566 μF	570.2 μF	0.75%	4 kW

5.7.2 ANN5 Boundaries Training

In this case study, the impact of training data amount, type and source is investigated. The purpose is to analyse the ANN behaviour and estimation error with respect to the considered training dataset. The same structure of ANN5 is studied in this section and referred to as $ANN5_{BOUNDARY}$. The considered training dataset for $ANN5_{BOUNDARY}$ is shown in Fig. 5.26.

It can be seen that the considered training dataset are covering only the minimum and maximum boundaries. $ANN5_{BOUNDARY}$ is fed with a training dataset dimension of [1x12]. The regression response of $ANN5_{BOUNDARY}$ is shown in Fig. 5.27.

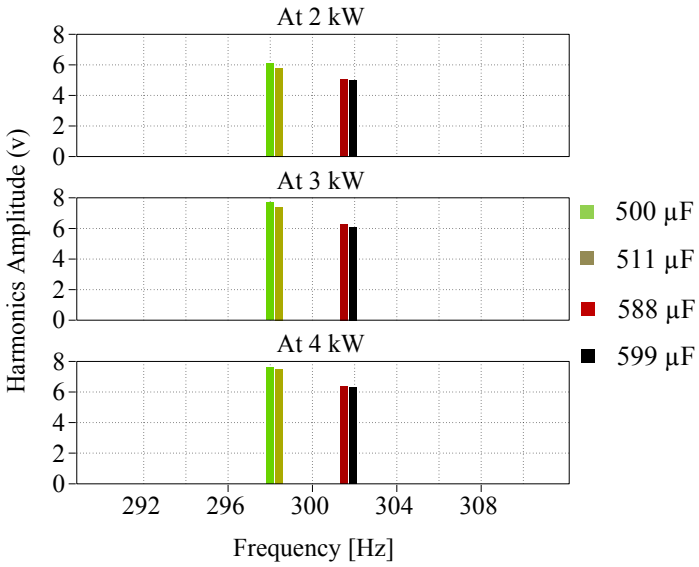

Fig. 5.26: Considered boundaries of dc-link voltage harmonics dataset for training $ANN5_{BOUNDARY}$.

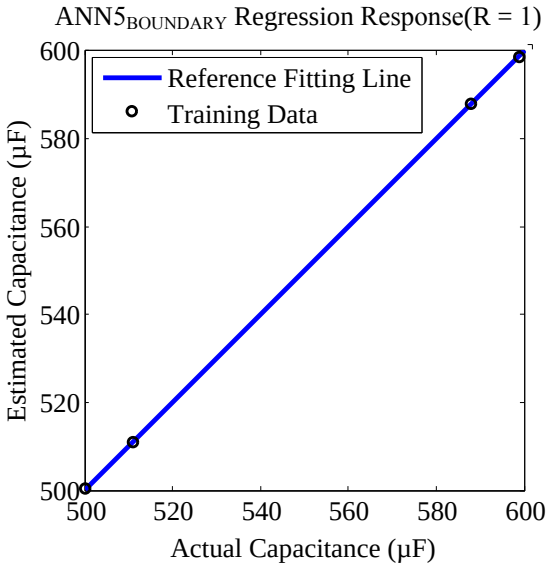

Fig. 5.27: Regression response of the proposed trained ANN5$_{BOUNDARY}$.

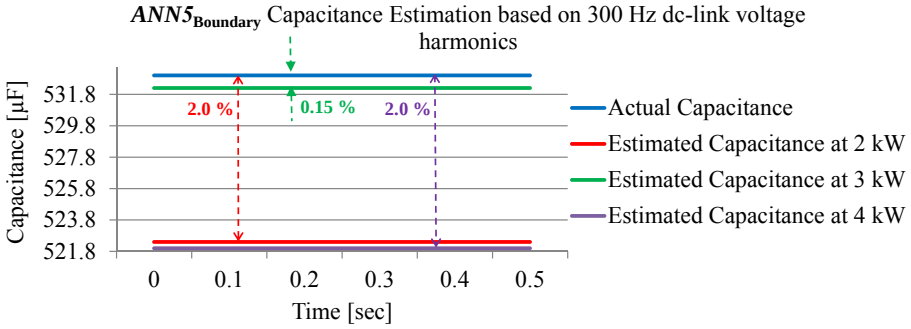

Fig. 5.28: The capacitance estimation of C = 533 μF by the trained $ANN5_{BOUNDARY}$ under different loading conditions.

The trained ANN5$_{BOUNDARY}$ is expected to estimate the values between these boundaries. Similar setting in 5.4.1 is considered. The estimated results and the estimation error by ANN5$_{BOUNDARY}$ are shown in Fig. 5.28. More capacitance estimation results are listed in Table 5.9.

Table 5.9: Experimental Results for Estimated Capacitance by $\boldsymbol{ANN5_{BOUNDARY}}$ Under Different Loading Conditions.

Actual Value	$ANN5_{Estimation}$	$ANN5_{Error}$	Power Level
566 μF	554.7 μF	2%	2 kW
555 μF	558.4 μF	0.6%	3 kW
544 μF	538.4 μF	1%	4 kW
566 μF	558.5 μF	1.3%	4 kW

5.8 Summary

An experimental validation of capacitor condition monitoring based on ANN is presented in this chapter. The experiments are conducted on a three-phase motor drive. A switchable capacitor bank is designed to change the capacitance value and connected to the existing dc-link capacitor for data collection and testing purposes. Importing the dc-link voltage and phase A output current to MATLAB have been applied. The imported parameters are used to train and test the ANN. Two proposed ANNs that estimate the capacitance value are studied with respect to the considered parameters. The dc-link voltage harmonic analysis is also discussed in this chapter. The dc-link voltage harmonics behaviour shows a linear relationship with respect to the capacitance variation. This linear relationship have been an advantage to the capacitor condition monitoring.

Two case studies are applied to the proposed ANNs. By comparing the estimated capacitance and their estimation error from Table 5.4 and Table 5.8, it can be seen that capacitance estimation based on dc-link voltage harmonics gave slightly lower estimation error. However, for both ANN4 and ANN5, the maximum estimation error is 1.3% and 1.2%, respectively. For the case study presented in Section 5.4.2 and Section 5.6.2, the estimation error for both $ANN4_{BOUNDARY}$ and $ANN5_{BOUNDARY}$ are much higher -as expected- comparing it to the case study in Section 5.4.1 and Section 5.6.1. The higher estimation error is due to the lower training dataset. It can be also noted that capacitance estimation based on dc-link voltage harmonics gave slightly higher estimation accuracy. However, the maximum estimation error based on dc-link voltage harmonics is 2%. While the maximum estimation error based on dc-link voltage ripple and current is 2.5%.

Chapter. 6

Conclusions

6.1 Summary and Future Work

This Chapter summarizes the main conclusions and the research outcomes. The main contribution and future research in the field of capacitor condition monitoring are also given.

The main goal of this project is to investigate the existing capacitor condition monitoring methodologies in order to develop a new cost-effective method to monitor the change of the electrical parameters of capacitors for dc-link application. The hypotheses of this project is that the health status of the dc-link capacitor can be estimated by estimating its capacitance value.

Chapter 1 in this thesis presents the introduction of this research project, which includes a background in dc-link capacitor types, their construction and mode of failure, general reliability assessment methods. It is also include problem formulation, project motivation, objectives and limitations assumptions done in the work.

In *Chapter 2*, the existing capacitor condition monitoring methodologies are reviewed and classified. The review identifies the limitations and shortcomings of the existing methodologies and the promising aspects of them. Moreover, through tracing the history of the technology evolution, the review is able to explore the points of strength. Thereby, development of future research that contribute to more practical applications can be achieved.

In *Chapter 3*, a discussion on the concept and structure of ANN algorithm

technology is given. Description of the training process, the ANN type and its mathematical structure is also presented.

Applying the proposed ANN on three-phase front-end diode bridge converter for capacitor condition monitoring purposes is presented as a contribution in *Chapter 4*. This Chapter can be divided into three stages with respect to the ANN training data amount, type and source. First, the ANN is trained based on an input/output terminal information that are corresponding to a certain value of capacitance. The input/output terminal information are currents and voltages in addition to dc-link ripple voltage. Secondly, in order to achieve high capacitance estimation accuracy with the least possible information, the amount of the training data is reduced by considering only input current and dc-link ripple voltage. Finally, in order to be convincing from practical applications in industry, the ANN considered the output current and dc-link ripple voltage for the purpose of capacitance estimation in order to use already existing signals.

As a proof of concept to the proposed methodology in *Chapter 4*, a *DSP* is used as a hardware platform. The ANN is trained in Matlab based on the information provided by the simulation converter, and afterwards trained ANN is generated as a SIMULINK model. The proof of the concept is to integrate the trained ANN into the DSP by converting the SIMULINK model into an equivalent C-code that is compatible with DSP. The ANN is tested and estimated accurate capacitance values. Since the ANN is trained on simulation information, it is also tested based on simulation information. Therefore, validating the proposed methodology based on practical information is essential in order to enrich the research in the field of capacitor condition monitoring.

A motor drive provided by Danfoss is used as a practical validation in *Chapter 5*. In order to apply data collection in practice, a PCB with capacitors is designed and connected in parallel to the existing dc-link capacitor. The capacitor board is also used for testing purposes. The connected capacitor PCB has no impact on the operation of the motor drive. Importing the dc-link voltage and phase A output current to MATLAB have been applied. The imported parameters are used to train and test the ANN. Two proposed ANNs that estimate the capacitance value are studied with respect to the considered parameter. The dc-link voltage harmonics analysis is also discussed. The dc-link voltage harmonics behaviour shows a linear relationship with respect to the capacitance variation. This linear relationship have been an advantage to capacitor condition monitoring.

6.2 Main Contributions

The main contributions in this research can be summarized in the following points:

- Review of existing capacitor condition monitoring methodologies: The most common methods of capacitor condition monitoring are reviewed and classified into 3 categories. It serves as the purpose to identify the existing limitations of the existing methodologies and exploring the points of strength to develop future research that contribute to more practical applications by tracing the process history of condition monitoring technology. The given review is also highlighting the life-time indicators that should be considered for capacitor condition monitoring nevertheless the methodology. Moreover, the review explains also the availability type of the existing methods and whether online or offline methodologies are essential for all the applications or just certain ones. Finally, the review gave a better understanding of the required methodology that could be the way-out of the existing shortcomings and to be more attracted to industry.

- Studying the impact of training data type, source and amount is also done. Generating the ANN after training process and integrating it inside a hardware platform -DSP- is successfully applied. The ANN performance evaluation under different structure is also presented.

- New software condition monitoring method: Using Artificial Neural Network (ANN) as a software algorithm for capacitor condition monitoring is proposed. Starting with a proposed ANN that estimate the capacitance of the dc-link capacitor in two different simulation topologies have presented. The first proposed ANN considered all the existing input/output terminal information. Afterwards, less information are considered in order to achieve high accuracy with less requirements. Therefore, the ANN succeed to estimate the capacitance based on dc-link voltage ripple and single phase output current. The ANN achieved high estimation accuracy under different capacitance and loading conditions. Analysing the dc-link voltage harmonics have been a great advantage for capacitor condition monitoring. Investigating into the capacitance value impact on the dc-link voltage harmonic amplitudes under different loading conditions is discussed. An experimental validation of the proposed ANNs is conducted. Whether the ANN is considering dc-link voltage ripple and single phase output current, or dc-link voltage harmonics, the capacitance estimation accuracy is high and

acceptable.

6.3 Future Work

- *Film-Capacitor condition monitoring*: As the Metallized Polypropylene Film Capacitors (*MPPF-Caps*) are discussed from construction and mode of failure aspects; as a future work, the proposed condition monitoring based on ANN algorithm can be applied. A Three-Phase Back-to-Back converter topology can be considered for this future work.

- *New methods to obtain the required training data*: As a future work, different criteria of training data collection is with interest. The new criteria in based on software, where the dc-link capacitance value itself will be varied as a replacement of the capacitor PCB. A designed code that change the operating frequency range, and hence, change the dc-link capacitor characteristic will be investigated. The impact of the intended criteria is not yet investigated.

- *Transient detection and discard of estimated capacitance during transients*: Taking into consideration some transient case studies could be an interesting investigation. The transient conditions will take place during operation and could be divided in tow-folds; a) changing the loading condition at a certain instant by speeding up the motor, and hence, increasing the power level, b) varying the capacitance value of the dc-link capacitor. For both folds, the corresponding waveforms of dc-link voltage and single phase output current will be captured. The captured waveforms will be applied for signal processing in order to feed them to the trained relevant ANN. The purpose is to investigate whether the ANN is able to estimate the capacitance value, and how high the estimation error and/or accuracy would be.

- *Experimental validation under un-balanced grid conditions*: As stated earlier in this project, the experimental part is conducted under balanced grid conditions. Considering un-balanced grid conditions is beneficial in order to generalize the proposed methodology and to apply it for wider operation conditions. Moreover, in case of un-balanced grid conditions, other frequency components than 300 Hz will be dominant. It is expected to have two more dominant features; a) $F3$ feature which will appear as a 100 Hz frequency component, b) $F4$ feature which will

appear as a 200 Hz frequency component. Both feature will be included as training data in addition to the 300 Hz components in order to generate general ANN the is able to estimate the capacitance under balanced and un-balanced grid conditions.

- *Clustering ANN and K-Nearest Neighbour (KNN)*: Investigate on new software algorithms is also intended as a future work. Since the proposed ANN for capacitance estimation considers different power levels, it can be noted that the capacitance steps are repeated in the target layer of the ANN. Therefore, it could also be considered as clustering problems, and hence, clustering and classifying solvers could be applied such as Clustering ANN and/or KNN. In the aforementioned algorithms, the capacitance value itself is no longer estimated, but the capacitance value will be classified in a pre-known category.

References

[1] Bayesian regularization backpropagation - matlab trainbr. [Online]. Available: http://se.mathworks.com/help/nnet/ref/nntool.html

[2] Digital signal controllers (dscs) - data manual. [Online]. Available: http://www.ti.com/lit/ds/symlink/tms320f28335.pdf.

[3] Electronics and electrical components information. [Online]. Available: http://anilcomponentengg.blogspot.dk/

[4] Electronics tutorials. [Online]. Available: http://www.electronics-tutorials.ws/category/capacitor

[5] General descriptions of aluminum electrolytic capacitors. [Online]. Available: http://www.nichicon.co.jp/english/products/pdf/aluminum.pdf

[6] House price estimation. [Online]. Available: https://se.mathworks.com/help/nnet/examples/house-price-estimation.html.

[7] Shenzhen electronics. [Online]. Available: http://www.szsrdz.com/English/

[8] Vishay. [Online]. Available: http://www.vishay.com/docs/40021/wtintro.pdf

[9] Vlt-danfoss automation drive. [Online]. Available: http://files.danfoss.com/documents/PE/MG33BF22.pdf

[10] "Capacitors age and capacitors have an end of life - white paper," in *Emerson Network Power*, 2015.

[11] K. Abdennadher, P. Venet, G. Rojat, J.-M. Retif, and C. Rosset, "A real-time predictive-maintenance system of aluminum electrolytic capacitors used in uninterrupted power supplies," *IEEE Transactions on Industry Applications*,, vol. 46, no. 4, pp. 1644–1652, July 2010.

[12] K. Abdennadher, P. Venet, G. Rojat, J. Retif, and C. Rosset, "Kalman filter used for on line monitoring and predictive maintenance system of aluminium electrolytic capacitors in ups," in *Proc. of IEEE Energy Conversion Congress and Exposition, (ECCE)*, Sept 2009, pp. 3188–3193.

[13] ——, "Online monitoring method and electrical parameter ageing laws of aluminium electrolytic capacitors used in ups," in *Proc. of 13th European Conference on Power Electronics and Applications, EPE '09.*, Sept 2009, pp. 1–9.

[14] A. Abo-Khalil and D.-C. Lee, "Dc-link capacitance estimation in ac/dc/ac pwm converters using voltage injection," *IEEE Transactions on Industry Applications,*, vol. 44, no. 5, pp. 1631–1637, Sept 2008.

[15] E. Aeloiza, J.-H. Kim, P. Enjeti, and P. Ruminot, "A real time method to estimate electrolytic capacitor condition in pwm adjustable speed drives and uninterruptible power supplies," in *Proc. of IEEE 36th Power Electronics Specialists Conference, (PESC)*, June 2005, pp. 2867–2872.

[16] M. Ahmad, A. Arya, and S. Anand, "An online technique for condition monitoring of capacitor in pv system," in *Proc. of IEEE International Conference on Industrial Technology (ICIT)*, March 2015, pp. 920–925.

[17] A. Amaral, G. Buatti, H. Ribeiro, and A. Cardoso, "Using dft to obtain the equivalent circuit of aluminum electrolytic capacitors," in *Proc. of 7th International Conference on Power Electronics and Drive Systems, PEDS '07.*, Nov 2007, pp. 434–438.

[18] A. Amaral and A. Cardoso, "Use of esr to predict failure of output filtering capacitors in boost converters," in *Proc. of IEEE International Symposium on Industrial Electronics,*, vol. 2, May 2004, pp. 1309–1314 vol. 2.

[19] ——, "An esr meter for high frequencies," in *Proc. of International Conference on Power Electronics and Drives Systems, (PEDS)*, vol. 2, 2005, pp. 1628–1633.

[20] ——, "An experimental technique for estimating the aluminum electrolytic capacitor equivalent circuit, at high frequencies," in *Proc. of IEEE International Conference on Industrial Technology, (ICIT)*, Dec 2005, pp. 86–91.

[21] ——, "An experimental technique for estimating the esr and reactance intrinsic values of aluminum electrolytic capacitors," in *Proc. of IEEE Instrumentation and Measurement Technology Conference, (IMTC)*, April 2006, pp. 1820–1825.

[22] ——, "Using newton-raphson method to estimate the condition of aluminum electrolytic capacitors," in *Proc. of IEEE International Symposium on Industrial Electronics, (ISIE)*, June 2007, pp. 827–832.

[23] ——, "An automatic technique to obtain the equivalent circuit of aluminum electrolytic capacitors," in *Proc. of 34th Annual Conference of IEEE Industrial Electronics, (IECON)*, Nov 2008, pp. 539–544.

[24] ——, "An economic offline technique for estimating the equivalent circuit of aluminum electrolytic capacitors," *IEEE Transactions on Instrumentation and Measurement,*, vol. 57, no. 12, pp. 2697–2710, Dec 2008.

[25] ——, "A non-invasive technique for fault diagnosis of smps," in *Proc. of IEEE Power Electronics Specialists Conference, (PESC)*, June 2008, pp. 2097–2102.

[26] ——, "A simple offline technique for evaluating the condition of aluminum electrolytic capacitors," *IEEE Transactions on Industrial Electronics,*, vol. 56, no. 8, pp. 3230–3237, Aug 2009.

[27] ——, "State condition estimation of aluminum electrolytic capacitors used on the primary side of atx power supplies," in *Proc. of 35th Annual Conference of IEEE Industrial Electronics, (IECON)*, Nov 2009, pp. 442–447.

[28] ——, "Using a sinosoidal pwm to estimate the esr of aluminum electrolytic capacitors," in *Proc. of International Conference on Power Engineering, Energy and Electrical Drives, (POWERENG).*, March 2009, pp. 691–696.

[29] ——, "Using input current and output voltage ripple to estimate the output filter condition of switch mode dc/dc converters," in *Proc. of IEEE International Symposium on Diagnostics for Electric Machines, Power Electronics and Drives, (SDEMPED)*, Aug 2009, pp. 1–6.

[30] ——, "Estimating aluminum electrolytic capacitors condition using a low frequency transformer together with a dc power supply," in *Proc. of IEEE International Symposium on Industrial Electronics (ISIE)*, July 2010, pp. 815–820.

[31] ——, "Simple experimental techniques to characterize capacitors in a wide range of frequencies and temperatures," *IEEE Transactions on Instrumentation and Measurement,*, vol. 59, no. 5, pp. 1258–1267, May 2010.

[32] ——, "On-line fault detection of aluminium electrolytic capacitors, in step-down dc-dc converters, using input current and output voltage ripple," *IET Power Electronics,*, vol. 5, no. 3, pp. 315–322, March 2012.

[33] C. M. Bishop, *Neural Networks for Pattern Recognition*. New York, NY, USA: Oxford University Press, Inc., 1995.

[34] M. A. Brubaker, D. E. Hage, T. A. Hosking, H. C. Kirbie, and E. D. Sawyer, "Increasing the life of electrolytic capacitor banks using integrated high performance film capacitors," presented at the europe power conversion intelligent motion (pcim), nuremberg, germany," 2013.

[35] G. Buiatti, A. Amaral, and A. Cardoso, "Esr estimation method for dc/dc converters through simplified regression models," in *Proc. of Conference Record of the IEEE Industry Applications Conference, 42nd IAS Annual Meeting.*, Sept 2007, pp. 2289–2294.

[36] G. Buiatti, A. Amaral, and A. Marques Cardoso, "Parameter estimation of a dc/dc buck converter using a continuous time model," in *Proc. of European Conference on Power Electronics and Applications*, Sept 2007, pp. 1–8.

[37] G. Buiatti, J. Martin-Ramos, A. Amaral, P. Dworakowski, and A. Marques Cardoso, "Condition monitoring of metallized polypropylene film capacitors in railway power trains," *IEEE Transactions on Instrumentation and Measurement,*, vol. 58, no. 10, pp. 3796–3805, Oct 2009.

[38] G. Buiatti, J. Martin-Ramos, C. Garcia, A. Amaral, and A. Marques Cardoso, "An online and noninvasive technique for the condition monitoring of capacitors in boost converters," *IEEE Transactions on Instrumentation and Measurement,*, vol. 59, no. 8, pp. 2134–2143, Aug 2010.

[39] Y.-M. Chen, H.-C. Wu, M.-W. Chou, and K.-Y. Lee, "Online failure prediction of the electrolytic capacitor for lc filter of switching-mode power converters," *IEEE Transactions on Industrial Electronics,*, vol. 55, no. 1, pp. 400–406, Jan 2008.

[40] H. Chung, H. Wang, F. Blaabjerg, and M. Pecht, *Reliability of Power Electronics Converter Systems*. The Institution of Engineering and Technology (IET), Dec. 2015.

[41] F. M. I. D. Astigarraga, F. Arizti and A. Galarza, "Estimation of dc-link capacitor equivalent series resistance for in-vehicle prognostic health monitoring," *Proc. of Energy Challenges and Machines, Third International Symposium on*, 2015.

[42] I. S. de Freitas, C. B. Jacobina, and E. C. dos Santos Jr., "Single-phase to single-phase full-bridge converter operating with reduced ac power in the dc-link capacitor," *IEEE Transactions on Power Electronics*, vol. 25, no. 2, pp. 272–279, Feb 2010.

[43] R. Deshpande, *Capacitors: Technology and Trends*. McGraw-Hill Education, 2014. [Online]. Available: https://books.google.dk/books?id=rFGoBAAAQBAJ

[44] M. Gasperi, "Life prediction model for aluminum electrolytic capacitors," in *Proc. of Conference Record of the IEEE Industry Applications Conference, Thirty-First IAS Annual Meeting, (IAS)*, vol. 3, Oct 1996, pp. 1347–1351 vol.3.

[45] ——, "Life prediction modeling of bus capacitors in ac variable-frequency drives," *IEEE Transactions on Industry Applications,*, vol. 41, no. 6, pp. 1430–1435, Nov 2005.

[46] K. Harada, A. Katsuki, and M. Fujiwara, "Use of esr for deterioration diagnosis of electrolytic capacitor," *IEEE Transactions on Power Electronics,*, vol. 8, no. 4, pp. 355–361, Oct 1993.

[47] J.-S. K. J.-M. K. Hong-Jun Heo, Won-Sang Im, "A Capacitance Estimation of Film Capacitors in an LCL-Filter of Grid-Connected PWM Converters," *Journal of Power Electronics*, vol. 13, pp. 94–103, 2013. [Online]. Available: http://www.dbpia.co.kr/Article/NODE02074217

[48] G.-B. Huang, "Learning capability and storage capacity of two-hidden-layer feedforward networks," *IEEE Transactions on Neural Networks*, vol. 14, no. 2, pp. 274–281, Mar 2003.

[49] A. Imam, D. Divan, R. Harley, and T. Habetler, "Real-time condition monitoring of the electrolytic capacitors for power electronics applications," in *Proc. of Twenty Second Annual IEEE Applied Power Electronics Conference, (APEC)*, Feb 2007, pp. 1057–1061.

[50] A. Imam, T. Habetler, R. Harley, and D. Divan, "Failure prediction of electrolytic capacitor using dsp methods," in *Proc. of Twentieth Annual IEEE Applied Power Electronics Conference and Exposition, (APEC)*, vol. 2, March 2005, pp. 965–970 Vol. 2.

[51] ——, "Condition monitoring of electrolytic capacitor in power electronic circuits using adaptive filter modeling," in *Proc. of IEEE 36th Power Electronics Specialists Conference, (PESC)*, June 2005, pp. 601–607.

[52] ——, "Condition monitoring of electrolytic capacitor in power electronic circuits using input current," in *Proc. of 5th IEEE International Symposium on Diagnostics for Electric Machines, Power Electronics and Drives, (SDEMPED)*, Sept 2005, pp. 1–7.

[53] ——, "Lms based condition monitoring of electrolytic capacitor," in *Proc. of 31st Annual Conference of IEEE Industrial Electronics Society, (IECON)*, Nov 2005, pp. 6 pp.–.

[54] Y.-J. Jo, T. H. Nguyen, and D.-C. Lee, "Condition monitoring of submodule capacitors in modular multilevel converters," in *Proc. of IEEE Energy Conversion Congress and Exposition (ECCE)*, Sept 2014, pp. 2121–2126.

[55] B. W. Johnson, "Fault-tolerant microprocessor-based systems," *IEEE Micro*, vol. 4, no. 6, pp. 6–21, Dec 1984.

[56] Y. Kai, H. Wenbin, T. Weijie, L. Jianguo, and C. Jingcheng, "A novel online esr and c identification method for output capacitor of buck converter," in *Proc. of IEEE Energy Conversion Congress and Exposition, (ECCE)*, Sept 2014, pp. 3476–3482.

[57] T. Kamel, Y. Biletskiy, and L. Chang, "Capacitor aging detection for the dc filters in the power electronic converters using anfis algorithm," in *Proc. of 28th Canadian Conference on Electrical and Computer Engineering (CCECE)*, May 2015, pp. 663–668.

[58] M. Kim, S.-K. Sul, and J. Lee, "Condition monitoring of dc-link capacitors in drive system for electric vehicles," in *Proc. of IEEE Vehicle Power and Propulsion Conference, (VPPC)*, Oct 2012, pp. 633–637.

[59] T. Kim, H. Adeli, R. J. Robles, and M. Balitanas, *Advanced Computer Science and Information Technology*. Springer, Sep. 2011.

[60] J. Koppinen, J. Kukkola, and M. Hinkkanen, "Parameter estimation of an lcl filter for control of grid converters," in *Proc. of 9th International Conference on Power Electronics and ECCE Asia, (ICPE-ECCE Asia)*, June 2015, pp. 1260–1267.

[61] A. Lahyani, P. Venet, G. Grellet, and P.-J. Viverge, "Failure prediction of electrolytic capacitors during operation of a switchmode power supply," *IEEE Transactions on Power Electronics,*, vol. 13, no. 6, pp. 1199–1207, Nov 1998.

[62] D.-C. Lee, K.-J. Lee, J.-K. Seok, and J.-W. Choi, "Online capacitance estimation of dc-link electrolytic capacitors for three-phase ac/dc/ac pwm converters using recursive least squares method," *in IEE Proceedings of Electric Power Applications,*, vol. 152, no. 6, pp. 1503–1508, Nov 2005.

[63] K.-W. Lee, M. Kim, J. Yoon, K.-W. Lee, and J.-Y. Yoo, "Condition monitoring of dc-link electrolytic capacitors in adjustable-speed drives," *IEEE Transactions on Industry Applications,*, vol. 44, no. 5, pp. 1606–1613, Sept 2008.

[64] P. Lipnicki, M. Orkisz, D. Lewandowski, and A. Tresch, "The effect of change in dc link series resistance on the ac/ac converter operation: Power converters embedded diagnostics," in *Proc. of IEEE 1st International Conference on Condition Assessment Techniques in Electrical Systems, (CATCON)*, Dec 2013, pp. 122–127.

[65] S. A. Makdessi M. and V. P., "Health monitoring of dc link capacitors," *Chemical Engineering Transactions*, vol. 33, pp. 1105–1110, 2013.

[66] J.-J. Moon, W.-S. Im, and J.-M. Kim, "Capacitance estimation of dc-link capacitor in brushless dc motor drive systems," in *Proc. of IEEE ECCE Asia Downunder (ECCE-Asia)*, June 2013, pp. 525–529.

[67] D. A. Murdock, J. E. R. Torres, J. J. Connors, and R. D. Lorenz, "Active thermal control of power electronic modules," *IEEE Transactions on Industry Applications*, vol. 42, no. 2, pp. 552–558, March 2006.

[68] T. H. Nguyen and D.-C. Lee, "Deterioration monitoring of dc-link capacitors in ac machine drives by current injection," *IEEE Transactions on Power Electronics,*, vol. 30, no. 3, pp. 1126–1130, March 2015.

[69] O. Ondel, E. Boutleux, and P. Venet, "A decision system for electrolytic capacitors diagnosis," in *Proc. of IEEE 35th Annual Power Electronics Specialists Conference, (PESC).*, vol. 6, June 2004, pp. 4360–4364 Vol.6.

[70] P. Pelletier, J. M. Guichon, J. L. Schanen, and D. Frey, "Optimization of a dc capacitor tank," *IEEE Transactions on Industry Applications*, vol. 45, no. 2, pp. 880–886, March 2009.

[71] X.-S. Pu, T. H. Nguyen, D.-C. Lee, K.-B. Lee, and J.-M. Kim, "Fault diagnosis of dc-link capacitors in three-phase ac/dc pwm converters by online estimation of equivalent series resistance," *IEEE Transactions on Industrial Electronics,*, vol. 60, no. 9, pp. 4118–4127, Sept 2013.

[72] X. Pu, T.-H. Nguyen, D.-C. Lee, and S.-G. Lee, "Capacitance estimation of dc-link capacitors for single-phase pwm converters," in *Proc. of IEEE 6th Internationa Conference on Power Electronics and Motion Control (IPEMC)*, May 2009, pp. 1656–1661.

[73] K. V. Rao and K. R. Sudha, *Electronic Devices and Circuits*. McGraw Hill Education, 2015.

[74] F. K. C. M. M. S. Rudolf Kruse, Christian Borgelt and P. Held, *Computational Intelligence: A methodological introduction*. Springer), Dec. 2013.

[75] V. Sankaran, F. Rees, and C. Avant, "Electrolytic capacitor life testing and prediction," in *Proc. of Conference Record of the IEEE Industry Applications Conference, Thirty-Second IAS Annual Meeting, IAS '97.*, vol. 2, Oct 1997, pp. 1058–1065 vol.2.

[76] P. Scherz and S. Monk, *Practical Electronics for Inventors, Fourth Edition*. McGraw-Hill Education, 2016. [Online]. Available: https://books.google.dk/books?id=HZgXswEACAAJ

[77] S. Shili, A. Hijazi, P. Venet, A. Sari, X. Lin-Shi, and H. Razik, "Balancing circuit control for supercapacitor state estimation," in *Proc. of Tenth International Conference on Ecological Vehicles and Renewable Energies, (EVER)*, March 2015, pp. 1–7.

[78] H. Soliman, H. Wang, and F. Blaabjerg, "Capacitance estimation for dc-link capacitors in a back-to-back converter based on artificial neural network algorithm," in *in Procc. of IEEE 8th International Power Electronics and Motion Control Conference (IPEMC-ECCE Asia)*, May 2016, pp. 3682–3688.

[79] H. Soliman, H. Wang, B. Gadalla, and F. Blaabjerg, "Artificial neural network algorithm for condition monitoring of dc-link capacitors based on capacitance estimation," *Journal of Renewable Energy and Sustainable Development*, vol. 1, no. 2, pp. 294–299, Jan. 2016.

[80] H. Soliman, H. Wang, and F. Blaabjerg, "A review of the condition monitoring of capacitors in power electronic converters," *IEEE Transactions on Industry Applications,*, vol. 50, no. 5, pp. 3569–3578, Sept 2016.

[81] H. Soliman, H. Wang, B. Gadalla, and F. Blaabjerg, "Condition monitoring of dc-link capacitors based on artificial neural network algorithm," in *Proc. of IEEE Fifth International Conference on Power Engineering, Energy and Electrical Drives (POWERENG)*, May 2015, pp. 1–5.

[82] G. Vachtsevanos, F. L. Lewis, M. Roemer, A. Hess, and B. Wu, *Intelligent Fault Diagnosis and Prognosis for Engineering Systems*. John Wiley Sons, Inc., Oct. 2006.

[83] P. Venet, F. Perisse, M. El-Husseini, and G. Rojat, "Realization of a smart electrolytic capacitor circuit," *Industry Applications Magazine, IEEE*, vol. 8, no. 1, pp. 16–20, Jan 2002.

[84] M. Vogelsberger, T. Wiesinger, and H. Ertl, "Life-cycle monitoring and voltage-managing unit for dc-link electrolytic capacitors in pwm converters," *IEEE Transactions on Power Electronics,*, vol. 26, no. 2, pp. 493–503, Feb 2011.

[85] G. Wang, Y. Guan, J. Zhang, L. Wu, X. Zheng, and W. Pan, "Esr estimation method for dc-dc converters based on improved emd algorithm," in *Proc. of IEEE Conference on Prognostics and System Health Management, (PHM)*, May 2012, pp. 1–6.

[86] ——, "Esr estimation method for dc-dc converters based on improved emd algorithm," in *Proc. of IEEE Conference on Prognostics and System Health Management (PHM)*, May 2012, pp. 1–6.

[87] H. Wang, H. S. H. Chung, and W. Liu, "Use of a series voltage compensator for reduction of the dc-link capacitance in a capacitor-supported system," *IEEE Transactions on Power Electronics*, vol. 29, no. 3, pp. 1163–1175, March 2014.

[88] H. Wang and F. Blaabjerg, "Reliability of capacitors for dc-link applications in power electronic converters - an overview," *IEEE Transactions on Industry Applications,*, vol. 50, no. 5, pp. 3569–3578, Sept 2014.

[89] H. Wang, D. A. Nielsen, and F. Blaabjerg, "Degradation testing and failure analysis of dc film capacitors under high humidity conditions," *Microelectronics Reliability*, vol. 55, no. 9–10, pp. 2007 – 2011, 2015, in Proc. of the 26th European Symposium on Reliability of Electron Devices, Failure Physics and Analysis, (ESREF). [Online]. Available: http://www.sciencedirect.com/science/article/pii/S0026271415001419

[90] Z. Waszczysznk, *Neural Networks in the Analysis and Design of Structures*, ser. CISM International Centre for Mechanical Sciences. Springer Vienna, 2014. [Online]. Available: https://books.google.dk/books?id=ceptCQAAQBAJ

[91] A. Wechsler, B. Mecrow, D. Atkinson, J. Bennett, and M. Benarous, "Condition monitoring of dc-link capacitors in aerospace drives," *IEEE Transactions on Industry Applications,*, vol. 48, no. 6, pp. 1866–1874, Nov 2012.

[92] T. Wiesinger and H. Ertl, "A novel real time monitoring unit for pwm converter electrolytic capacitors," in *Proc. of IEEE Power Electronics Specialists Conference, (PESC)*, June 2008, pp. 523–528.

[93] E. Wolfgang, "Examples for failures in power electronics systems," *ECPE Tutorial on Reliability of Power Electronic Systems*,, Germany, April 2007.

[94] S. Yang, D. Xiang, A. Bryant, P. Mawby, L. Ran, and P. Tavner, "Condition monitoring for device reliability in power electronic converters: A review," *IEEE Transactions on Power Electronics*,, vol. 25, no. 11, pp. 2734–2752, Nov 2010.

[95] Y. Yu, T. Zhou, M. Zhu, and D. Xu, "Fault diagnosis and life prediction of dc-link aluminum electrolytic capacitors used in three-phase ac/dc/ac converters," in *Proc. of Second International Conference on Instrumentation, Measurement, Computer, Communication and Control (IMCCC)*, Dec 2012, pp. 825–830.

CV

Name	Hammam A. H. Soliman
Date of Birth	1^{st} *June*1986
Place of Birth	Al-Ain City, United Arab Emirates
Citizen of	Egypt
Education	2005-2010 B.Sc. in Electrical and Control Engineering, Specialization:Power System Substations, Arab Academy for Science, Technology and Maritime Transport. Cairo-Egypt. 2010-2013 M.Sc. in Electrical and Control Engineering, Specialization: Wind Energy, Arab Academy for Science, Technology and Maritime Transport, Cairo-Egypt. 2014-2017 Ph.D. Studies at Aalborg University, Department of Energy Technology, Denmark
Work	2010-2013 Teaching Assistant, Electrical and Control Department, Arab Academy for Science, Technology and Maritime Transport, Cairo-Egypt. 2011-2012 Design Engineer, Al-Bahrawy Consultancy Group, Cairo-Egypt. 2014-2017 PhD Fellow at Aalborg University, Department of Energy Technology, Denmark.

A Review of the Condition Monitoring of Capacitors in Power Electronic Converters

Soliman, Hammam Abdelaal Hammam; Wang, Huai; Blaabjerg, Frede

Published in:
I E E E Transactions on Industry Applications

DOI (link to publication from Publisher):
10.1109/TIA.2016.2591906

Publication date:
2016

Document Version
Publisher's PDF, also known as Version of record

A Review of the Condition Monitoring of Capacitors in Power Electronic Converters

Hammam Soliman, *Student Member, IEEE*, Huai Wang, *Member, IEEE*, and Frede Blaabjerg, *Fellow, IEEE*

***Abstract*—Capacitors are one type of reliability-critical components in power electronic systems. In the last two decades, many efforts in academic research have been devoted to the condition monitoring of capacitors to estimate their health status. Industry applications are demanding more reliable power electronics products with preventive maintenance. Nevertheless, most of the developed capacitor condition monitoring technologies are rarely adopted by industry due to the complexity, increased cost, and other relevant issues. An overview of the prior-art research in this area is therefore needed to justify the required resources and the corresponding performance of each key method. It serves to provide a guideline for industry to evaluate the available solutions by technology benchmarking, as well as to advance the academic research by discussing the history development and the future opportunities. Therefore, this paper first classifies the capacitor condition monitoring methods into three categories, then the respective technology evolution in the last two decades is summarized. Finally, the state-of-the-art research and the future opportunities targeting for industry applications are given.**

***Index Terms*—Capacitance estimation, capacitance measurement, capacitor health status, condition monitoring, electrolytic capacitors (E-Caps), film capacitors, reliability.**

I. Introduction

CONDITION monitoring is an important method to estimate the health condition of power electronic components, converters, and systems. It is widely applied in reliable or safety-critical applications, such as wind turbines, electrical aircrafts, electric vehicles, etc., enabling the indication of future failure occurrences and preventive maintenance.

In [1], the condition monitoring of semiconductor devices used in power electronics is well reviewed. Besides active semiconductor devices, capacitors are another type of components that fail more frequently than other components in power electronic systems [2]. In the last two decades, there are a large number of scientific publications on the condition monitoring of capacitors, of which the relevant ones are discussed in this paper [3]–[64]. Nevertheless, the developed technologies are rarely adopted in industrial applications, due to the complexity, increased cost, and other relevant issues. Therefore, an overview of the existing methods is beneficial to both the industry application and academic research. It serves the following two purposes.

1) Benchmark different condition monitoring solutions and identify the promising aspects and limitations of them.
2) Trace the process history of the technology evolution and explore the future research opportunities that have the potential to contribute to more practical applications.

Three types of capacitors are generally available for power electronic applications, which are electrolytic capacitors (E-Caps), metallized poly propylene film capacitors (MPPF), and multilayer ceramic capacitors [65]. These types can be used in power conversion systems, filter applications, and snubber circuits.

In power electronics conversion systems, a single capacitor or a capacitor bank is usually used. The systems may malfunction if the single capacitor reaches the end of life. For the systems with capacitor banks, the time to failure of the multiple capacitors could vary. Once one of them fails, the other capacitors may withstand increased stresses, which accelerates their degradation. To ensure a reliable operation, it is recommended to replace the entire bank once one of the capacitors reaches the end of life [66].

The majority of the condition monitoring methods for both individual capacitors and capacitor banks are based on the

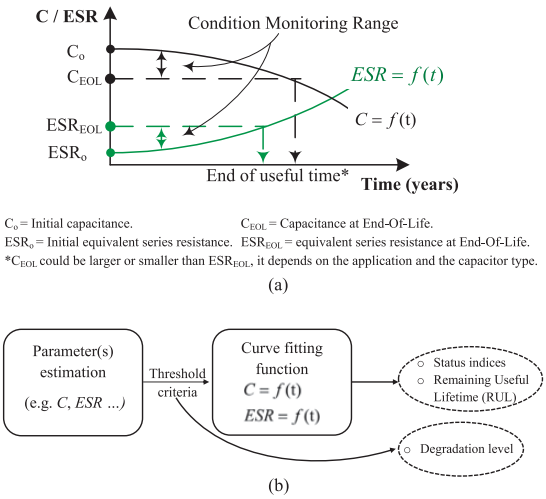

Fig. 1. Key indicators of condition monitoring and their steps. (a) Capacitance and ESR curves as an indication of capacitor degradation level. (b) Major steps of condition monitoring of capacitors.

Manuscript received December 17, 2015; revised May 1, 2016; accepted July 6, 2016. Date of publication July 19, 2016; date of current version November 18, 2016. Paper 2015-PEDCC-0996.R1, presented at the 2015 International Aegean Conference on Electrical Machines and Power Electronics, the 2015 International Conference on Optimization of Electrical and Electronic Equipment, and the 2015 International Symposium on Advanced Electromechanical Motion Systems, Side, Turkey, Sept. 2–4, and approved for publication in the IEEE TRANSACTIONS ON INDUSTRY APPLICATIONS by the Power Electronic Devices and Components Committee of the IEEE Industry Applications Society.

The authors are with the Department of Energy Technology, Aalborg University, Aalborg 9220, Denmark (e-mail: has@et.aau.dk; hwa@et.aau.dk; fbl@et.aau.dk).

Color versions of one or more of the figures in this paper are available online at http://ieeexplore.ieee.org.

Digital Object Identifier 10.1109/TIA.2016.2591906

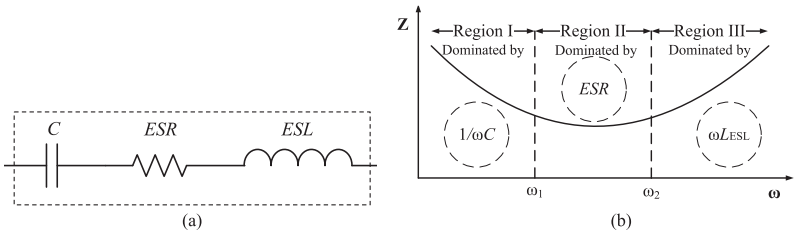

Fig. 2. Equivalent model and impedance characteristics of capacitors. (a) Simplified equivalent model of capacitors. (b) Impedance characteristics of capacitors.

estimation of the capacitance C and equivalent series resistance (ESR), which are typical indicators of the degradation of capacitors [67]. Based on the degradation curves in Fig. 1(a), and according to the block diagram shown in Fig. 1(b), an end of life or threshold criterion is needed before going further and decide the health condition of the capacitor. For aluminum E-Caps, the widely accepted end-of-life criterion is 20% capacitance reduction or double of the ESR. For film capacitors, a reduction of 2%–5% capacitance may indicate the reach of end of life. The range in between the initial value of capacitance/ESR and the aged value is the condition monitoring range, as shown in Fig. 1(a).

In [68], [69], the selection of those end-of-life criteria is based on two aspects to consider.

1) The capacitor degradation rate becomes considerably faster (e.g., dC/dt , dESR$/dt$) after the capacitance or ESR reaches the specified end-of-life criteria.
2) The power electronic conversion systems may not function appropriately when the capacitance drops or the ESR increases to a specified level.

The first aspect of the above consideration is usually the primary reason for the choice of the end-of-life criteria. The estimated capacitance or ESR value can be correlated to the capacitor health conditions in one of the following three ways.

1) An indication whether the capacitor fails or not, by comparing the estimated value to the specific end-of-life criteria.
2) A degradation level of the capacitor, by observing the difference between the estimated value and the specific end-of-life criteria. For this purpose, detailed capacitance or ESR degradation curve is not necessary.
3) An estimation of the remaining useful lifetime (RUL). It requires the knowledge of the capacitance or ESR degradation curves under specific operation conditions, which are usually obtained from the accelerated degradation testing data.

Fig. 2(a) shows a simplified equivalent model of capacitors and Fig. 2(b) plots the corresponding frequency characteristics. It can be noted that the capacitor impedance is distinguished by three frequency regions dominated by capacitance (C), the ESR and the equivalent series inductance (ESL), respectively. An overview of the reliability of capacitors in dc-link application is presented in [67]. The failure mechanisms, lifetime models, and dc-link design solutions are discussed. A brief discussion on the condition monitoring of capacitors is also given. Since the scope of [67] does not focus on the condition monitoring, no detailed discussion and critical comparison of the prior-art methods are provided. This paper intends to fill the gap in the literature and conducts a comprehensive overview on the research topic. Section II gives the classification of the existing condition monitoring methods. Section III outlines the technology development history of capacitor condition monitoring for the last two decades and the benchmark of these technologies. Section IV presents the future research opportunities.

II. Classification of Condition Monitoring Technologies for Capacitors

The condition monitoring methods for capacitors can be classified from three perspectives as shown in Fig. 3. The first perspective is the availability. If the health indicator can be obtained during the operation of the system, it is called an online condition monitoring. If an interruption of the system is required to obtain the health indicator, it is called an offline condition monitoring. The second perspective shows the type of the health indicator that is used for the condition monitoring. The third perspective is the methods to obtain the values of the specific indicator.

Accordingly, Fig. 3 shows the classification of the methods to obtain different health indicators. They are divided into three categories to be discussed in this paper.

The condition monitoring methods reviewed in this paper are mainly applied for single-stage dc–dc converters, dc–ac inverters, and two-stage ac/dc/ac converters. Figs. 4 and 5 show the topologies that will be discussed in this section. Fig. 4(a) is a boost converter and Fig. 4(b) is a buck converter.

Fig. 5 shows a generic structure of ac/dc/ac converters with either a diode-bridge rectifier or pulse-width modulation (PWM) rectifier as the first ac–dc stage. The definitions of the voltages, currents, and components are shown in the figure. Part of the representative condition monitoring methods discussed in [3]–[64] are listed in Table I. Table I shows the category of the respective method, the applied health indicator, and the principle for the indicator estimation. The information of the application case in terms of topology, power rating, and capacitance value are listed. A brief discussion of the advantages and disadvantages is also included. More specific details of these methods and applications will be discussed in this section.

A. Capacitor Ripple Current Sensor Based Methods

The basic concept in this category is to obtain the capacitance and/or ESR by using the capacitor voltage and ripple current information at regions I and II, respectively [as illustrated in

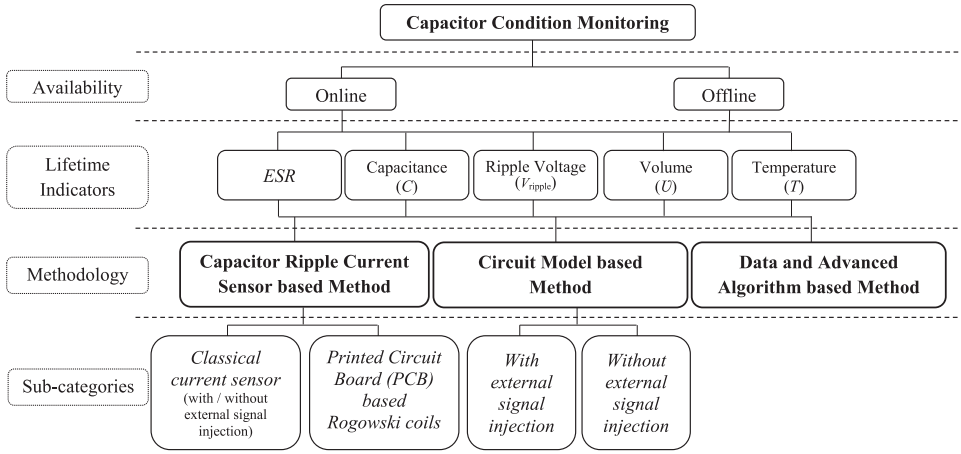

Fig. 3. Classification of capacitor condition monitoring technology and their indicators.

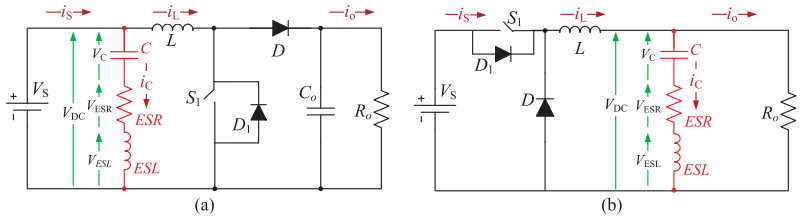

Fig. 4. Condition monitoring applications for single-stage dc–dc converters discussed in this paper. (a) Boost converter circuit. (b) Buck converter circuit.

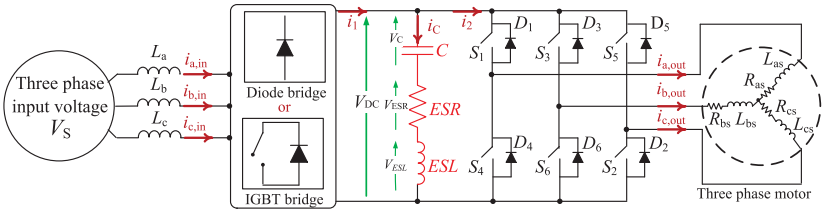

Fig. 5. Condition monitoring applications for two-stage ac/dc/ac power converters to be discussed in this paper.

Fig. 2(b)]. Some of the presented methods in the literature have applied this concept [8]–[17]. To obtain the voltage and current information at a certain frequency, external signals are injected. The signal is injected into the power electronic circuits with the frequency of interest. A large number of papers discuss the methods in this category. The capacitor voltage information is readily available since it is usually required for the control of power electronic converters (e.g., the dc-link voltage). The ripple current is measured by an additional current sensor. The current sensors used for capacitor current measurements can be divided into classical current sensors (e.g., resistors, hall sensors) and printed circuit board (PCB) based Rogowski coils. PCB-based Rogowski coils are designed PCBs that are fixed to the capacitor terminal to sense both capacitor's current and voltages.

1) Classical Current Sensors:

a) Without signal injection: Methods that are using direct classical current sensors are not very common. Three examples illustrate the concept of using a direct sensor [3]–[5]. All are using a direct current sensor to obtain the capacitor ripple current, in addition to the ripple voltage obtained through an existing voltage sensor. In [3], the root-mean-square (rms) value of the capacitor current measured by a current sensor is obtained. The average capacitor power (P_C) can be calculated by multiplying the capacitor's current and capacitor's ripple voltage. The calculation of the ESR is achieved by (1)

$$\mathrm{ESR} = \frac{P_C}{i_C^2} \tag{1}$$

where i_C is the current flowing through the dc-link capacitor.

TABLE I
CONDITION MONITORING METHODS OF CAPACITORS IN POWER ELECTRONIC CONVERTERS

Methodology	*C* /ESR	Used Approach	Topologies	Advantages/ Disadvantages	Capacitance; Power rating	Used in Ref.
I	*C* (E-Caps)	$C = \frac{1}{\Delta v_c}\int i_c dt$	Fig. 5 Diode bridge	Avoids the use of extensive filters.	4700 μF; 15 kW	[6]
					2200 μF; 15 kW	[7]
	ESR (E-Caps)	$\mathrm{ESR} = \frac{V_{\mathrm{DC}}-V_c}{i_c}$	Fig. 5 PWM IGBT bridge	Extra effort and many filters to be used because of the current injection.	2500 μF; 3 kW	[21]
					63.5 mΩ	
	ESR (E-Caps)	$\mathrm{ESR} = \frac{\Delta V_{\mathrm{cf}}}{\Delta i_{cf}}$	Fig. 4(b) Buck converter	Requires additional hardware for implementation.	2200 μF; 40 W	[5]
						[55]
	ESR (E-Caps)	$\frac{\mathrm{ESR}}{\mathrm{ESR}_o} = \left(\frac{\vartheta_{\mathrm{o1},O}}{\vartheta_{\mathrm{o1}}}\right)^2$	Fig. 5 Diode bridge	High accuracy level of ESR estimation.	470 μF; 0.4 Ω	[41]
		$\mathrm{ESR}_{\mathrm{HOT}} = \frac{\Delta T \times H \times S}{I^2}$				[42]
	C (E-Caps)	$C = \frac{1}{\Delta v_c}\int i_c dt$	Fig. 5 PWM IGBT bridge	Extra effort and many filters to be used because of the current injection.	6150 μF; 3 kW	[22]
	ESR (E-Caps)	$\mathrm{ESR} = \frac{P_c}{i_c^2}$	Fig. 5 Diode bridge	Simple analog circuit is required for the capacitor voltage measurement.	1800/5600 μF; 6 kW	[4]
II	ESR (E-Caps)	$\mathrm{ESR} \propto V_c$	Fig. 4(b) Buck converter	Forming an LC filter is important for achieving the proposed approach.	68 μF; 72 W	[29]
	C (MPPF-Caps)	$C\frac{dv_c}{dt} + \frac{1}{R_{\mathrm{rh}}}V_c = -i_{2f}$	Fig. 11 Fig. 12	Applied for specific kind of application systems (traction systems).	9 mF; 1.2 MW	[38]
	ESR (E-Caps)	$\mathrm{ESR} \propto V_c$	Fig. 4(b) Buck converter	Difficult due to requirement for additional measurements and prior data for the reference model.	2200 μF; 40 W	[34]
	ESR (E-Caps)	$\mathrm{ESR} = \frac{\Delta v_c \times R}{R \times \Delta I_L - \Delta v_c}$	Fig. 4(a) Boost converter	The temperature effect is considered.	N/A	[39]
	ESR (E-Caps)	$\mathrm{ESR} = \frac{\Delta v_c \times R}{R \times \Delta I_L - \Delta v_c}$	Fig. 4(b) Buck converter	The temperature effect is considered.	N/A	[59]
	C(E-Caps and MPPFCaps)	$C = \frac{1}{\Delta v_c}\int i_c dt$	Fig. 5 Diode bridge	Low accuracy under dynamic operation.	80 μF; 1.1 kW	[28]
	C(E-Caps and MPPFCaps)	$C = \frac{1}{\Delta v_c}\int i_c dt$	Fig. 5 Diode bridge	Applied on both E-Caps and MPPFCaps.	470 $/ mu$F; 250 mΩ	[43]
	C(E-Caps)	$C = \frac{1}{\Delta v_c}\int i_c dt$	Fig. 5 Diode bridge	Low accuracy under dynamic operation.	3280 μF; 100 W	[44]
	C and *ESR* (E-Caps)	$C = \frac{V_s D T_s}{8L\left(V_{S_{t=\frac{DT_s}{2}}} - V_{S_{t=\frac{(1+D)Ts}{2}}}\right)}$	Fig. 4(a) Boost converter	The condition monitoring method can be implemented in the same microcontroller used for MPPT purpose.	47 μF; 750 W	[45]
III	*C*(E-Caps)	$C = \frac{\mathrm{BPF}[P_C]}{\mathrm{BPF}\left[1/2\,\frac{\Delta v_c^2}{dt}\right]}$	Fig. 5 PWM IGBT bridge	Current measurement is not required.	3950 μF; 3 kW	[20]
	C(E-Caps)	Trained information on ANFIS	Fig. 16(b)	Based on software no extra hardware is required.	1500/2500 μF; 12 kW	[32]
	C(E-Caps)	Trained information on ANN	Fig. 5 Diode bridge	Based on software and existing information no extra hardware or extra sensors are required.	5000 μF; 10 kW	[31]

i_{2f}—current through the capacitance in the frequency filter; R_{rh}—braking rheostat; V_{dc}—dc-link voltage; V_C—capacitor voltage; i_C—capacitor current; V_{Cf}—capacitor voltage at certain switching frequency; $i_{\mathrm{Cf\_}}$—capacitor current at certain switching frequency; Δv_C—capacitor ripple voltage; Δi_{Cf}—fundamental capacitor ripple current; Δv_{Cf}—fundamental capacitor ripple voltage; $\vartheta_{\mathrm{o1},0}$!—initial volume of E-Caps; ϑ_{o1}—volume of E-Caps; ESR_o—initial value of ESR; $\mathrm{ESR}_{\mathrm{HOT}}$—ESR at operating temperature; *H*—heat transfer per surface area; *S*—surface area; ΔT—element temperature rise; ΔI_L—inductor ripple current; *R*—load resistance; V_S—solar PV voltage; T_S—switching time; *D*—duty cycle; *L*—inductor; $\mathrm{BPF}[P_C]$—output capacitor power from band pass filter; ANFIS—Adaptive Neuro Fuzzy Inference System; ANN—Artificial Neural Network.

In [4], the measured capacitor current is filtered by a band pass filter (BPF) before calculating the rms value. The usage of the filter is due to the calculation of ESR in a certain range of frequencies—as discussed previously—and is given in (2) as

$$\mathrm{ESR} = \frac{V_{\mathrm{Cf}}}{i_{\mathrm{Cf}}} \tag{2}$$

where V_{Cf} and i_{Cf} are the dc-link capacitor voltage and current at a certain switching frequency, respectively.

In [5], an electronic module is designed and integrated with an electrolytic capacitor. The electronic circuit is able to calculate the ESR by sensing the capacitor ripple current and voltage. The calculated ESR value are then compared with the initial value of the ESR_o to decide the capacitor status. The computational circuit is shown in Fig. 6.

Although this method requires additional hardware and the maximum error of the ESR estimation is 10%, the main advantage is the usage of a toroidal core in sensing the ripple current. The authors claimed that the additional parasitic inductance due to the usage of the toroidal core is negligible in this application case.

It is important to notice that the estimation of ESR based on the average capacitor power is achieved with 10% estimation error, which is acceptable in some applications. Moreover, it is achieved without the usage of filters, which reduces time and cost. But in some applications, the usage of the filter is required

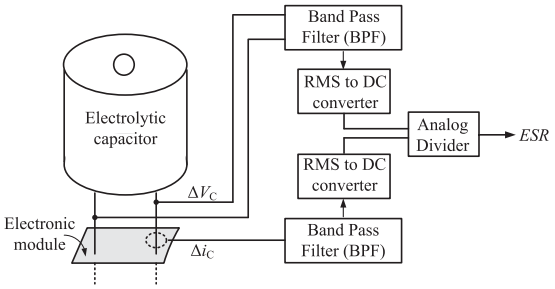

Fig. 6. ESR computational circuit in capacitors [5].

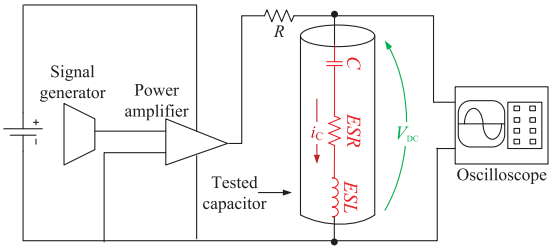

Fig. 7. Experimental setup with signal injection used in [8]–[17].

in order to achieve higher accuracy with estimation error lower than 10%.

b) With signal injection: An alternative way is to externally inject a desirable signal of current or voltage at a certain frequency into the circuit where the capacitor of interest is located. This methodology is the most widely used methodology. Various applications and different methodologies can be used, and most of the methodologies are applied on an experimental setup as illustrated in Fig. 7.

In [8] and [9], an experimental technique that allows the determination of the ESR value of aluminum E-Caps based on sinusoidal analysis technique and close to their resonance frequencies is reported. The technique has been applied on a capacitor existing in an LCfilter with 25 V input voltage, and 4700 μF filter capacitor. However, the technique presented some drawbacks due to the fact that both capacitance and inductance values are frequency dependent. In these two references, the estimated ESRs from the experimental test are not compared with the simulations. This is due to the fact that both tests are done at different frequencies. Moreover, the obtained results are not compared to the initial values; this is due to a lack of information from the manufacturer of the tested capacitors. The manufacturer is typically providing the data sheets with dissipation factor (DF) at 120 Hz.

In order to overcome the aforementioned shortcomings, different algorithms were used in [10]–[17]. Laplace transform algorithm in [10], Newton–Raphson (NR) in [11] and [16], discrete Fourier transform (DFT) in [12], [13], and [17], and least mean square (LMS) in [14] and [15]. All the algorithms are used to calculate the relationship between the input voltage and the output voltage of the experimental circuit shown in Fig. 7. The differences between these algorithms are summarized at the end of this section.

TABLE II
SUMMARY OF CONDITION MONITORING ANALYSIS ALGORITHMS

Analysis Algorithm	Operating frequency		(C) Estimation error percentage	(ESR) Estimation error percentage
Laplace Transform	120 Hz		17.6%[10]	N/A
	750 Hz		N/A	18%[11]
	10 kHz		N/A	5%[10]
Discrete Fourier Transform (DFT)	750 Hz		N/A	8% [11]
	1 kHz		2.8%[12]	11%[12]
	10 kHz		N/A	10% [10] 12% [16]
Newton–Raphson (NR)	120 Hz		1.5%[10]	8.4%[15]
Least Mean Square (LMS)	1 kHz	Method (1)*	2.6%[13] 1.0%[14]	0.4%[14]
		Method (2)*	0.3%[14]	9.7%[14]

*Method (1): based on sinusoidal generator. Method (2): based on charge/discharge circuit.

In [11] and [12], the same setup (as shown in Fig. 7) is used to estimate the equivalent circuit of the capacitor by using the NR method and DFT, respectively, instead of Laplace analysis. The measured values of capacitance and ESR are compared with those obtained in [10]. The NR–based method gave values, which were very close to the measured values using an LCR meter with maximum error of 1.5%. Comparing the obtained values based on the DFT method in [12] with the values obtained by the Laplace transform method in [10], the DFT method estimated the ESR with a maximum error of 8%, and the method using the Laplace method estimated the ESR with a maximum error of 18%.

Another method based on *DFT* analysis is considered in [13] and it is applied on the same setup as shown in Fig. 7. The method estimated the ESR and capacitance with a maximum error of 11% and 2.8%, respectively. In [14], a simple modification to the same setup in Fig. 7 is carried out to estimate the ESR and capacitance. The modified circuit uses a control circuit to charge and discharge the capacitor. Therefore, from the relationship between the capacitor current and the capacitor voltage, the capacitance value is estimated by applying an *LMS* algorithm using a sinusoidal curve fitting technique instead of using Laplace.

Based on the same method proposed in [14] and the setup shown in Fig. 7, a wider range of frequencies and temperatures are considered in [15] for the estimation of ESR and capacitance. In addition, [15] uses two methods: 1) based on a sinusoidal generator; and 2) based on charge/discharge circuit, and compares each method. It is concluded that for the ESR estimation the first method is better, while the opposite is correct for the capacitance estimation.

Table II summarizes the comparison between all algorithms with respect to the operating frequency. Based on the review of

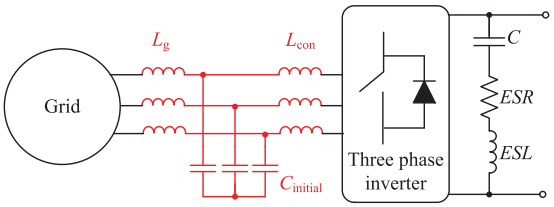

Fig. 8. LCL filter interfaced between grid and PWM inverter [19].

these algorithms, the following can be concluded.

1) In order to use the Laplace transform algorithm, a certain requirement must be fulfilled. The requirement is that the input resistance *R* must be two to three times higher than both the ESR and the capacitor reactance. Otherwise, the Laplace transform algorithm shows high error percentages.
2) The NR Algorithm is an iteration-based algorithm, and from the results listed in Table II, NR is recommended for the frequency region I, and hence, for capacitance estimation.
3) The DFT algorithm is considering only the first harmonic component in the computation of the gain and phase displacement between the input and output voltage, and hence, it takes low effort.
4) All of the four algorithms are applied for offline condition monitoring of capacitors.

For the LCL filter of the grid-connected PWM converter shown in Fig. 8, a condition monitoring method is proposed in [18] and [19].

This methodology is based on using the corresponding variation in the filter capacitor operating frequency region as the capacitance drop is an indication to the health status. Assuming that the capacitance is reduced up to 80% of the initial value, the frequency caused due the drop is calculated by

$$f = \frac{1}{2\pi} \times \sqrt{\frac{L_{\text{con}} + L_g}{L_{\text{con}} \times L_g \times 0.8 C_{\text{initial}}}} \tag{3}$$

where L_{con} is the line inductance on the converter side, L_g is the line inductance on the grid side, and C_{initial} is the initial value of the capacitance. To obtain the frequency of the aged capacitor, a voltage is injected into the reference voltage of the capacitor in the LCL filter with the frequency calculated previously. Although this method is similar to the one proposed in [20] since both are using voltage injection, the difference is the usage of measured capacitance frequency and comparing it to the initial frequency to identify the deterioration of the capacitor. Moreover, the replacement time of the capacitors is determined according to the following condition:

$$(\alpha - \beta) \geq 80\% \tag{4}$$

where (α) and (β) are the dB frequency magnitude of the initial and degraded capacitance, respectively.

2) PCB-Based Rogowski Coils: Capacitor condition monitoring based on PCB-based *Rogowski* coils is summarized in this section. The methods described in [6] and [7] are based on the *Rogowski* current sensor concept, where a designed PCB is fixed to the capacitor terminal to sense both capacitor's current $i_{c,\text{ac}}$ and voltages $V_{c,\text{ac}}$. The difference between *Rogowski* based methods and the method in [5] is illustrated in Fig. 9. The advantage in the *Rogowski* based methods is the avoidance of using extensive filters since the total active power P_c drawn by the capacitor is represented by the ESR. Where, V_{cf} and i_{cf} are the capacitor voltage and current at a certain switching frequency, respectively.

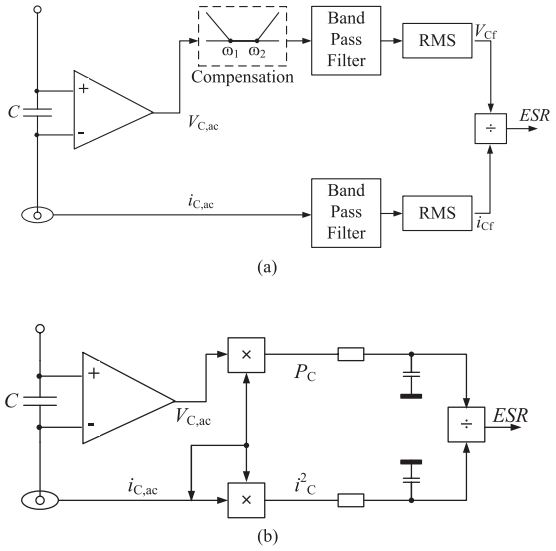

Fig. 9. Condition monitoring by ESR estimation based on designed PCBs. (a) ESR estimation done within the capacitors ohmic frequency range as illustrated in Fig. 2(b) [5]. (b) ESR estimation based on Rogowski coil current sensor [6], [7].

B. Circuit Model-Based Methods

1) Without Signal Injection: Instead of the current sensors connected in series with the capacitors, capacitor ripple currents can also be obtained indirectly based on the operation principle of PWM switching converters [28], and the switching status of dc–dc power converters with the LC filters [29].

An online condition monitoring method based on capacitance estimation by (10) is presented in [28]. As referring to Fig. 5, the electrical information i_1, $i_{a,\text{out}}$, $i_{b,\text{out}}$ and V_{dc} are obtained by using the three existing current sensors and one voltage sensor, respectively. These sensors are already existing for the control purpose of the converter. The electrical information i_C, i_2, $i_{c,\text{out}}$ are estimated indirectly.

The capacitor ripple current i_C is calculated using the difference between the input current sensor i_1 and the current flows to the inverter i_2 which is based on the transistor switching sequences. The assumption of this calculation is that the three phase output currents are balanced.

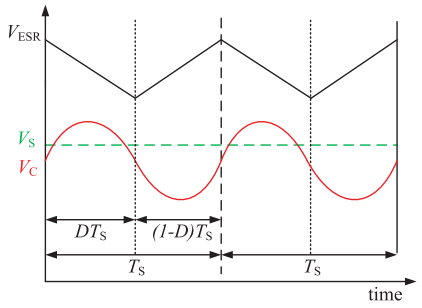

Fig. 10. Voltages waveform with respect to sampling time and duty cycle [45].

Due to the high switching frequency in dc–dc converters, the impedance of the electrolytic capacitor is dominated by the ESR. Since the ESR is very small compared to the load resistance, the output ripple voltage is determined by the capacitor ESR and the inductor ripple current. For a dc–dc power converter operated in a steady state, three factors in which the inductor current depends on remains unchanged. The factors are duty cycle, the inductance, and the difference between input and output voltage. Therefore, the amplitude of the output ac ripple voltage is determined directly by the ESR. The experimental test is based on a comparison between the output ripple voltage in the case of using predetermined unaged capacitor, with the output ripple voltage in case of using an aged capacitor.

In [45], an online methodology that belongs to this category and requires no signal injection is proposed. The methodology is applied on a dc-link capacitor in a boost converter as shown in Fig. 4(a). The boost converter is supplied from a photovoltaic (PV) panel. The main advantage in this methodology is that the sensing voltage for the maximum power point tracking (MPPT) purpose is utilized for the ESR and capacitance estimation according to (5) and (6), respectively

$$\text{ESR} = \frac{\left[V_S|_{t=0} - V_S|_{t=DTs}\right] \times L}{V_S \times DTs} \tag{5}$$

$$C = \frac{V_S \times DTs}{8} \times L \times \left[V_{S|t=\frac{DTs}{2}} - V_{S|_{t=\frac{(1+D)Ts}{2}}}\right] \tag{6}$$

where V_S, T_s, D, and L are the solar PV voltage, switching time, duty cycle, and the inductor, respectively, as illustrated in Fig. 10.

However, the ESR and the capacitance can be estimated only during a steady state, when the MPPT system settles to a point. Since the same sensing voltage is used for the MPPT purpose is used for ESR and capacitance estimation, therefore, the condition monitoring method is implemented in the same microcontroller which is also used for the MPPT. This helps to avoid additional hardware, and hence reduces the cost.

Another methodology that is applied to the capacitor condition monitoring based on the circuit model is presented in [38]. The condition monitoring is based on capacitance estimation of a dc-link MPPF capacitor in a traction system. The general traction scheme of the railway trains is shown in Fig. 11. Regarding to the operation nature of the traction systems, during

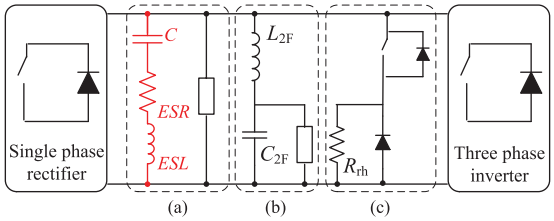

Fig. 11. General traction scheme. (a) dc-link capacitor. (b) Frequency filter. (c) Braking chopper [38].

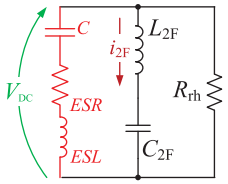

Fig. 12. Equivalent dc-link circuit during dc-link capacitor discharge [38].

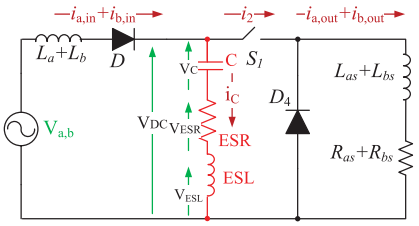

Fig. 13. Equivalent circuit of the three-phase ac/dc/ac converter shown in Fig. 5 when the motor is stopped [43].

the capacitor discharge period, the obtained equivalent circuit of the dc-link is shown in Fig. 12. Normally in the traction system applications both current and voltage sensors are already installed and available in some auxiliary measurement blocks. Thereby, an insertion of an additional current sensor in series with the dc-link capacitor or a voltage sensor is avoided, and the dc-link capacitor will be obtained by applying the LMS algorithm to

$$C\frac{dv_{\text{DC}}}{dt} + \frac{1}{R_{\text{rh}}} \times V_{\text{DC}} = -i_{2F} \tag{7}$$

where C, i_{2F}, L_{2F}, C_{2F}, R_{rh}, and V_{DC} are the dc-link capacitor, current passes through the frequency filter, frequency filter inductance, frequency filter capacitance, braking rheostat, and dc-link voltage, respectively.

A similar concept that estimates the ESR and the capacitance at a certain time is also presented in [43]. The estimation is applied on a dc-link capacitor in a three phase diode bridge ac/dc/ac converter that drives an induction motor as shown in Fig. 5. The main idea is to apply the condition monitoring method whenever the motor is stopped. During this instant, the equivalent circuit is given as shown in Fig. 13.

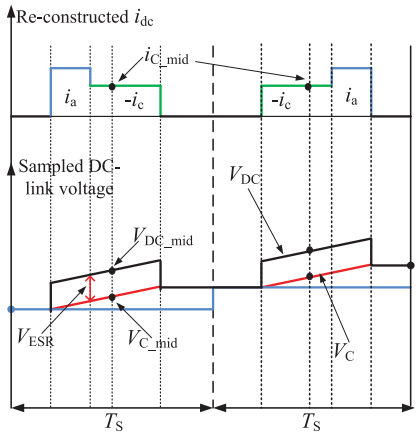

Fig. 14. Behavior of the dc-link current and voltage according to the gating pulses in an ac/dc/ac converter shown in Fig. 5 [21].

In Fig. 13, L_a, L_b, L_{as}, L_{bs}, R_{as}, R_{bs}, are the line inductances of phase A and phase B, the stator inductances and resistances of phase A and phase B, respectively.

2) With Signal Injection: A few examples that are based on the circuit model methodology, in addition to external signal injection, are proposed in [21]–[26]. The current injection methods in [21], [22], [24], and [26] are applied on the PWM ac/dc/ac converter, while in [23] and [25] they are applied to a submodule capacitor in a modular multilevel converter, and a drive system for electric vehicles, respectively. The injected current is of a frequency lower than the line frequency, inducing two voltages which follows the relationship of

$$V_{DC} = V_C + V_{ESR}. \tag{8}$$

By considering the generation of the zero voltage vectors at switching periods, the values at the mid-point of the switching periods are used in [21] to obtain the ESR value as

$$\text{ESR} = \frac{V_{ESR}}{i_C} = \frac{V_{dc\_mid} - V_{C\_mid}}{i_{C\_mid}} \tag{9}$$

where the term (mid) in the subscripts indicates the quantities measured at the mid-point of the normal sampling period as in the signals shown in Fig. 14.

In [22] the estimated capacitance is obtained by

$$C = \frac{1}{\Delta V_{DC}} \int i_C \, dt. \tag{10}$$

Although it can be noticed that the current injection method is applied on various applications, the need of external signals, extra hardware, and filters is the main shortcoming in such a method.

C. Data and Advanced Algorithm Based Methods

In this category, the power electronic converters are treated as a black box or semiblack box. Black-box approaches are based on the information of voltages and currents at the input side and output side only. The internal properties of the converters are assumed unknown. Semiblack-box approaches use also some of the available information inside the power converter structure. The relationship between the parameters to be estimated and the available parameters (e.g., input and output side terminal voltage and current information, dc-link voltage) are obtained through data training.

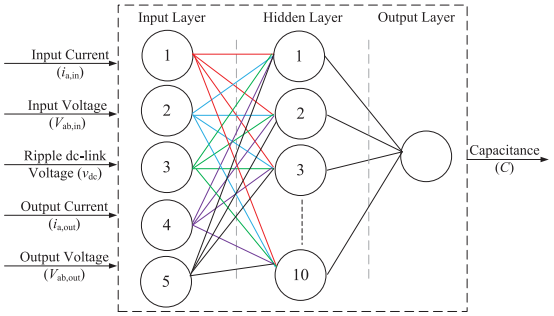

Fig. 15. Structure of ANN of capacitance estimation [31].

In [20], a low-frequency ac voltage is injected to the dc-link reference, which is used as training data in sake of finding the identification model based on support vector regression (SVR). After using a set of training data, a function that finds the relationship between the capacitor's power and its corresponding capacitance is designed, and the capacitance is determined according to

$$C = \frac{\text{BPF}[P_C]}{\text{BPF}[1/2][\frac{\Delta V_C^2}{dt}]} \tag{11}$$

where the term BPF$[P_C]$ refers to the capacitor's power filtered by using the BPF and it equals to 3 kW. The cut-off frequency of the used BPF equals to 30 Hz. As claimed in [20], this method is simpler than the current injection, since the estimation is based on the capacitor power and no dc-link ripple current information is required. Since the SVR is an algorithm, which is based on offline trained data, the recursive least-squares algorithm is applied to allow the estimated capacitance to be updated, when new data become available [30].

Two recent methods for condition monitoring of capacitors based on data training using software algorithms are presented recently in [31] and [32]. Their structures are shown in Figs. 15 and 16, respectively.

The method described in [31] is based on the artificial neural network (ANN) algorithm. It is applied for the dc-link capacitor condition monitoring in a diode-bridge front-end three phase motor drive as shown in Fig. 5.

The main motivation behind using ANN for capacitance estimation is to avoid the usage of a direct/indirect current sensor. The capacitance value is estimated based on the existing control information and the power level of the power converter. This is convenient for the industry applications, where input/output current of the converter and the dc-link voltage are already existing information. No extra hardware circuitry and no injection

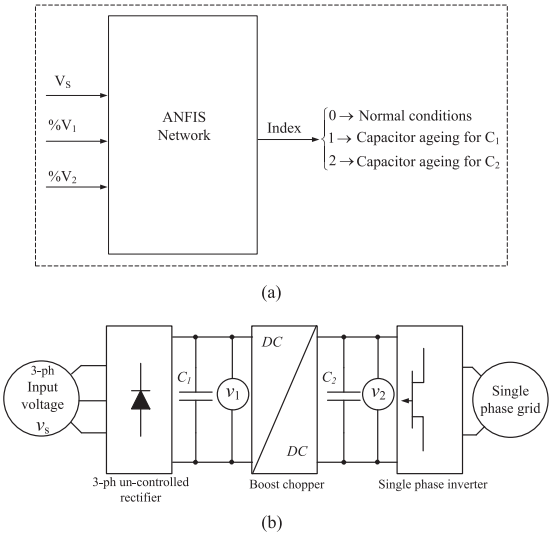

Fig. 16. Condition monitoring of capacitors based on data training proposed by [32]. (a) ANFIS network [32]. (b) Power electronic converter circuit [32].

TABLE III
SIMULATION RESULTS FOR ESTIMATED CAPACITANCE (AT 7 KW) USING METHODOLOGY III

$C_{\text{act.}} = 1300\ \mu\text{F}$	$C_{\text{est.}} = 1296\ \mu\text{F}$	$\text{Error} = 0.3\%$
$C_{\text{act.}} = 1743\ \mu\text{F}$	$C_{\text{est.}} = 1747\ \mu\text{F}$	$\text{Error} = 0.23\%$
$C_{\text{act.}} = 2600\ \mu\text{F}$	$C_{\text{est.}} = 2589\ \mu\text{F}$	$\text{Error} = 0.5\%$
$C_{\text{act.}} = 3200\ \mu\text{F}$	$C_{\text{est.}} = 3203\ \mu\text{F}$	$\text{Error} = 0.09\%$
$C_{\text{act.}} = 3854\ \mu\text{F}$	$C_{\text{est.}} = 3850\ \mu\text{F}$	$\text{Error} = 0.1\%$
$C_{\text{act.}} = 4265\ \mu\text{F}$	$C_{\text{est.}} = 4257\ \mu\text{F}$	$\text{Error} = 0.18\%$

of external signals are required, and thereby minimizing both complexity and cost. In Fig. 15, the basic structure of the ANN is illustrated; normally, the structure of any neural network consists of three types of layers: input layer, hidden layer, and output layer. In this ANN, the capacitance value is the target to be estimated, while the input/output terminal information of the converter and the dc-link voltage are the inputs to the ANN. Parts of the results are shown in Table III. The maximum estimated error is 0.5%, where $C_{\text{act.}}$ and $C_{\text{est.}}$ refer to the actual and estimated capacitance, respectively.

The method described in [32] is applied to a power electronic converter shown in Fig. 16(b) and based on adaptive neuro-fuzzy inference system (ANFIS) algorithm.

The methodology is based on collecting data and training the ANFIS on them for the sake of predicting future nontrained outputs according to the basic structure shown in Fig. 16(a). The supply voltage *V*s and ripple voltages *V*1 and *V*2 of both filter capacitors *C*1 and *C*2 are inputs to the ANFIS. Both *V*1 and *V*2 are going through an interpolation process before implementing them in order to assure that a strong mapping between the inputs and outputs is obtained.

In order to investigate the ageing process, *V*1 and *V*2 are calculated at the end-of-life states and denoted by *V*1th and *V*2th, respectively. A relationship between the supply voltage and the end-of-life voltages is linearly interpolated using curve fitting techniques. The two factors $\hat{V}_{1\text{th}}$ and $\hat{V}_{2\text{th}}$ are obtained, where $\hat{V}_{1\text{th}}$ and $\hat{V}_{2\text{th}}$ are the estimated values of *V*1th and *V*2th according to *V*s, respectively. Finally, in order to obtain the data implemented as input to the ANFIS, a percentage value is calculated as the following:

$$\%V_1 = \frac{V_{1m}}{V_{1\text{th}}} \times 100 \tag{12}$$

$$\%V_2 = \frac{V_{2m}}{V_{2\text{th}}} \times 100 \tag{13}$$

where *V*1m and *V*2m are the measured values of *V*1 and *V*2, respectively, at any current level.

The ANFIS network is trained on 366 pairs of inputs and outputs. The network estimates one index out of two indices for capacitance and ESR of both capacitors in the converter. Moreover, the ANFIS can show decreasing/increasing percentages in the capacitance and the ESR, respectively. The method based on the ANFIS gives a high accuracy (0.5% maximum error) according to the results and it is useful for fault detection.

III. History Development and Benchmark of Capacitor Condition Monitoring Methods

The technology evolution of the capacitor condition monitoring technologies is illustrated in Fig. 17 with respect to history. Different methods are represented according to the selected indicators, online or offline, and the methodologies discussed in Section II. The maximum estimation error percentages corresponding to each methodology are also given in Fig. 17.

Since the estimation accuracy is an important performance factor, Fig. 18 compares the estimation errors with respect to the range of capacitance *C* and ESR. The comparison is according to the available data in different literatures and with respect to the methodologies classified earlier in Section II. It can be seen that the lowest error percentages are captured by the methods that belong to Methodology III. This concludes that software solutions have a strong potential to be considered in condition monitoring.

Fig. 19 summarizes the share of the considered lifetime indicators, and the share of each methodology listed in this review. Almost 60% of the used health indicator is captured by the ESR. This percentage conclude that E-Caps are the widely used capacitor type in power electronic applications.

IV. Remarks on the Condition Monitoring for Capacitors

Based on the above analysis, the following remarks are given to the overview.

1) Fig. 18 shows that the condition monitoring methods based on Methodology III achieved a relatively higher accuracy than those based on Methodologies I and II.
2) The majority of the condition monitoring methods are based on the first methodology as shown in Fig. 19.
3) Fig. 19 shows that the ripple voltage estimation is the lowest considered indicator. However, the capacitor

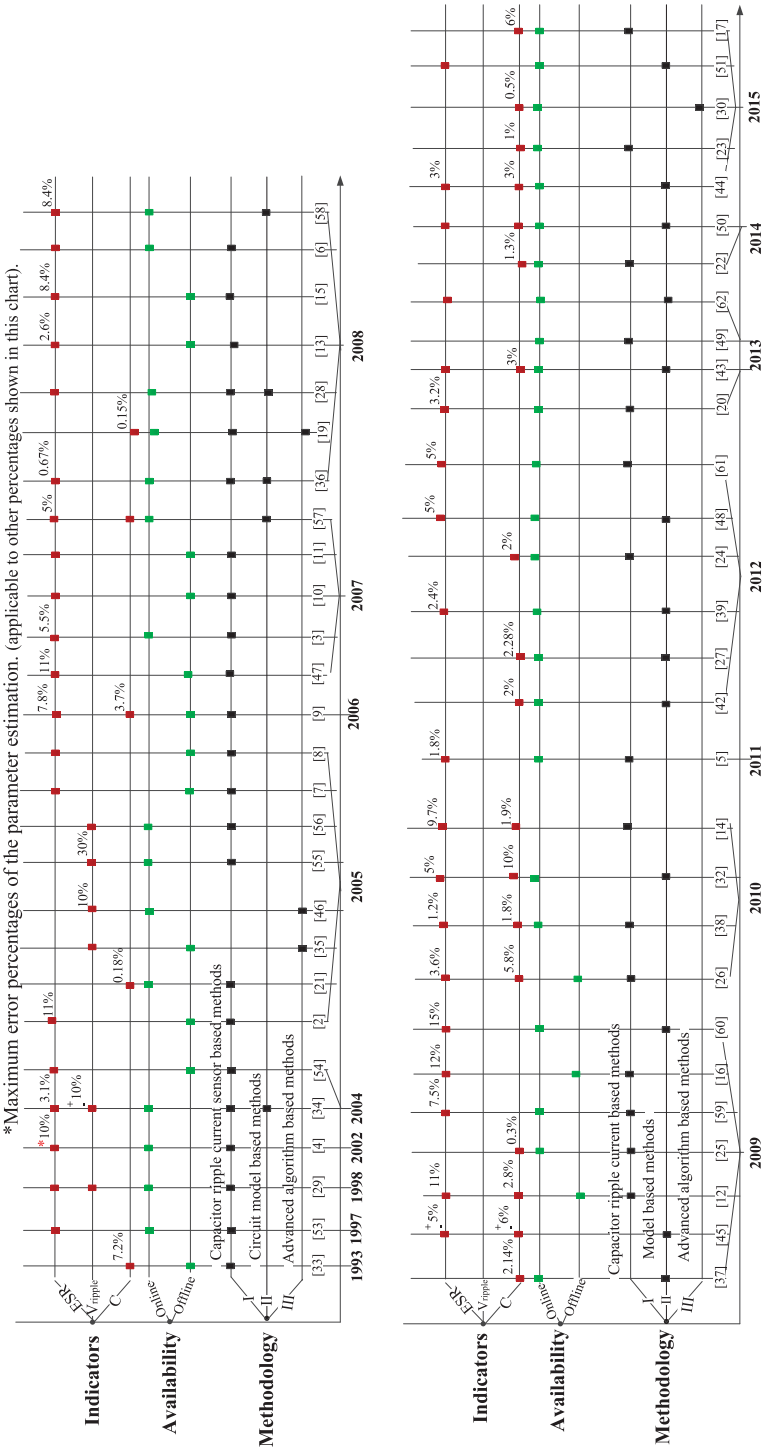

Fig. 17. Development history of the condition monitoring technology for capacitors.

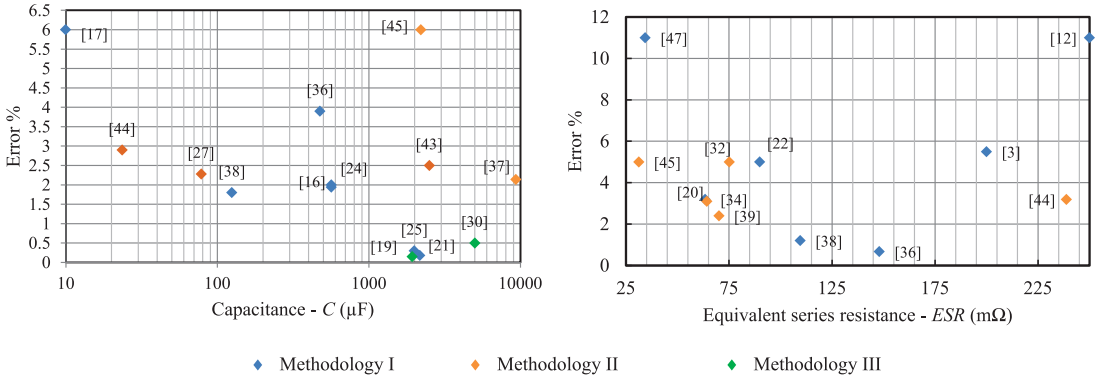

Fig. 18. Comparison of the capacitor parameter estimation in prior-art literatures.

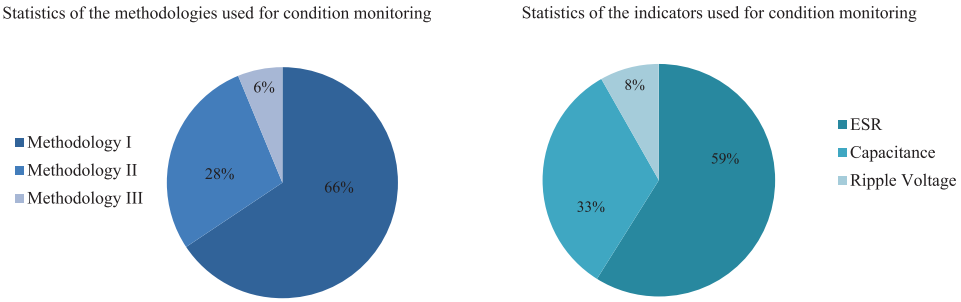

Fig. 19. Sharing of the used methods for condition monitoring and the considered indicators.

ripple voltage is the main factor in ESR and capacitance estimation.

4) According to the development history shown in Fig. 17, ESR is a common indicator for capacitor condition monitoring due to the wide usage of E-Caps where both capacitance and ESR can indicate the health status. For film capacitors, the capacitance is a preferred indicator, since the ESR of film capacitors are significantly smaller than that of the E-Caps.
5) Leakage current or insulation resistance can also be used as an indicator for E-Caps and film capacitors. They are mainly used in offline condition monitoring since it is relatively more difficult to estimate it online, compared to that of ESR or capacitance.
6) It can be noted from Fig. 17 that the majority of the condition monitoring methods are online. By considering that the degradation of capacitors are usually very slow, offline condition monitoring is sufficient in most applications (e.g., in motor drives) to detect the wear out of capacitors. It implies that much simpler estimation methods can be applied (e.g., during the start-up of motor drives).
7) The capacitor ripple current sensor based methods are not attractive for practical industry applications due to its addition of hardware circuitry, cost, and the reliability issues of the introduced circuit. Table IV shows the hardware/software complexity with respect to each methodology. It can be seen that the hardware complexity is reduced against the increase in software complexity.
8) Condition monitoring of capacitors discussed here is limited to the wear out detection. To extend the scope, in reliability critical applications, the online monitoring of the operation status (e.g., hot spot temperature, abnormal voltage, and current stresses) is of much interest. For this perspective, the online monitoring of capacitance and ESR value might be necessary to indirectly monitor the temperature and other abnormal stressors.
9) New methods based on software solutions and existing feedback signals, without adding any hardware cost, could be attractive for industry applications.

TABLE IV
ASSOCIATED LEVELS OF COMPLEXITY WITH RESPECT TO EACH METHODOLOGY

Methodology	Hardware Complexity	Software Complexity
I	+ + +	+
II	++	++
III	+	+ + +

V. CONCLUSION

The condition monitoring technologies are classified by the authors into three categories from their methodology point

of view. The indicators that represent the health status of the capacitor and the used approach to calculate them are also reviewed. Different iteration/estimation algorithms used for capacitor condition monitoring applications are grouped. A comparison between these algorithms and the estimated maximum percentage error by each of the algorithms are discussed in detail. Moreover, remarks on whether the health indicator is useful to be considered or not are also discussed. The technology evolution and benchmark of the state-of-the-art condition monitoring methods for capacitors from 1993 to present are listed. Remarks on both the promising aspects and shortcomings of the key methods and their applicability in practical industry applications are provided. From the authors point of view, future research opportunities in the condition monitoring of capacitors include the following main aspects.

1) Software-based methods with reduced or no additional hardware efforts expect to be attractive for industry applications which requires high reliability performance. The advantages of this kind of methods lie in twofold: it could be applied for both new power converters or existing power converters by upgrading the algorithms in the digital controllers and it is a trend that the cost of digital controllers and computation resources is reducing.
2) Cost-effective and low-inductive current sensing methods could overcome many of the shortcomings of existing current sensor based methods. PCB-based Rogowski coils are promising for the capacitor current measurement, while more research efforts are needed to achieve better integration with the capacitors and more robust and cost-effective design.
3) Integrated implementation of condition monitoring, protection, and other ancillary functions for capacitors in applications requiring high reliability performance.

REFERENCES

[1] S. Yang, D. Xiang, A. Bryant, P. Mawby, L. Ran, and P. Tavner, "Condition monitoring for device reliability in power electronic converters: A review," *IEEE Trans. Power Electron.*, vol. 25, no. 11, pp. 2734–2752, Nov. 2010.

[2] Power supply failure survey part II. [Online]. Available: http://www.rs-online.com/designspark/electronics/knowledge-item/power-supply-failure-survey-part-ii

[3] E. Aeloiza, J.-H. Kim, P. Enjeti, and P. Ruminot, "A real time method to estimate electrolytic capacitor condition in PWM adjustable speed drives and uninterruptible power supplies," in *Proc. IEEE 36th Power Electron. Spec. Conf.*, Jun. 2005, pp. 2867–2872.

[4] A. Imam, D. Divan, R. Harley, and T. Habetler, "Real-time condition monitoring of the electrolytic capacitors for power electronics applications," in *Proc. 22nd Annu. Appl. Power Electron. Conf.*, Feb. 2007, pp. 1057–1061.

[5] P. Venet, F. Perisse, M. El-Husseini, and G. Rojat, "Realization of a smart electrolytic capacitor circuit," *IEEE Ind. Appl. Mag.*, vol. 8, no. 1, pp. 16–20, Jan. 2002.

[6] M. Vogelsberger, T. Wiesinger, and H. Ertl, "Life-cycle monitoring and voltage-managing unit for dc-link electrolytic capacitors in PWM converters," *IEEE Trans. Power Electron.*, vol. 26, no. 2, pp. 493–503, Feb. 2011.

[7] T. Wiesinger and H. Ertl, "A novel real time monitoring unit for PWM converter electrolytic capacitors," in *Proc. IEEE Power Electron. Spec. Conf.*, Jun. 2008, pp. 523–528.

[8] A. Amaral and A. Cardoso, "An experimental technique for estimating the aluminum electrolytic capacitor equivalent circuit, at high frequencies," in *Proc. IEEE Int. Conf. Ind. Technol.*, Dec. 2005, pp. 86–91.

[9] A. Amaral and A. Cardoso, "An ESR meter for high frequencies," in *Proc. Int. Conf. Power Electron. Drives Syst.*, vol. 2, 2005, pp. 1628–1633.

[10] A. Amaral and A. Cardoso, "An experimental technique for estimating the ESR and reactance intrinsic values of aluminum electrolytic capacitors," in *Proc. IEEE Instrum. Meas. Technol. Conf.*, Apr. 2006, pp. 1820–1825.

[11] A. Amaral and A. Cardoso, "Using Newton-Raphson method to estimate the condition of aluminum electrolytic capacitors," in *Proc. IEEE Int. Symp. Ind. Electron.*, Jun. 2007, pp. 827–832.

[12] A. Amaral, G. Buatti, H. Ribeiro, and A. Cardoso, "Using DFT to obtain the equivalent circuit of aluminum electrolytic capacitors," in *Proc. 7th Int. Conf. Power Electron. Drive Syst.*, Nov. 2007, pp. 434–438.

[13] A. Amaral and A. Cardoso, "A simple offline technique for evaluating the condition of aluminum electrolytic capacitors," *IEEE Trans. Ind. Electron.*, vol. 56, no. 8, pp. 3230–3237, Aug. 2009.

[14] A. Amaral and A. Cardoso, "An automatic technique to obtain the equivalent circuit of aluminum electrolytic capacitors," in *Proc. IEEE 34th Annu. Conf. Ind. Electron.*, Nov. 2008, pp. 539–544.

[15] A. Amaral and A. Cardoso, "Simple experimental techniques to characterize capacitors in a wide range of frequencies and temperatures," *IEEE Trans. Instrum. Meas.*, vol. 59, no. 5, pp. 1258–1267, May 2010.

[16] A. Amaral and A. Cardoso, "An economic offline technique for estimating the equivalent circuit of aluminum electrolytic capacitors," *IEEE Trans. Instrum. Meas.*, vol. 57, no. 12, pp. 2697–2710, Dec. 2008.

[17] A. Amaral and A. Cardoso, "Using a sinosoidal PWM to estimate the ESR of aluminum electrolytic capacitors," in *Proc. Int. Conf. Power Eng., Energy Elect. Drives*, Mar. 2009, pp. 691–696.

[18] J. Koppinen, J. Kukkola, and M. Hinkkanen, "Parameter estimation of an LCL filter for control of grid converters," in *Proc. 9th Int. Conf. Power Electron.*, Jun. 2015, pp. 1260–1267.

[19] J.-S. K. J.-M. K. Hong-Jun Heo and W.-S. Im, "A capacitance estimation of film capacitors in an LCL-filter of grid-connected PWM converters," *J. Power Electron.*, vol. 13, pp. 94–103, 2013. [Online]. Available: http://www.dbpia.co.kr/Article/NODE02074217

[20] A. Abo-Khalil and D.-C. Lee, "Dc-link capacitance estimation in ac/dc/ac PWM converters using voltage injection," *IEEE Trans. Ind. Appl.*, vol. 44, no. 5, pp. 1631–1637, Sep. 2008.

[21] X.-S. Pu, T. H. Nguyen, D.-C. Lee, K.-B. Lee, and J.-M. Kim, "Fault diagnosis of dc-link capacitors in three-phase ac/dc PWM converters by online estimation of equivalent series resistance," *IEEE Trans. Ind. Electron.*, vol. 60, no. 9, pp. 4118–4127, Sep. 2013.

[22] D.-C. Lee, K.-J. Lee, J.-K. Seok, and J.-W. Choi, "Online capacitance estimation of dc-link electrolytic capacitors for three-phase ac/dc/ac PWM converters using recursive least squares method," in *IEE Proc. Elect. Power Appl.*, vol. 152, no. 6, pp. 1503–1508, Nov. 2005.

[23] Y.-J. Jo, T. H. Nguyen, and D.-C. Lee, "Condition monitoring of submodule capacitors in modular multilevel converters," in *Proc. IEEE Energy Convers. Congr. Expo.*, Sep. 2014, pp. 2121–2126.

[24] T. H. Nguyen and D.-C. Lee, "Deterioration monitoring of dc-link capacitors in ac machine drives by current injection," *IEEE Trans. Power Electron.*, vol. 30, no. 3, pp. 1126–1130, Mar. 2015.

[25] M. Kim, S.-K. Sul, and J. Lee, "Condition monitoring of dc-link capacitors in drive system for electric vehicles," in *Proc. IEEE Veh. Power Prop. Conf.*, Oct. 2012, pp. 633–637.

[26] X. Pu, T.-H. Nguyen, D.-C. Lee, and S.-G. Lee, "Capacitance estimation of dc-link capacitors for single-phase PWM converters," in *Proc. IEEE 6th Int. Power Electron. Motion Control Conf.*, May 2009, pp. 1656–1661.

[27] A. Amaral and A. Cardoso, "Estimating aluminum electrolytic capacitors condition using a low frequency transformer together with a dc power supply," in *Proc. IEEE Int. Symp. Ind. Electron.*, Jul. 2010, pp. 815–820.

[28] A. Wechsler, B. Mecrow, D. Atkinson, J. Bennett, and M. Benarous, "Condition monitoring of dc-link capacitors in aerospace drives," *IEEE Trans. Ind. Appl.*, vol. 48, no. 6, pp. 1866–1874, Nov. 2012.

[29] Y.-M. Chen, H.-C. Wu, M.-W. Chou, and K.-Y. Lee, "Online failure prediction of the electrolytic capacitor for lc filter of switching-mode power converters," *IEEE Trans. Ind. Electron.*, vol. 55, no. 1, pp. 400–406, Jan. 2008.

[30] A. Lahyani, P. Venet, G. Grellet, and P.-J. Viverge, "Failure prediction of electrolytic capacitors during operation of a switchmode power supply," *IEEE Trans. Power Electron.*, vol. 13, no. 6, pp. 1199–1207, Nov. 1998.

[31] H. Soliman, H. Wang, B. Gadalla, and F. Blaabjerg, "Condition monitoring of dc-link capacitors based on artificial neural network algorithm," in *Proc. IEEE 5th Int. Conf. Power Eng., Energy Elect. Drives*, May 2015, pp. 587–591.

[32] T. Kamel, Y. Biletskiy, and L. Chang, "Capacitor aging detection for the dc filters in the power electronic converters using Anfis algorithm," in *Proc. 28th Can. Conf. Elect. Comput. Eng.*, May 2015, pp. 663–668.
[33] K. Abdennadher, P. Venet, G. Rojat, J.-M. Retif, and C. Rosset, "A real-time predictive-maintenance system of aluminum electrolytic capacitors used in uninterrupted power supplies," *IEEE Trans. Ind. Appl.*, vol. 46, no. 4, pp. 1644–1652, Jul. 2010.
[34] K. Harada, A. Katsuki, and M. Fujiwara, "Use of ESR for deterioration diagnosis of electrolytic capacitor," *IEEE Trans. Power Electron.*, vol. 8, no. 4, pp. 355–361, Oct. 1993.
[35] O. Ondel, E. Boutleux, and P. Venet, "A decision system for electrolytic capacitors diagnosis," in *Proc. IEEE 35th Annu. Power Electron. Spec. Conf.*, vol. 6, Jun. 2004, pp. 4360–4364.
[36] A. Imam, T. Habetler, R. Harley, and D. Divan, "Condition monitoring of electrolytic capacitor in power electronic circuits using adaptive filter modeling," in *Proc. IEEE 36th Power Electron. Spec. Conf.*, Jun. 2005, pp. 601–607.
[37] K.-W. Lee, M. Kim, J. Yoon, K.-W. Lee, and J.-Y. Yoo, "Condition monitoring of dc-link electrolytic capacitors in adjustable-speed drives," *IEEE Trans. Ind. Appl.*, vol. 44, no. 5, pp. 1606–1613, Sep. 2008.
[38] G. Buiatti, J. Martin-Ramos, A. Amaral, P. Dworakowski, and A. M. Cardoso, "Condition monitoring of metallized polypropylene film capacitors in railway power trains," *IEEE Trans. Instrum. Meas.*, vol. 58, no. 10, pp. 3796–3805, Oct. 2009.
[39] G. Buiatti, J. Martin-Ramos, C. Garcia, A. Amaral, and A. M. Cardoso, "An online and noninvasive technique for the condition monitoring of capacitors in boost converters," *IEEE Trans. Instrum. Meas.*, vol. 59, no. 8, pp. 2134–2143, Aug. 2010.
[40] A. Amaral and A. Cardoso, "On-line fault detection of aluminium electrolytic capacitors, in step-down dc-dc converters, using input current and output voltage ripple," *IET Power Electron.*, vol. 5, no. 3, pp. 315–322, Mar. 2012.
[41] M. Gasperi, "Life prediction modeling of bus capacitors in ac variable-frequency drives," *IEEE Trans. Ind. Appl.*, vol. 41, no. 6, pp. 1430–1435, Nov. 2005.
[42] M. Gasperi, "Life prediction model for aluminum electrolytic capacitors," in *Proc. Conf. Record IEEE 31st Ind. Appl. Conf.*, vol. 3, Oct. 1996, pp. 1347–1351.
[43] Y. Yu, T. Zhou, M. Zhu, and D. Xu, "Fault diagnosis and life prediction of dc-link aluminum electrolytic capacitors used in three-phase ac/dc/ac converters," in *Proc. 2nd Int. Conf. Instrum., Meas., Comput., Commun. Control*, Dec. 2012, pp. 825–830.
[44] J.-J. Moon, W.-S. Im, and J.-M. Kim, "Capacitance estimation of dc-link capacitor in brushless dc motor drive systems," in *Proc. IEEE ECCE Asia Downunder*, Jun. 2013, pp. 525–529.
[45] M. Ahmad, A. Arya, and S. Anand, "An online technique for condition monitoring of capacitor in PV system," in *Proc. IEEE Int. Conf. Ind. Technol.*, Mar. 2015, pp. 920–925.
[46] K. Abdennadher, P. Venet, G. Rojat, J. Retif, and C. Rosset, "Kalman filter used for on line monitoring and predictive maintenance system of aluminium electrolytic capacitors in ups," in *Proc. IEEE Energy Convers. Congr. Expo.*, Sep. 2009, pp. 3188–3193.
[47] A. Imam, T. Habetler, R. Harley, and D. Divan, "Condition monitoring of electrolytic capacitor in power electronic circuits using input current," in *Proc. 5th IEEE Int. Symp. Diagn. Elect. Mach. Power Electron. Drives*, Sep. 2005, pp. 1–7.
[48] G. Buiatti, A. Amaral, and A. Cardoso, "ESR estimation method for dc/dc converters through simplified regression models," in *Proc. Conf. Record IEEE 42nd Ind. Appl. Conf.*, Sep. 2007, pp. 2289–2294.
[49] G. Wang, Y. Guan, J. Zhang, L. Wu, X. Zheng, and W. Pan, "ESR estimation method for dc-dc converters based on improved EMD algorithm," in *Proc. IEEE Conf. Progn. Syst. Health Manage.*, May 2012, pp. 1–6.
[50] P. Lipnicki, M. Orkisz, D. Lewandowski, and A. Tresch, "The effect of change in dc link series resistance on the ac/ac converter operation: Power converters embedded diagnostics," in *Proc. IEEE 1st Int. Conf. Condition Assess. Techn. Elect. Syst.*, Dec. 2013, pp. 122–127.
[51] Y. Kai, H. Wenbin, T. Weijie, L. Jianguo, and C. Jingcheng, "A novel online ESR and C identification method for output capacitor of buck converter," in *Proc. IEEE Energy Convers. Congr. Expo.*, Sep. 2014, pp. 3476–3482.
[52] S. Shili, A. Hijazi, P. Venet, A. Sari, X. Lin-Shi, and H. Razik, "Balancing circuit control for supercapacitor state estimation," in *Proc. 10th Int. Conf. Ecological Veh. Renew. Energies*, Mar. 2015, pp. 1–7.
[53] K. Abdennadher, P. Venet, G. Rojat, J. Retif, and C. Rosset, "Online monitoring method and electrical parameter ageing laws of aluminium electrolytic capacitors used in ups," in *Proc. 13th Eur. Conf. Power Electron. Appl.*, Sep. 2009, pp. 1–9.
[54] V. Sankaran, F. Rees, and C. Avant, "Electrolytic capacitor life testing and prediction," in *Proc. Conf. Record IEEE 32nd Ind. Appl. Conf.*, vol. 2, Oct. 1997, vol. 2, pp. 1058–1065.
[55] A. Amaral and A. Cardoso, "Use of ESR to predict failure of output filtering capacitors in boost converters," in *Proc. IEEE Int. Symp. Ind. Electron.*, vol. 2, May 2004, pp. 1309–1314.
[56] A. Imam, T. Habetler, R. Harley, and D. Divan, "LMS based condition monitoring of electrolytic capacitor," in *Proc. 31st Annu. Conf. IEEE Ind. Electron. Soc.*, Nov. 2005, pp. 848–853.
[57] A. Imam, T. Habetler, R. Harley, and D. Divan, "Failure prediction of electrolytic capacitor using DSP methods," in *Proc. 20th Annu. IEEE Appl. Power Electron. Conf. Expo.*, Mar. 2005, vol. 2, pp. 965–970.
[58] G. Buiatti, A. Amaral, and A. M. Cardoso, "Parameter estimation of a dc/dc buck converter using a continuous time model," in *Proc. Power Electron. Appl., Eur. Conf.*, Sep. 2007, pp. 1–8.
[59] A. Amaral and A. Cardoso, "A non-invasive technique for fault diagnosis of SMPS," in *Proc. Power Electron. Spec. Conf.*, Jun. 2008, pp. 2097–2102.
[60] A. Amaral and A. Cardoso, "State condition estimation of aluminum electrolytic capacitors used on the primary side of ATX power supplies," in *Proc. 35th Annu. Conf. IEEE Ind. Electron.*, Nov. 2009, pp. 442–447.
[61] A. Amaral and A. Cardoso, "Using input current and output voltage ripple to estimate the output filter condition of switch mode dc/dc converters," in *Proc. IEEE Int. Symp. Diagn. Elect. Mach., Power Electron. Drives*, Aug. 2009, pp. 1–6.
[62] G. Wang, Y. Guan, J. Zhang, L. Wu, X. Zheng, and W. Pan, "ESR estimation method for dc-dc converters based on improved EMD algorithm," in *Proc. IEEE Conf. Progn. Syst. Health Manage.*, May 2012, pp. 1–6.
[63] S. A. Makdessi M., and V. P., "Health monitoring of dc link capacitors," *Chem. Eng. Trans.*, vol. 33, pp. 1105–1110, 2013.
[64] F. M. I. D. Astigarraga, F. Arizti, and A. Galarza, "Estimation of dc-link capacitor equivalent series resistance for in-vehicle prognostic health monitoring," in *Proc. 3rd Int. Symp. Energy Challenges Mach.*, vol. 2, 2015.
[65] A survey of electrochemical supercapacitor technology. [Online]. Available: http://services.eng.uts.edu.au/cempe/subjects_JGZ/eet/Capstone _ AN.pdf
[66] "Capacitors age and capacitors have an end of life - white paper," in *Emerson Network Power*, 2015.
[67] H. Wang and F. Blaabjerg, "Reliability of capacitors for dc-link applications in power electronic converters—an overview," *IEEE Trans. Ind. Appl.*, vol. 50, no. 5, pp. 3569–3578, Sep. 2014.
[68] H. Wang, D. A. Nielsen, and F. Blaabjerg, "Degradation testing and failure analysis of dc film capacitors under high humidity conditions," *Microelectron. Reliability*, vol. 55, no. 910, pp. 2007–2011, 2015. [Online]. Available: http://www.sciencedirect.com/science/article/pii/S0026271415001419
[69] H. Wang, D. A. Nielsen, and F. Blaabjerg, "Degradation testing and failure analysis of dc film capacitors under high humidity conditions," in *Proc. 26th Eur. Symp. Rel. Electron Devices, Failure Phys. Anal.*, 2015, pp. 2007–2011. [Online]. Available: http://www.sciencedirect.com/science/article/pii/S0026271415001419

Hammam Soliman (S'011) received the bachelor's and master's degrees in electrical and control engineering from the Arab Academy for Science, Technology, and Maritime Transport (AASTMT), Cairo, Egypt, in 2010 and 2013, respectively. He is currently working toward the Ph.D. degree in the Energy Technology Department, Aalborg University, Aalborg, Denmark.

He is a Team Member with the Center of Reliable Power Electronics, Energy Technology Department, Aalborg University. He was a Teaching Assistant in the Electrical Engineering Department, AASTMT, from September 2010 to November 2013. He was also a part-time Design Engineer at Bahrawy Consultancy Group, Cairo. His current research interests include the reliability of power electronic systems, reliability of capacitors, and monitoring the health conditions of capacitors in dc-link applications.

Huai Wang (S'07–M'12) received the B.E. degree in electrical engineering from the Huazhong University of Science and Technology, Wuhan, China, in 2007, and the Ph.D. degree in power electronics from the City University of Hong Kong, Hong Kong, China, in 2012.

He is currently an Associate Professor and a Work Package Leader with the Center of Reliable Power Electronics, Aalborg University, Aalborg, Denmark. He was a Visiting Scientist at ETH Zurich, Zurich, Switzerland, from August to September 2014, and at the Massachusetts Institute of Technology, Cambridge, MA, USA, from September to November 2013. He was at the ABB Corporate Research Center, Baden, Switzerland, in 2009. His current research interests include the reliability of power electronic systems, reliability of capacitors and IGBT modules, multiobjective life-cycle performance optimization of power electronic systems, time-domain control of converters, and emerging power electronics applications. He has coedited a book on Reliability of Power Electronic Converter Systems in 2015, filed four patents, and contributed more than 30 journal papers.

Dr. Wang received the Richard M. Bass Outstanding Young Power Electronics Engineer Award from the IEEE Power Electronics Society in 2016, and the Green Talents Award from the German Federal Ministry of Education and Research in 2014. He has received six Best Paper and Project Awards from industry, IEEE, and the Hong Kong Institution of Engineers. He serves as the Guest Editor-in-Chief of the IEEE JOURNAL OF EMERGING AND SELECTED TOPICS IN POWER ELECTRONICS Special Issue on Power Electronics for Energy Efficient Buildings, and is an Associate Editor of the IEEE TRANSACTIONS ON POWER ELECTRONICS.

Frede Blaabjerg (S'86–M'88–SM'97–F'03) received the Ph.D. degree in power electronics from Aalborg University, Aalborg, Denmark, in 1992.

He was at ABB-Scandia, Randers, Denmark, from 1987 to 1988. He became an Assistant Professor in 1992, an Associate Professor in 1996, and a Full Professor of Power Electronics and Drives with Aalborg University in 1998. He has been a part time Research Leader in wind turbines with the Research Center Risoe, Roskilde, Denmark. From 2006 to 2010, he was the Dean of the Faculty of Engineering, Science, and Medicine, and became a Visiting Professor at Zhejiang University, Hangzhou, China, in 2009. His current research interests include power electronics and its applications such as in wind turbines, photovoltaic systems, reliability, harmonics, and adjustable speed drives.

Dr. Blaabjerg received the 1995 Angelos Award for his contribution in the modulation technique and the Annual Teacher Prize from Aalborg University. In 1998, he received the Outstanding Young Power Electronics Engineer Award from the IEEE Power Electronics Society (PELS). He has received 15 IEEE Prize Paper Awards and another Prize Paper Award from the International Conference on Power Electronics and Intelligent Control for Energy Conservation Poland in 2005. He received the IEEE PELS Distinguished Service Award in 2009, the International Conference on Power Electronics and Motion Control Council Award in 2010 and the IEEE William E. Newell Power Electronics Award in 2014. He has received a number of major research awards in Denmark, including the largest individual Danish research award, the Villum Kann Rasmussen Annual Award for Technical and Scientific Research in 2014. He was an Editor-in-Chief of the IEEE TRANSACTIONS ON POWER ELECTRONICS from 2006 to 2012. He was a Distinguished Lecturer for the IEEE PELS from 2005 to 2007 and for the IEEE Industry Applications Society from 2010 to 2011. He was the Chairman of EPE in 2007 and the International Symposium on Power Electronics for Distributed Generation Systems in 2012.

Artificial Neural Network Algorithm for Condition Monitoring of DC-link Capacitors Based on Capacitance Estimation

Soliman, Hammam Abdelaal Hammam; Wang, Huai; Gadalla, Brwene Salah Abdelkarim; Blaabjerg, Frede

Published in:
Journal of Renewable Energy and Sustainable Development (RESD)

Publication date:
2015

Document Version
Accepted author manuscript

Artificial Neural Network Algorithm for Condition Monitoring of DC-link Capacitors Based on Capacitance Estimation

Hammam Soliman, Huai Wang, IEEE Member, Brwene Gadalla, Frede Blaabjerg, IEEE Fellow
Department of Energy Technology, Aalborg University,
Aalborg 9220, Denmark,
has@et.aau.dk, hwa@et.aau.dk, bag@et.aau.dk, fbl@et.aau.dk

Abstract - In power electronic converters, reliability of DC-link capacitors is one of the critical issues. The estimation of their health status as an application of condition monitoring have been an attractive subject for industrial field and hence for the academic research filed as well. More reliable solutions are required to be adopted by the industry applications in which usage of extra hardware, increased cost, and low estimation accuracy are the main challenges. Therefore, development of new condition monitoring methods based on software solutions could be the new era that covers the aforementioned challenges. A capacitance estimation method based on Artificial Neural Network (ANN) algorithm is therefore proposed in this paper. The implemented ANN estimated back converter. Analysis of the error of the capacitance estimation is also given. The presented method enables a pure software based approach with high parameter estimation accuracy.

Keywords - Capacitor condition monitoring; capacitor health status; Capacitance estimation.

I. INTRODUCTION

Condition monitoring is an important strategy to estimate the health condition of power electronic components, convert- ers and systems. It is widely applied in reliability or safety critical applications, such as wind turbines, electrical aircraft, electric vehicles, etc., enabling the indication of future failure occurrences and preventive maintenances. In [1], the condition monitoring of semiconductor devices used in power electronics is well reviewed. Besides the power devices, and according to [2], electrolytic capacitors are sharing 60% of the failure distribution for power converter elements as shown in Fig.1, therefore, capacitors are another type of reliability critical components.

In the last two decades, a large number of research results on condition monitoring of capacitors has been published. The majority of the condition monitoring methods for capacitors are based on estimation of the capacitance C and equivalent series resistance (ESR), which are indicators of the degradation of capacitors [3]. For aluminum electrolytic capacitors, the widely accepted end-of-life criteria are 20% capacitance reduction or double of the ESR. For film capacitors, a reduction of 2% to 5% capacitance may indicate the reach of end-of-life. Therefore, a method which can estimate the C value could be applied on both aluminum electrolytic and film capacitors. However, obtaining the values of C or ESR is an important step since it gives an indication of the ageing process and its acceleration. Fig. 2(a) shows a simplified equivalent model of capacitors and Fig. 2(b) plots the corresponding frequency characteristics. It can be noted that the capacitor impedances are distinguished by three frequency regions dominated by capacitance, ESR and the Equivalent Series Inductance (ESL), respectively.

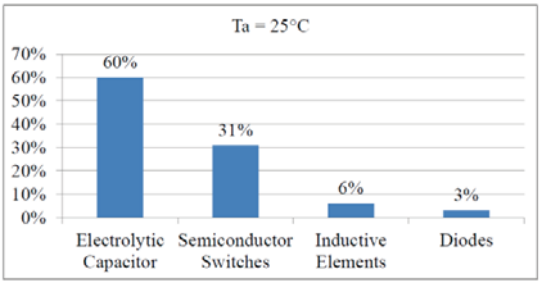

Fig .1. Distribution of failure for power converetr elements [2

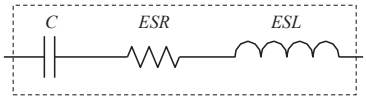

(a) Simplified equivalent model of capacitors

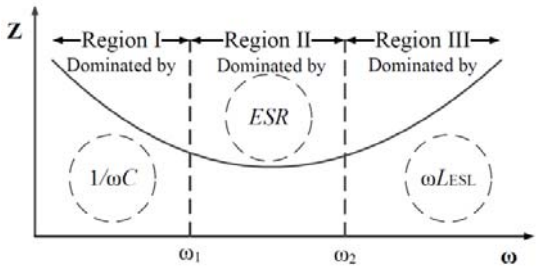

(b) Impedance characteristic of capacitors

Fig .2. Equivalent model and impedance characteristics of capacitors.

From the methodology point of view in [4], condition monitoring methods in the literature are classified into three categories as the following: a) Capacitor ripple current sensor based methods, b) Circuit model based methods, and c) Data and advanced algorithm based methods. The following three subsections are defining the principle of each category with its corresponding examples from the literature.

A. Capacitor ripple current sensor based methods

The basic principle of the this category is to estimate the capacitance and/or the ESR by using the capacitor ripple voltage and current information at region I and II (as shown in Fig. 2(b)). In [2, 5–7], an external current injection at low fre-quency is the main approach to achieve condition monitoring, it has been applied to PWM AC/DC/AC converter in [2], [5], and [7], while in [6] it has been applied to a sub-module capacitor in moulder multilevel converter.

B. Circuit model based methods

This category is based on that instead of injecting external signals, the capacitor current can be obtained indirectly de- pending on both the circuit model and the operation principle of PWM switching converters. In [8], an on-line condition monitoring based on capacitance estimation is proposed, the capacitor ripple current is calculated using the difference between the input current sensor, and the output current flows to the inverter which is based on the transistor switching statues.

C. Data and advanced algorithm based methods

This category, obtaining a strong correlation between the available parameters and the parameters to be estimated is the main concept. In [9], an external voltage is injected to the reference voltage of the capacitor at low frequency, the obtained capacitor power is used as a training data in sake of finding an identification model based on Support Vector Regression (SVR). After using a group of training data, a generated function is used to analyse the correlation between the known capacitor power and its corresponding capacitance value. Although the previous mentioned methods have been ver- ified by simulation and experimental work, errors, complex-ity, and cost increasing due to extra hardware are common shortcomings. Therefore, the developed technologies are rarely adopted in practical industry applications, implying that new condition monitoring methods based on software solutions and existing feedback signals, without adding any hardware cost, could be more promising in practical applications.

This paper aims to propose a condition monitoring method based on Artificial Neural Network (ANN) that uses existing power stage and control information and existing spare re- sources of digital controllers. It requires no extra hardware cir- cuitry (e.g., current sensors and corresponding signal condition circuits), no external signal injection, and therefore minimises the increased complexity and cost. Main sections in this paper are as the following: Section II gives the basic principle of ANN applied for capacitor condition monitoring. Section III

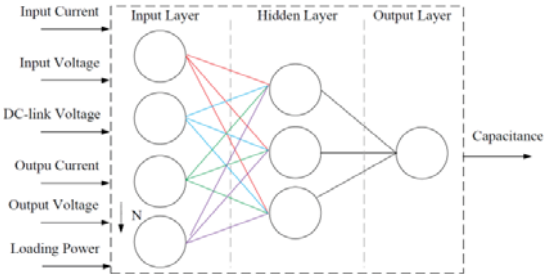

Fig .3. The structure of the Artificial Neural Network.

illustrates the applied ANN to a back to back converter study case. Section IV presents the results achieved by the proposed method based on ANN, followed by the conclusion.

II. ANN FOR CAPACITOR CONDITION MONITORING

Implementation of capacitor condition monitoring

using ANN is motivated by the shortcomings that have been investigated earlier in this paper. Avoiding the usage of direct/indirect current sensors is one of the main advantages of using ANN to obtain the estimated value of C. Instead of sensing the capacitor current iC, only the input terminal and output terminal information of the power converters are used as inputs to the ANN, while the capacitance is the ANN's target, and then the network is responsible for estimating the value of C when using different inputs than the trained ones. Normally, during the operation of the power converter, the required terminal information to train the ANN is supposed to be available. Taking the power level of the applied converter into consideration while the network is trained, is improving the ANN's estimated results by being more robust against dynamic variations of the loading power. Fig.3 illustrates the structure of the proposed ANN. The basic structure of any neural network consists of three layers, input, hidden, and output layers. The input layer is where the available amount of data N fed to the ANN will be stored. The hidden layer job is to transform the inputs into a function that the output layer can use, while the output layer transforms the hidden layer activations into a scale which the operator wanted the output to be on target.

III. CAPACITANCE ESTIMATION BASED ON ANN

Capacitance estimation based on ANN is applied to a back to back converter as shown in Fig. 4. The specifications of the converter are listed in Table I.

Capacitance values in the range between (1000μF and 5000μF) with 100μF step are used as targets to the network, each value of these 41 samples corresponds respectively to the single phase RMS input/output voltages, currents, and the DC-link voltage. Since the different loading condition of the back-to-back converter is also considered, three groups of 41 samples under the respective loading level of 10 kW, 7 kW and 4 kW are used.

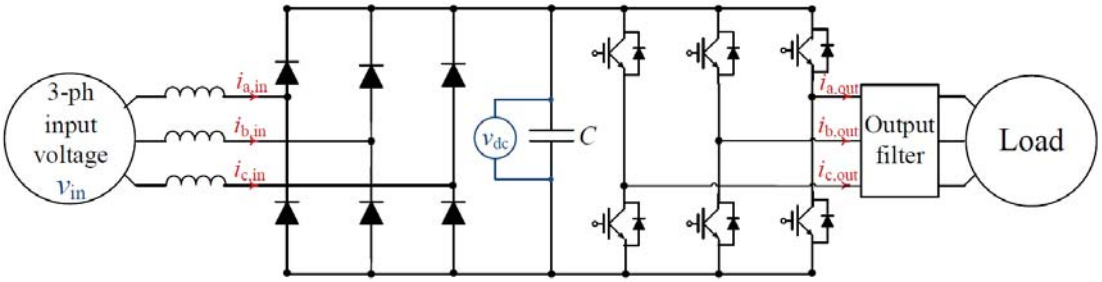

Fig .4. A back-to-back converter.

Table 1. THE SPECIFICATIONS OF THE BACK-TO-BACK CONVERTER PARAMETERS.

Input AC Voltage (*VL−L*)	600 V
Output AC Voltage (*VL−L*)	380 V
Rated DC-link Voltage (*Vdc*)	780 V
Full Power Level (*Po*)	10 kW
Capacitance (*C*)	5000 *μ*F

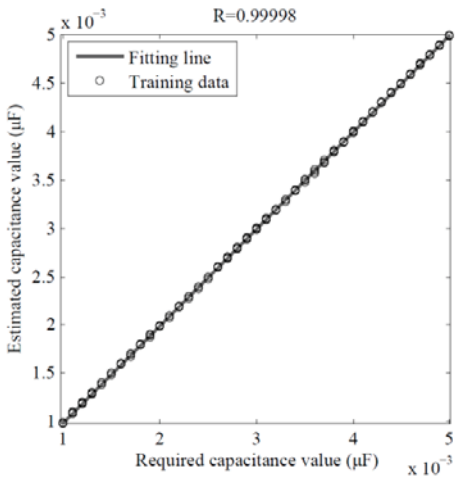

Fig .5. Regression responce of the trained network..

All the 123 samples are fed to a single hidden layer ANN consisting of 10 neurons using the Neural Fitting Tool (nftool) in MATLAB software. This tool is usually used for estimation and prediction of problems in which the neural network maps between a data set of numeric inputs and a set of numeric targets. The iteration algorithm used in this training is Levenberg-Marquardt, which typically takes more memory but less time. The training automatically stops when generalisation stops improving, as indicated by an increase in the mean square error of the validation samples. During the training observing the Regression value R is important, since Regression values measure the correlation between outputs and targets. An R value of 1 means a close relationship, while 0 means a random relationship. Fig. 5 shows the regression response of the trained network in this paper. It can be noted that all the

123 input data are exactly aligned on the fitting line and the values of R are close to 1. Based on this result, the network stopped training and the ANN is generated to be used.

IV. SIMULATION RESULTS AND DISCUSSION

In this section, the trained network is tested for verification purpose. The inputs to the ANN are stored in the Matlab work- space, and they are sent to the ANN as a group set every 0.2 seconds. Each group set is resulting in one corresponding output (estimated C value). The same group set of inputs is sent until a new set is available in the work-space. The same back to back converter as shown in Fig. 4 is used for the simulation test, but with two capacitors C1 and C2 connected in parallel through switches to have the option to switch between them to simulate the degradation of C. At the timing (5 sec) the capacitor C2 will be switched on instead of C1 . Fig.6 shows the capacitance value estimated by the trained ANN. The simulation results for the estimated parameters and their corresponding errors are shown in Table II. The estimated results verify that the trained ANN is responding for the changes in the capacitance value, and the statues of the capacitor could be easily identified.

Table 2. SIMULATION RESULTS FOR ESTIMATED CAPACITANCE..

$C1_{actual}$=5000μF	$C1_{estimated}$=4991μF	Error=0.18%
$C2_{actual}$=4000μF	$C2_{estimated}$=3996μF	Error=0.1%

Moreover, to prove the accuracy of the trained ANN, the network is tested to identify the reduction of 50μF out of 5000μF and the resulted estimation is shown in Fig. 7. For the initial stage, the estimated value is 4991μF and for the degraded case, the estimated value is 4945μF, which gives a 0.18% error as a maximum.

To test the robustness of the trained ANN against loading power variations, the ANN is tested to estimate a capacitance

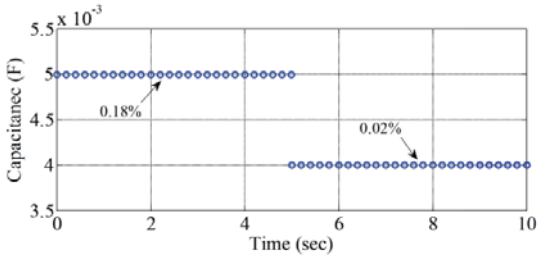

Fig .6. Tested DC-link capacitor change in a back-to-back converter.

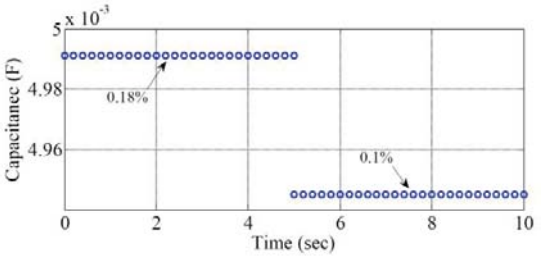

Fig .7. Trained ANN accuracy for the capacitance change shown in Fig. 6.

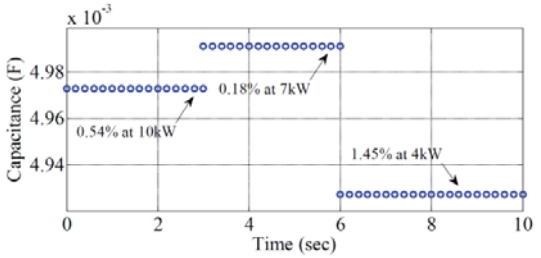

Fig .8. Trained ANN accuracy for the loading power change.

value of 5000μF during a loading power change. The esti- mated results with their corresponding errors percentage are shown in Fig. 8.

Moreover, for further verification of the ANN accuracy, a set of random values of capacitance between the ranges of (1000μF-5000μF) are applied under three different power levels, their actual and estimated values are shown in Fig.9. The actual and estimated values of capacitance of the set applied under 70% power level are presented in Table III.

In sake of showing the impact of the training data amount on the accuracy of the trained ANN, another network (ANN2) is trained by using 63 samples instead of 123 samples considering the same conditions of (ANN1) which have been trained earlier in this paper. Fig. 10 shows that the errors estimated by ANN2 are higher than the ones estimated previously by ANN1, implying the trade-off between estimation accuracy and required computation resource.

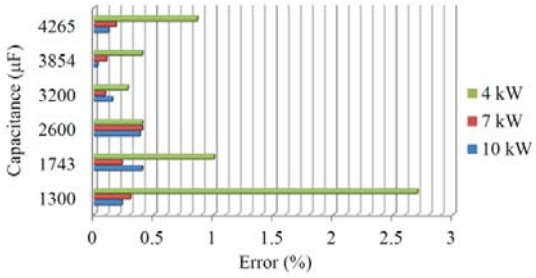

Fig .9. Estimation error analysis under different level of power.

Table 3. SIMULATION RESULTS FOR ESTIMATED CAPACITANCE (AT 7KW).

C_{actual}=1300μF	$C_{estimated}$=1296μF	Error=0.3%
C_{actual}=1743μF	$C_{estimated}$=1747μF	Error=0.23%
C_{actual}=2600μF	$C_{estimated}$=2589μF	Error=0.4%
C_{actual}=3200μF	$C_{estimated}$=3203μF	Error=0.09%
C_{actual}=3854μF	$C_{estimated}$=3850μF	Error=0.1%
C_{actual}=4265μF	$C_{estimated}$=4257μF	Error=0.18%

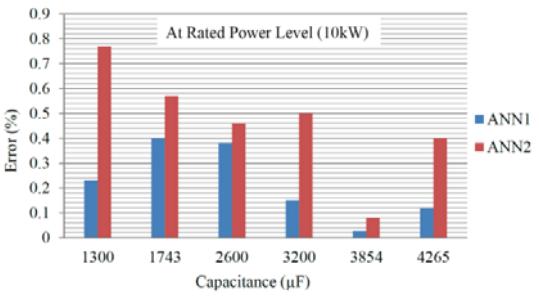

Fig .10. Estimation error analysis by different trained ANNs.

The last accuracy analysis is performed to observe the error percentage of the estimated capacitance with respect to different degree of changes of the original value of 5000μF, the results are shown in Fig. 11. It can be noted that the estimation errors of the proposed ANN are below 0.25%. It can respond and estimate correctly the capacitance values even under a very low level of capacitance reduction of 0.2% changes.

The following remarks are given from the results presented in this section:

- The simulation results of the proposed method based on ANN verify that condition monitoring methods based on software solutions could be an attractive alternative for the practical industry applications.

- It can be noted from the results that trained ANN is capable to respond to a very small change of capacitance

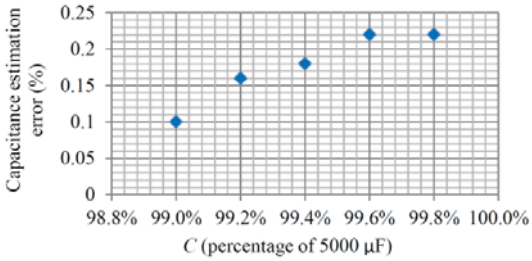

Fig .11. Estimation error analysis under different level of capacitance reduction at rated power level.

and estimate the capacitance value within the range in which the network is trained.

- It should be noted that the accuracy of the trained ANN strongly depends on the amount, quality, and accuracy of the data used in the training.

V. CONCLUSIONS

A new capacitor condition monitoring method based on Artificial Neural Network algorithm is proposed in this paper. It is applied to a back-to-back converter study case to estimate the capacitance value change of the DC-link capacitor. The proposed method requires no additional hardware circuit and could be implemented by using the spare resources of existing

digital controllers in most of power electronic systems, implying a minimum increased cost (e.g., only in the research and development part). The error analysis under different DC-link capacitance values and different level of capacitance reduction with respect to the initial value are given, achieving a maximum estimation error that is well below 0.5%, which could be acceptable in many practical applications. The impact of training data amount on the error analysis is also given.

REFERENCES

[1] S. Yang, D. Xiang, A. Bryant, P. Mawby, L. Ran, and P. Tavner, "Condition monitoring for device reliability in power electronic converters: A review," IEEE Transactions on Power Electronics, vol. 25, no. 11, pp. 2734–2752, Nov 2010.

[2] X.-S. Pu, T. H. Nguyen, D.-C. Lee, K.-B. Lee, and J.-M. Kim, "Fault diagnosis of dc-link capacitors in three-phase ac/dc pwm converters by online estima- tion of equivalent series resistance," *IEEE Transac- tions on Industrial Electronics*, vol. 60, no. 9, pp. 4118–4127, Sept 2013.

[3] H. Wang and F. Blaabjerg, "Reliability of capac- itors for dc-link applications in power electronic converters-an overview," *IEEE Transactions on Industry Applications*, vol. 50, no. 5, pp. 3569–3578, Sept 2014.

[4] H. Soliman, H. Wang, and F. Blaabjerg, "A review of the condition monitoring of capacitors in power electronic converters," in *Electromotion Joint International Conference (ACEMP - OPTIM), 2015 IEEE*, August 2015, pp. 243–249.

[5] D.-C. Lee, K.-J. Lee, J.-K. Seok, and J.-W. Choi, "Online capacitance estimation of dc-link electrolytic capacitors for three-phase ac/dc/ac pwm converters using recursive least squares method," *in Proceedings of Electric Power Applications*, vol. 152, no. 6, pp. 1503–1508, Nov 2005.

[6] Y.-J. Jo, T. H. Nguyen, and D.-C. Lee, "Condition monitoring of submodule capacitors in modular multilevel converters," in *Energy Conversion Congress and Exposition (ECCE), 2014 IEEE*, Sept 2014, pp. 2121–2126.

[7] T. H. Nguyen and D.-C. Lee, "Deterioration mon- itoring of dc-link capacitors in ac machine drives by current injection," *IEEE Transactions on Power Electronics*, vol. 30, no. 3, pp. 1126–1130, March 2015.

[8] A. Wechsler, B. Mecrow, D. Atkinson, J. Bennett, and M. Benarous, "Condition monitoring of dc-link capacitors in aerospace drives," *IEEE Transactions on Industry Applications*, vol. 48, no. 6, pp. 1866– 1874, Nov 2012.

[9] A. Abo-Khalil and D.-C. Lee, "Dc-link capacitance estimation in ac/dc/ac pwm converters using voltage injection," *IEEE Transactions on Industry Applications*, vol. 44, no. 5, pp. 1631–1637, Sept 2008.

Condition Monitoring for DC-link Capacitors Based on Artificial Neural Network Algorithm

Soliman, Hammam Abdelaal Hammam; Gadalla, Brwene Salah Abdelkarim; Wang, Huai; Blaabjerg, Frede

Published in:
IEEE 5th International Conference on Power Engineering, Energy, and Electrical Drives

Publication date:
2015

Document Version
Publisher final version (usually the publisher pdf)

Condition Monitoring for DC-link Capacitors Based on Artificial Neural Network Algorithm

Hammam Soliman, Huai Wang, *IEEE Member*, Brwene Gadalla, Frede Blaabjerg, *IEEE Fellow*
Department of Energy Technology, Aalborg University
Aalborg 9220, Denmark
has@et.aau.dk, hwa@et.aau.dk, bag@et.aau.dk, fbl@et.aau.dk

***Abstract*—In power electronic systems, capacitor is one of the reliability critical components . Recently, the condition monitoring of capacitors to estimate their health status have been attracted by the academic research. Industry applications require more reliable power electronics products with preventive maintenances. However, the existing capacitor condition monitoring methods suffer from either increased hardware cost or low estimation accuracy, being the challenges to be adopted in industry applications. New development in condition monitoring technology with software solutions without extra hardware will reduce the cost, and therefore could be more promising for industry applications. A condition monitoring method based on Artificial Neural Network (ANN) algorithm is therefore proposed in this paper. The implementation of the ANN to the DC-link capacitor condition monitoring in a back-to-back converter is presented. The error analysis of the capacitance estimation is also given. The presented method enables a pure software based approach with high parameter estimation accuracy.**

I. Introduction

Condition monitoring is an important strategy to estimate the health condition of power electronic components, converters and systems. It is widely applied in reliability or safety critical applications, such as wind turbines, electrical aircraft, electric vehicles, etc., enabling the indication of future failure occurrences and preventive maintenances. In [1], the condition monitoring of semiconductor devices used in power electronics is well reviewed. Besides the power devices, capacitors are another type of reliability critical components. In the last two decades, a large number of research results on condition monitoring of capacitors have been published. From this paper point of view, condition monitoring methods in the prior-art are classified into three categories according to their methodologies, as the following: a) Capacitor ripple current sensor based methods, b) Circuit model based methods, and c) Data and advanced algorithm based methods. The basic principle of the first category is to estimate the capacitance and/or the Equivalent Series Resistance *ESR* by using the capacitor ripple voltage and current information at low and medium frequencies (as shown in Fig. 1(b)). In [3-6], an external current injection at low frequency is the main approach to achieve condition monitoring, it have been applied on PWM AC/DC/AC converter in [3], [4], and [6], while in [5] is applied to a sub-module capacitor in moulder multilevel converter. In the second category, instead of injecting external signals, the capacitor current can be obtained indirectly depending on both the circuit model and the operation principle of PWM switching converters. In [7], an on-line condition monitoring based on capacitance estimation is proposed, the capacitor ripple current is calculated using the difference between the input current sensor, and the output current flows to the inverter which is based on the transistor switching statues. In the third category, obtaining a strong correlation between the available parameters and the parameters to be estimated is the main concept. In [8], an external voltage is injected to the reference voltage of the capacitor at low frequency, the obtained capacitor power is used as a training data in sake of finding an identification model based on Support Vector Regression (*SVR*). After using a group of training data, a generated function is used to analyse the correlation between the known capacitor power and its corresponding capacitance value. Although the previous mentioned methods have been verified by simulation and experimental work, errors, complexity, and cost increasing due to extra hardware are common shortcomings. Therefore, the developed technologies are rarely adopted in practical industry applications, implying that new condition monitoring methods based on software solutions and existing feedback signals, without adding any hardware cost, could be more promising in practical applications.

The majority of the condition monitoring methods for capacitors are based on estimation of the capacitance C and (*ESR*), which are indicators of the degradation of capacitors [2]. For aluminum electrolytic capacitors, the widely accepted end-of-life criteria is 20% capacitance reduction or double of the *ESR*. For film capacitors, a reduction of 2% to 5% capacitance may indicate the reach of end-of-life. Therefore, a method which can estimate the C value could be applied on both aluminum electrolytic and film capacitors. However, obtaining the values of C or *ESR* is an important step. Fig. 1(a) shows a simplified equivalent model of capacitors and Fig. 1(b) plots the corresponding frequency characteristics. It can be noted that the capacitor impedances is distinguished by three frequency regions dominated by capacitance, *ESR* and the Equivalent Series Inductance (*ESL*), respectively.

This paper aims to propose a condition monitoring method based on Artificial Neural Network (ANN) that uses existing

978-1-4799-9978-1/15/$31.00 ©2015 European Union

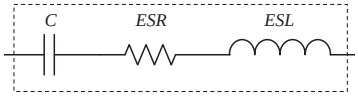

(a) Simplified equivalent model of capacitors

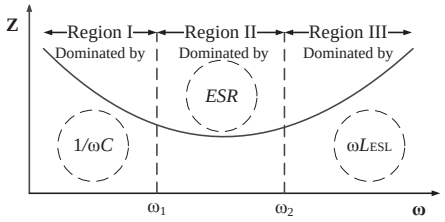

(b) Impedance characteristic of capacitors

Fig. 1. Equivalent model and impedance characteristics of capacitors.

power stage and control information and existing spare resources of digital controllers. It requires no hardware circuitry (e.g., current sensors and corresponding signal condition circuits), no external signal injection, and therefore minimizes the increased complexity and cost. Main sections in this paper are as the following: Section II gives the basic principle of ANN applied for capacitor condition monitoring. Section III illustrates the applied ANN to a back to back converter study case. Section IV presents the results accomplished by the proposed method based on ANN, followed by the conclusion.

II. ANN for Capacitor Condition Monitoring

The motivation behind using the ANN for condition monitoring is that, instead of sensing the capacitor current i_C using direct/indirect sensors, it is possible to obtain the estimated value of *C* by applying the ANN, of which only the input terminal and output terminal information of the power converters are needed. Normally the required terminal information to train the ANN supposed to be available during the operation, the aforementioned information are used as an *inputs* to the training network, while the corresponding *C* value is used as a *target*, and then the network is responsible for estimating the value of *C* when using different inputs than the trained ones. The power level of the applied converter is also taken into consideration while the network is trained. Fig.2 illustrates the structure of the proposed ANN. The basic structure of any neural network consists of three layers, input, hidden, and output layers. The input layer is where the available amount of data *N* fed to the ANN will be stored. The hidden layer job is to transform the inputs into a function that the output layer can use, while the output layer transforms the hidden layer activations into a scale which the operator wanted the output to be on target.

III. Capacitance Estimation based on ANN

Capacitance estimation based on ANN is applied on a back to back converter shown in Fig. 3. The ratings of the converter

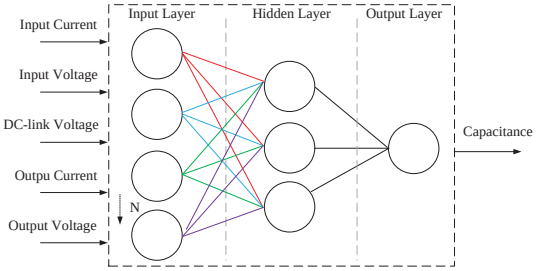

Fig. 2. Structure of the Artificial Neural Network.

are listed in Table I.

TABLE I
Ratings of the Back-to-Back Converter Parameters.

Input AC Voltage (V_{L-L})	600 V
Output AC Voltage (V_{L-L})	380 V
Rated DC-link Voltage (V_{dc})	780 V
Full Power Level (P_o)	10 kW
Capacitance (C)	5000 μF

Capacitance values in the range between (1000μF and 5000μF) with 100μF step are used as targets to the network, each value of these 41 samples are corresponded respectively to the single phase (phase A) *RMS* input/output voltages, currents, and the DC-link voltage. Since the different loading condition of the back-to-back converter is also considered, three group of 41 samples under the respective loading level of 10 kW, 7 kW and 4 kW are used.

All the 123 samples are fed to a single hidden layer ANN consisting of 10 neurons using the Neural Fitting Tool *nftool* in MATLAB software. This tool is usually used for estimation and prediction problems in which the neural network maps between a data set of numeric inputs and a set of numeric targets. The iteration algorithm used in this training is *Levenberg-Marquardt*, which typically takes more memory but less time. The training automatically stops when generalization stops improving, as indicated by an increase in the mean square error of the validation samples. During the training observing the Regression value *R* is important, since Regression values measure the correlation between outputs and targets. An *R* value of 1 means a close relationship, while 0 means a random relationship. Fig. 4 shows the regression response of the trained network in this paper, it can be noted that all the 123 input data are exactly aligned on the fitting line and the values of *R* is close to 1. Based on this result, the network stopped training and the ANN is generated to be used.

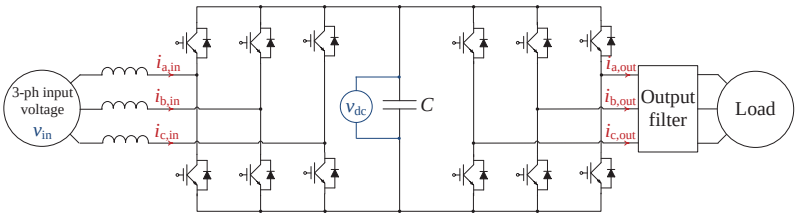

Fig. 3. A back-to-back converter.

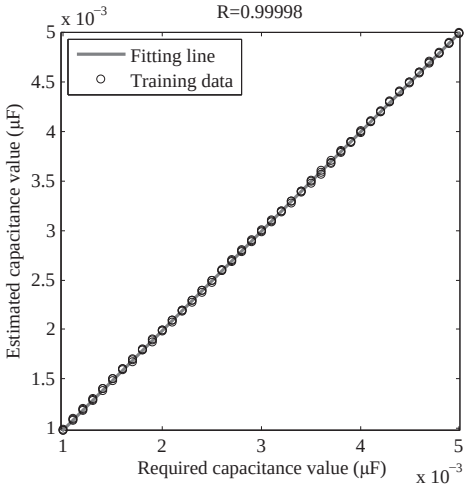

Fig. 4. Regression responce of the trained network.

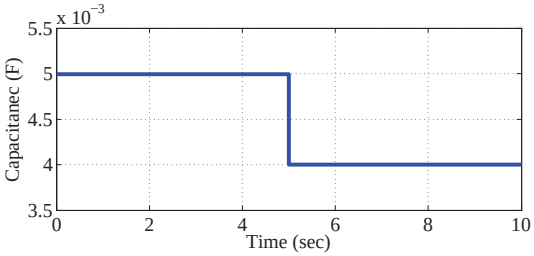

Fig. 5. Tested DC-link capacitor change in a back-to-back converter.

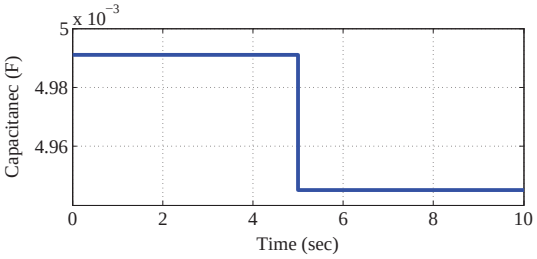

Fig. 6. Trained ANN accuracy for the capacitance change shown in Fig. 5.

IV. Simulation Results and Discussion

In this section, the generated network is tested for verification purpose, the same back to back converter as shown in Fig. 3 is used for the simulation test, but with two capacitors C_1 and C_2 connected in parallel through switches to have the option to switch between them to simulate the degradation of C. At the timing (5 sec) the capacitor C_2 will be switched on instead of C_1. Fig.5 shows the capacitance value estimated by the trained ANN.

The simulation results for the estimated parameters and their corresponding errors are shown in Table II. The estimated results verify that the trained ANN is responding for the changes in the capacitance value, and the statues of the capacitor could be easily identified. Moreover, to prove the accuracy of the trained ANN, the network is tested to identify the reduction of 50μF out of 5000μF and the resulted estimation is shown in Fig. 6. For the initial stage, the estimated value is 4991μF and for the degraded case, the estimated value is 4945μF, which gives a 0.18% error as a maximum. Moreover, for further verification of the ANN accuracy, a set of random values of capacitance between the ranges of (1000μF-5000μF) are applied under three different power levels, their actual and estimated values are shown in Fig. 7. The actual and estimated values of capacitance of the set applied under 70% power level are presented in Table III.

TABLE II
Simulation Results for Estimated Capacitance.

$C_{1actual}$=5000μF	$C_{1estimated}$=4991μF	Error=0.18%
$C_{2actual}$=4000μF	$C_{2estimated}$=3996μF	Error=0.1%

In sake of showing the impact of the training data amount on the accuracy of the trained ANN, another network (ANN2) is trained by using 63 samples instead of 123 samples considering the same conditions of (ANN1) which trained earlier in this paper. Fig. 8 shows that the error percentages estimated by ANN2 are higher than the ones estimated previously by ANN1, implying the trade-off between estimation accuracy and required computation resource.

The last accuracy analysis is performed to observe the

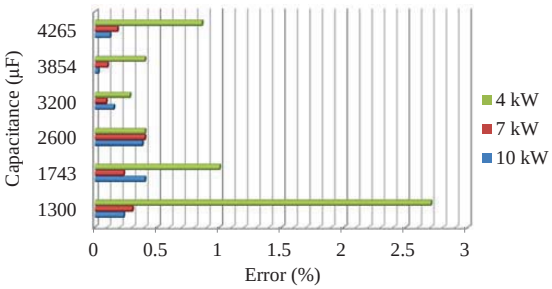

Fig. 7. Estimation error analysis under different level of power.

TABLE III
SIMULATION RESULTS FOR ESTIMATED CAPACITANCE (AT 7KW).

C_{actual}=1300μF	$C_{estimated}$=1296μF	Error=0.3%
C_{actual}=1743μF	$C_{estimated}$=1747μF	Error=0.23%
C_{actual}=2600μF	$C_{estimated}$=2589μF	Error=0.4%
C_{actual}=3200μF	$C_{estimated}$=3203μF	Error=0.09%
C_{actual}=3854μF	$C_{estimated}$=3850μF	Error=0.1%
C_{actual}=4265μF	$C_{estimated}$=4257μF	Error=0.18%

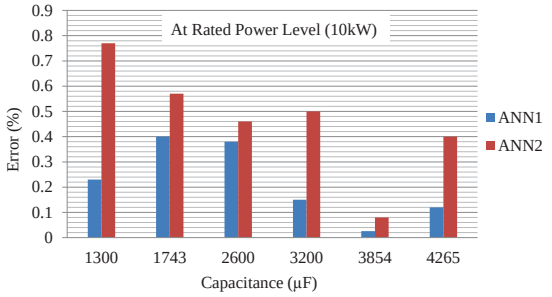

Fig. 8. Estimation error analysis by different trained ANNs.

error percentage of the estimated capacitance with respect to different degree of changes of the original value of 5000μF, the results are shown in Fig. 9. It can be noted that the estimation errors of the proposed ANN are below 0.25%. It can respond and estimate correctly the capacitance values even under a very low level of capacitance reduction of 0.2% changes.

The following remarks are given from the results presented in this section:

a) Simulation results of the proposed method based on ANN verifies that condition monitoring methods based on software solutions could be an attractive alternative for the practical industry applications.
b) It can be noted from the results estimated by the trained ANN that ANN is sensitive since it can respond for any percentage of change, and estimate any capacitance value within the range which the network is trained.
c) It should be noted that the accuracy of the trained ANN strongly depends on the amount, quality, and accuracy of the data used in the training.

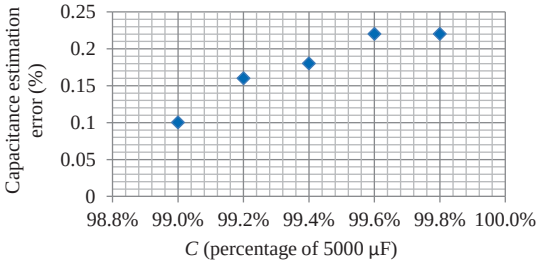

Fig. 9. Estimation error analysis under different level of capacitance reduction at rated power level.

V. CONCLUSIONS

A new capacitor condition monitoring method based on Artificial Neural Network algorithm is proposed in this paper. It is applied for a back-to-back converter study case to estimate the capacitance value change of the DC-link capacitor. The proposed method requires no additional hardware circuit and could be implemented by using the spare resources of existing digital controllers in most of power electronic systems, implying a minimum increased cost (e.g., only in the research and development part). The error analysis under different DC-link capacitance values and different level of capacitance reduction with respect to the initial value are given, achieving a maximum estimation error that is well below 0.5%, which could be acceptable in many practical applications. The impact of training data amount on the error analysis are also given.

REFERENCES

[1] S. Yang, D. Xiang, A. Bryant, P. Mawby, L. Ran, and P. Tavner, "Condition monitoring for device reliability in power electronic converters: a review," *IEEE Trans. Power Electron.*, vol. 25, no. 11, pp. 2734-2752, Nov. 2010.

[2] H. Wang and F. Blaabjerg, "Reliability of capacitors for DC-link applications in power electronic converters an overview," *IEEE Trans. Ind. Appl.*, vol. 50, no. 5, pp. 3569-3578, Sep./Oct. 2014.

[3] X. Pu, T. Nguyen, D. Lee, K. Lee, and J. Kim, "Fault diagnosis of DC-Link capacitors in three-phase AC/DC PWM converters by online estimation of equivalent series Resistance," *IEEE Trans. Ind. Appl.*, vol. 60, no. 9, pp. 4118-4127, Sep. 2013.

[4] D. Lee, K. Lee, J. Seok, and J. Choi, "Online capacitance estimation of DC-link electrolytic capacitors for three-phase AC/DC/AC PWM converters using recursive least squares method," *IEEE Trans. Ind. Appl.*, vol. 152,

no. 6, pp. 1503-1508, Nov./Dec. 2005.
[5] Y. Jo, T. Nguyen, K. Lee, and D. Lee, "Condition monitoring of submodule capacitors in modular multi-level converters," in *Proc. of ECCE*, pp. 2121-2126, Sep. 2014.
[6] T. Nguyen, and D. Lee, "Deterioration monitoring of DC-link capacitors in AC machine drives by current injection," *IEEE Trans. Power Electron.*, vol. 30, no. 3, pp. 1126-1130, Mar. 2015.
[7] A. Wechsler, B. Mecrow, D. Atkinson, J. Bennett, and M. Benarous, "Condition monitoring of DC-link capacitors in aerospace drives," *IEEE Trans. Ind. Appl.*, vol. 48, no. 6, pp. 1866-1874, Nov./Dec. 2012.
[8] A. Abo-Khalil, and D. Lee, "DC-link capacitance estimation in AC/DC/AC PWM converters using voltage injection," *IEEE Trans. Ind. Appl.*, vol. 44, no. 5, pp. 1631-1637, Sep./Oct. 2008.

A Review of the Condition Monitoring of Capacitors in Power Electronic Converters

Soliman, Hammam Abdelaal Hammam; Wang, Huai; Blaabjerg, Frede

Published in:
2015 IEEE INTERNATIONAL ACEMP - OPTIM - ELECTROMOTION JOINT CONFERENCE

Publication date:
2015

A Review of the Condition Monitoring of Capacitors in Power Electronic Converters

Hammam Soliman, Huai Wang, *IEEE Member*, Frede Blaabjerg, *IEEE Fellow*
Department of Energy Technology, Aalborg University
Aalborg 9220, Denmark
has@et.aau.dk, hwa@et.aau.dk, fbl@et.aau.dk

***Abstract*—Capacitor is one of the reliability critical components in power electronic systems. In the last two decades, many efforts in the academic research have been devoted to the condition monitoring of capacitors to estimate their health status. Industry applications demand more reliable power electronics products with preventive maintenances. Nevertheless, most of the developed capacitor condition monitoring technologies are rarely adopted by industry due to the complexity, increased cost and other relevant issues. An overview of the prior-art research in this area is therefore needed to justify the required resources and the corresponding performance of each of the key method. It serves to provide a guideline for industry to evaluate the available solutions by technology benchmarking, as well as to advance the academic research by discussing the history development and the future opportunities. Therefore, this paper firstly classifies the capacitor condition monitoring methods into three categories, then the respective technology evolution from 1993 to 2015 is summarized. Remarks on the state-of-the-art research and the future opportunities targeting for practical industry applications are given.**

I. Introduction

Condition monitoring is an important strategy to estimate the health condition of power electronic components, converters and systems. It is widely applied in reliability or safety critical applications, such as wind turbines, electrical aircrafts, electric vehicles, etc., enabling the indication of future failure occurrences and preventive maintenances. In [1], the condition monitoring of semiconductor devices used in power electronics is well reviewed. Besides the power devices, capacitors are another type of reliability critical components. In the last two decades, a large number of research results on condition monitoring of capacitors have been published, to be listed part of them in this paper [3]-[30]. Nevertheless, to the best knowledge of the authors, the developed technologies are rarely adopted in practical industry applications, due to the complexity, increased cost and other relevant issues. Therefore, a critical overview of the existing literatures is beneficial to both industry application and academic research. It severs to the following two purposes: a) benchmark of different condition monitoring solutions and identify the promising aspects and limitations of them; b) trace the history of the technology evolution and explore the future research opportunities that have the potential to contribute more to practical applications.

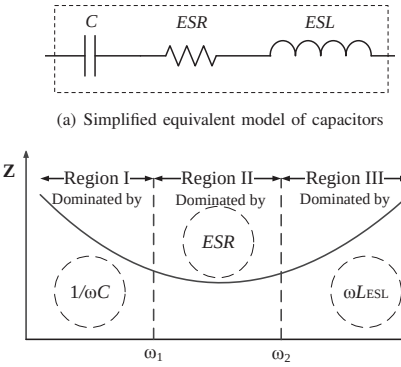

(a) Simplified equivalent model of capacitors

(b) Impedance characteristic of capacitors

Fig. 1. Equivalent model and impedance characteristics of capacitors.

In power electronics conversion systems, a single capacitor or a capacitor bank is usually used. The systems may be malfunction if the single capacitor reaches end-of-life. For the systems with capacitor banks, the time-to-failure of the multiple capacitors could vary. Once one of them fails, the other capacitors may withstand increased stresses, which accelerate the degradation of them. For ensuring the reliable operation, it is recommended that all the capacitors in the bank may be replaced once the first capacitor reaches the end-of-life.

The majority of the condition monitoring methods for both individual capacitors and capacitor banks are based on estimation of the capacitance *C* and Equivalent Series Resistance (*ESR*), which are indicators of the degradation of capacitors [2]. For aluminum electrolytic capacitors, the widely accepted end-of-life criteria is 20% capacitance reduction or double of the *ESR*. For film capacitors, a reduction of 2 to 5% capacitance may indicate the reach of end-of-life. Therefore, obtain the values of *C* or *ESR* is an important step. The selection of those end-of-life criteria are based on two aspects of considerations: 1) The capacitor degradation rate becomes faster (e.g. *dC/dt* , *dESR/dt*) after the capacitance or *ESR* reaches the specified end-of-life criteria, 2) The power electronic conversion systems may not function probably when

978-1-4763-7239-8/15/$31.00 ©2015 IEEE

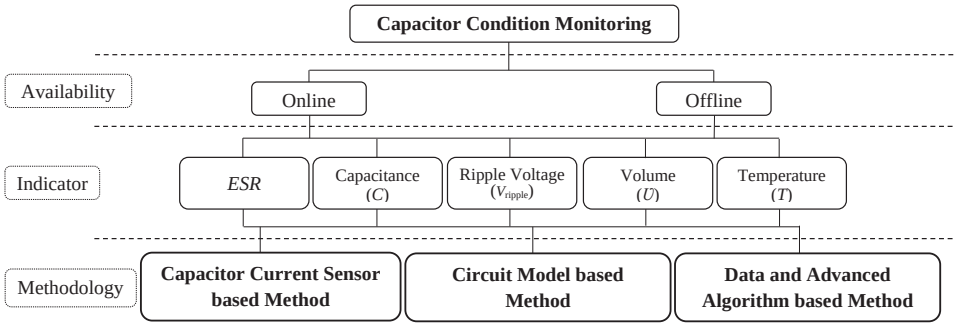

Fig. 2. Classification of capacitor condition monitoring technology.

the capacitance drops or the *ESR* increases to the specified level. The first aspect of the above consideration is usually the primary reason for the choice of the end-of-life criteria.

Fig. 1(a) shows a simplified equivalent model of capacitors and Fig. 1(b) plots the corresponding frequency characteristics. It can be noted that the capacitor impedance is distinguished by three frequency regions dominated by capacitance, *ESR* and the Equivalent Series Inductance (*ESL*), respectively.

An overview of the reliability of capacitors in DC-link application is presented in [2]. The failure mechanisms, lifetime models and DC-link design solutions are discussed. A brief discussion on the condition monitoring of capacitors is also given. Since the scope of [2] does not focus on the condition monitoring, no detailed discussion and critical comparison of the prior-art methods are provided. This paper intends to fill the gap in the literature and conducts a comprehensive overview on the research topic. Section II gives the classification of the existing condition monitoring methods. Section III outlines the technology development history of capacitor condition monitoring from 1993 to 2015 and the benchmark of these technologies. Section IV presents the views from the authors and addresses future research opportunities.

II. Classification of Condition Monitoring Technologies for Capacitors

The condition monitoring technologies for capacitors can be classified from the perspectives of health condition indicators and the methods to obtain the values of the specific indictors. Accordingly, Fig. 2 shows the classifications. Especially, the way to obtain the specific electrical parameters can be classified into three categories to be briefly discussed in this paper in the following subsections.

A. Capacitor ripple current sensor based methods

The use of a current sensor to measure the ripple current flowing through the monitored capacitor is the widely studied method in literatures. The basic concept is to obtain the capacitance or *ESR* by using the capacitor voltage and ripple current information at a low frequency and a specific medium frequency (as illustrated in Fig. 1(b)), respectively. An alternative way is to externally inject a desirable current at certain frequency into the capacitor [3]-[6]. The current injection methods in [3], [4], and [6] are applied in a PWM AC/DC/AC converter, while in [5] it is applied to a sub-module capacitor in modular multilevel converter. The injected current is in a frequency lower than the line frequency, which induces two voltage components across both *ESR* (V_{ESR}) and *C* (V_C), as follows

$$V_{dc} = V_C + V_{ESR} \tag{1}$$

and considering the generation of the zero voltage vectors at switching periods, the values at the mid-point are used in [3] to obtain the ESR value as in (2), and in [4] the estimated capacitance is obtained by (3).

$$ESR = \frac{V_{ESR.mid}}{i_{dc}} = \frac{V_{dc.mid} - V_{C.mid}}{i_{dc.mid}} \tag{2}$$

$$C = \frac{1}{\Delta V_{dc}} \int i_{dc} dt \tag{3}$$

where the term "mid" in the subscripts indicates the quantities measured at the midpoint of the normal sampling period.

B. Circuit model based methods

Instead of using current sensors connected in series with the capacitors, capacitor ripple currents can also be obtained indirectly based on the operation principle of PWM switching converters. To illustrate it by one example, an on-line condition monitoring based on capacitance estimation by (3) is presented in [7]. As shown in Fig. 3, the electrical parameters i_1, i_2, i_3 and v_C are three existing current sensors and one voltage sensor, respectively, for the control purpose of the converter. The parameters highlighted by red color are estimated indirectly. The capacitor ripple current i_C is calculated using the difference between the input current sensor i_1 and the current flows to the inverter i_5 which is based on the transistor switching sequences. The assumption of this calculation is that the three phase output currents are balanced.

C. Data and advanced algorithm based methods

In this category, the power electronic converters are treated as a black-box or semi-black-box. The mapping relationship

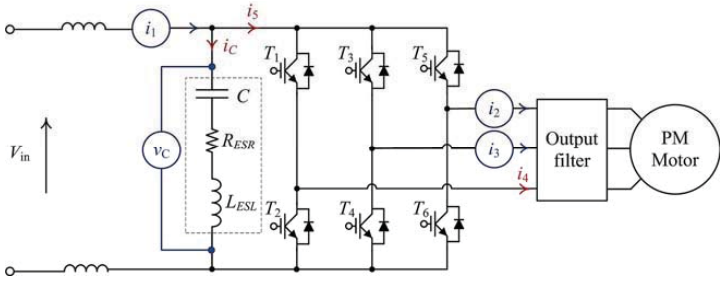

Fig. 3. An example of condition monitoring of DC-link capacitor based on circuit model [7].

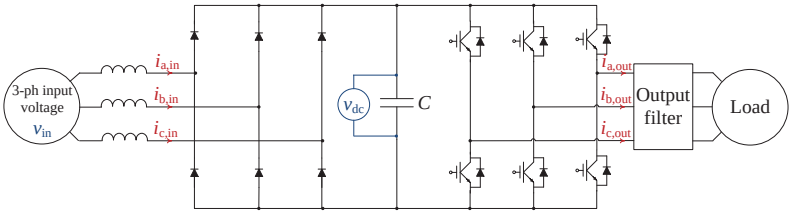

Fig. 4. An AC-AC power conversion system with a capacitor dc-link [23].

between the parameters to be estimated and the available parameters (e.g., input and output side terminal voltage and current information, DC-link voltage) are obtained through data training. In [8], a low frequency AC voltage is injected to the DC-link reference, which is used as a training data in sake of finding the identification model based on Support Vector Regression (SVR). After using a set of training data, a function that analyses the relation between a known capacitor power and its corresponding capacitance is designed, and the capacitance is determined according to

$$C = \frac{BPF[P_{cap}]}{BPF[1/2][\frac{\Delta V^2}{dt}]} \tag{4}$$

where, the *BPF* term refers to the usage of the band pass filter. As claimed by the author, this method is simpler than current injection, since the estimation is based only on the capacitor power and no DC-link ripple current information is required. Since the SVR is an algorithm which based on an off-line trained data, the Recursive Least Square (RLS) algorithm is applied to allow the estimated capacitance to be updated when new data become available [11].

One of the most recent methods proposed by the same author of this paper is presented in [23]. The method is based on the Artificial Neural Network (ANN) algorithm and applied on a power electronic converter shown in Fig. 4. The main motivation behind using ANN for capacitance estimation is that, to avoid the usage of direct/indirect current sensor to sense the capacitor current i_C, while the capacitance value is estimated based on the existing control information and existing power level of the power converter. No hardware circuitry is required and no injection of external signals, therefore, minimizing both complexity and cost is achieved. In

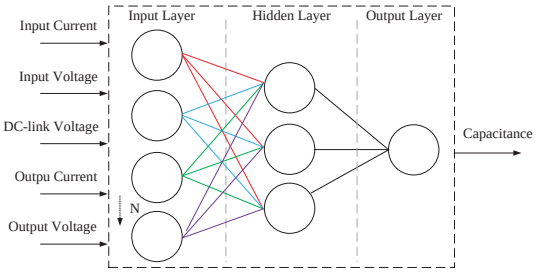

Fig. 5. Structure of the Artificial Neural Network [23].

Fig.5 the basic structure of the ANN is illustrated, normally the structure of any neural network consists of three main layers, input layer, hidden layer, and output layer. In this ANN the capacitance value is the target which should be estimated, while the input/output terminal information of the converter and the dc-link voltage are the inputs to ANN. Part of the results is shown in Table I. The maximum estimated error is 0.5%.

III. History Development and Benchmark of Capacitor Condition Monitoring Methods

The technology evolution of the capacitor condition monitoring technologies is illustrated in Fig. 6 with respect to years. Different methods are represented according to the selected indicators, online or offline, and the methodologies as discussed in Section II. Moreover, the maximum error of the parameter estimation of some of the methods are also included

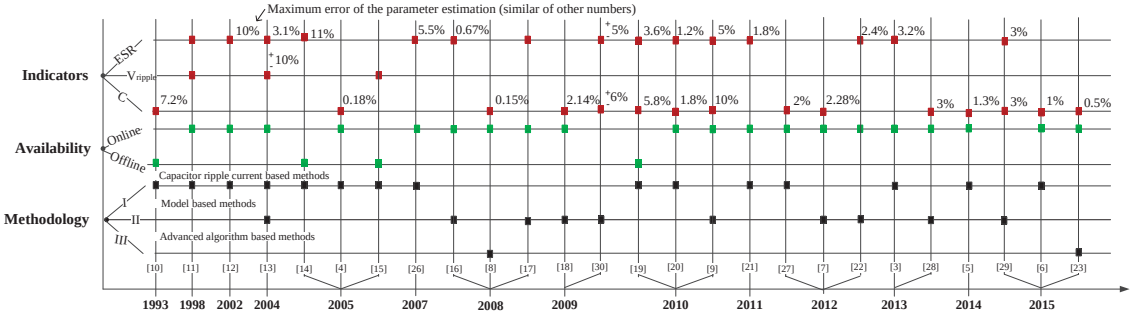

Fig. 6. Development history of the condition monitoring technology for capacitors.

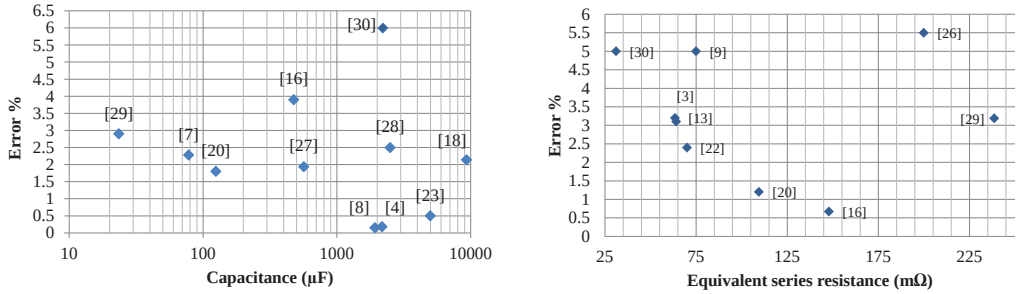

Fig. 7. Comparisons of the parameter estimation in prior-art literatures.

TABLE I
SIMULATION RESULTS FOR ESTIMATED CAPACITANCE (AT 7KW).

C_{actual}=1300μF	$C_{estimated}$=1296μF	Error=0.3%
C_{actual}=1743μF	$C_{estimated}$=1747μF	Error=0.23%
C_{actual}=2600μF	$C_{estimated}$=2589μF	Error=0.5%
C_{actual}=3200μF	$C_{estimated}$=3203μF	Error=0.09%
C_{actual}=3854μF	$C_{estimated}$=3850μF	Error=0.1%
C_{actual}=4265μF	$C_{estimated}$=4257μF	Error=0.18%

in the figure. Since the estimation accuracy is an important performance factor, Fig.7 compares the estimation errors with respect to the range of capacitance and *ESR* according to the available data in respective literatures. The benchmark of various condition monitoring methods are briefly summarized in Table II. This development history figure is very important since it gives many quick facts such as the following:

1) The majority of the condition monitoring methods are based on the first methodology, where most of the shortcomings are coming from.

2) The first methodology contains the highest estimation error percentage (11%).

3) Condition monitoring methods based on the third methodology need to be focused on, specially it contains the minimum estimation error (0.15%).

More remarks are given in the following section.

IV. REMARKS ON THE CONDITION MONITORING FOR CAPACITORS

Based on the above literature study and analysis, the following remarks are given from the authors viewpoint:

1) Capacitor ripple current sensor based methods is not attractive for practical industry applications due to its addition of hardware circuitry, cost and reliability issue of the introduced circuit.

2) It can be noted from Fig. 4 that the majority of condition monitoring methods are online. By considering that the degradation of capacitors are usually very slow, offline condition monitoring is sufficient in most applications (e.g., motor drives) to detect the wear out of capacitors. It implies that some much simpler estimation methods can be applied (e.g., during the start-up of motor drives).

3) Condition monitoring of capacitors discussed here is limited to the wear out detection. To extend the scope, in reliability critical applications, the online monitoring of the operation status (e.g., hot spot

TABLE II. A summary of condition monitoring methods.

Method	C/ESR	Used Approach	Applied Application	Advantages/Dis-advantages	Ref.
I	C (MPPF-caps)	$C_{dc}\frac{dV_C}{dt}+\frac{1}{R_{rh}}V_C=-i_{2f}$	single phase rectifier to 3-phase inverter	Applied for specific kind of application systems (traction systems).	[18]
	ESR (E-caps)	$ESR=\frac{V_{dc\_mid}-V_{c\_mid}}{i_{dc\_mid}}$	PWM back to back converter	Extra effort and many filters to be used because of the current injection.	[3]
	ESR (E-Caps)	$ESR\propto V_C$	Switch-mode power supply	Difficult due to requirement for additional measurements and prior data for the reference model	[13]
	ESR (E-Caps)	$ESR=\frac{\Delta V_{cf}}{\Delta i_{cf}}$	DC-DC Converter	Requires additional hardware for implementation	[12]
	ESR (E-Caps)	$\frac{ESR}{ESR_O}=\left(\frac{\vartheta_{ol,O}}{\vartheta_{ol}}\right)^2$ $ESR_{HOT}=\frac{\Delta T\times H\times S}{I^2}$	AC Drives	High accuracy level of ESR estimation	[24] [25]
	C (E-caps)	$C=\frac{1}{\Delta V_C}\int i_C dt$	PWM back to back converter	Extra effort and many filters to be used because of the current injection.	[4]
	C (E-caps and MPPF-caps)	$C=\frac{1}{\Delta V_C}\int i_C dt$	3-phase inverter	Applied on both E-caps and MPPF-caps.	[27]
	ESR (E-Caps)	$ESR=\frac{V_{Cf}}{i_{Cf}}$	Boost Converter	Simple analog circuit is required for the capacitor voltage measurement.	[26]
II	ESR (E-caps)	$ESR\propto V_{1p}$	DC-DC converter	Forming an LC filter is important for achieving the proposed approach.	[17]
	ESR (E-Caps)	$ESR=\frac{\Delta V_C\times R}{R\times\Delta I_L-\Delta V_C}$	Buck converter	The temperature effect is considered.	[22]
	C (E-Caps)	$C=\frac{1}{\Delta V_C}\int i_C dt$	Aerospace application	Low accuracy under dynamic operation.	[7]
	C (E-Caps)	$C=\frac{1}{\Delta V_C}\int i_C dt$	DC motor drive systems	Low accuracy under dynamic operation.	[28]
	C and ESR (E-Caps)	$C=\frac{V_{PV}DT_S}{8L\left(V_{PV_{t=\frac{DTs}{2}}}-V_{PV_{t=\frac{(1+D)Ts}{2}}}\right)}$ $ESR=\frac{\left(V_{PV_{t=0}}-V_{PV_{t=DTs}}\right)L}{V_{PV}DT_S}$	PV boost converter	The condition monitoring method can be implanted in the same microcontroller used for MPPT purpose.	[29]
III	C (E-caps)	$C=\frac{BPF[P_C]}{BPF\left[\frac{1}{2}\frac{\Delta V_C^2}{dt}\right]}$	PWM back to back converter	Current measurement is not required.	[8]

i_{2f} - current through the capacitance in the frequency filter, V_{dc_mid}, V_{c_mid}, i_{dc_mid}-dc-link voltage, capacitor voltage, dc-link current respectively all at midpoint, V_C- capacitor ripple voltage, Δi_{Cf} – fundamental capacitor ripple current, Δv_{Cf} – fundamental capacitor ripple voltage, ϑ_0 –initial volume of E-Caps, ϑ –volume of E-Caps, ESR_o –initial value of equivalent series resistance, ESR_{HOT} –ESR at operating temperature, H- heat transfer per surface area, S- surface area, ΔT- element temperature rise, ΔV_C- output ripple voltage of dc-link capacitor, i_C- capacitor dc-link current, I_{Cf} – RMS capacitor ripple current at switching frequency, V_{Cf} – RMS capacitor ripple voltage at switching frequency, V_{lp}-output voltage of the low pass filter , ΔI_L –inductor ripple current, R-load resistance, V_{PV}-solar PV voltage, T_S-switching time, D-duty cycle, L- inductor, $BPF[P_C]$- output capacitor power from band pass filter.

temperature, abnormal voltage and current stresses) is of much interest. For this perspective, the online monitoring of capacitance and *ESR* value might be necessary to indirectly monitor the temperature and other abnormal stressors.

4) New methods based on software solutions and existing feedback signals, without adding any hardware cost, could be attractive for industry applications.

V. Conclusions

The classification, technology evolution and benchmark of the state-of-the-art condition monitoring methods for capacitors are reviewed in this paper. Remarks on both the promising aspects and shortcomings of key methods and their applicability in practical industry applications are provided. New research opportunities, such as software based condition monitoring methods, and online monitoring of capacitor hot spot temperature and abnormal stresses, are addressed, which may find themselves more attractive to be adopted in industry products.

References

[1] S. Yang, D. Xiang, A. Bryant, P. Mawby, L. Ran, and P. Tavner, "Condition monitoring for device reliability in power electronic converters: a review," *IEEE Trans. Power Electron.*, vol. 25, no. 11, pp. 2734-2752, Nov. 2010.

[2] H. Wang and F. Blaabjerg, "Reliability of capacitors for DC-link applications in power electronic converters an overview," *IEEE Trans. Ind. Appl.*, vol. 50, no. 5, pp. 3569-3578, Sep./Oct. 2014.

[3] X. Pu, T. Nguyen, D. Lee, K. Lee, and J. Kim, "Fault diagnosis of DC-Link capacitors in three-phase AC/DC PWM converters by online estimation of equivalent series Resistance," *IEEE Trans. Ind. Appl.*, vol. 60, no. 9, pp. 4118-4127, Sep. 2013.

[4] D. Lee, K. Lee, J. Seok, and J. Choi, "Online capacitance estimation of DC-link electrolytic capacitors for three-phase AC/DC/AC PWM converters using recursive least squares method," *IEEE Trans. Ind. Appl.*, vol. 152, no. 6, pp. 1503-1508, Nov./Dec. 2005.

[5] Y. Jo, T. Nguyen, K. Lee, and D. Lee, "Condition monitoring of submodule capacitors in modular multilevel converters," in *Proc. of ECCE*, pp. 2121-2126, Sep. 2014.

[6] T. Nguyen, and D. Lee, "Deterioration monitoring of DC-link capacitors in AC machine drives by current injection," *IEEE Trans. Power Electron.*, vol. 30, no. 3, pp. 1126-1130, Mar. 2015.

[7] A. Wechsler, B. Mecrow, D. Atkinson, J. Bennett, and M. Benarous, "Condition monitoring of DC-link capacitors in aerospace drives," *IEEE Trans. Ind. Appl.*, vol. 48, no. 6, pp. 1866-1874, Nov./Dec. 2012.

[8] A. Abo-Khalil, and D. Lee, "DC-link capacitance estimation in AC/DC/AC PWM converters using voltage injection," *IEEE Trans. Ind. Appl.*, vol. 44, no. 5, pp. 1631-1637, Sep./Oct. 2008.

[9] K. Abdennadher, P. Venet, G. Rojat, J.M. Retif, and C. Rosset, "A real-time predictive-maintenance system of aluminum electrolytic capacitors used in uninterrupted power supplies," *IEEE Trans. Ind. App.*, vol. 46, no. 4,pp. 1644-1652, Jul. 2010.

[10] K. Harada, A. Katsuki, and M. Fujiwara, "Use of ESR for deterioration diagnosis of electrolytic capacitor," *IEEE Trans. Power Electron.*, vol. 8, no. 4,pp. 355-361, Oct. 1993.

[11] A. Lahyani, P. Venet, G. Grellet, and P. J. Vivergr, "Failure prediction of the electrolytic capacitors during operation of a switch-mode power supply," *IEEE Trans. Power Electorn.*, vol. 13, no. 6, pp. 1199-1207, Nov. 1998.

[12] P. Venet, F. Perisse, M.H. El-Husseini, and G. Rojat, "Realization of a smart electrolytic capacitor circuit," *IEEE Ind. App.*, vol. 8, no. 1, pp. 1620, Jan./Feb. 2002.

[13] O. Ondel, E. Boutleux, and P. Venet, "A decision system for electrolytic capacitors diagnosis," *Proc. of PESC*, pp. 4360-4364, Jun. 2004.

[14] E.C. Aeloiza, J.H. Kim, P.N. Enjeti, and P. Ruminot, "A real time method to estimate electrolytic capacitor condition in PWM adjustable speed drives and uninterruptible power supplies," *Proc. of PESC*, pp. 2867-2872, Jun. 2005.

[15] A.M. Imam, T.G. Habetler, R.G. Harley, and D.M. Divan, "Condition monitoring of electrolytic capacitor in power electronic circuits using adaptive filter modeling," *Proc. of PESC*, pp. 601-607, Jun. 2005.

[16] K.W. Lee, M. Kim, J. Yoon, and J.Y. Yoo, "Condition monitoring of dc-link electrolytic capacitors in adjustable-speed drives," *IEEE Ind. App.*, vol. 44, no. 5, pp. 1606-1613, Sep. 2008.

[17] Y. M. Chen, H. C. Wu, M. W. Chou, and K. Y. Lee, "Online failure prediction of the electrolytic capacitors for LC filter of switching mode power converters," *IEEE Ind. Electron.*, vol. 55, no. 1, pp. 400 406, Jan. 2008.

[18] G. M. Buiatti, J. A. Martn-Ramos, A. M. Amaral, P. Dworakowski, and A. J. Cardoso, "Condition monitoring of metallized polypropylene film capacitors in railway power trains," *IEEE Trans. Inst. and Measur.*, vol. 58, no. 10, pp. 3796 3805, Oct. 2009.

[19] A. M. Amaral, and A. J. Cardoso, "Estimating aluminum electrolytic capacitors condition using a low frequency transformer together with a DC power supply," *Proc. of ISIE*, pp. 815-820, Jul. 2010.

[20] G. M. Buiatti, J. A. Martn-Ramos, A. M. Amaral, C.H.R. Garcia, and A. J. Cardoso, "An online and noninvasive technique for the condition monitoring of capacitors in boost converters," *IEEE Trans. Inst. and Measur.*, vol. 59, no. 8, pp. 2134-2143, Aug. 2010.

[21] M.A. Vogelsberger, T. Wiesinger, and H. Ertl, "Life-Cycle monitoring and voltage-managing unit for dc-link electrolytic capacitors in PWM converters," *IEEE Trans. Power. Electron.*, vol. 26, no. 2, pp. 493-503, Feb. 2011.

[22] A. M. Amaral, and A. J. Cardoso, "On-line fault detection of aluminium electrolytic capacitors, in step-

down DC-DC converters, using input current and output voltage ripple," *IET Trans. Power. Electron.*, vol. 5, no. 3, pp. 315-322, Mar. 2012.

[23] H. Soliman, H. Wang, B. Gadalla, and F. Blaabjerg, "Condition monitoring of dc-link capacitors based on artificial neural network algorithm,"*Proc. of POWERENG*, pp. 1-5, Apr. 2015.

[24] M. Gasperi, "Life prediction modeling of bus capacitors in AC variable frequency drives," *IEEE Trans. Ind. Appl.*, vol. 41, no. 6, pp. 14301435, Nov./Dec. 2005.

[25] M. Gasperi, "Life prediction model for aluminum electrolytic capacitors," *in Proc. IEEE Industrial Application Conference*, 1996, pp. 13471351.

[26] A.M. Imam, D.M. Divan, R.G. Harley, T.G. Habetler, "Real-Time Condition Monitoring of the Electrolytic Capacitors for Power Electronics Applications," *Proc. of APEC*, pp. 1057-1061, Feb. 2007.

[27] Y. Yu; T. Zhou; M. Zhu; D. Xu, "Fault Diagnosis and Life Prediction of DC-link Aluminum Electrolytic Capacitors Used in Three-phase AC/DC/AC Converters," *Proc. of IMCC*, pp. 825-830, Dec. 2012.

[28] J.J. Moon, W.S. Im, J.M. Kim, "Capacitance estimation of DC-link capacitor in brushless DC motor drive systems," *Proc. of ECCE*, pp. 525-529, June 2013.

[29] M.W. Ahmad, A. Arya, S. Anand, "An online technique for condition monitoring of capacitor in PV system," *Proc. of ICIT*, pp. 920-925, Mar. 2015.

[30] K. Abdennadher, P. Venet, G. Rojat, J.M. Retif, C. Rosset, "Kalman filter used for on line monitoring and predictive maintenance system of aluminium electrolytic capacitors in UPS," *Proc. of ECCE*, pp. 3188-3193, Sep. 2009.

Capacitance Estimation for DC-link Capacitors in a Back-to-Back Converter Based on Artificial Neural Network Algorithm

Soliman, Hammam Abdelaal Hammam; Wang, Huai; Blaabjerg, Frede

Published in:
Proceedings of the 2016 IEEE International Power Electronics and Motion Control Conference - ECCE Asia (IPEMC 2016-ECCE Asia).

Publication date:
2016

Document Version
Publisher's PDF, also known as Version of record

Capacitance Estimation for DC-link Capacitors in a Back-to-Back Converter Based on Artificial Neural Network Algorithm

Hammam Soliman, Huai Wang, *IEEE Member*, Frede Blaabjerg, *IEEE Fellow*
Department of Energy Technology, Aalborg University
Aalborg 9220, Denmark
has@et.aau.dk, hwa@et.aau.dk, fbl@et.aau.dk

***Abstract*—The reliability of dc-link capacitors in power electronic converters is one of the critical aspects to be considered in modern power converter design. The observation of their ageing process and the estimation of their health status have been an attractive subject for the industrial field and hence for the academic research field as well. The existing condition monitoring methods suffer from shortcomings such as low estimation accuracy, extra hardware, and also increased cost. Therefore, the developed methods of condition monitoring that are based on software solutions and algorithms could be the way out of the aforementioned challenges and shortcomings. In this paper, a pure software condition monitoring method based on Artificial Neural Network (ANN) algorithm is proposed. The implemented ANN estimates the capacitance of the dc-link capacitor in a back-to-back converter. The error analysis of the estimated results is also studied. The developed ANN algorithm has been implemented in a Digital Signal Processor (DSP) in order to have a proof of concept of the proposed method.**

I. Introduction

DC-link capacitors are an important element in the field of power electronic converters. They strongly contribute to the size, cost, efficiency, failure rate, and therefore reliability of the power converters. Moreover, according to [1], electrolytic capacitors are sharing 60% of the failure rate in power electronics component. Therefore, reliability study on the DC-link capacitors is very important in sake of achieving reliable and robust converters. Fig. 1 from [2] shows that today's perspective of power electronics reliability should consider three main aspects. Condition monitoring is an important way to ensure reliable operation and to achieve predictive maintenance of power electronic components and systems.

The general principle of condition monitoring is defined as a real-time measure of a component, such that if it drifts away from the healthy condition an appropriate action to be taken [5]. This real-time measure in some application is difficult to be reached directly with a measurement equipment and therefore, an estimation of this parameter is an alternative method. Moreover, a signature of the health status should be presented in this component. Different parameters can indicate

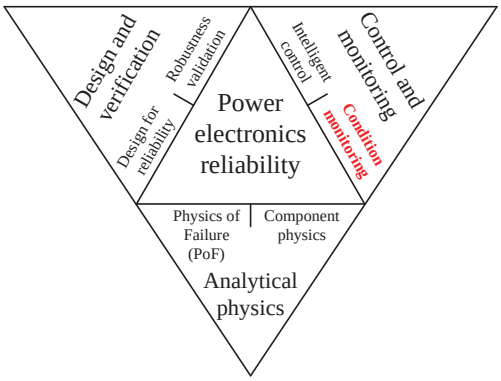

Fig. 1. Aspects of power electronics reliabilty assessment [2].

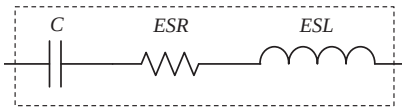

(a) Simplified equivalent model of capacitors.

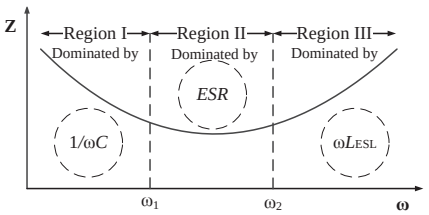

(b) Impedance characteristic of capacitors.

Fig. 2. Equivalent model and impedance characteristics of capacitors.

the health status of a capacitor such as, the capacitance C, the Equivalent Series Resistance (ESR), the Equivalent Series Inductance (L_{ESL}), the capacitor's volume and/or temperature. Fig. 2(a) shows a simplified equivalent model of capacitors and Fig. 2(b) plots the corresponding frequency characteristics. It

978-1-5090-1210-7/16/$31.00 ©2016 IEEE

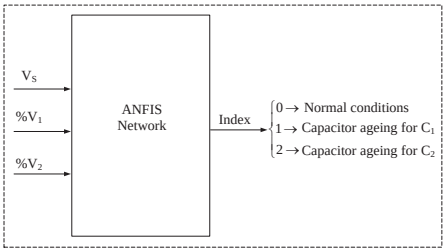

(a) Structure of Adaptive Neuro-Fuzzy Inference System (ANFIS) network [3].

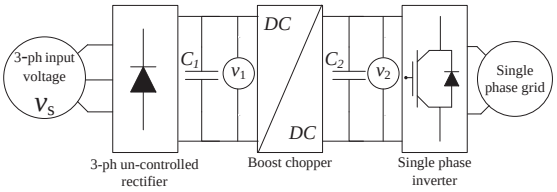

(b) Power electronic converter circuit [3].

Fig. 3. Condition monitoring of capacitors based on data training proposed by [3].

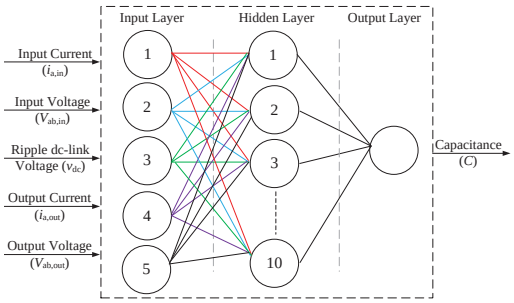

(a) Structure of Artificial Neural Network (ANN) [4].

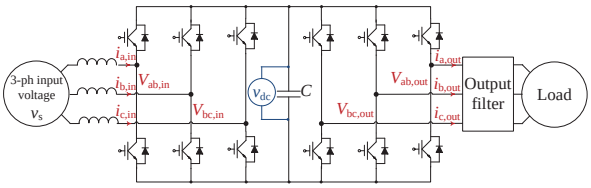

(b) A back-to-back converter.

Fig. 4. Condition monitoring of dc-link capacitor in a back-to-back converter based on data training proposed by [4].

can be noted that the capacitor impedances are distinguished by three frequency regions dominated by capacitance, *ESR* and the L_{ESL}, respectively.

The majority of the condition monitoring methods for capacitors are based on the estimation of the capacitance and the *ESR*, which are indicators of the degradation in the capacitors [6]. The degradation level and the end-of-life criteria vary with capacitor type. For aluminium electrolytic capacitors, the widely accepted end-of-life criteria is 20% capacitance reduction or double of the *ESR*. For film capacitors, a reduction of 2% to 5% capacitance may indicate the reach of end-of-life. Therefore, a method which can estimate the *C* value could be interesting for both aluminium electrolytic and film capacitors.

From a methodology point of view, the condition monitoring methods in the prior-art are classified into three categories [7], as the following: a) capacitor ripple current sensor based methods, b) circuit model based methods, and c) data and advanced algorithm based methods. Methodologies that belongs to the third category are listed in [3, 4, 8–11]. Since this paper focuses on software solutions, some recent methodologies in the third category are reviewed. In [3, 4], two recent condition monitoring methods based on software solutions are presented.

In [3], an Adaptive Neuro-Fuzzy Inference System (ANFIS) algorithm is applied on the power converter converter shown in Fig. 3(b). Based on data training, the ANFIS is able to predict the health status of the capacitor. According to the basic structure shown in Fig. 3(a), the ANFIS is using the supply voltage V_s and ripple voltages V_1 and V_2 of both filter capacitors C_1 and C_2 as inputs. While the health condition of the capacitors are expressed in terms of index. The network estimates one index out of two incidences for capacitance and *ESR* of both capacitors in the converter.

To assure that a strong mapping between ANFIS inputs and output, a relationship between the supply voltage and the end-of-life- voltages is linearly interpolated using curve fitting techniques. The two factors $\hat{V}_{1th}$ and $\hat{V}_{2th}$ are obtained, where $\hat{V}_{1th}$ and $\hat{V}_{2th}$ are the estimated values of V_{1th} and V_{2th} according to V_s respectively. Finally, in order to obtain the data implemented as inputs to the ANFIS, a percentage value is calculated as the following:

$$\%V_1 = \frac{V_{1m}}{V_{1th}} \times 100 \tag{1}$$

$$\%V_2 = \frac{V_{2m}}{V_{2th}} \times 100 \tag{2}$$

where V_{1m} and V_{2m} are the measured values of V_1 and V_2 respectively at any current status.

In [4] a recent method that based on the Artificial Neural Network (ANN) algorithm is applied on the back-to-back converter shown in Fig. 4(b). No hardware circuitry is required and no injection of external signals, therefore, minimizing

complexity and cost are achieved. In this ANN the capacitance value is the target, which should be estimated, while the input/output terminal information of the converter and the dc-link voltage are the inputs to ANN. However, some of the voltage and phase current information may not be available in practical applications. It is still an open question of the performance of the ANN based method in [4] with the absence of information about some of the voltages and currents.

To overcome the above mentioned limitation, this paper proposes an ANN based method requiring one input side phase current and the dc-link voltage information only. Moreover, in order to leverage the limited available information while achieving comparable capacitance estimation accuracy, the available data are pre-processed before feeding to the ANN. The proposed method retains the advantages as that presented in [4]. It requires no hardware circuitry (e.g., current sensors and corresponding signal condition circuits), no external signal injection, and therefore minimizes the increased complexity and cost. This paper is organized as the following: Section II gives the basic principle of ANN applied for capacitor condition monitoring. Section III illustrates the applied ANN to a back to back converter study case. Section IV presents the results accomplished by the proposed method based on ANN, followed by a conclusion.

II. ANN for Capacitor Condition Monitoring

The use of ANN for capacitance estimation has been inspired by [4] where the main motivation is to estimate the capacitance values based on the available input and output terminal information of the converter, without adding sensors and hardware circuits. The available information will be used as *inputs* to the ANN, while the corresponding value of C is used as a *target* as shown in Fig. 4(a).

The basic structure of neural network consists of three layers, input, hidden, and output layers. The input layer is where the available data fed to the ANN are stored. The task of the hidden layer is to transform the inputs into a function that the output layer can use. The task of the output layer is to transform the activations inside the hidden layer into a scale. Based on this scale, the data entered as targets are adjusted to fit as the desired output.

In this paper the same basic structure in [4] is used, but with two kinds of inputs to the ANN instead of five, and different training algorithms. As shown in Fig. 5(a), only the phase A input current $i_{a,in}$, and ripple dc-link voltage ΔV_{dc} are used as the ANN inputs. The details of the ANN's structure and the criteria of training data selection are further discussed in the following section.

III. Implementation of the Proposed ANN

The proposed ANN method is applied to a back-to-back converter as shown in Fig. 4(b). Its specifications are listed in Table I. The implementation of the ANN method is discussed as below.

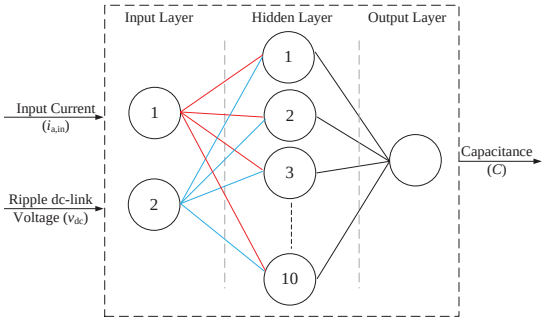

(a) Structure of ANN network.

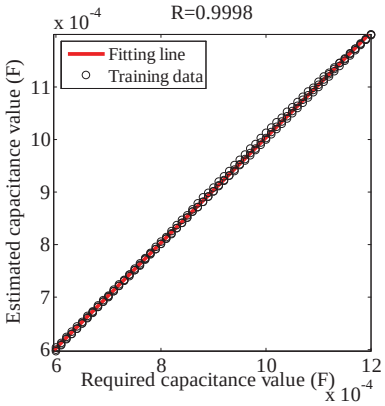

(b) Regression response of the trained network.

Fig. 5. The structure of the trained ANN and its regression response.

TABLE I
Ratings of the Back-to-Back Converter Parameters.

Input AC Voltage (V_{L-L})	400 V
Output AC Voltage (V_{L-L})	400 V
Rated dc-link Voltage (V_{dc})	750 V
Full Power Level (P_o)	10 kW
Capacitance (C)	1000 μF

A. Training data preparation

Since the dc-link voltage ripple depends on both the capacitance and the loading conditions, the prepared training data include the information from the operation under three power levels. For each power level, there are 61 data of the capacitance values used to train the ANN, covering the range between 600 μF and 1200 μF with 10 μF step. Each capacitance value is corresponding to one value of the input current and one value of the dc-link voltage ripple. The process of the training data collection is as following:

1) Starting from the lower boundary of the capacitance range (600 μF), the back-to-back converter SIMULINK model starts running with 1 μs sampling time.
2) During the simulation, Root Mean Square (*RMS*) values of phase A input current $i_{a,in}$, and ripple dc-link voltage ΔV_{dc} are sent to the workspace.
3) After the simulation under a specific dc-link capacitance finishes, there will be $1^6 + 1$ instantaneous values for each parameter. A designed Matlab code calculates the average of the last 7,000 instantaneous values saved in the workspace to generate only one value for each parameter. So, by the end of each single run, there will be one average RMS value for the phase A input current $i_{a,in}$, and one average RMS value of the ripple dc-link voltage ΔV_{dc}.
4) When reaching the upper boundary of the capacitance range (1200 μF), there are 3 datasets. One dataset for phase A input current $i_{a,in}$, one dataset for ripple dc-link voltage ΔV_{dc}, and one dataset for the capacitance. Each dataset consists of 61 data.
5) The above process is repeated for the operating power level of 10 kW, 7 kW, respectively. and 4 kW. Finally, there are 183 data in each dataset.

The datasets of phase A input current $i_{a,in}$ and ripple dc-link voltage ΔV_{dc} are loaded to the ANN's input layer as a matrix with a dimension of 2×183. While the dataset of the capacitance is loaded to the output layer as a matrix with a dimension of 1×183. Due to the usage of average values, the error of the estimated capacitance is reduced. The trained ANN can be used to estimate the dc-link capacitance under different loading conditions with a capacitor within the set lower and upper limits.

B. ANN structure and training algorithm

After all the datasets loaded to respective layers, an amount of 50 hidden neurons is selected. The Neural Fitting Tool *nftool* in MATLAB software [12] is used. This tool is usually used for estimation and prediction problems in which the neural network maps between a set of numeric inputs and a set of numeric targets. The iteration algorithm used in this training is *Bayesian Regularization* [13], which typically takes longer time but it is definitely better for challenging problems. Moreover, the used training algorithm avoids the overfitting issues by stopping the training automatically when the generated results stops improving. During the training, the Regression factor *R* is important to be observed, which measures the correlation between the desired outputs and trained targets. An *R* value of 1 means a close relationship, while 0 means a random relationship. The regression response of the trained ANN is shown in Fig. 5(b). It can be noted that all the 183 input data are exactly aligned to the fitting line and the values of *R* is close to 1. Based on this result, the network stopped training and the ANN is generated and ready to be used.

IV. Capacitance Estimation Based on the Proposed ANN

The proposed ANN is applied for dc-link capacitance estimation under different operation conditions. The ANN is fed with updated information on phase A input current $i_{a,in}$, and ripple dc-link voltage ΔV_{dc} every 0.1 sec. Three cases are studied for the trained ANN as presented below.

A. Case I: Constant capacitance conditions

In this case, the trained ANN is tested to check whether is able to estimate the correct value of capacitance or not. A random value chosen for this test within the trained capacitance range. The estimated values of the capacitance corresponding to each set is shown in Fig. 6.

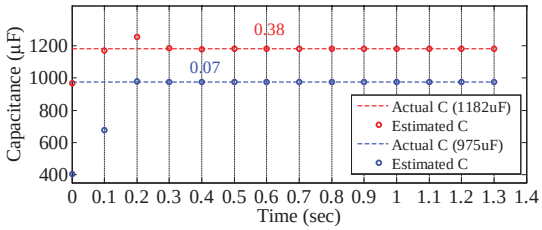

Fig. 6. The capacitance estimation by the trained ANN at 10 kW load.

B. Case II: Varying load conditions

In this test, the impact of the load (power) variation on the estimation accuracy is analysed. The load power is dropped from 10 kW to 4 kW at the moment of 0.7 sec is simulated. The estimation of capacitance values and their corresponding errors are shown in Fig. 7 and Fig. 8, respectively. It can be seen that the variation effect takes place just after 0.1 sec.

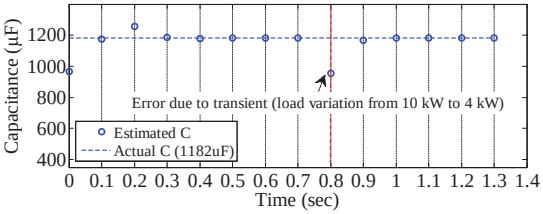

Fig. 7. The trained ANN accuracy under load variation.

C. Case III: Varying capacitance conditions

In sake of proving that the trained ANN is able to detect the degradation of a capacitor, in this test a 1% drop in capacitance is simulated to test the ANNs estimation behaviour. The drop is simulated with two capacitors C_1 and C_2 connected in parallel, where C_1 equals to 600 μF, and C_2 equals to 1 μF and connected through a switch to have the option to switch between 601 μF and 600 μF. Fig. 9 shows the estimated capacitance value with the corresponding estimation error for each estimation.

TABLE II
REMARKS ON SIMULATION RESULTS FROM SIMULINK.

Case study	Remarks / Comments
Case I	- It can be seen that the trained ANN estimates the actual value in steady state with a maximum error of 0.38%.
Case II	- An error of 19% is observed during transient, which should be discarded in the estimation.
	- The trained ANN estimates the correct value during the steady state operation with error less than 1%.
Case III	- The trained ANN detects 1% variation in the capacitance value.

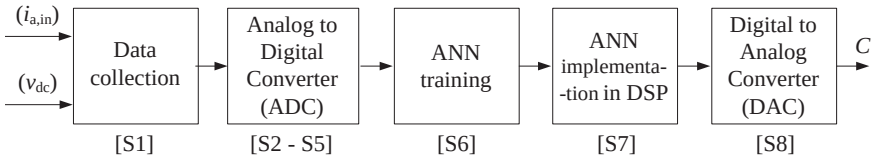

Fig. 10. The process of ANN implementation in DSP

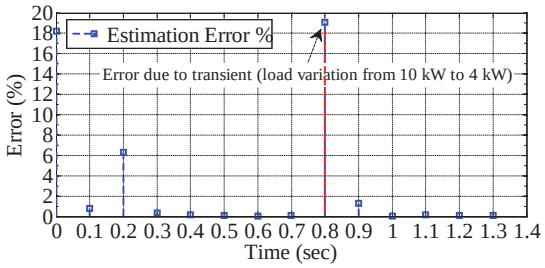

Fig. 8. The estimation error corresponding to Fig.7 under load variation.

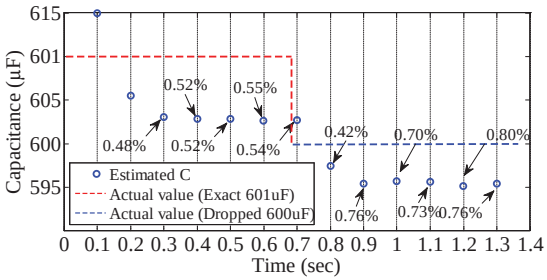

Fig. 9. The estimation error analysis with capacitance variation at 10 kW load. (Case III)

A a general observation on all the results is that the estimated capacitance values before 0.3 sec should be discarded in the estimation. The low estimation accuracy before 0.3 sec is due to the ANN's inputs affected by the transient. This shows that the estimated results from the trained ANN should be considered only during steady state operation of the back-to-back converter. Remarks to the studies are shown in Table II.

V. PROOF OF CONCEPT

The ANN discussed in the last two sections is implemented in a Digital Signal Processor (DSP) to verify the proposed concept. The DSP used is Texas Instrument TMS320F28335 [14]. The block diagram shown in Fig. 10 illustrates the implementation process with the following steps:

S1) The training datasets obtained from the back-to-back SIMULINK model and used earlier in this paper, are collected and stored in an excel sheet.

S2) In real prototype applications, readings of current and voltage are fed to the DSP into a digital form. The validation part in this paper aims to proof the concept by feeding the DSP with digital data, but those data are obtained from the back-to-back SIMULINK model. Therefore, three gain factors are calculated to obtain the equivalent digital values of phase A input current $i_{a,in}$, ripple dc-link voltage ΔV_{dc}, and capacitance values.

S3) The DSP maximum voltage rating of a digital input $DSP_{max,volt_1}$ equals to 3 V, and the maximum number of bits $DSP_{max,bits}$ are 4096 bits, therefore, the calculated gain factors are based on 2.7 V $DSP_{max,volt_2}$, and 4096 bits as usable limits. Moreover, 16 Amp, 0.158 V, and 1200 μF are used as the maximum limits for phase A input current $i_{max,a,in}$, ripple dc-link voltage $\Delta V_{max,dc}$, and capacitance C_{max}, respectively.

S4) Based on the previous considerations in mentioned in S3, the gains are calculated as following:

$$K_I = \frac{DSP_{max,volt_2} \times DSP_{max,bits}}{i_{max,a,in} \times DSP_{max,volt_1}} = \frac{2.7 \times 4096}{16 \times 3} = 230 \quad (3)$$

$$K_V = \frac{DSP_{max,volt_2} \times DSP_{max,bits}}{\Delta V_{max,dc} \times DSP_{max,volt_1}} = \frac{2.7 \times 4096}{0.158 \times 3} = 23331 \quad (4)$$

$$K_C = \frac{DSP_{max,volt_2} \times DSP_{max,bits}}{C_{max} \times DSP_{max,volt_1}} = \frac{2.7 \times 4096}{0.0012 \times 3} = 3072000 \quad (5)$$

Where, K_I, K_V, and K_C, are the gain factors, phase A input current $i_{a,in}$, ripple dc-link voltage ΔV_{dc}, and capacitance, respectively.

S5) Afterwards, all the collected datasets stored in the excel sheet are multiplied by the corresponding gain factor, and hence, three datasets each consisting of 183 data but into a digital form are ready to be used as training data.

S6) The same ANN structure shown in Fig. 5(a) is applied to train the available digital data. The regression response is the same as that in Fig. 5(b).

S7) The implementation of the trained ANN in the DSP is achieved by generating a C-code that is equivalent to the generated SIMULINK trained ANN model. Afterwards, this C-code is compiled using the Code Composer Studio (*CCS*), and then, a new ANN is built by the DSP

S8) In sake of testing the ANN project by the DSP, the streaming of data coming from the back-to-back converter SIMULINK model are first converted into digital forms according to (3), (4) and (5). The estimated capacitance value in digital format is converted into the physical value according to (5).

Five random capacitance values are selected to be estimated by ANN on the *DSP* system. The estimated results by the *DSP* is presented in Table III.

TABLE III
ESTIMATED CAPACITANCE VALUES AND THE CORRESPONDING ERRORS PERCENTAGE BY DSP USED IN A BACK-TO-BACK CONVERTER.

Actual C value	Estimated by *DSP*	Estimation error
1182 μF	1182.2 μF	0.02 %
1093 μF	1093.2 μF	0.02 %
975 μF	974.9 μF	0.01 %
786 μF	785.8 μF	0.03 %
606 μF	605.5 μF	0.09 %

The error of the estimated capacitance values from the DSP is less than 0.1%. To verify the simulation results shown in Section IV, the estimated capacitance results by using DSP are presented in Fig. 11 to Fig. 14. It can be seen in Fig. 11 that the maximum error is 0.25% and 0.027%, respectively, for the two estimated capacitors.

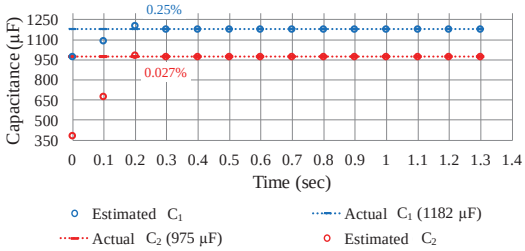

Fig. 11. The capacitance estimation by the trained ANN in DSP at 10 kW load. (Case I)

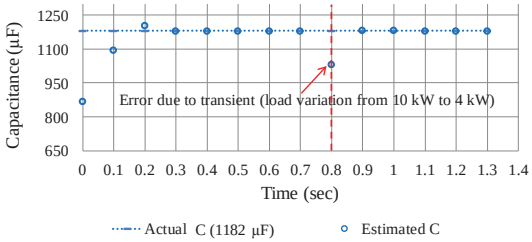

Fig. 12. The trained ANN in DSP accuracy under load variation. (Case II)

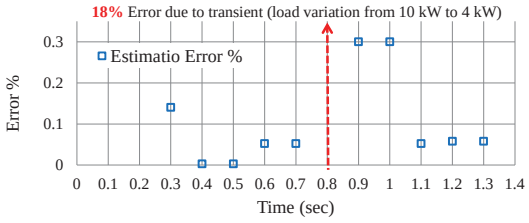

Fig. 13. The estimation error by ANN in DSP corresponding to Fig.12 under load vriation. (Case II)

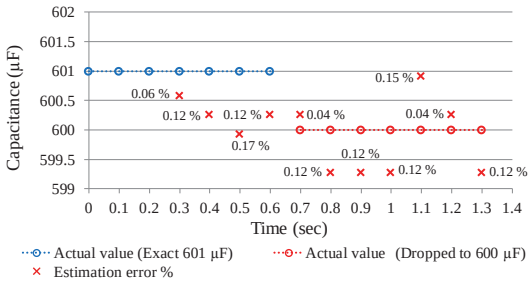

Fig. 14. The estimation error analysis by DSP with capacitance variation at 10 kW load. (Case III)

In Fig. 12 and Fig. 13, it can be noted that the maximum error is 18% during the transient load variation from 10 kW to 4 kW. While during steady state, the errors are below 0.35%. The summary of the comments is shown in Table IV.

TABLE IV
REMARKS ON RESULTS FROM DSP.

Case study	Remarks / Comments
Case I	- It can be seen that the trained ANN estimates the actual value in steady state with a maximum error of 0.25%.
Case II	- An error of 18% is observed during transient, which should then be discarded when operating. - The trained ANN estimates the correct value during the steady state operation with error less than 0.35%.
Case III	- The trained ANN detects 1% variation in the capacitance value with maximum error equal to 0.04% at the instant of drop.

VI. CONCLUSIONS

A new capacitor condition monitoring method based on Artificial Neural Network (ANN) algorithm is proposed in this paper. It is applied for a back-to-back converter study case in order to estimate the capacitance value change of the dc-link capacitor. The proposed method requires no additional hardware circuit and can be implemented by using the extra resources of existing digital controllers in most of power electronic systems, implying a minimum additional investment. The method is implemented in both simulation software and DSP. The capacitance estimation results under different capacitance values and loading conditions are presented. It reveals that the estimation errors are below 0.4% and 0.35%, respectively for the simulations and the proof-of-concept by the DSP.

REFERENCES

[1] A. Imam, T. Habetler, R. Harley, and D. Divan, "Lms based condition monitoring of electrolytic capacitor," in *Proc. of Industrial Electronics Society, IECON 31st Annual Conference of IEEE*, Nov 2005, pp. 848–853.

[2] H. Chung, H. Wang, F. Blaabjerg, and M. Pecht, *Reliability of Power Electronics Converter Systems*. The Institution of Engineering and Technology (IET), Dec. 2015.

[3] T. Kamel, Y. Biletskiy, and L. Chang, "Capacitor aging detection for the dc filters in the power electronic converters using anfis algorithm," in *Proc. of IEEE Canadian Conference on Electrical and Computer Engineering (CCECE)*, 2015, pp. 663–668.

[4] H. Soliman, H. Wang, B. Gadalla, and F. Blaabjerg, "Condition monitoring for dc-link capacitors based on artificial neural network algorithm," in *Proc. of IEEE Power Engineering, Energy and Electrical Drives (POWERENG)*, 2015, pp. 587–591.

[5] S. Yang, D. Xiang, A. Bryant, P. Mawby, L. Ran, and P. Tavner, "Condition monitoring for device reliability in power electronic converters: A review," *IEEE Transactions on Power Electronics*, vol. 25, no. 11, pp. 2734–2752, Nov. 2010.

[6] H. Wang and F. Blaabjerg, "Reliability of capacitors for dc-link applications in power electronic converters - an overview," *IEEE Trans. on Industry Applications*, vol. 50, no. 5, pp. 3569–3578, Sept 2014.

[7] H. Soliman, H. Wang, and F. Blaabjerg, "A review of the condition monitoring of capacitors in power electronic converters," in *Proc. of IEEE Electromotion Joint Conference (ACEMP-OPTIM)*, 2015, pp. 243–249.

[8] H. Soliman, H. Wang, B. Gadalla, and F. Blaabjerg, "Artificial neural network algorithm for condition monitoring of dc-link capacitors based on capacitance estimation," *Journal of Renewable Energy and Sustainable Development*, vol. 1, no. 2, pp. 294–299, Jan. 2016.

[9] A. Imam, T. Habetler, R. Harley, and D. Divan, "Condition monitoring of electrolytic capacitor in power electronic circuits using adaptive filter modeling," in *Proc. of Power Electronics Specialists Conference, PESC '05. IEEE 36th*, 2005, pp. 601–607.

[10] A. Imam, T. Habetler, R. Harley, and D. Divan, "Condition monitoring of electrolytic capacitor in power electronic circuits using input current," in *Proc. of Diagnostics for Electric Machines, Power Electronics and Drives, SDEMPED 5th IEEE International Symposium on*, 2005, pp. 1–7.

[11] A. Abo-Khalil and D.-C. Lee, "Dc-link capacitance estimation in ac/dc/ac pwm converters using voltage injection," *IEEE Transactions on Industry Applications,*, vol. 44, no. 5, pp. 1631–1637, Sep. 2008.

[12] Open network/data manager - matlab nntool. [Online]. Available: http://se.mathworks.com/help/nnet/ref/nntool.html.

[13] Bayesian regularization backpropagation - matlab trainbr. [Online]. Available: http://se.mathworks.com/help/nnet/ref/nntool.html

[14] Digital signal controllers (dscs) - data manual. [Online]. Available: http://www.ti.com/lit/ds/symlink/tms320f28335.pdf.

Artificial Neural Network based DC-link Capacitance Estimation in a Diode-bridge Front-end Inverter System

Hammam Soliman, Ibrahim Abdelsalam*, Huai Wang, *IEEE Member*, Frede Blaabjerg, *IEEE Fellow*
Department of Energy Technology, Aalborg University - Aalborg 9220, Denmark
*Electrical and Control Department, Arab Academy for Science, Technology and Maritime Transport - Cairo, Egypt
has@et.aau.dk, I.abdelsalam@aast.edu, hwa@et.aau.dk, fbl@et.aau.dk

***Abstract*—In modern design of power electronic converters, reliability of DC-link capacitors is an essential aspect to be considered. The industrial field have been attracted to the monitoring of their health condition and the estimation of their ageing process status. The existing condition monitoring methods suffer from shortcomings such as, low estimation accuracy, extra hardware, and increased cost. Therefore, development of new condition monitoring methodologies that are based on advanced software algorithms could be the way out of the aforementioned challenges and shortcomings. In this paper, a proposed software condition monitoring methodology based on Artificial Neural Network (ANN) algorithm is presented. Matlab software is used to train and generate the proposed ANN. The proposed methodology estimates the capacitance of the DC-link capacitor in a three phase front-end diode bridge AC/DC/AC converter. The estimation is based on the usage of single phase output current and dc-link voltage ripple. The impact of training data type, source and amount are also investigated for estimation accuracy analysis. Experimental validation of the proposed method is also conducted.**

I. Introduction

Condition monitoring is an important method to observe and estimate the health condition of power electronic components, converters and systems. It is widely applied and demanded in safety-critical or reliable applications, such as wind turbines, electrical air-crafts, electric vehicles, etc., enabling the indication of future failure occurrences and preventive maintenance. In [1], the condition monitoring principle is defined as an online measurement of a component, such that if it drifts away from the healthy condition an appropriate action to be taken.

According to the review on the condition monitoring of semiconductor devices used in power electronics in [1], capacitors are another type of components that which fail more frequently than other components in power electronic systems. The health status of a capacitor can be indicated by three parameters; the capacitance *C*, the Equivalent Series Resistance (*ESR*), and the Equivalent Series Inductance (L_{ESL}) [2].

Moreover, each of the aforementioned parameters are distinguished by three frequency regions. The majority of the condition monitoring methods for capacitors are based on the estimation of the capacitance and the *ESR* due to their direct correlation to the capacitor degradation [3].

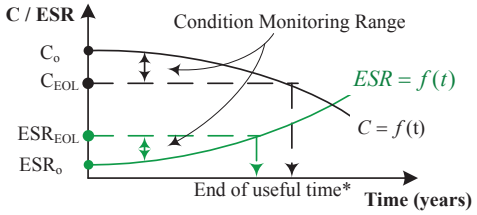

C_o = Initial capacitance. C_{EOL} = Capacitance at End-Of-Life.
ESR_o = Initial equivalent series resistance. ESR_{EOL} = equivalent series resistance at End-Of-Life.
*C_{EOL} could be larger or smaller than ESR_{EOL}, it depends on the application and the capacitor type.

Fig. 1. Capacitance and ESR curves as an indication of capacitor degradation level [4].

Based on the degradation curves in Fig. 1, an end-of-life or threshold criteria is needed before going further and decide the health condition of the capacitor. For Electrolytic capacitors (*E-Caps*), the widely accepted end-of-life criteria is 20% capacitance reduction or double of the *ESR*.

This paper aims to experimentally validate a proposed condition monitoring method by capacitance estimation using Artificial Neural Network (ANN) that uses the single phase A output current $i_{out,a}$ and dc-link ripple voltage Δv_{dc} as inputs. It requires no hardware circuitry (e.g., current sensors and corresponding signal condition circuits), no external signal injection, and therefore minimizes the increased complexity and cost. Moreover, investigation of the training data type, amount and source is also presented in sake of analysing the estimation accuracy.

The main sections in this paper are as the following: Section II gives the basic principle of ANN applied for capacitor condition monitoring and illustrates the applied ANN to a front-end diode bridge converter study case. Section III presents the results obtained by the proposed method based on ANN validated in a hardware prototype, followed by the conclusion in Section IV.

II. ANN for Capacitor Condition Monitoring

Using ANN for capacitance estimation have firstly been applied by [5] where the main motivation is that the estimated

978-1-5090-5157-1/17/$31.00 ©2017 IEEE

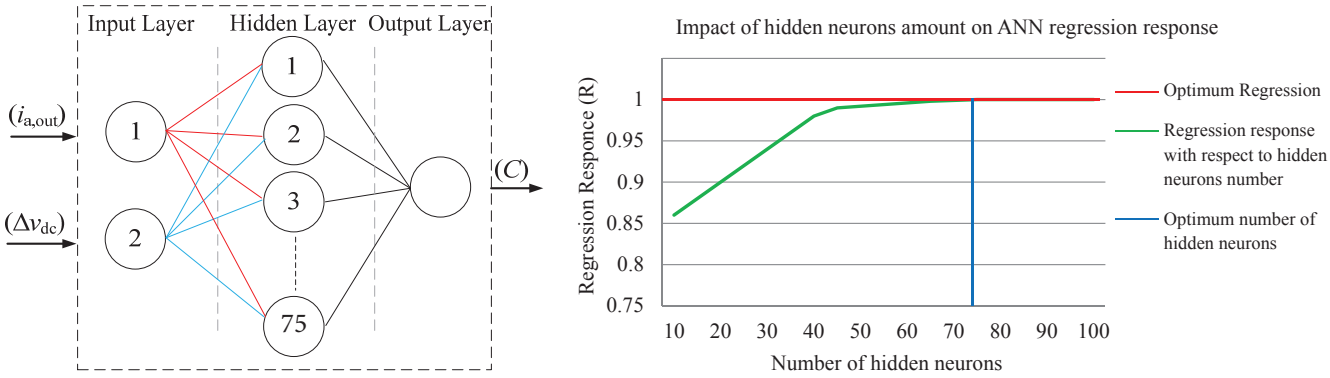

(a) Proposed ANN structure.

(b) Impact of hidden neurons amount on ANN regression response.

Fig. 2. Optimum hidden neurons amount selection with respect to the proposed ANN structure.

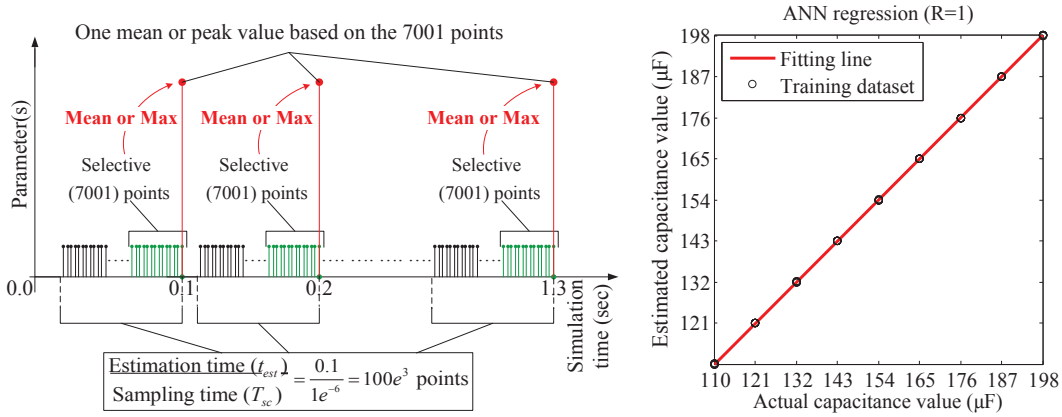

(a) Explanation of the designed Matlab code to prepare the training data of Phase A output current and ripple dc-link voltage.

(b) Regression response of the trained ANN.

Fig. 3. Training data selection criteria and the trained ANN regression response.

value of C is possible to be obtained using the available input voltage and current and output voltage and current terminal information of the converter, in addition to the dc-link voltage ripple, without sensing the capacitor current i_C. In order to optimize an efficient ANN that requires less information, hence less amount of iteration; an ANN is proposed by [4] that considered single phase A input current $i_{in,a}$ and dc-link ripple voltage Δv_{dc} as inputs. In [4] the ANN is trained based on training data obtained from simulation, afterwards, in order to validate the concept, the trained ANN is integrated into a Digital Signal Processor (*DSP*).

In this paper the ANN is trained based on training data obtained from an experimental platform. Moreover, the ANN is trained to estimate the capacitance value using only the single phase A output current $i_{out,a}$ and dc-link ripple voltage Δv_{dc}.

A. Proposed ANN structure

As stated earlier, the ANN is considering the single phase A output current $i_{out,a}$ and dc-link ripple voltage Δv_{dc} as inputs. The basic structure of any neural network consists of three layers, input, hidden, and output layers. The input layer is where the available amount of data fed to the ANN will be stored. The hidden layer task is to transform the inputs into a function that the output layer can use, while the output layer transforms the hidden layer activations into a scale, this is the scale where the data entered as targets will be adjusted to be as the desired output. In this section, the similar architecture as in [4] is applied as given in Fig. 2(a). Amount of hidden neurons selection is discussed in [6]. It is stated that the common selection criteria of hidden neurons amount is trial and error. Fig. 2(b) illustrates the impact of hidden neurons amount on the ANN regression response, hence, the ANN estimation accuracy. For the proposed ANN in this paper, the optimum hidden neurons number is 75. In the following subsection, the selection criteria of training data and the ANN structure are discussed.

B. Training data selection

Illustration of the data collection process is shown in Fig. 3(a). It can be seen that one average value of $i_{out,a}$ is calculated based on 7001 points and stored every 0.1 sec. In

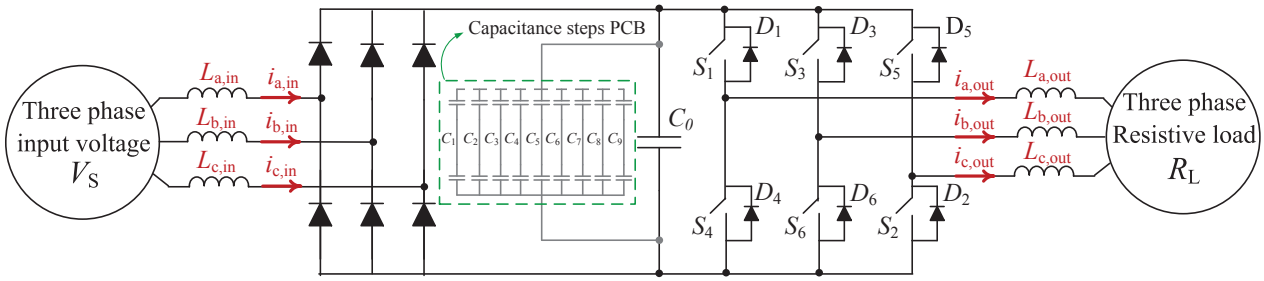

Fig. 4. An AC-AC power conversion system with a capacitor dc-link.

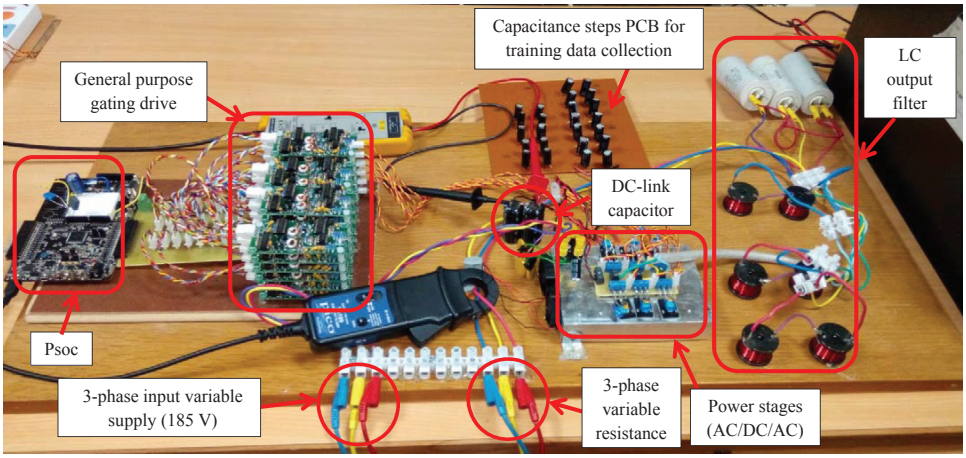

Fig. 5. Experimental platform for the proposed capacitor condition monitoring validation.

addition, one peak value of Δv_{dc} is calculated based on 7001 points and stores every 0.1 sec.

In order to collect training data with different capacitance values, a designed Printed Circuit Board (*PCB*) with 9 capacitance step is connected in parallel with the nominal dc-link capacitors as shown in Fig. 4. Each capacitance step equals to 11 μF. Therefore, the capacitance boundaries are between 110 μF and 198 μF. As considered in the simulation case, different loading conditions are considered, therefore, the training data are collected five times starting by 40 Ω and ending by 80 Ω resistive load. Eventually, 45 training data sets are available to be fed to the ANN layers. For the proposed ANN in this paper, the Neural Fitting Tool nftool in MATLAB software [7] is used. This tool is usually used for estimation and prediction problems in which the neural network maps between a set of numeric inputs and a set of numeric targets. The iteration algorithm used in this training is Bayesian Regularization [8], which typically takes longer time but it is suitable for challenging problems. Moreover, the used training algorithm avoids the overfitting issues by stopping the training automatically when the generated results stops improving. The regression response of the trained ANN equals to 0.9996 as shown in Fig. 3(b). Therefore, a very strong correlation between the inputs ($i_{out,a}$, ΔV_{dc}) and the target (C). Since the regression response of the trained ANN is satisfactory, the trained ANN is generated as a SIMULINK model for capacitance estimation purposes.

III. Experimental Results and Discussion

In order to validate the proposed concept, an experimental study is carried out in this section.

TABLE I
Specifications of the Experimental Front-End Diode Bridge Prototype Converter Parameters.

Input AC Voltage (V_{L-L})	185 V
Output AC Voltage (V_{L-L})	185 V
Rated DC-link Voltage (V_{dc})	250 V
Full Power Level ($P_{o,max}$)	850 W
Resistive load corresponded to ($P_{o,max}$) (R_L)	40 Ω
Nominal Capacitance ($C0$)	110 μF

A front-end diode bridge converter prototype is built. The circuit diagram of the built prototype is shown in Fig. 4. The experimental platform is shown in Fig. 5 and its specifications are listed in Table I. The training data are collected as described earlier. In order to collect training data with different capacitance values, a designed Printed Circuit Board (*PCB*) with 9 capacitance step is connected in parallel with the nominal dc-link capacitors as shown in Fig. 4.

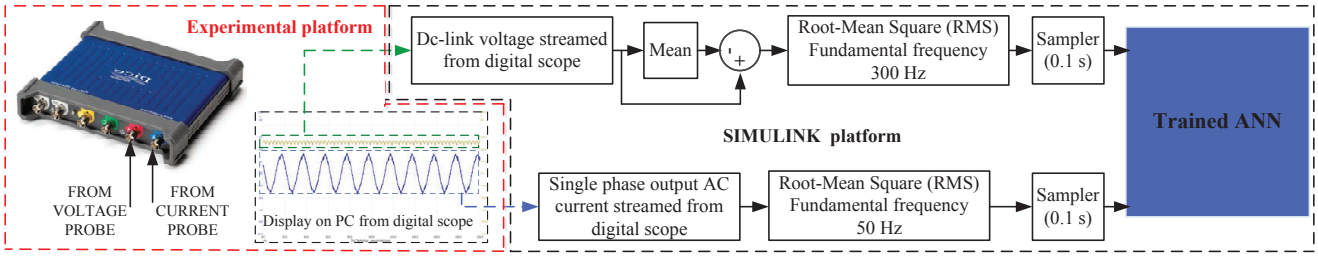

Fig. 6. Process of the proposed capacitor condition monitoring methodology.

TABLE II
EXPERIMENTAL RESULTS FOR ESTIMATED CAPACITANCE BY *ANN1* UNDER DIFFERENT LOADING CONDITIONS.

Actual Capacitance Value	Estimated Capacitance Value	Estimation Error	Loading Condition
C_{actual} = 110 μF	$C_{estimated}$ = 109.6 μF	Error = 0.36%	R_L = 70 Ω
C_{actual} = 143 μF	$C_{estimated}$ = 142.5 μF	Error = 0.35%	R_L = 50 Ω
C_{actual} = 176 μF	$C_{estimated}$ = 176.2 μF	Error = 0.1%	R_L = 40 Ω
C_{actual} = 187 μF	$C_{estimated}$ = 187.8 μF	Error = 0.42%	R_L = 60 Ω
C_{actual} = 198 μF	$C_{estimated}$ = 197 μF	Error = 0.5%	R_L = 80 Ω

The corresponding $i_{a,out}$ and ΔV_{dc} from each capacitance step are obtained in MATLAB according to the block digram shown in Fig. 6. The dc-link voltage ripple and RMS current of phase A are obtained based on the input signals as illustrated in Fig. 6. In the following subsections, the trained ANN is tested under different conditions.

A. Constant capacitance condition

In order to test the trained ANN, the dc-lnik capacitor in the prototype is adjusted to 132 μF under full power level. The behaviour of the dc-link voltage and single phase output current are shown in Fig. 7.

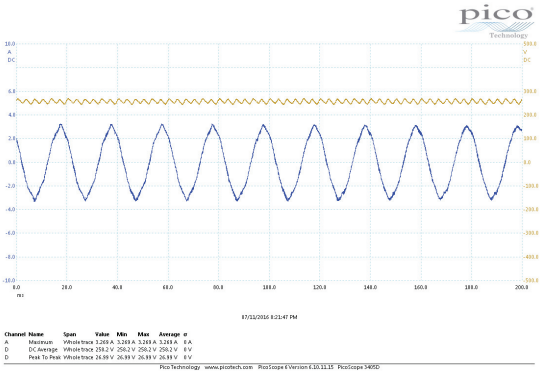

Fig. 7. DC-link voltage and single phase AC output current.

The trained ANN estimated the correct capacitance value as shown in Fig. 8. More estimated capacitance and their corresponding estimation error percentages are listed in Table II. It can be seen the ANN is tested under different loading conditions achieving 0.5% as maximum estimation error.

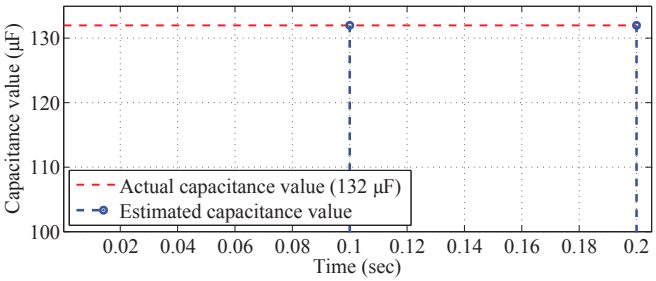

Fig. 8. Estimated capacitance by the trained ANN1.

B. Beyond the trained boundaries condition

In this subsection, the trained ANN is tested to estimate the capacitance under loading condition of 90 Ω resistive load which is beyond the considered training boundaries. the dc-lnik capacitor in the prototype is adjusted to its nominal value (110 μF). The trained ANN estimated 108.5 μF capacitance value with 1.5% estimation error as shown in Fig. 9.

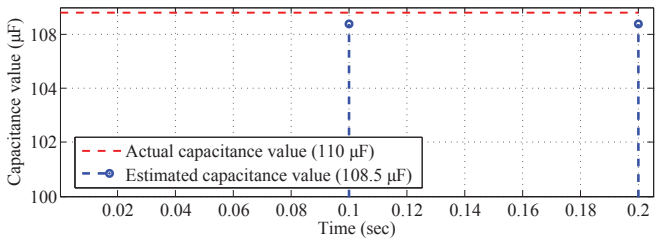

Fig. 9. Estimated capacitance by the trained ANN2.

TABLE III
EXPERIMENTAL RESULTS FOR ESTIMATED CAPACITANCE BY ***ANN2*** UNDER DIFFERENT LOADING CONDITIONS.

Actual Capacitance Value	Estimated Capacitance Value	Estimation Error	Loading Condition
C_{actual} = 165 μF	$C_{estimated}$ = 168.4 μF	Error = 2.0%	R_L = 40 Ω
C_{actual} = 176 μF	$C_{estimated}$ = 179.4 μF	Error = 1.9%	R_L = 40 Ω
C_{actual} = 187 μF	$C_{estimated}$ = 188.7 μF	Error = 0.9%	R_L = 40 Ω
C_{actual} = 143 μF	$C_{estimated}$ = 142.7 μF	Error = 0.2%	R_L = 50 Ω
C_{actual} = 154 μF	$C_{estimated}$ = 151.7 μF	Error = 1.5%	R_L = 50 Ω
C_{actual} = 132 μF	$C_{estimated}$ = 130 μF	Error = 1.5%	R_L = 70 Ω

C. ANN boundaries training

Training data amount, type and source have a strong impact on the ANN behaviour. It can be noted that the trained ANN is tested for capacitance values that are in the range of the training data. In order to investigate the ANN robustness with respect to training data amount specifications, (*ANN2*) with regression responce shown in Fig. 10 is studied.

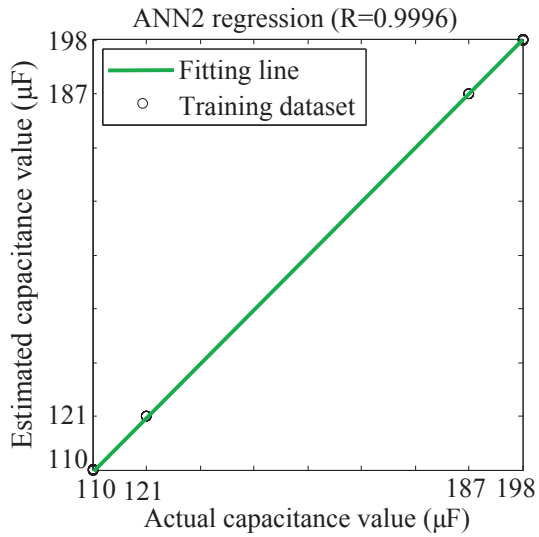

Fig. 10. Regression response of the trained ANN for experimental validation.

It can be seen that ANN2 is trained based on the first two minimum and last two maximum boundaries of the capacitance range ($(C0)$, $(C1)$, $(C8)$, and $(C9)$). Since 5 loading conditions are considered, eventually, 20 dataset are used in training ANN2. The estimated capacitance and their corresponding estimation error percentages are listed in Table III. Although that the estimation error percentages are higher than the ones listed in Table II, but they are worthy to be accepted in sake of saving time and effort in collecting larger capacitance steps for training purposes.

IV. CONCLUSIONS

The major contribution of this paper is divided in twofold; one is to experimentally validate a proposed condition monitoring method by capacitance estimation using ANN, two is to validate a proposed ANN that is trained based on the minimum and maximum boundaries. The proposed methodology is applied for a front-end diode bridge converter study case in order to estimate the capacitance value change of the dc-link capacitor. The proposed method requires no additional hardware circuit and can be implemented by using the extra resources of existing digital controllers in most of power electronic systems, implying a minimum additional investment. An accuracy analysis that shows the impact of hidden neurons amount on ANN accuracy is discussed. The capacitance estimation results under different capacitance values and loading conditions are also presented. Two different training approaches are analysed. It reveals that the maximum estimation error is 0.5% in case of considering the whole range of the collected data for training purpose. In addition, estimation error of 1.5% is obtained in capacitance estimation under non-trained loading condition. For an ANN trained based on the boundaries information, the estimation error is not exceeding 2%. ANN trained on boundaries are beneficial in sake of saving time and effort. Considering un-balanced and/or transient conditions is intended in the future work.

REFERENCES

[1] S. Yang, D. Xiang, A. Bryant, P. Mawby, L. Ran, and P. Tavner, "Condition monitoring for device reliability in power electronic converters: A review," *IEEE Transactions on Power Electronics*, vol. 25, no. 11, pp. 2734–2752, Nov. 2010.

[2] H. Soliman, H. Wang, and F. Blaabjerg, "A review of the condition monitoring of capacitors in power electronic converters," *IEEE Transactions on Industry Applications*, vol. 52, no. 6, pp. 4976–4989, Nov 2016.

[3] H. Wang and F. Blaabjerg, "Reliability of capacitors for dc-link applications in power electronic converters - an overview," *IEEE Trans. on Industry Applications*, vol. 50, no. 5, pp. 3569–3578, Sept 2014.

[4] H. Soliman, H. Wang, and F. Blaabjerg, "Capacitance estimation for dc-link capacitors in a back-to-back converter based on artificial neural network algorithm," in *2016 IEEE 8th International Power Electronics and Motion*

Control Conference (IPEMC-ECCE Asia), May 2016, pp. 3682–3688.

[5] H. Soliman, H. Wang, B. Gadalla, and F. Blaabjerg, "Condition monitoring for dc-link capacitors based on artificial neural network algorithm," in *Proc. of IEEE Power Engineering, Energy and Electrical Drives (POWERENG)*, 2015, pp. 587–591.

[6] G.-B. Huang, "Learning capability and storage capacity of two-hidden-layer feedforward networks," *IEEE Transactions on Neural Networks*, vol. 14, no. 2, pp. 274–281, Mar 2003.

[7] Open network/data manager - matlab nntool. [Online]. Available: http://se.mathworks.com/help/nnet/ref/nntool.html.

[8] Bayesian regularization backpropagation - matlab trainbr. [Online]. Available: http://se.mathworks.com/help/nnet/ref/nntool.html

ISSN (online): 2446-1636
ISBN (online): 978-87-7112-957-1

AALBORG UNIVERSITY PRESS